



21

Diffraction techniques



Crystal structure

- 21.1 Lattices and unit cells
- 21.2 The identification of lattice planes

X-ray diffraction

- 21.3 Bragg's law
- 21.4 The powder method
- 21.5 Single-crystal X-ray diffraction

Information from X-ray analysis

- 21.6 The packing of identical spheres: metal crystals
- 21.7 Ionic crystals
- 21.8 Absolute configurations

Neutron and electron diffraction

- 21.9 Neutron diffraction
- 21.10 Electron diffraction

Checklist of key ideas

Further reading.

Exercises

Problems

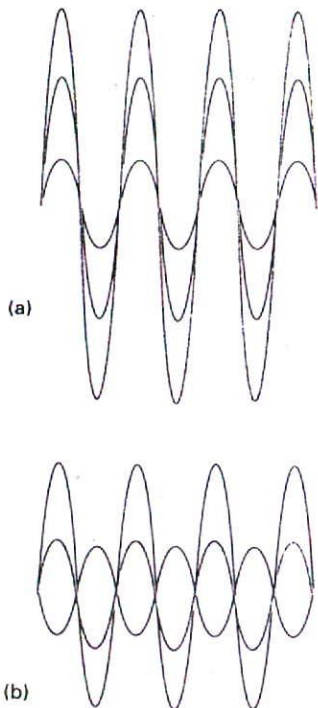
In this chapter we return to the techniques that are used to determine structure, but now the emphasis is on the geometrical arrangement of atoms and the distribution of electrons rather than energy levels. All the techniques described in this chapter make use of the property of diffraction of waves by objects with similar dimensions to the wavelength of the waves.

First, we see how to describe the regular arrangement of atoms in crystals and the symmetry of their arrangement. Then we consider the basic principles of X-ray diffraction, and show how the dimensions of unit cells and their symmetries can be inferred from experiments on powdered samples. After that, we turn to the most valuable technique, single-crystal X-ray diffraction, and show how the diffraction pattern can be interpreted in terms of the distribution of electron density in a unit cell. We then explore some of the principles that govern the crystal structures that X-ray diffraction reveals.

In the concluding sections of the chapter we see how neutron diffraction and electron diffraction bear close similarities to X-ray diffraction, but provide complementary information.

A characteristic property of waves is that they interfere with one another, giving a greater displacement where peaks or troughs coincide and a smaller displacement where peaks coincide with troughs (Fig. 20.1). According to classical electromagnetic theory, the intensity of electromagnetic radiation is proportional to the square of the amplitude of the waves. Therefore, the regions of constructive or destructive interference show up as regions of enhanced or diminished intensities. The phenomenon of diffraction is the interference caused by an object in the path of waves, and the pattern of varying intensity that results is called the **diffraction pattern**. Diffraction occurs when the dimensions of the diffracting object are comparable to the wavelength of the radiation.

X-rays have wavelengths comparable to bond lengths in molecules and the spacing of atoms in crystals (about 100 pm). By analysing an X-ray diffraction pattern, it is possible to draw up a detailed picture of the location of atoms even in such complex molecules as



21.1 When two waves are in the same region of space they interfere. Depending on their relative phase, they may interfere (a) constructively, to give an enhanced amplitude, or (b) destructively, to give a smaller amplitude. The component waves are shown in black and the resultant in green.

proteins. Electrons moving at about $20\,000\text{ km s}^{-1}$ (after acceleration through about 4 kV) have wavelengths of 40 pm , and may also be diffracted by molecules, surfaces, and thin slices of solids. Neutrons generated in a nuclear reactor, and then slowed, to thermal velocities, have similar wavelengths and may also be used for diffraction studies.

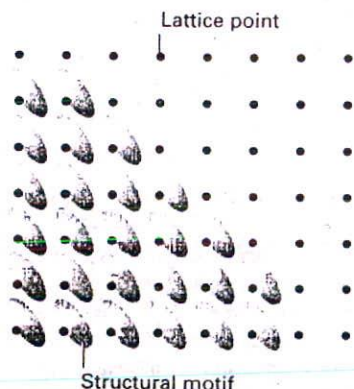
Crystal structure

Early in the history of modern science it was suggested that the regular external form of crystals implied an internal regularity of their constituents. In this section we see how to describe the arrangement of atoms inside crystals.

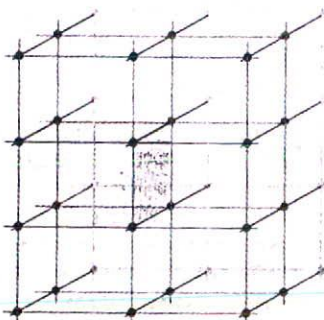
21.1 Lattices and unit cells

A crystal is built up from regularly repeating 'structural motifs', which may be atoms, molecules, or groups of atoms, molecules, or ions. A **space lattice** is the pattern formed by points representing the locations of these motifs (Fig. 21.2). The space lattice is, in effect, an abstract scaffolding for the crystal structure. More formally, the space lattice is a three-dimensional, infinite array of points, each of which is surrounded in an identical way by its neighbours, and which defines the basic structure of the crystal. In some cases there may be a structural motif centred on each lattice point, but that is not necessary. The **crystal structure** itself is obtained by associating with each lattice point an identical structural motif.

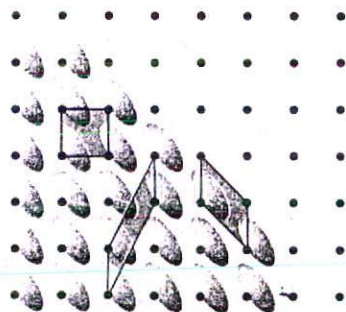
The **unit cell** is an imaginary parallelepiped (parallel-sided figure) that contains one unit of the translationally repeating pattern (Fig. 21.3). A unit cell can be thought of as the fundamental region from which the entire crystal may be constructed by purely translational displacements (like bricks in a wall). A unit cell is commonly formed by joining neighbouring lattice points by straight lines (Fig. 21.4). Such unit cells are called **primitive**. It is sometimes more convenient to draw non-primitive unit cells that also have lattice points at their centres or on pairs of opposite faces. An infinite number of different unit cells can describe the same lattice, but we normally choose the one with sides that have the shortest lengths and that are most nearly perpendicular to one another. The lengths of the sides of a



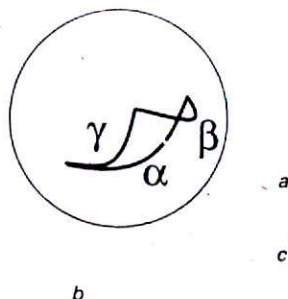
21.2 Each lattice point specifies the location of a structural motif (for example, a molecule or a group of molecules). The crystal lattice is the array of lattice points; the crystal structure is the collection of structural motifs arranged according to the lattice.



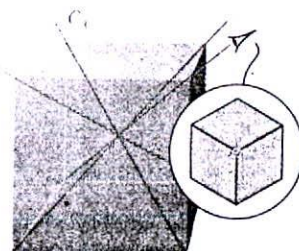
21.3 A unit cell is a parallel-sided (but not necessarily rectangular) figure from which the entire crystal structure can be constructed by using only translations (not reflections, rotations, or inversions).



21.4 A unit cell can be chosen in a variety of ways, as shown here. It is conventional to choose the cell that represents the full symmetry of the lattice. In this rectangular lattice, the rectangular unit cell would normally be adopted.



21.5 The notation for the sides and angles of a unit cell. Note that the angle α lies in the plane (b, c) and perpendicular to the axis a .



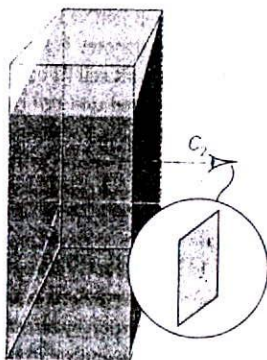
21.6 A unit cell belonging to the cubic system has four threefold axes arranged tetrahedrally. The insert shows the threefold symmetry.

Table 21.1 The seven crystal systems

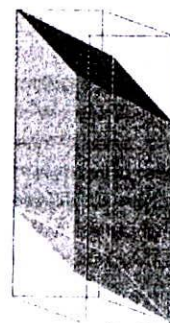
System	Essential symmetries
Triclinic	None
Monoclinic	One C_2 axis
Orthorhombic	Three perpendicular C_2 axes
Rhombohedral	One C_3 axis
Tetragonal	One C_4 axis
Hexagonal	One C_6 axis
Cubic	Four C_3 axes in a tetrahedral arrangement

unit cell are denoted a , b , and c , and the angles between them are denoted α , β , and γ (Fig. 21.5).

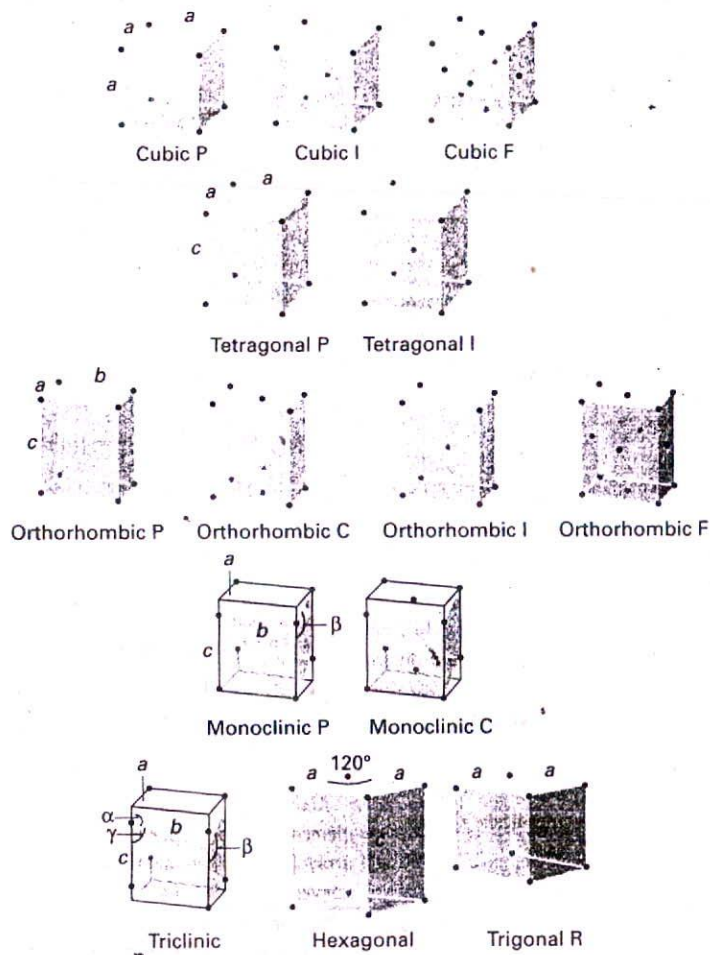
Unit cells are classified into seven crystal systems by noting the rotational symmetry elements they possess. A cubic unit cell, for example, has four threefold axes in a tetrahedral array (Fig. 21.6). A monoclinic unit cell has one twofold axis; the unique axis is by convention the b -axis (Fig. 21.7). A triclinic unit cell has no rotational symmetry, and typically all three sides and angles are different (Fig. 21.8). The essential symmetries, the elements that must be present for the unit cell to belong to a particular crystal system, are listed in Table 21.1.



21.7 A unit belonging to the monoclinic system has a twofold axis (shown in more detail in the insert).



21.8 A triclinic unit cell has no axes of rotational symmetry.

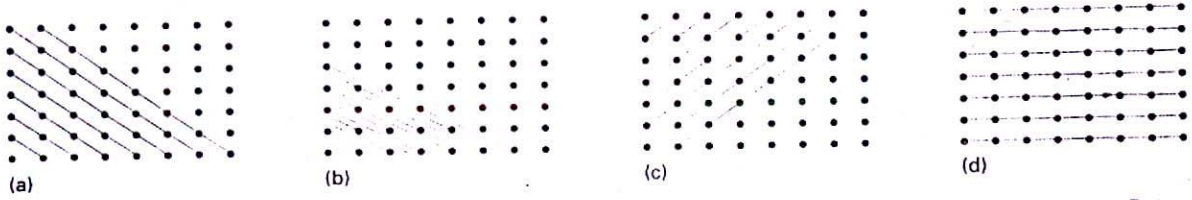


21.9 The fourteen Bravais lattices. The points are lattice points, and are not necessarily occupied by atoms. P denotes a primitive unit cell (R is used for a trigonal lattice), I a body-centred unit cell, F a face-centred unit cell, and C (or A or B) a cell with lattice points on two opposite faces.

There are only 14 distinct crystal lattices in three dimensions. These Bravais lattices are illustrated in Fig. 21.9. It is conventional to portray these lattices by primitive unit cells in some cases and by non-primitive unit cells in others. Primitive unit cells (with lattice points only at the corners) are denoted P. A **body-centred unit cell** (I) also has a lattice point at its centre. A **face-centred unit cell** (F) has lattice points at its corners and also at the centres of its six faces. A **side-centred unit cell** (A, B, or C) has lattice points at its corners and at the centres of two opposite faces. For simple structures, it is often convenient to choose an atom belonging to the structural motif, or the centre of a molecule, as the location of a lattice point or the vertex of a unit cell, but that is not a necessary requirement.

21.2 The identification of lattice planes

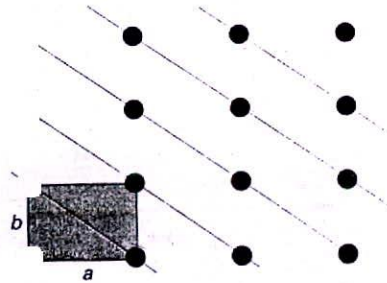
The spacing of the lattice points in a crystal is an important quantitative aspect of its structure and its investigation by diffraction techniques. However, there are many different sets of planes (Fig. 21.10), and we need to be able to label them. Two-dimensional lattices are easier to visualize than three-dimensional lattices, so we shall introduce the concepts involved by referring to two dimensions initially, and then extend the conclusions by analogy to three dimensions.



21.10 Some of the planes that can be drawn through the points of the space lattice and their corresponding Miller indices (hkl): (a) (110), (b) (230), (c) $\bar{1}10$, (d) (010).

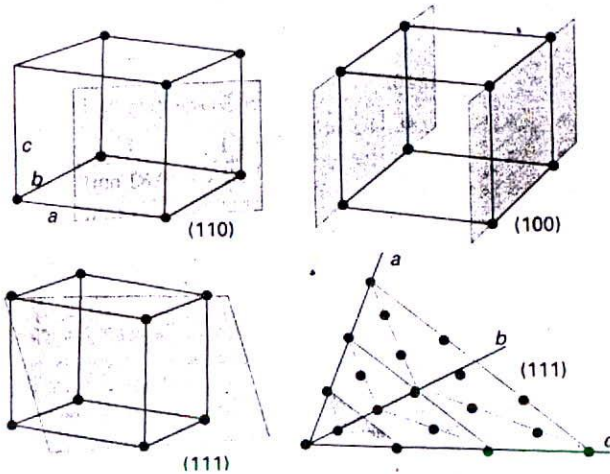
(a) The Miller indices

Consider a two-dimensional rectangular lattice formed from a unit cell of sides a , b (as in Fig. 21.11). Each plane in the illustration (except the plane passing through the origin) can be distinguished by the distances at which it intersects the a - and b -axes. One way of labelling each set of parallel planes would therefore be to quote the smallest intersection distances. For example, we could denote the four sets in Fig. 21.10a as $(1a, 1b)$, $(\frac{1}{2}a, \frac{1}{3}b)$, $(-1a, 1b)$, and $(\infty a, 1b)$. However, if we agree to quote distances along the axes as multiples of the lengths of the unit cell, we can label the planes more simply as $(1, 1)$, $(\frac{1}{2}, \frac{1}{3})$, $(-1, 1)$, and $(\infty, 1)$. If the lattice in Fig. 21.10 is the top view of a three-dimensional orthorhombic lattice in which the unit cell has a length c in the z -direction, all four sets of planes intersect the z -axis at infinity. Therefore, the full labels are $(1, 1, \infty)$, $(\frac{1}{2}, \frac{1}{3}, \infty)$, $(-1, 1, \infty)$, and $(\infty, 1, \infty)$.

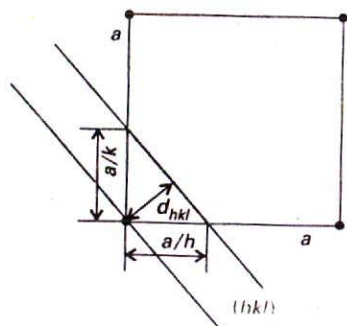


21.11 The dimensions of a unit cell and their relation to the plane passing through the lattice points.

The presence of fractions and ∞ in the labels is inconvenient. They can be eliminated by taking the reciprocals of the labels. As we shall see, taking reciprocals turns out to have further advantages. The Miller indices, (hkl) , are the reciprocals of intersection distances (with fractions cleared by multiplying through by an appropriate factor, if taking the reciprocal results in a fraction). For example, the $(1, 1, \infty)$ planes in Fig. 21.10a are the (110) planes in the Miller notation. Similarly, the $(\frac{1}{2}, \frac{1}{3}, \infty)$ planes are denoted (230). Negative indices are written with a bar over the number, and Fig. 21.10c shows the $\bar{1}10$ planes. The Miller indices for the four sets of planes in Fig. 21.10 are therefore (110), (230), $\bar{1}10$, and (010). A three-dimensional representation of a selection of planes, including one in a lattice with a non-orthogonal axes, is shown in Fig. 21.12.



21.12 Some representative planes in three dimensions and their Miller indices. Note that a 0 indicates that a plane is parallel to the corresponding axis, and that the indexing may also be used for unit cells with non-orthogonal axes.



21.13 The calculation of the separation of the planes (hkl) in terms of the Miller indices for a square lattice.

A helpful feature to remember is that, the smaller the absolute value of h in (hkl) , the more nearly parallel the plane is to the a -axis.¹ The same is true of k and the b -axis and l and the c -axis. When $h = 0$, the planes intersect the a -axis at infinity, so the $(0kl)$ planes are parallel to the a -axis. Similarly, the $(h0l)$ planes are parallel to b and the $(hk0)$ planes are parallel to c .

(b) The separation of planes

The Miller indices are very useful for expressing the separation of planes. The separation of the $(hk0)$ planes, in the square lattice shown in Fig. 21.13 is given by

$$\frac{1}{d_{hk0}^2} = \frac{h^2 + k^2}{a^2} \quad \text{or} \quad d_{hk0} = \frac{a}{(h^2 + k^2)^{1/2}} \quad (1)$$

By extension to three dimensions, the separation of the (hkl) planes of a cubic lattice is given by

$$\frac{1}{d_{hkl}^2} = \frac{h^2 + k^2 + l^2}{a^2} \quad \text{or} \quad d_{hkl} = \frac{a}{(h^2 + k^2 + l^2)^{1/2}} \quad (2)$$

The corresponding expression for a general orthorhombic lattice is the generalization of this expression:

$$\frac{1}{d_{hkl}^2} = \frac{h^2}{a^2} + \frac{k^2}{b^2} + \frac{l^2}{c^2} \quad (3)$$

Example 21.1 Using the Miller indices

Calculate the separation of (a) the (123) planes and (b) the (246) planes of an orthorhombic cell with $a = 0.82$ nm, $b = 0.94$ nm, and $c = 0.75$ nm.

Method For the first part, simply substitute the information into eqn 3. For the second part, instead of repeating the calculation, note that, if all three Miller indices are multiplied by n , their separation is reduced by that factor (Fig. 21.14):

$$\frac{1}{d_{nh,nk,nl}^2} = \frac{(nh)^2}{a^2} + \frac{(nk)^2}{b^2} + \frac{(nl)^2}{c^2} = n^2 \left(\frac{h^2}{a^2} + \frac{k^2}{b^2} + \frac{l^2}{c^2} \right) = \frac{n^2}{d_{hkl}^2}$$

which implies that

$$d_{nh,nk,nl} = \frac{d_{hkl}}{n}$$

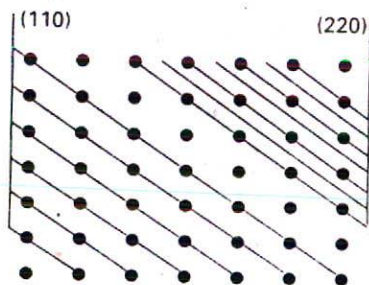
Answer Substituting the indices into eqn 3 gives

$$\frac{1}{d_{123}^2} = \frac{1^2}{(0.82 \text{ nm})^2} + \frac{2^2}{(0.94 \text{ nm})^2} + \frac{3^2}{(0.75 \text{ nm})^2} = 22 \text{ nm}^{-2}$$

Hence, $d_{123} = 0.21$ nm. It then follows immediately that d_{246} is one-half this value, or 0.11 nm.

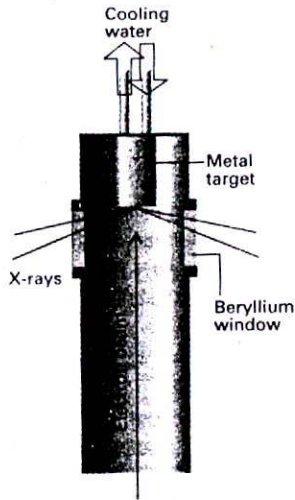
Self-test 21.1 Calculate the separation of (a) the (133) planes and (b) the (399) planes in the same lattice.

[0.19 nm, 0.063 nm]



21.14 The separation of the (220) planes is half that of the (110) planes. In general, the separation of the planes (nh, nk, nl) is n times smaller than the separation of the (hkl) planes.

1 The $(h00)$ planes are exceptions.



21.15 X-rays are generated by directing an electron beam on to a cooled metal target. Beryllium is transparent to X-rays (on account of the small number of electrons in each atom) and is used for the windows.

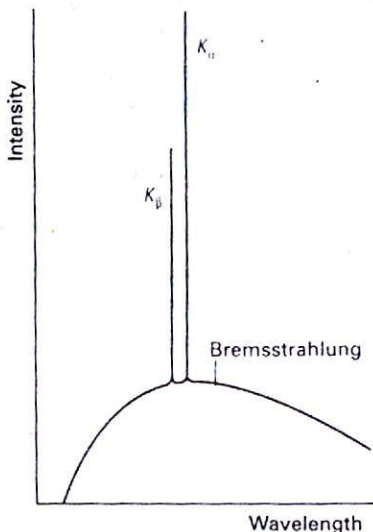
X-ray diffraction

X-rays, which are electromagnetic radiation with wavelengths of the order of 10^{-10} m, are typically generated by bombarding a metal with high-energy electrons (Fig. 21.15). The electrons decelerate as they plunge into the metal and generate radiation with a continuous range of wavelengths called *Bremsstrahlung*.² Superimposed on the continuum are a few high-intensity, sharp peaks (Fig. 21.16). These peaks arise from collisions of the incoming electrons with the electrons in the inner shells of the atoms. A collision expels an electron from an inner shell, and an electron of higher energy drops into the vacancy, emitting the excess energy as an X-ray photon (Fig. 21.17). If the electron falls into a *K* shell (that is, a shell with $n = 1$), the X-rays are classified as *K*-radiation, and similarly for transitions into the *L* ($n = 2$) and *M* ($n = 3$) shells. Strong, distinct lines are labelled K_{α} , K_{β} , and so on.

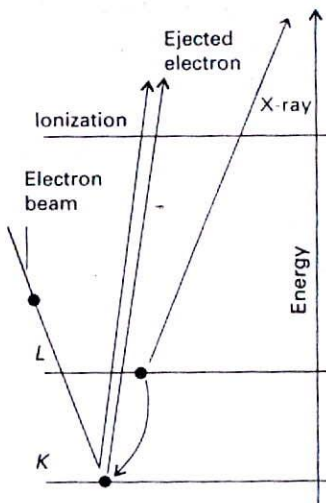
21.3 Bragg's law

Wilhelm Röntgen discovered X-rays in 1895. Seventeen years later, Max von Laue suggested that they might be diffracted when passed through a crystal, for by then he had realized that their wavelengths are comparable to the separations of lattice planes. von Laue's suggestion was confirmed almost immediately by Walter Friedrich and Paul Knipping, and has grown since then into a technique of extraordinary power.

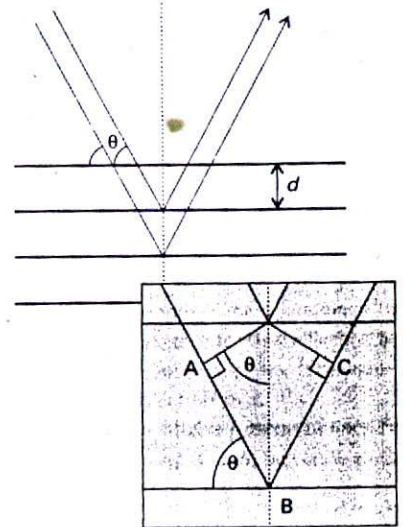
An early approach to the analysis of diffraction patterns produced by crystals was to regard a lattice plane as a mirror, and to model a crystal as stacks of reflecting lattice planes of separation d (Fig. 21.18). The model makes it easy to calculate the angle the crystal must



21.16 The X-ray emission from a metal consists of a broad, featureless *Bremsstrahlung* background, with sharp transitions superimposed on it. The label *K* indicates that the radiation comes from a transition in which an electron falls into a vacancy in the *K* shell of the atom.



21.17 The processes that contribute to the generation of X-rays. An incoming electron collides with an electron (in the *K* shell), and ejects it. Another electron (from the *L* shell in this illustration) falls into the vacancy and emits its excess energy as an X-ray photon.



21.18 The conventional derivation of the Bragg law treats each lattice plane as a reflecting plane and incident radiation. The path lengths differ by $AB + BC$, which depends on the glancing angle, θ . Constructive interference (a 'reflection') occurs when $AB + BC$ is equal to an integer number of wavelengths.

² *Bremse* is German for deceleration, *Strahlung* for ray.

make to the incoming beam of X-rays for constructive interference to occur. It has also given rise to the name reflection to denote an intense beam arising from constructive interference.

The path-length difference of the two rays shown in Fig. 21.18 is

$$AB + BC = 2d \sin \theta$$

where θ is the glancing angle. For many glancing angles the path-length difference is not an integer number of wavelengths, and the waves interfere largely destructively. However, when the path-length difference is an integer number of wavelengths ($AB + BC = n\lambda$), the reflected waves are in phase and interfere constructively. It follows that a bright reflection should be observed when the glancing angle satisfies Bragg's law:

$$n\lambda = 2d \sin \theta \quad (4)$$

Reflections with $n = 2, 3, \dots$ are called second-order, third-order, and so on; they correspond to path-length differences of $2, 3, \dots$ wavelengths. In modern work it is normal to absorb the n into d , to write Bragg's law as

$$\lambda = 2d \sin \theta \quad (5)$$

and to regard the n th-order reflection as arising from the (nh, nk, nl) planes (see Example 21.1).

The primary use of Bragg's law is in the determination of the spacing between the layers in the lattice for, once the angle θ corresponding to a reflection has been determined, d may readily be calculated.

Example 21.2 Using Bragg's law

A reflection from the (111) planes of a cubic crystal was observed at a glancing angle of 11.2° when $\text{Cu } K_\alpha$ X-rays of wavelength 154 pm were used. What is the length of the side of the unit cell?

Method The separation of the planes can be determined from Bragg's law. Because the crystal is cubic, the separation is related to the length of the side of the unit cell, a , by eqn 2, which may therefore be solved for a .

Answer According to eqn 5, the (111) planes responsible for the diffraction have separation

$$d_{111} = \frac{\lambda}{2 \sin \theta}$$

The separation of the (111) planes of a cubic lattice of side a is given by eqn 2 as

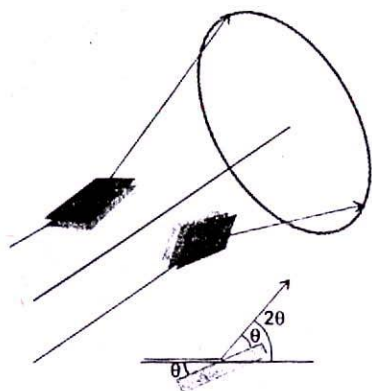
$$d_{111} = \frac{a}{3^{1/2}}$$

Therefore,

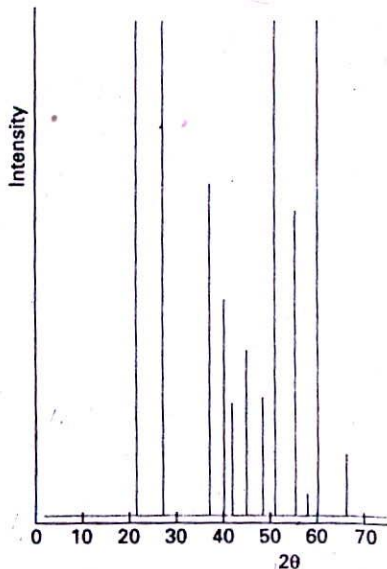
$$a = \frac{3^{1/2} \lambda}{2 \sin \theta} = \frac{3^{1/2} \times (154 \text{ pm})}{2 \sin 11.2^\circ} = 687 \text{ pm}$$

Self-test 21.2 Calculate the angle at which the same crystal will give a reflection from the (123) planes.

[24.8°]



21.19 The same set of planes in two microcrystallites with different orientations around the direction of the incident beam gives diffracted rays that lie on a cone. The full powder diffraction pattern is formed by cones corresponding to reflections from all the sets of (hkl) planes that satisfy Bragg's law. (A reflection at a glancing angle θ gives rise to a reflection at an angle 2θ to the direction of the incident beam; see inset.)



21.20 In the Debye-Scherrer method, a monochromatic X-ray beam is diffracted by a powder sample. The crystallites give rise to cones of intensity, which are detected electronically to give a pattern like that shown here.

21.4 The powder method

von Laue's original method consisted of passing a broad-band beam of X-rays into a single crystal, and recording the diffraction pattern photographically. The idea behind the approach was that a crystal might not be suitably orientated to act as a diffraction grating for a single wavelength but, whatever its orientation, Bragg's law would be satisfied for at least one of the wavelengths if a range of wavelengths was used. There is currently a resurgence of interest in this approach because synchrotron radiation spans a range of X-ray wavelengths (Section 16.1a).

(a) The Debye-Scherrer method

An alternative technique to von Laue's was developed by Peter Debye and Paul Scherrer and independently by Albert Hull. They used monochromatic radiation and a powdered sample. When the sample is a powder, at least some of the crystallites will be orientated so as to satisfy the Bragg condition for each set of planes (hkl) . For example, some of the crystallites will be orientated so that their (111) planes, of spacing d_{111} , give rise to diffracted intensity at the glancing angle θ (Fig. 21.19). The crystallites with this glancing angle will lie at all possible angles around the incoming beam, so the diffracted beams lie on a cone around the incident beam of half-angle 2θ . Other crystallites will be orientated with different planes satisfying the Bragg condition. They give rise to a cone of diffracted intensity with a different half-angle. In principle, each set of (hkl) planes gives rise to a diffraction cone, because some of the randomly orientated crystallites will have the correct angle to diffract the incident beam. In modern powder diffractometers the intensities of the reflections are monitored electronically as the detector is rotated around the sample in a plane containing the incident ray (Fig. 21.20).

Powder diffraction techniques are used to identify a sample of a solid substance by comparison of the positions of the diffraction lines and their intensities with a large data bank (*The powder diffraction file*, which is maintained by the International Centre for Diffraction Data, ICDD, and contains information on about 50 000 crystalline phases). Powder diffraction data are also used to determine phase diagrams, for different solid phases result in different diffraction patterns, and to determine the relative amounts of each phase present in a mixture. The technique is also used for the initial determination of the dimensions and symmetries of unit cells, as the following section explains.

(b) Indexing the reflections

Bragg's law is used to interpret the angle θ of a reflection in terms of the separation of the lattice planes. If the values of h , k , and l for the planes responsible for that reflection are known, the dimensions of the unit cell can be deduced. The crux of the technique is therefore the indexing of the reflection, or ascribing the indices hkl to it.

Some types of unit cell give characteristic and easily recognizable patterns of lines. For example, in a cubic lattice of unit cell dimension a the spacing is given by eqn 2, so the angles at which the (hkl) planes give reflections are given by

$$\sin \theta = (h^2 + k^2 + l^2)^{1/2} \frac{\lambda}{2a} \quad (6)$$

The reflections are then predicted by substituting the values of h , k , and l :

(hkl)	(100)	(110)	(111)	(200)	(210)	(211)	(220)	(300)	(221)	(310)	...
$h^2 + k^2 + l^2$	1	2	3	4	5	6	8	9	9	10	...

Notice that 7 (and 15, ...) is missing because the sum of the squares of three integers cannot equal 7 (or 15, ...). Therefore the pattern has omissions that are characteristic of the cubic P lattice.

Example 21.3 Identifying the unit cell

A powder diffraction photograph of the element polonium gave lines at the following values of 2θ (in degrees) when 71.0 pm Mo X-rays were used: 12.1, 17.1, 21.0, 24.3, 27.2, 29.9, 34.7, 36.9, 38.9, 40.9, 42.8. Identify the unit cell and determine its dimensions.

Method From eqn 6 we write

$$\sin^2 \theta = A(h^2 + k^2 + l^2) \quad A = \left(\frac{\lambda}{2a}\right)^2$$

We need to determine the common factor A , and then find $h^2 + k^2 + l^2$.

Answer We draw up the following table:

$2\theta/^\circ$	12.1	17.1	21.0	24.3	27.2	29.9	34.7	36.9	38.9	40.9	42.8
$\theta/^\circ$	6.05	8.55	10.5	12.2	13.6	15.0	17.4	18.5	19.5	20.5	21.4
$100 \sin^2 \theta$	1.11	2.21	3.32	4.47	5.53	6.70	8.94	10.1	11.1	12.3	13.3

The common divisor is 1.11/100. Divide through to identify $h^2 + k^2 + l^2$:

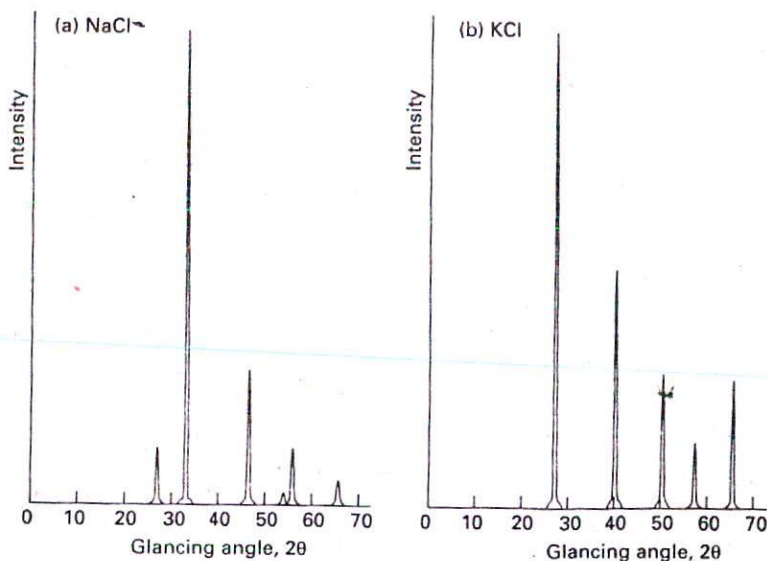
$h^2 + k^2 + l^2$	1	2	3	4	5	6	8	9	10	11	12
-------------------	---	---	---	---	---	---	---	---	----	----	----

The corresponding indices are

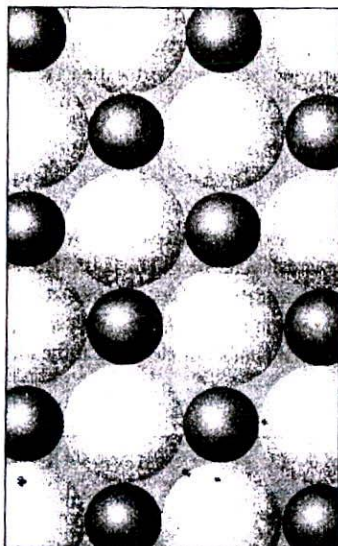
$$(100) (110) (111) (200) (210) (211) (220) (300) (310) (311) (222)$$

Note that indices like (120) and (012) are equivalent to (210) in this list. We have now indexed the lines. Note the absence of $h^2 + k^2 + l^2 = 7$, which indicates a primitive cubic (cubic P) cell. From $(\lambda/2a)^2 = 0.0111$, we find $a = 337$ pm.

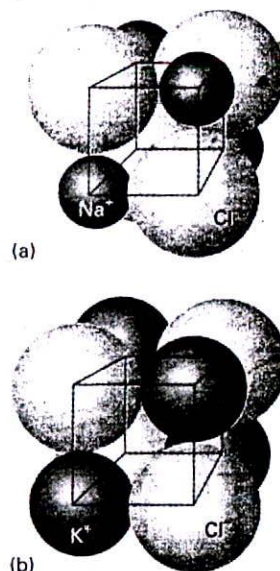
Comment Later we shall see that additional information comes from the intensities of the lines.



21.21 X-ray powder photographs of (a) NaCl, (b) KCl and the indexed reflections. The smaller number of lines in (b) is a consequence of the similarity of the K^+ and Cl^- scattering factors, as discussed later in the chapter.



21.22 A fragment of the structure of NaCl and KCl: showing one plane of ions. Each cation (small spheres) has anions (large spheres) as its nearest neighbours. (For the three-dimensional structure, see Fig. 21.40.)



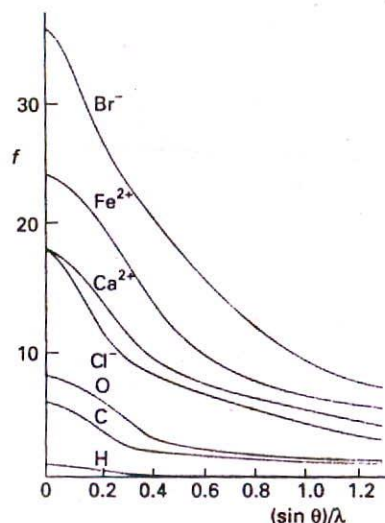
21.23 (a) One octant of the unit cell of NaCl; the Na^+ ions and Cl^- ions have different numbers of electrons and hence have different scattering factors. (b) One octant of the unit cell of KCl; the K^+ ions and Cl^- ions have the same numbers of electrons and hence have similar scattering factors. The diffraction pattern in this case is that of a primitive cubic lattice.

Self-test 21.3 In the same camera, another cubic crystal gave reflections at the following values of 2θ (in degrees): 10.4, 14.8, 18.2, 21.0, 23.6, 25.8, 27.7. Identify the unit cell and determine its dimension. See Fig. 21.26 for assistance.

[Cubic I; 550 pm]

(c) Systematic absences

The X-ray powder diffraction patterns for NaCl and KCl are remarkably different for two such similar structures (Fig. 21.21). Both crystals consist of two mutually interpenetrating face-centred cubic arrays of ions, one of Na^+ ions or K^+ ions and the other of Cl^- ions (Fig. 21.22). The explanation of the difference is found in the scattering strengths of the ions and the interference between waves scattered by the cations and anions. Thus, some reflections from the Na^+ ions are in phase with the Cl^- reflections, and the two reflections augment one another to give more intense maxima. For other orientations, the two sets of reflections may be out of phase, and tend to cancel, but, as the scattering strengths of the two ions are different, the cancellation is incomplete. For KCl, however, the scattering strengths of K^+ and Cl^- , which have the same numbers of electrons, are very similar, and cancellation is complete. The ions in KCl therefore all look very similar (Fig. 21.23) and, instead of appearing to be face-centred cubic, the powder diffraction pattern is that typical of a lattice with a primitive cubic unit cell.



21.24 The variation of the scattering factor of atoms and ions with atomic number and angle. The scattering factor in the forward direction (at $\theta = 0$, and hence at $(\sin \theta)/\lambda = 0$) is equal to the number of electrons present in the species.

The general form of the diffraction pattern of a crystal composed of atoms and ions with different scattering strengths can be predicted by considering a crystal composed of A and B atoms with scattering strengths measured by their scattering factors, f_A and f_B . If the scattering factor is large, the atoms scatter X-rays strongly. The scattering factor of an atom is related to the electron density distribution in the atom, $\rho(r)$, by

$$f = 4\pi \int_0^\infty \rho(r) \frac{\sin kr}{kr} r^2 dr \quad k = \frac{4\pi}{\lambda} \sin \theta \quad (7)$$

The value of f is greatest in the forward direction and smaller for directions away from the forward direction (Fig. 21.24). The detailed analysis of the intensities of reflections must take this dependence on direction into account (in single-crystal studies as well as for powders). We show in the *Justification* below that, in the forward direction (for $\theta = 0$), f is equal to the total number of electrons in the atom.

Justification 21.1

As $\theta \rightarrow 0$, so $k \rightarrow 0$. Because $\sin x = x - \frac{1}{6}x^3 + \dots$,

$$\lim_{x \rightarrow 0} \frac{\sin x}{x} = \lim_{x \rightarrow 0} \frac{x - \frac{1}{6}x^3 + \dots}{x} = \lim_{x \rightarrow 0} (1 - \frac{1}{6}x^2 + \dots) = 1$$

The factor $(\sin kr)/kr$ is therefore equal to 1 for forward scattering. It follows that in the forward direction

$$f = 4\pi \int_0^\infty \rho(r) r^2 dr$$

The integral over the electron density ρ (the number of electrons in an infinitesimal region divided by the volume of the region) multiplied by the volume element $4\pi r^2 dr$ is the total number of electrons, N_e , in the atom. Hence, in the forward direction, $f = N_e$. For example, the scattering factors of Na^+ , K^+ , and Cl^- are 8, 18, and 18, respectively.

The scattering factor is smaller in non-forward directions because $(\sin kr)/kr < 1$ for $\theta > 0$, so the integral is smaller than the value calculated above.

We shall now calculate the diffraction pattern to expect when two kinds of atom are present in a unit cell. We begin by showing in the following *Justification* that, if in the unit cell there is an A atom at the origin and a B atom at the coordinates (xa, yb, zc) , where x , y , and z lie in the range 0 to 1, then the phase difference between the hkl reflections of the A and B atoms is

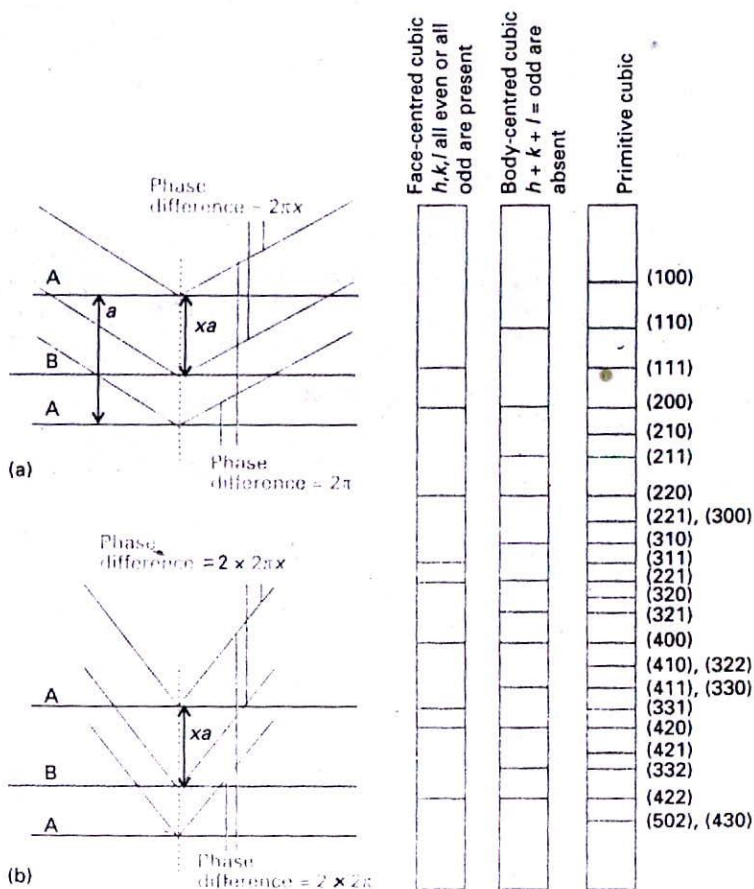
$$\phi_{hkl} = 2\pi(hx + ky + lz) \quad (8)$$

Justification 21.2

Consider the crystal shown schematically in Fig. 21.25. The reflection corresponds to two waves from adjacent A planes, the phase difference of the waves being 2π . If there is a B atom at a fraction x of the distance between the two A planes, then it gives rise to a wave with a phase difference $2\pi x$ relative to an A reflection. To see this conclusion, note that, if $x = 0$, there is no phase difference; if $x = \frac{1}{2}$ the phase difference is π ; if $x = 1$, the B atom lies where the lower A atom is and the phase difference is 2π . Now consider a (200) reflection. There is now a $2 \times 2\pi$ difference between the waves from the two A layers, and if B were to lie at $x = 0.5$ it would give rise to a wave that differed in phase by 2π from the wave from the upper A layer. Thus, for a general fractional position x , the phase difference

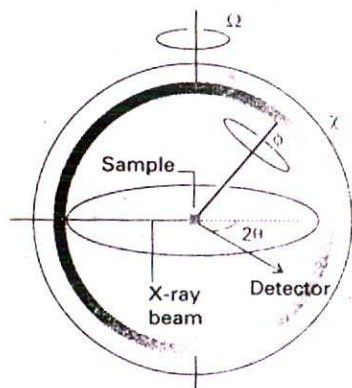
for a (200) reflection is $2 \times 2\pi x$. For a general ($h00$) reflection, the phase difference is therefore $h \times 2\pi x$. For three dimensions, this result generalizes to eqn 8.

The A and B reflections interfere destructively when the phase difference is π , and the total intensity is zero if the atoms have the same scattering power. For example, if the unit cells are cubic I with a B atom at $x = y = z = \frac{1}{2}$, then the A, B phase difference is $(h + k + l)\pi$. Therefore, all reflections for odd values of $h + k + l$ vanish because the waves are displaced in phase by π . Hence the diffraction pattern for a cubic I lattice can be constructed from that for the cubic P lattice (a cubic lattice without points at the centre of its unit cells) by striking out all reflections with odd values of $h + k + l$. Recognition of these systematic absences in a powder spectrum immediately indicates a cubic I lattice (Fig. 21.26).



21.25 Diffraction from a crystal containing two kinds of atom. (a) For a (100) reflection from the A planes there is a phase difference of 2π between waves reflected by neighbouring planes, but (b) for a (200) reflection the phase difference is 4π . The reflection from a B plane at a fractional distance xa from an A plane has a phase that is x times these phase differences.

21.26 The powder diffraction patterns and the systematic absences of three versions of a cubic cell. Comparison of the observed pattern with patterns like these enables the unit cell to be identified. The locations of the lines give the cell dimensions.



21.27 A four-circle diffractometer. The settings of the orientations (ϕ , χ , θ , and Ω) of the components are controlled by computer; each (hkl) reflection is monitored in turn, and their intensities are recorded.

If the amplitude of the waves scattered from A is f_A at the detector, that of the waves scattered from B is $f_B e^{i\phi_{hkl}}$, with ϕ_{hkl} the phase difference given in eqn 8. The total amplitude at the detector is therefore

$$F_{hkl} = f_A + f_B e^{i\phi_{hkl}} \quad (9)$$

Because the intensity is proportional to the square modulus of the amplitude of the wave, the intensity, I_{hkl} , at the detector is

$$I_{hkl} \propto F_{hkl}^* F_{hkl} = \{f_A + f_B e^{-i\phi_{hkl}}\} \{f_A + f_B e^{i\phi_{hkl}}\} \quad (10)$$

This expression expands to

$$I_{hkl} \propto f_A^2 + f_B^2 + f_A f_B (e^{i\phi_{hkl}} + e^{-i\phi_{hkl}}) = f_A^2 + f_B^2 + 2f_A f_B \cos \phi_{hkl} \quad (11)$$

The cosine term either adds to or subtracts from $f_A^2 + f_B^2$ depending on the value of ϕ_{hkl} , which in turn depends on h , k , and l and x , y , and z (through eqn 8). Hence, there is a variation in the intensities of the lines with different hkl , which is exactly what is observed for NaCl (Fig. 21.21a).

21.5 Single-crystal X-ray diffraction

The method developed by the Braggs (William and his son Lawrence, who later jointly won the Nobel Prize) is the foundation of almost all modern work in X-ray crystallography. They used a single crystal and a monochromatic beam of X-rays, and rotated the crystal until a reflection was detected. There are many different sets of planes in a crystal, so there are many angles at which a reflection occurs. The complete set of data consists of the list of angles at which reflections are observed and their intensities.

(a) The technique

The diffraction pattern produced by a single crystal is measured by using a four-circle diffractometer (Fig. 21.27). The computer linked to the diffractometer determines the unit cell dimensions and the angular settings of the diffractometer's four circles that are needed to observe any particular (hkl) reflection. The computer controls the settings, and moves the crystal and the detector for each one in turn. At each setting, the diffraction intensity is measured, and background intensities are assessed by making measurements at slightly different settings. Computing techniques are now available that lead not only to automatic indexing but also to the automated determination of the shape, symmetry, and size of the unit cell. Moreover, several techniques are now available for sampling large amounts of data, including area detectors and image plates, which sample whole regions of diffraction patterns simultaneously.

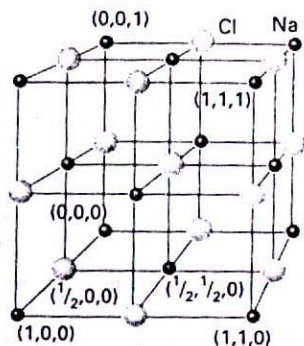
(b) Structure factors

The problem we now address is how to interpret the data from a diffractometer in terms of the structure of the crystal. To do so, we must go beyond Bragg's law.

Suppose the unit cell contains several atoms with scattering factors f_j and coordinates (x_j, y_j, z_j) . The overall amplitude of a wave diffracted by the (hkl) planes is a generalization of the expression $F_{hkl} = f_A + f_B e^{i\phi_{hkl}}$ obtained earlier:

$$F_{hkl} = \sum_j f_j e^{i\phi_{hkl}(j)} \quad \phi_{hkl}(j) = 2\pi(hx_j + ky_j + lz_j) \quad (12)$$

The sum is over all the atoms in the unit cell. The quantity F_{hkl} is called the structure factor, and the intensity of the (hkl) reflection is proportional to $|F_{hkl}|^2$.



21.28 The location of the atoms for the structure factor calculation in Example 21.4. The dark spheres are Na^+ , the light spheres are Cl^- .

Example 21.4 Calculating a structure factor

Calculate the structure factors for the unit cell in Fig. 21.28.

Method The structure factor is given by eqn 12. To use this equation, consider the ions at the locations specified in Fig. 21.28. Write f^+ for the Na^+ scattering factor and f^- for the Cl^- scattering factor. Note that ions in the body of the cell contribute to the scattering with a strength f . However, ions on faces are shared between two cells (use $\frac{1}{2}f$), those on edges by four cells (use $\frac{1}{4}f$), and those at corners by eight cells (use $\frac{1}{8}f$). Two useful relations are

$$e^{i\pi} = -1 \quad \cos \phi = \frac{1}{2}(e^{i\phi} + e^{-i\phi})$$

Answer From eqn 12, and summing over the coordinates of all 27 atoms in the illustration:

$$F_{hkl} = f^+ \left(\frac{1}{8} + \frac{1}{8}e^{2\pi i l} + \dots + \frac{1}{2}e^{2\pi i(\frac{1}{2}h + \frac{1}{2}k + l)} \right) \\ + f^- \left(e^{2\pi i(\frac{1}{2}h + \frac{1}{2}k + \frac{1}{2}l)} + \frac{1}{4}e^{2\pi i(\frac{1}{2}h)} + \dots + \frac{1}{4}e^{2\pi i(\frac{1}{2}h + l)} \right)$$

To simplify this 27-term expression, we use

$$e^{2\pi i h} = e^{2\pi i k} = e^{2\pi i l} = 1$$

because h , k , and l are all integers:

$$F_{hkl} = f^+ \{ 1 + \cos(h+k)\pi + \cos(h+l)\pi + \cos(k+l)\pi \} \\ + f^- \{ (-1)^{h+k+l} + \cos k\pi + \cos l\pi + \cos h\pi \}$$

Then, because $\cos h\pi = (-1)^h$,

$$F_{hkl} = f^+ \{ 1 + (-1)^{h+k} + (-1)^{h+l} + (-1)^{l+k} \} \\ + f^- \{ (-1)^{h+k+l} + (-1)^h + (-1)^k + (-1)^l \}$$

Now note that:

$$\text{if } h, k, \text{ and } l \text{ are all even, } F_{hkl} = f^+ \{ 1 + 1 + 1 + 1 \} \\ + f^- \{ 1 + 1 + 1 + 1 \} = 4(f^+ + f^-)$$

$$\text{if } h, k, \text{ and } l \text{ are all odd, } F_{hkl} = 4(f^+ - f^-)$$

$$\text{if one index is odd and two are even, or vice versa, } F_{hkl} = 0$$

Comment The hkl all-odd reflections are less intense than the hkl all-even.

Self-test 21.4 Deduce the rule for the systematic absences of a cubic I lattice.

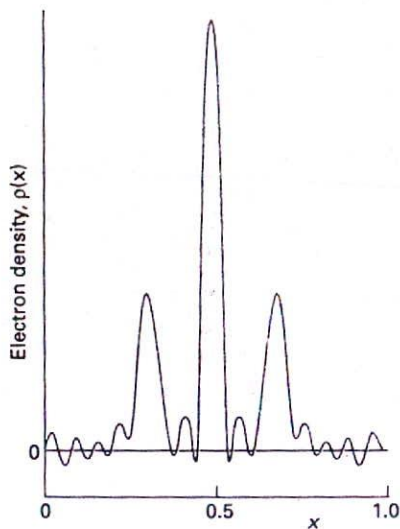
$$[\text{for } h + k + l \text{ odd, } F_{hkl} = 0]$$

(c) The electron density

If we knew all the structure factors F_{hkl} , we could calculate the electron density distribution, $\rho(\mathbf{r})$, in the unit cell by using the expression

$$\rho(\mathbf{r}) = \frac{1}{V} \sum_{hkl} F_{hkl} e^{-2\pi i(hx + ky + lz)} \quad (13)$$

where V is the volume of the unit cell. Equation 13 is called a Fourier synthesis of the electron density.



21.29 The plot of the electron density calculated in Example 21.5.

Example 21.5 Calculating an electron density by Fourier synthesis

Consider the $(h00)$ planes of a crystal extending indefinitely in the x -direction. In an X-ray analysis the structure factors were found as follows:

h :	0	1	2	3	4	5	6	7	8	9
F_h :	16	-10	2	-1	7	-10	8	-3	2	-3
h :	10	11	12	13	14	15				
F_h :	6	-5	3	-2	2	-3				

(and $F_{-h} = F_h$). Construct a plot of the electron density projected on to the x -axis of the unit cell.

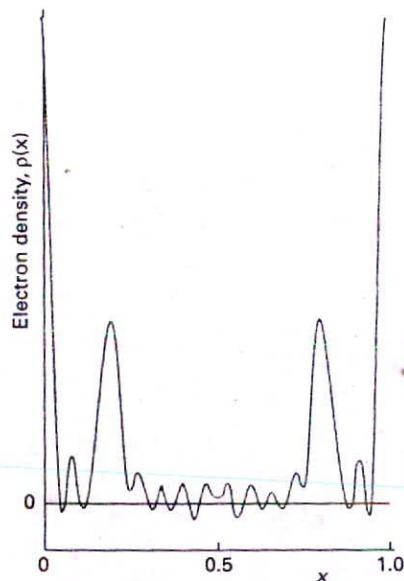
Method Because $F_{-h} = F_h$, it follows from eqn 13 that

$$\begin{aligned} V\rho(x) &= \sum_{h=-\infty}^{\infty} F_h e^{-2\pi i h x} = F_0 + \sum_{h=1}^{\infty} (F_h e^{-2\pi i h x} + F_{-h} e^{2\pi i h x}) \\ &= F_0 + \sum_{h=1}^{\infty} F_h (e^{-2\pi i h x} + e^{2\pi i h x}) = F_0 + 2 \sum_{h=1}^{\infty} F_h \cos(2\pi h x) \end{aligned}$$

and we evaluate the sum (truncated at $h = 15$) for points $0 \leq x \leq 1$ using mathematical software.

Answer The results are plotted in Fig. 21.29.

Comment The positions of three atoms can be discerned very readily. The more terms that are included, the more accurate the density plot. Terms corresponding to high values of h (short-wavelength cosine terms in the sum) account for the finer details of the electron density; low values of h account for the broad features.



21.30 The plot of the electron density calculated in Self-test 21.5. Note how a different choice of phases for the structure factors leads to a markedly different structure.

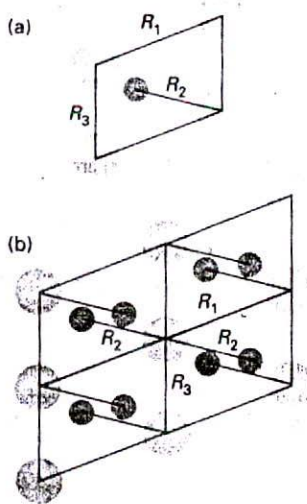
Self-test 21.5 Use mathematical software to experiment with different structure factors (including changing signs as well as amplitudes). For example, use the same values of F_h as above, but with positive signs throughout.

[Fig. 21.30]

(d) The phase problem

From the measured intensities, I_{hkl} , we get the structure factors, F_{hkl} , and then evaluate eqn 13 to find the electron density, $\rho(\mathbf{r})$, throughout the unit cell. Unfortunately, I_{hkl} is proportional to the square modulus $|F_{hkl}|^2$, so we cannot say whether we should use $+|F_{hkl}|$ or $-|F_{hkl}|$ in the sum. In fact, the difficulty is more severe for non-centrosymmetric unit cells because, if we write F_{hkl} as the complex number $|F_{hkl}|e^{i\alpha}$, where α is the phase of F_{hkl} and $|F_{hkl}|$ is its magnitude, the intensity lets us determine $|F_{hkl}|$ but tells us nothing of its phase, which may lie anywhere from 0 to 2π . This ambiguity is called the **phase problem**; its consequences are illustrated by comparing Figs. 21.29 and 21.30. Some way must be found to assign phases to the structure factors, for otherwise the sum for ρ could not be evaluated and the method would be useless.

The phase problem can be overcome to some extent by a variety of methods. One procedure that is widely used for inorganic materials with a reasonably small number of atoms in a unit cell and for organic molecules with a small number of heavy atoms, is the **Patterson synthesis**. Instead of the structure factors F_{hkl} , the values of $|F_{hkl}|^2$, which can be



21.31 The Patterson synthesis corresponding to the pattern in (a) is the pattern in (b). The distance and orientation of each spot from the origin gives the orientation and separation of one atom-atom separation in (a). Some of the typical distances and their contribution to (b) are shown as R_1 , etc.

obtained without ambiguity from the intensities, are used in an expression that resembles eqn 13:

$$P(\mathbf{r}) = \frac{1}{V} \sum_{hkl} |F_{hkl}|^2 e^{-2\pi i(hx+ky+lz)} \quad (14)$$

The outcome of a Patterson synthesis is a map of the *vector separations* of the atoms (the distances and directions between atoms) in the unit cell. Thus, if atom A is at the coordinates (x_A, y_A, z_A) and atom B is at (x_B, y_B, z_B) , then there will be a peak at $(x_A - x_B, y_A - y_B, z_A - z_B)$ in the Patterson map. There will also be a peak at the negative of these coordinates, because there is a vector from B to A as well as a vector from A to B. The height of the peak in the map is proportional to the product of the atomic numbers of the two atoms, $Z_A Z_B$. For example, if the unit cell has the structure shown in Fig. 21.31a, the Patterson synthesis would be the map shown in Fig. 21.31b, where the location of each spot relative to the origin gives the separation and relative orientation of each pair of atoms in the original structure.

If some atoms are heavy, they dominate the scattering (because their scattering factors are large, of the order of their atomic number) and their locations may be deduced quite readily. The sign of F_{hkl} can now be calculated from the locations of the heavy atoms in the unit cell, and to a high probability the phase calculated for them will be the same as the phase for the entire unit cell. To see why this is so, we have to note that a structure factor of a centrosymmetric cell has the form

$$F = (\pm)f_{\text{heavy}} + (\pm)f_{\text{light}} + (\pm)f_{\text{light}} + \dots \quad (15)$$

where f_{heavy} is the scattering factor of the heavy atom and f_{light} the scattering factors of the light atoms. (An expression of this form, but for atoms of similar atomic number, was derived in Example 21.4.) The f_{light} are all much smaller than f_{heavy} , and their phases are more or less random if the atoms are distributed throughout the unit cell. Therefore, the net effect of the f_{light} is to change F only slightly from f_{heavy} , and we can be reasonably confident that F will have the same sign as that calculated from the location of the heavy atom. This phase can then be combined with the observed $|F|$ (from the reflection intensity) to perform a Fourier synthesis of the full electron density in the unit cell, and hence to locate the light atoms as well as the heavy atoms.

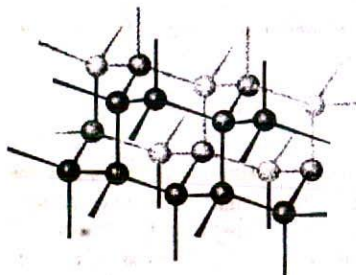
Modern structural analyses make extensive use of direct methods. Direct methods are based on the possibility of treating the atoms in a unit cell as being virtually randomly distributed (from the radiation's point of view), and then to use statistical techniques to compute the probabilities that the phases have a particular value. It is possible to deduce relations between some structure factors and sums (and sums of squares) of others, which have the effect of constraining the phases to particular values (with high probability, so long as the structure factors are large). For example, the Sayre probability relation has the form

$$\text{sign of } F_{h+H, k+K, l+L} \text{ is probably equal to } (\text{sign of } F_{hkl}) \times (\text{sign of } F_{HKL}) \quad (16)$$

For example, if F_{122} and F_{232} are both large and negative, then it is highly likely that F_{354} , provided it is large, will be positive.

(e) Structure refinement

In the final stages of the determination of a crystal structure, the parameters describing the structure (atom positions, for instance) are adjusted systematically to give the best fit between the observed intensities and those calculated from the model of the structure deduced from the diffraction pattern. This process is called **structure refinement**. Not only does the procedure give accurate positions for all the atoms in the unit cell, but it also gives



21.32 A fragment of the structure of diamond. Each C atom is tetrahedrally bonded to four neighbours. This framework-like structure results in a rigid crystal with a high thermal conductivity.

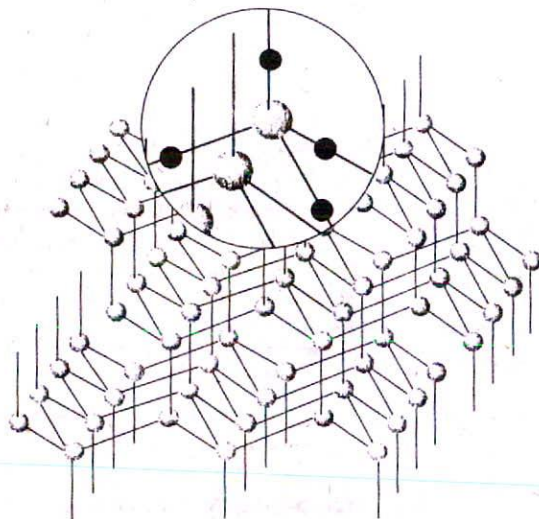
an estimate of the errors in those positions and in the bond lengths and angles derived from them. The procedure also provides information on the vibrational amplitudes of the atoms.

Information from X-ray analysis

The bonding within a solid may be of various kinds. Simplest of all (in principle) are metals, where electrons are delocalized over arrays of identical cations and bind them together into a rigid but ductile and malleable whole. In many cases the crystal structures of metals can be rationalized in terms of a model in which spherical metal cations pack together into an orderly array. In an ionic solid, both cations and anions are packed together.

In covalent solids, covalent bonds in a definite spatial orientation link the atoms in a network extending through the crystal. The demands of directional bonding, which have only a small effect on the structures of many metals, now override the geometrical problem of packing spheres together, and elaborate and extensive structures may be formed. A famous example of a covalent solid is diamond (Fig. 21.32), in which each sp^3 -hybridized C atom is bonded tetrahedrally to its four neighbours.

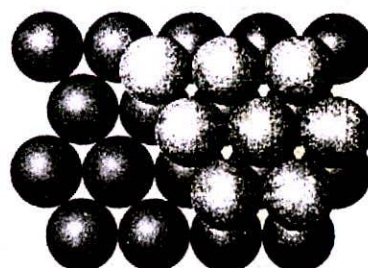
Molecular solids, which are the subject of the overwhelming majority of modern structural determinations, are bonded together by van der Waals interactions (Chapter 22). The observed crystal structure is nature's solution to the problem of condensing objects of various shapes into an aggregate of minimum energy (actually, for temperatures above zero, of minimum Gibbs energy). The prediction of the structure is a very difficult task, and rarely possible. The problem is made more complicated by the role of hydrogen bonds, which in some cases dominate the crystal structure, as in ice (Fig. 21.33), but in others (for example, phenol) distort a structure that is determined largely by the van der Waals interactions. X-ray diffraction studies of molecular compounds reveal a huge amount of information, including interatomic distances, bond angles, the stereochemistry of the molecules, and vibrational parameters.



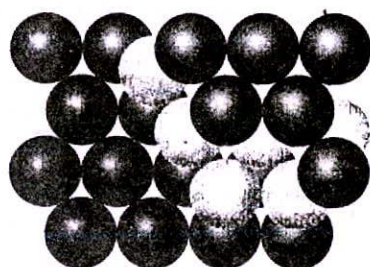
21.33 A fragment of the crystal structure of ice (ice-I). Each O atom is at the centre of a tetrahedron of four O atoms at a distance of 276 pm. The central O atom is attached by two short O-H bonds to two H atoms and by two long hydrogen bonds to the H atoms of two of the neighbouring molecules. Overall, the structure consists of planes of hexagonal puckered rings of H_2O molecules (like the chair form of cyclohexane).



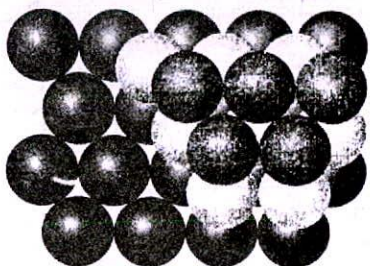
21.34 The first layer of close-packed spheres used to build a three-dimensional close-packed structure.



21.35 The second layer of close-packed spheres occupies the dips of the first layer. The two layers are the AB component of the close-packed structure.



(a)



(b)

21.36 (a) The third layer of close-packed spheres might occupy the dips lying directly above the spheres in the first layer, resulting in an ABA structure, which corresponds to hexagonal close-packing. (b) Alternatively, the third layer might lie in the dips that are not above the spheres in the first layer, resulting in an ABC structure, which corresponds to cubic close-packing.

21.6 The packing of identical spheres: metal crystals

Most metallic elements crystallize in one of three simple forms, two of which can be explained in terms of rigid spheres packing together in the closest possible arrangement.

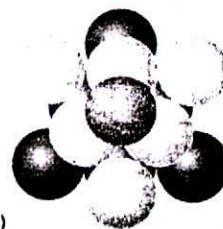
(a) Close packing

A close-packed layer of identical spheres, one with maximum utilization of space, is shown in Fig. 21.34. A close-packed three-dimensional structure can be envisaged as formed by stacking such close-packed layers on top of one another. However, this stacking can be done in different ways and can result in close-packed polytypes, or structures that are identical in two dimensions (the close-packed layers) but differ in the third dimension.

In all polytypes, the spheres of the second close-packed layer lie in the depressions of the first layer (Fig. 21.35). The third layer may be added in either of two ways. In one, the spheres are placed so that they reproduce the first layer (Fig. 21.36a), to give an ABA pattern of layers. Alternatively, the spheres may be placed over the gaps in the first layer (Fig. 21.36b), so giving an ABC pattern. Two polytypes are formed if the two stacking patterns are repeated in the vertical direction. If the ABA pattern is repeated, to give the sequence of layers ABABAB..., the spheres are hexagonally close-packed (hcp). Alternatively, if the ABC pattern is repeated, to give the sequence ABCABC..., the spheres are cubic close-packed (ccp). The origins of these names can be seen by referring to Fig. 21.37. The ccp structure gives rise to face-centred unit cells, so may also be denoted cubic F (or fcc, for

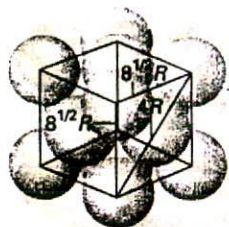


(a)

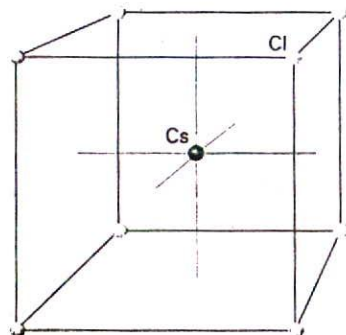


(b)

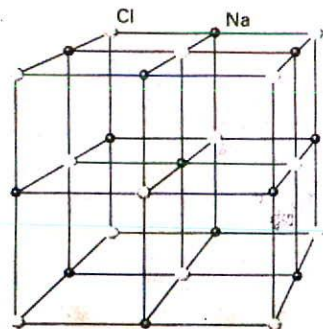
21.37 A fragment of the structure shown in Fig. 21.36 revealing the (a) hexagonal (b) cubic symmetry. The tints on the spheres are the same as for the layers in Fig. 21.36.



21.38 The calculation of the packing fraction of a ccp unit cell.



21.39 The caesium-chloride structure consists of two interpenetrating simple cubic arrays of ions, one of cations and the other of anions, so that each cube of ions of one kind has a counter-ion at its centre.



21.40 The rock-salt (NaCl) structure consists of two mutually interpenetrating slightly expanded face-centred cubic arrays of ions. The entire assembly shown here is the unit cell.

Table 21.2 The crystal structures of some elements

Structure	Element
hcp*	Be, Cd, Co, He, Mg, Sc, Ti, Zn
fcc* (ccp, cubic F)	Ag, Al, Ar, Au, Ca, Cu, Kr, Ne, Ni, Pd, Pb, Pt, Rh, Rn, Sr, Xe
bcc (cubic I)	Ba, Cs, Cr, Fe, K, Li, Mn, Mo, Rb, Na, Ta, W, V
cubic P	Po

*Close-packed structures.

face-centred cubic). It is also possible to have ABCABAB... structures and even random sequences; however, the hcp and ccp polytypes are the most important. Some elements possessing these structures are listed in Table 21.2.

The compactness of close-packed structures is indicated by their **coordination number**, the number of atoms immediately surrounding any selected atom, which is 12 in all cases. Another measure of their compactness is the **packing fraction**, the fraction of space occupied by the spheres, which is 0.740 (see the *Justification* below). That is, in a close-packed solid of identical spheres, only 26.0 per cent of the volume is empty space. The fact that many metals are close-packed accounts for their high densities.

Justification 21.3

To calculate a packing fraction of a ccp structure, we first calculate the volume of a unit cell, and then calculate the total volume of the spheres that fully or partially occupy it. The first part of the calculation is a straightforward exercise in geometry. The second part involves counting the fraction of spheres that occupy the cell.

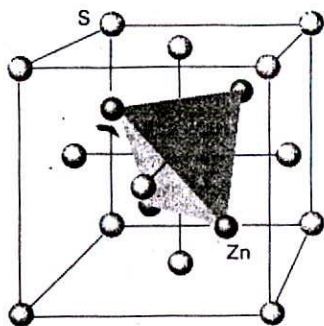
Refer to Fig. 21.38. Because a diagonal of any face passes completely through one sphere and half way through two other spheres, its length is $4R$. The length of a side is therefore $8^{1/2}R$ and the volume of the unit cell is $8^{3/2}R^3$. Because each cell contains the equivalent of $6 \times \frac{1}{2} + 8 \times \frac{1}{8} = 4$ spheres, and the volume of each sphere is $\frac{4}{3}\pi R^3$, the total occupied volume is $\frac{16}{3}\pi R^3$. The fraction of space occupied is therefore $\frac{16}{3}\pi R^3 / 8^{3/2}R^3 = 16\pi / 8^{3/2}3$, or 0.740. Because an hcp structure has the same coordination number, its packing fraction is the same. The packing fractions of structures that are not close-packed are calculated similarly (see Problem 21.13).

(b) Less closely packed structures

As shown in Table 21.2, a number of common metals adopt structures that are less than close-packed. The departure from close packing suggests that specific covalent bonding between neighbouring atoms is beginning to influence the structure and impose a specific geometrical arrangement. One such arrangement results in a cubic I (bcc, for body-centred cubic) structure, with one sphere at the centre of a cube formed by eight others. The coordination number of a bcc structure is only 8, but there are six more atoms not much further away than the eight nearest neighbours. The packing fraction of 0.68 is not much smaller than the value for a close-packed structure (0.74), and shows that about two-thirds of the available space is actually occupied.

21.7 Ionic crystals

When crystals of compounds of monatomic ions are modelled by stacks of spheres it is essential to allow for the different ionic radii (typically with the cations smaller than the anions) and different charges. The coordination number of an ion is the number of nearest



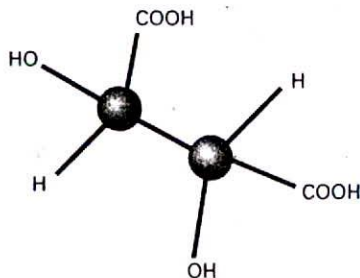
21.41 The structure of the spherulite form of ZnS showing the location of the Zn atoms in the tetrahedral holes formed by the array of S atoms. (There is an S atom at the centre of the cube inside the tetrahedron of Zn atoms.)

Table 21.3* Ionic radii, R/pm

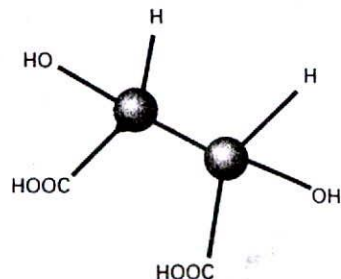
Na^+	102(6†), 116(8)
K^+	138(6), 151(8)
F^-	128(2), 131(4)
Cl^-	181 (close packing)

* More values are given in the *Data* section at the end of this volume.

† Coordination number.



1 D(+)-Tartaric acid



2 L(-)-Tartaric acid

neighbours of opposite charge; the structure itself is characterized as having (n_+, n_-) coordination, where n_+ is the coordination number of the cation and n_- that of the anion.

Even if, by chance, the ions have the same size, the problems of ensuring that the unit cells are electrically neutral make it impossible to achieve 12-coordinate close-packed structures. As a result, ionic solids are generally less dense than metals. The best packing that can be achieved is the (8, 8)-coordinate caesium-chloride structure in which each cation is surrounded by eight anions and each anion is surrounded by eight cations (Fig. 21.39). In this structure, an ion of one charge occupies the centre of a cubic unit cell with eight counter-ions at its corners. The structure is adopted by CsCl itself and also by CaS, CsCN (with some distortion), and CuZn.

When the radii of the ions differ more than in CsCl, even eight-coordinate packing cannot be achieved. One common structure adopted is the (6, 6)-coordinate rock-salt structure typified by NaCl (Fig. 21.40). In this structure, each cation is surrounded by six anions and each anion is surrounded by six cations. The rock-salt structure can be pictured as consisting of two interpenetrating slightly expanded cubic F (fcc) arrays, one of cations and the other of anions. This structure is adopted by NaCl itself and also by several other MX compounds, including KBr, AgCl, MgO, and ScN.

The switch from the caesium-chloride structure to the rock-salt structure occurs (sometimes) in accord with the radius-ratio rule, which is based on the value of the radius ratio, γ :

$$\gamma = \frac{r_{\text{smaller}}}{r_{\text{larger}}} \quad [17]$$

The two radii are those of the larger and smaller ions in the crystal. The radius-ratio rule is derived by considering the geometrical problem of packing the maximum number of hard spheres of one radius around a hard sphere of a different radius. The rule states that the caesium-chloride structure should be expected when

$$\gamma > 3^{1/2} - 1 = 0.732$$

and that the rock-salt structure should be expected when

$$2^{1/2} - 1 = 0.414 < \gamma < 0.732$$

For $\gamma < 0.414$, the most efficient packing leads to four-coordination of the type exhibited by the spherulite (or zinc blende) form of ZnS (Fig. 21.41). The deviation of a structure from that expected on the basis of the radius-ratio rule is often taken to be an indication of a shift from ionic towards covalent bonding; however, a major source of unreliability is the arbitrariness of ionic radii and their variation with coordination number.

Ionic radii are derived from the internuclear distance between adjacent ions in a crystal. However, we need to apportion the total distance between the two ions by defining the radius of one ion and then inferring the radius of the other ion. One scale that is widely used is based on the value 140 pm for the radius of the O^{2-} ion (Table 21.3). Other scales are also available (such as one based on F^- for discussing halides), and it is essential not to mix values from different scales. Because ionic radii are so arbitrary, predictions based on them must be viewed cautiously.

21.8 Absolute configurations

Although it has long been possible to separate enantiomers (mirror-image chiral isomers, Section 15.3b), it was not until X-ray diffraction techniques were developed that the absolute stereochemical configuration of an isomer could be determined. We now know, for example, that D-tartaric acid (1) is the isomer responsible for rotating light clockwise (that is, it is the (+) isomer), and that L-tartaric acid (2) is the (–) isomer. The X-ray method is not

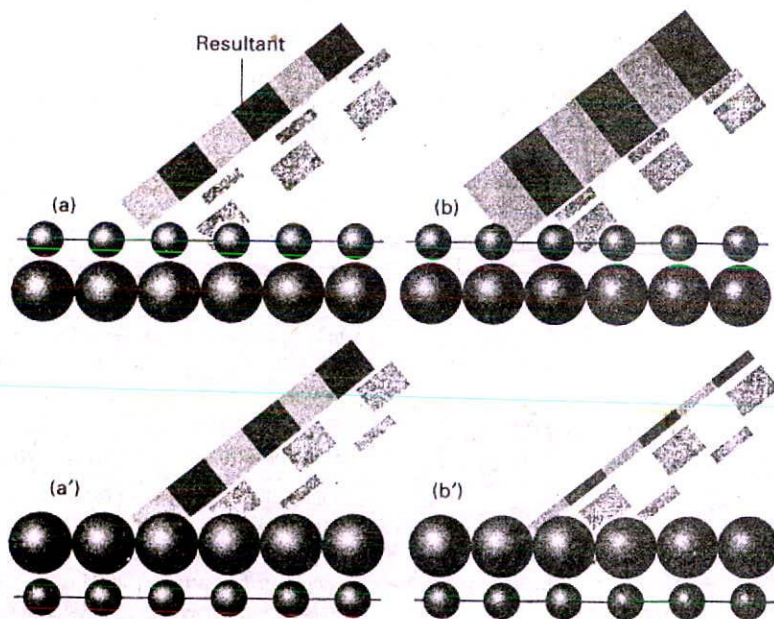
trivial, because enantiomers give almost identical diffraction patterns. The information about the absolute configuration is contained in small differences in diffraction intensities and is based on a technique developed by J.M. Bijvoet.

Consider first the diagrams in Fig. 21.42, which represent an idealized crystal and its mirror image. This model resembles the arrangement of Zn and S atoms in zinc blende, which was the first absolute configuration to be determined. The technique we are about to describe was used to show that the shiny (111) faces of the crystal have S atoms on the surface whereas the dull (111) faces have Zn atoms on the surface (Fig. 21.43). Each plane of atoms gives rise to a scattered wave, and their superpositions are shown on the left of Fig. 21.42. Note that the two superpositions have the same amplitude but differ in phase. The diffraction pattern therefore has the same intensity for each enantiomer and, at this stage, cannot be used to distinguish them.

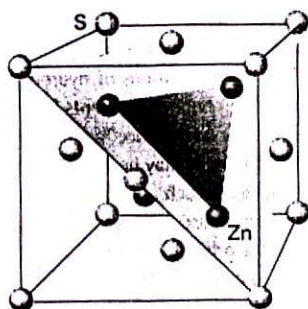
The essence of the method is to use X-rays that are close to an absorption frequency of one species of atom in the sample. In the examination of ZnS, for instance, gold L_{α} radiation (127.6 pm) was used, which is close to the beginning of a zinc absorption band (which commences at 128.3 pm). In Bijvoet's development of this approach for a study of tartaric acid, a Rb atom is incorporated into the compound (he used sodium rubidium tartrate) with X-rays from a zirconium target. Atoms with absorptions close to the X-ray frequency introduce an extra phase shift in the scattered X-ray. A simple way to picture the additional phase shift is to imagine the X-rays as exciting the atom before being re-emitted, and being delayed in the process. The effect is called **anomalous scattering**.

Suppose the layer marked A in the crystal contains the anomalous scatterers; then the scattered waves are as shown on the right of Fig. 21.42. The essential point is that the superpositions now differ slightly in amplitude, not only phase, so the diffracted intensities are slightly different in each case. Therefore, the enantiomers can in fact be distinguished because the scattering intensities differ.

Modern diffractometers are so sensitive that the incorporation of a heavy atom is no longer strictly necessary. It is now possible to detect the small intensity variations arising from the light atoms normally present. However, the procedure is much easier and more



21.42 The two versions (top and bottom) of the two layers of atoms represent enantiomers. The interference between their scattered waves results in composite waves that differ in phase (a and a'), but the absolute phase cannot be determined, and the intensities of the reflections are identical. If, however, the atoms represented by the larger spheres modify the phase of the waves they scatter, then the resultant superpositions differ in amplitude as well as phase (b and b'), the reflections have different intensities, and the absolute configuration can be established. The green bands represent the waves scattered by the layers, with alternating positive and negative regions shown as light and dark. The width of a band indicates its intensity. The resultant in each instance is indicated by the grey band.



21.43 The (111) faces of the sphalerite crystal have either S atoms above Zn atoms or, as shown here, Zn atoms above S atoms.

reliable if some moderately heavy atoms (such as S or Cl) are present. Anomalous scattering depends strongly on the wavelength of the X-radiation. Thus, atoms lighter than S and Cl give little effect for Mo K_α radiation, and until recently Cu K_α radiation had to be used.

Neutron and electron diffraction

A neutron generated in a reactor and slowed to thermal velocities by repeated collisions with a moderator (such as graphite) until it is travelling at about 4 km s^{-1} has a wavelength of about 100 pm. Because 100 pm is comparable to X-ray wavelengths, similar diffraction phenomena can be expected. In practice, a range of wavelengths occurs in a neutron beam, but a monochromatic beam can be selected by diffraction from a germanium crystal.

Electrons can be accelerated to precisely controlled energies by a known potential difference. When accelerated from rest through 10 keV they acquire a wavelength of 12 pm, which makes them suitable for structural studies too.

Example 21.6 Calculating the typical wavelength of thermal neutrons

Calculate the typical wavelength of neutrons that have reached thermal equilibrium with their surroundings at 100°C .

Method We need to relate the wavelength to the temperature. There are two linking steps. First, the de Broglie relation expresses the wavelength in terms of the linear momentum. Then the linear momentum can be expressed in terms of the kinetic energy, the mean value of which is given in terms of the temperature by the equipartition theorem (see the Introduction and Section 20.3).

Answer The de Broglie relation states that $\lambda = h/p$. Then, from the equipartition theorem we know that the mean translational kinetic energy of a neutron at a temperature T travelling in the x -direction is $E_K = \frac{1}{2}kT$. The kinetic energy is also equal to $p^2/2m$, where p is the momentum of the neutron and m is its mass. Hence, $p = (mkT)^{1/2}$. It follows that the neutron's wavelength is

$$\lambda = \frac{h}{(mkT)^{1/2}}$$

Therefore, at 100°C ,

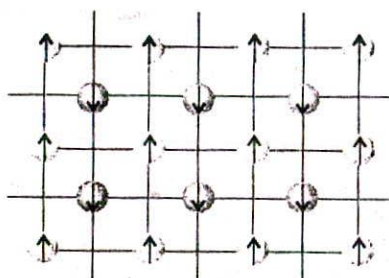
$$\lambda = \frac{6.626 \times 10^{-34} \text{ J s}}{\{(1.675 \times 10^{-27} \text{ kg}) \times (1.381 \times 10^{-23} \text{ JK}^{-1}) \times (373 \text{ K})\}^{1/2}} = 226 \text{ pm}$$

Self-test 21.6 Calculate the temperature needed for the average wavelength of the neutrons to be 100 pm.

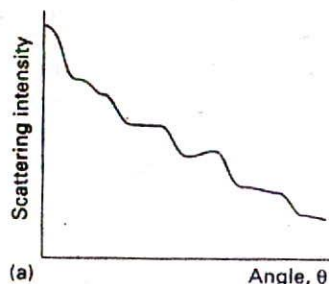
[$1.6 \times 10^3 \text{ }^\circ\text{C}$]

21.9 Neutron diffraction

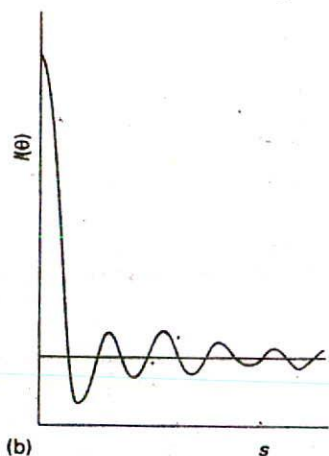
The scattering of X-rays is caused by the oscillations an incoming electromagnetic wave generates in the electrons of atoms. In contrast, the scattering of neutrons is a nuclear phenomenon. Neutrons pass through the electronic structures of atoms and interact with the nuclei through the strong nuclear force that is responsible for binding nucleons together. As a result, the intensity with which neutrons are scattered is independent of the number of electrons. Whereas X-ray scattering factors increase strongly with atomic



21.44 If the spins of atoms at lattice points are orderly, as in this antiferromagnetic material, where the spins of one set of atoms are aligned antiparallel to those of the other set, neutron diffraction detects two interpenetrating simple cubic lattices on account of the magnetic interaction of the neutron with the atoms, but X-ray diffraction would see only a single bcc lattice.



(a)



(b)

21.45 (a) The scattering intensity consists of a smoothly varying background with undulations superimposed. (b) The undulations are emphasized if a sector is rotated in front of the screen, and then the densitometer trace taken from the photograph plotted against $s = (4\pi/\lambda) \sin \frac{1}{2}\theta$.

number, neutron scattering factors vary much less strongly; nor do they vary with angle. As a result, in contrast to X-rays, neutron diffraction is not dominated by the heavy atoms present in a molecule. Neutron diffraction therefore shows up the positions of hydrogen nuclei much more clearly than X-rays do. Similarly, although neighbouring elements in the periodic table have almost identical X-ray scattering factors, and hence are almost indistinguishable in X-ray diffraction, their neutron scattering lengths may be significantly different. As a result, it is possible to distinguish atoms of elements such as Ni and Co that are present in the same compound and to study order-disorder phase transitions in FeCo.

The difference in sensitivity to hydrogen nuclei can have a pronounced effect on the measurement of C-H bond lengths. Because X-rays respond to accumulations of electrons, the weak peaks in an X-ray diffraction map represent the locations of the bulk of the electron density in the bonds, and this density may be shifted towards the C atom. For example, X-ray measurements on sucrose give $R(\text{C-H}) = 96 \text{ pm}$; neutron measurements, which respond to the location of the nuclei, give $R(\text{C-H}) = 109.5 \text{ pm}$. The O-H bond lengths in sucrose show similar differences, being 79 pm by X-rays but 97 pm by neutrons.

Another property of neutrons that distinguishes them from X-ray photons is their possession of a magnetic moment due to their spin. This magnetic moment can couple to the magnetic fields of ions in a crystal (if the ions have unpaired electrons) and modify the diffraction pattern. A simple example of this magnetic scattering is provided by metallic chromium. The lattice is cubic I (bcc), and the diffraction pattern using X-rays has systematic absences. These absences are not observed when neutrons are used, because the structure is such that atoms at the body-centre location have magnetic moments opposite to those at the corners, and the structure is better regarded as consisting of two interpenetrating arrays of magnetically different Cr atoms (Fig. 21.44). Therefore, although the atoms are identical as far as X-rays are concerned, they are different from the viewpoint of neutrons, and diffraction intensity is observed at the predicted systematic X-ray absences. Neutron diffraction is especially important for investigating these magnetically ordered lattices.

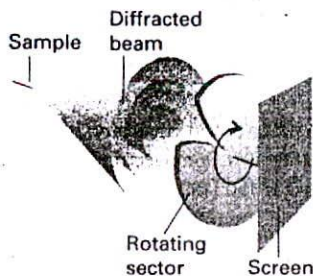
21.10 Electron diffraction

Electrons are scattered strongly by their interaction with the charges of electrons and nuclei, and so until recently could not be used to study the interiors of solid samples. However, they have been used for some time to study molecules in the gas phase, on surfaces, and in thin films. The application to surfaces, which is called 'low-energy electron diffraction' (LEED), is a major use of the technique and is discussed in Section 28.2e. Recent developments have extended electron diffraction techniques to solids, where they have certain advantages over X-ray diffraction. For instance, they are applicable to very small samples, and so may be used when single-crystal X-ray diffraction is impractical or powder diffraction too complex to interpret (see *Further reading*). A sample size of about 10^4 unit cells can be used for electron diffraction studies on solids, which is several million times smaller than for X-ray crystallography, even using synchrotron radiation.

In a typical gas-phase electron diffraction apparatus, electrons are emitted from a hot filament and are then accelerated through a potential gradient. They then pass through the stream of gas, and on to a fluorescent screen. The wavelength of electrons accelerated from rest through a potential difference \mathcal{V} is

$$\lambda = \frac{h}{(2m_e e \mathcal{V})^{1/2}} \quad (18)$$

(see Example 11.2). For an accelerating potential difference of 40 kV, the wavelength is 6.1 pm.



21.46 The layout of an electron diffraction apparatus. The diffraction pattern is photographed from the fluorescent screen. A rotating heart-shaped sector emphasizes the scattering from the nuclear positions and suppresses the smoothly varying background due to scattering from the continuous electron distribution in the molecules.

The gaseous sample presents all possible orientations of atom-atom separations to the electron beam. The resulting diffraction pattern consists of a series of concentric undulations on a background with an intensity that decreases steadily with increasing scattering angle (Fig. 21.45). The undulations are due to the molecular scattering, the sharply defined scattering from the nuclear positions. The background is due largely to the atomic scattering. One way of levelling the total intensity and hence to emphasize the undulations is to insert a rotating heart-shaped disk in front of the screen (Fig. 21.46).

The scattering from a pair of nuclei separated by a distance R_{ij} and orientated at a definite angle to the incident beam can be calculated. The overall diffraction pattern is then calculated by allowing for all possible orientations of this pair of atoms. When the molecule consists of a number of atoms, we sum over the contribution from all pairs, and find that the total intensity has an angular variation given by the Wierl equation:

$$I(\theta) = \sum_{i,j} f_i f_j \frac{\sin sR_{ij}}{sR_{ij}} \quad s = \frac{4\pi}{\lambda} \sin \frac{1}{2}\theta \quad (19)$$

where λ is the wavelength of the electrons in the beam and θ is the scattering angle. The electron scattering factor, f , is a measure of the intensity of the electron scattering powers of the atoms.

The electron diffraction pattern gives the distances between all possible pairs of atoms in the molecule (not just to those bonded together). When there are only a few atoms, the peaks can be analysed reasonably quickly, and the analysis proceeds by assuming a geometry and calculating the intensity pattern by using the Wierl equation. The best fit is then taken as the actual molecular geometry.

Checklist of key ideas

- diffraction
- diffraction pattern

Crystal structure

21.1 Lattices and unit cells

- space lattice
- crystal structure
- unit cell
- primitive unit cell
- crystal system
- essential symmetry
- Bravais lattice
- body-centred unit cell
- face-centred unit cell
- side-centred unit cell

21.2 The identification of lattice planes

- Miller indices

X-ray diffraction

- Bremsstrahlung

21.3 Bragg's law

- X-ray reflection
- glancing angle
- Bragg's law (5)

21.4 The powder method

- indexing
- scattering factor
- systematic absence

21.5 Single-crystal X-ray diffraction

- four-circle diffractometer
- structure factor
- Fourier synthesis (13)
- phase problem
- Patterson synthesis (14)
- direct methods

- Sayre probability relation (16)

- structure refinement

Information from X-ray analysis

- metal
- ionic solid
- covalent solid
- molecular solid

21.6 The packing of identical spheres: metal crystals

- close-packed
- polytype
- hexagonal close-packed (hcp)
- cubic close-packed (ccp)
- coordination number
- packing fraction

21.7 Ionic crystals

- coordination number (of ionic lattice)
- caesium-chloride structure
- rock-salt structure
- radius-ratio rule

21.8 Absolute configurations

- anomalous scattering

Neutron and electron diffraction

21.9 Neutron diffraction

- magnetic scattering

21.10 Electron diffraction

- molecular scattering,
- atomic scattering
- Wierl equation (19)
- electron scattering factor

Further reading

Articles of general interest

- J.P. Glusker, Teaching crystallography to noncrystallographers. *J. Chem. Educ.* **65**, 474 (1988).
- J.H. Enemark, Introducing chemists to X-ray structure determination. *J. Chem. Educ.* **65**, 491 (1988).
- Crystallographic resource list. *J. Chem. Educ.* **65**, 512 (1988).
- C.G. Pope, X-ray diffraction and the Bragg equation. *J. Chem. Educ.* **74**, 129 (1997).
- J.P. Chesick, Fourier transforms in chemistry. Part III. X-ray crystal structure analysis. *J. Chem. Educ.* **66**, 413 (1989).
- T. Li and J.H. Worrell, Construction of the seven basic crystallographic units. *J. Chem. Educ.* **66**, 73 (1989).
- S.F.A. Kettle and L.J. Norrby, Really, your lattices are all primitive, Mr. Bravais! *J. Chem. Educ.* **70**, 959 (1993).
- J.P. Birk and P.R. Coffman, Finding the face-centred cube in the cubic close-packed structure. *J. Chem. Educ.* **69**, 953 (1992).
- J. Toofan, A simple expression between critical radius ratio and coordination number. *J. Chem. Educ.* **71**, 147 (1994).
- S.R. Elliott, Structure of amorphous materials. In *Encyclopedia of applied physics* (ed. G.L. Trigg), **1**, 559. VCH, New York (1991).
- A.I. Goldman, Crystalline state. In *Encyclopedia of applied physics* (ed. G.L. Trigg), **4**, 365. VCH, New York (1992).
- W.B. Pearson and C. Chieh, Crystallography. In *Encyclopedia of applied physics* (ed. G.L. Trigg), **4**, 385. VCH, New York (1992).
- E. Schönherr, Crystal growth. In *Encyclopedia of applied physics* (ed. G.L. Trigg), **4**, 335. VCH, New York (1992).
- T. Vogt, Neutron diffraction. In *Encyclopedia of applied physics* (ed. G.L. Trigg), **11**, 339. VCH, New York (1994).
- F. Ebrahimi and M.J. Kaufman, Structure of metals and alloys. In *Encyclopedia of applied physics* (ed. G.L. Trigg), **10**, 199. VCH, New York (1994).
- R.M. Hanson and S.A. Bergman, Data-driven chemistry: building models of molecular structure (literally) from electron diffraction data. *J. Chem. Educ.* **71**, 150 (1994).
- J.M. Cowley, Electron diffraction. In *Encyclopedia of applied physics* (ed. G.L. Trigg), **5**, 405. VCH, New York (1993).

Texts and sources of data and information

- M.F.C. Ladd and R.A. Palmer, *Structure determination by X-ray crystallography*. Plenum, New York (1985).
- J.P. Glusker and K.N. Trueblood, *Crystal structure analysis*. Oxford University Press (1985).
- E.A.V. Ebsworth, D.W.H. Rankin, and S. Craddock, *Structural methods in inorganic chemistry*. Blackwell Scientific, Oxford (1991).
- R. Drago, *Physical methods for chemists*. Saunders, Philadelphia (1992).
- C. Giacovazzo (ed.), *Fundamentals of crystallography*. Oxford University Press (1992).
- A.F. Wells, *Structural inorganic chemistry*. Clarendon Press, Oxford (1984).
- R.W.G. Wyckoff, *Crystal structure* (five sections, and supplements). Wiley-Interscience, New York (1959).
- I. Hargittai and M. Hargittai (ed.), *Stereochemical applications of gas-phase electron diffraction*. VCH, Weinheim (1988).
- J.M. Cowley, *Electron diffraction techniques*. Oxford University Press (1992).
- C. Hammond, *The basics of crystallography and diffraction*. Oxford University Press (1997).

Exercises

- 21.1 (a)** Equivalent lattice points within the unit cell of a Bravais lattice have identical surroundings. What points within a face-centred cubic unit cell are equivalent to the point $(\frac{1}{2}, 0, 0)$?
- 21.1 (b)** Equivalent lattice points within the unit cell of a Bravais lattice have identical surroundings. What points within a body-centred cubic unit cell are equivalent to the point $(\frac{1}{2}, 0, \frac{1}{2})$?
- 21.2 (a)** Find the Miller indices of the planes that intersect the crystallographic axes at the distances $(2a, 3b, 2c)$ and $(2a, 2b, \infty c)$.
- 21.2 (b)** Find the Miller indices of the planes that intersect the crystallographic axes at the distances $(1a, 3b, -c)$ and $(2a, 3b, 4c)$.
- 21.3 (a)** Calculate the separations of the planes (111) , (211) , and (100) in a crystal in which the cubic unit cell has side 432 pm .
- 21.3 (b)** Calculate the separations of the planes (121) , (221) , and (244) in a crystal in which the cubic unit cell has side 523 pm .

21.4 (a) The glancing angle of a Bragg reflection from a set of crystal planes separated by 99.3 pm is 20.85°. Calculate the wavelength of the X-rays.

21.4 (b) The glancing angle of a Bragg reflection from a set of crystal planes separated by 128.2 pm is 19.76°. Calculate the wavelength of the X-rays.

21.5 (a) What are the values of 2θ of the first three diffraction lines of bcc iron (atomic radius 126 pm), when the X-ray wavelength is 58 pm?

21.5 (b) What are the values of 2θ of the first three diffraction lines of fcc (gold atomic radius 144 pm) when the X-ray wavelength is 154 pm?

21.6 (a) Copper K_α radiation consists of two components of wavelengths 154.433 pm and 154.051 pm. Calculate the separation of the diffraction lines arising from the two components in a powder diffraction pattern recorded in a circular camera of radius 5.74 cm (with the sample at the centre) from planes of separation 77.8 pm.

21.6 (b) A synchrotron source produces X-radiation at a range of wavelengths. Consider two components of wavelengths 95.401 and 96.035 pm. Calculate the separation of the diffraction lines arising from the two components in a powder diffraction pattern recorded in a circular camera of radius 5.74 cm (with the sample at the centre) from planes of separation 82.3 pm.

21.7 (a) The compound Rb_3TlF_6 has a tetragonal unit cell with dimensions $a = 651$ pm and $c = 934$ pm. Calculate the volume of the unit cell.

21.7 (b) Calculate the volume of the hexagonal unit cell of sodium nitrate, for which the dimensions are $a = 1692.9$ pm and $c = 506.96$ pm.

21.8 (a) The orthorhombic unit cell of NiSO_4 has the dimensions $a = 634$ pm, $b = 784$ pm, and $c = 516$ pm, and the density of the solid is estimated as 3.9 g cm^{-3} . Determine the number of formula units per unit cell and calculate a more precise value of the density.

21.8 (b) An orthorhombic unit cell of a compound of molar mass $135.01 \text{ g mol}^{-1}$ has the dimensions $a = 589$ pm, $b = 822$ pm, and $c = 798$ pm. The density of the solid is estimated as 2.9 g cm^{-3} . Determine the number of formula units per unit cell and calculate a more precise value of the density.

21.9 (a) The unit cells of SbCl_3 are orthorhombic with dimensions $a = 812$ pm, $b = 947$ pm, and $c = 637$ pm. Calculate the spacing of the (411) planes.

21.9 (b) An orthorhombic unit cell has dimensions $a = 679$ pm, $b = 879$ pm, and $c = 860$ pm. Calculate the spacing of the (322) planes.

21.10 (a) A substance known to have a cubic unit cell gives reflections with Cu K_α radiation (wavelength 154 pm) at glancing angles 19.4°, 22.5°, 32.6°, and 39.4°. The reflection at 32.6° is known to be due to the (220) planes. Index the other reflections.

21.10 (b) A substance known to have a cubic unit cell gives reflections with radiation of wavelength 137 pm at the glancing angles 10.7°, 13.6°, 17.7°, and 21.9°. The reflection at 17.7° is known to be due to the (111) planes. Index the other reflections.

21.11 (a) Potassium nitrate crystals have orthorhombic unit cells of dimensions $a = 542$ pm, $b = 917$ pm, and $c = 645$ pm. Calculate the glancing angles for the (100), (010), and (111) reflections using Cu K_α radiation (154 pm).

21.11 (b) Calcium carbonate crystals in the form of aragonite have orthorhombic unit cells of dimensions $a = 574.1$ pm, $b = 796.8$ pm, and $c = 495.9$ pm. Calculate the glancing angles for the (100), (010), and (111) reflections using radiation of wavelength 83.42 pm (from aluminium).

21.12 (a) Copper(I) chloride forms cubic crystals with four formula units per unit cell. The only reflections present in a powder photograph are those with either all even indices or all odd indices. What is the symmetry of the unit cell?

21.12 (b) A powder diffraction photograph from tungsten shows lines which index as (110), (200), (211), (220), (310), (222), (321), (400), ... Identify the symmetry of the unit cell.

21.13 (a) The coordinates, in units of a , of the atoms in a simple cubic lattice are (0, 0, 0), (0, 1, 0), (0, 0, 1), (0, 1, 1), (1, 0, 0), (1, 1, 0), (1, 0, 1), and (1, 1, 1). Calculate the structure factors F_{hkl} when all the atoms are identical.

21.13 (b) The coordinates, in units of a , of the atoms in a body-centred cubic lattice are (0, 0, 0), (0, 1, 0), (0, 0, 1), (0, 1, 1), (1, 0, 0), (1, 1, 0), (1, 0, 1), (1, 1, 1), and $(\frac{1}{2}, \frac{1}{2}, \frac{1}{2})$. Calculate the structure factors F_{hkl} when all the atoms are identical.

21.14 (a) Calculate the packing fraction for close-packed cylinders.

21.14 (b) Calculate the packing fraction for equilateral triangular rods stacked as shown in (3).



3

21.15 (a) Verify that the radius ratio for sixfold coordination is 0.414.

21.15 (b) Verify that the radius ratio for eightfold coordination is 0.732.

21.16 (a) From the data in Table 21.3 determine the radius of the smallest cation that can have (a) sixfold and (b) eightfold coordination with the O^{2-} ion.

21.16 (b) From the data in Table 21.3 determine the radius of the smallest cation that can have (a) sixfold and (b) eightfold coordination with the K^+ ion.

21.17 (a) Calculate the atomic packing factor for diamond.

21.17 (b) Calculate the atomic packing factor for a cubic C unit cell.

21.18 (a) The carbon-carbon bond length in diamond is 154.45 pm. If diamond were considered to be a close-packed structure of hard spheres with radii equal to half the bond length, what would be its expected density? The diamond lattice is face-centred cubic and its actual density is 3.516 g cm^{-3} . Can you explain the discrepancy?

21.18 (b) Although the crystallization of large biological molecules may not be as readily accomplished as that of small molecules, their crystal lattices are no different. Tobacco seed globulin forms face-centred cubic crystals with unit cell dimension of 12.3 nm and a density of 1.287 g cm^{-3} . Determine the globulin's molar mass.

21.19 (a) Is there an expansion or a contraction as titanium transforms from hcp to body-centred cubic? The atomic radius of titanium is 145.8 pm in hcp but 142.5 pm in bcc.

21.19 (b) Is there an expansion or a contraction as iron transforms from hcp to bcc? The atomic radius of iron is 126 pm in hcp but 122 pm in bcc.

21.20 (a) In a Patterson synthesis, the spots correspond to the lengths and directions of the vectors joining the atoms in a unit cell. Sketch the pattern that would be obtained for a planar, triangular isolated BF_3 molecule.

21.20 (b) In a Patterson synthesis, the spots correspond to the lengths and directions of the vectors joining the atoms in a unit cell. Sketch the pattern that would be obtained from the C atoms in an isolated benzene molecule.

21.21 (a) What velocity should neutrons have if they are to have wavelength 50 pm?

21.21 (b) Calculate the wavelength of neutrons that have reached thermal equilibrium by collision with a moderator at 300 K.

21.22 (a) What accelerating potential difference must be applied to electrons to generate a beam with wavelength 18 pm?

21.22 (b) Calculate the wavelengths of electrons that have been accelerated through (a) 1.0 kV, (b) 10 kV, (c) 40 kV.

21.23 (a) Predict from the Wierl equation the positions of the first maximum and first minimum in the neutron and electron diffraction patterns of the Cl_2 molecule obtained with neutrons of wavelength 80 pm and electrons of wavelength 4.0 pm.

21.23 (b) Predict from the Wierl equation the positions of the first maximum and first minimum in the neutron and electron diffraction patterns of a Br_2 molecule obtained with neutrons of wavelength 78 pm and electrons of wavelength 4.0 pm.

Problems

Numerical problems

21.1 In the early days of X-ray crystallography there was an urgent need to know the wavelengths of X-rays. One technique was to measure the diffraction angle from a mechanically ruled grating. Another method was to estimate the separation of lattice planes from the measured density of a crystal. The density of NaCl is 2.17 g cm^{-3} and the (100) reflection using $\text{Pd } K_\alpha$ radiation occurred at 6.0° . Calculate the wavelength of the X-rays.

21.2 The element polonium crystallizes in a cubic system. Bragg reflections, with X-rays of wavelength 154 pm, occur at $\sin \theta = 0.225, 0.316,$ and 0.388 from the (100), (110), and (111) sets of planes. The separation between the sixth and seventh lines in the powder spectrum is larger than between the fifth and sixth lines. Is the unit cell simple, body-centred, or face-centred? Calculate the unit cell dimension.

21.3 The unit cell dimensions of NaCl, KCl, NaBr, and KBr, all of which crystallize in face-centred cubic lattices, are 562.8 pm, 627.7 pm, 596.2 pm, and 658.6 pm, respectively. In each case, anion and cation are in contact along an edge of the unit cell. Do the data support the contention that ionic radii are constants independent of the counterion?

21.4 The powder diffraction patterns of (a) tungsten, (b) copper obtained in a camera of radius 28.7 mm are shown in Fig. 21.47. Both were obtained with 154 pm X-rays and the scales are marked. Identify

the unit cell in each case, and calculate the lattice spacing. Estimate the metallic radii of W and Cu.

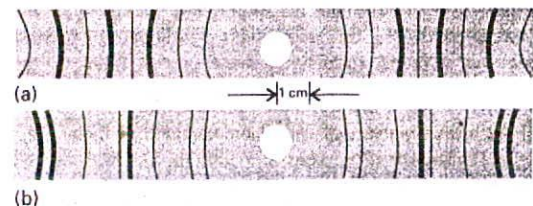


Fig. 21.47

21.5 Elemental silver reflects X-rays of wavelength 154.18 pm at angles of $19.076^\circ, 22.171^\circ,$ and 32.256° . However, there are no other reflections at angles of less than 33° . Assuming a cubic unit cell, determine its type and dimension. Calculate the density of silver.

21.6 Genuine pearls consist of concentric layers of calcite crystals (CaCO_3) in which the trigonal axes are oriented along the radii. The nucleus of a cultured pearl is a piece of mother-of-pearl that has been worked into a sphere on a lathe. The oyster then deposits concentric layers of calcite on the central seed. Suggest an X-ray method for distinguishing between real and cultured pearls.

21.7 In their book *X-rays and crystal structures* (which begins "It is now two years since Dr. Laue conceived the idea...") the Braggs give a number of simple examples of X-ray analysis. For instance, they report that the reflection from (100) planes in KCl occurs at $5^\circ 23'$, but for NaCl it occurs at $6^\circ 0'$ for X-rays of the same wavelength. If the side of the NaCl unit cell is 564 pm, what is the side of the KCl unit cell? The densities of KCl and NaCl are 1.99 g cm^{-3} and 2.17 g cm^{-3} , respectively. Do these values support the X-ray analysis?

21.8 The volume of a monoclinic unit cell is $abc \sin \beta$. Naphthalene has a monoclinic unit cell with two molecules per cell and sides in the ratio 1.377 : 1 : 1.436. The angle β is $122^\circ 49'$ and the density of the solid is 1.152 g cm^{-3} . Calculate the dimensions of the cell.

21.9 Calculate the coefficient of thermal expansion of diamond given that the (111) reflection shifts from $22^\circ 2' 25''$ to $21^\circ 57' 59''$ on heating a crystal from 100 K to 300 K and 154.0562 pm X-rays are used.

21.10 Use the Wierl equation to predict the appearance of the electron diffraction pattern of CCl_4 with an (as yet) undetermined C-Cl bond length but of known tetrahedral symmetry. Take $f_{\text{Cl}} = 17f$ and $f_{\text{C}} = 6f$ and note that $R(\text{Cl}, \text{Cl}) = (\frac{8}{3})^{1/2} R(\text{C}, \text{Cl})$. Plot I/f^2 against $x = sR(\text{C}, \text{Cl})$. In an actual experiment using 10.0 keV electrons the positions of the maxima occurred at $3^\circ 10'$, $5^\circ 22'$, and $7^\circ 54'$ and minima occurred at $1^\circ 46'$, $4^\circ 6'$, $6^\circ 40'$, and $9^\circ 10'$. What is the C-Cl bond length in CCl_4 ?

Theoretical problems

21.11 Show that the separation of the (hkl) planes in an orthorhombic crystal with sides a , b , and c is given by eqn 3.

21.12 Show that the volume of a triclinic unit cell of sides a , b , and c and angles α , β , and γ is

$$V = abc(1 - \cos^2 \alpha - \cos^2 \beta - \cos^2 \gamma + 2 \cos \alpha \cos \beta \cos \gamma)^{1/2}$$

Use this expression to derive expressions for monoclinic and orthorhombic unit cells. For the derivation, it may be helpful to use the result from vector analysis that $V = \mathbf{a} \cdot \mathbf{b} \times \mathbf{c}$ and to calculate V^2 initially.

21.13 Calculate the packing fractions of (a) a primitive cubic lattice, (b) a bcc unit cell, (c) an fcc unit cell.

21.14 The coordinates of the four I atoms in the unit cell of KIO_4 are $(0, 0, 0)$, $(0, \frac{1}{2}, \frac{1}{2})$, $(\frac{1}{2}, \frac{1}{2}, \frac{1}{2})$, $(\frac{1}{2}, 0, \frac{3}{4})$. By calculating the phase of the I reflection in the structure factor, show that the I atoms contribute no net intensity to the (114) reflection.

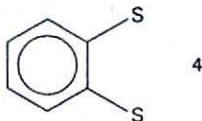
21.15 The coordinates, in units of a , of the A atoms, with scattering factor f_A , in a cubic lattice are $(0, 0, 0)$, $(0, 1, 0)$, $(0, 0, 1)$, $(0, 1, 1)$, $(1, 0, 0)$, $(1, 1, 0)$, $(1, 0, 1)$, and $(1, 1, 1)$. There is also a B atom, with scattering factor f_B , at $(\frac{1}{2}, \frac{1}{2}, \frac{1}{2})$. Calculate the structure factors F_{hkl} and predict the form of the powder diffraction pattern when (a) $f_A = f$, $f_B = 0$, (b) $f_B = \frac{1}{2}f_A$, and (c) $f_A = f_B = f$.

Additional problems supplied by Carmen Giunta and Charles Trapp

21.16 B.A. Bovenzi and G.A. Pearce, Jr (*J. Chem. Soc. Dalton Trans.* (accepted, 1997)) synthesized coordination compounds of the

tridentate ligand pyridine-2,6-diamidoxime ($\text{C}_7\text{H}_9\text{N}_5\text{O}_2$). The compound, which they isolated from the reaction of the ligand with $\text{CuSO}_4(\text{aq})$, did not contain a $[\text{Cu}(\text{C}_7\text{H}_9\text{N}_5\text{O}_2)_2]^{2+}$ complex cation as expected. Instead, X-ray diffraction analysis revealed a linear polymer of formula $[\text{Cu}(\text{Cu}(\text{C}_7\text{H}_9\text{N}_5\text{O}_2)(\text{SO}_4) \cdot 2\text{H}_2\text{O})_n]$, which features bridging sulfate groups. The unit cell was primitive monoclinic with $a = 1.0427 \text{ nm}$, $b = 0.8876 \text{ nm}$, $c = 1.3777 \text{ nm}$, and $\beta = 93.254^\circ$. The mass density of the crystals is 2.024 g cm^{-3} . How many monomer units are there per unit cell?

21.17 D. Sellmann, M.W. Wemple, W. Donaübauer, and F.W. Heinemann (*Inorg. Chem.* 36, 1397 (1997)) describe the synthesis and reactivity of the ruthenium nitrido compound $[\text{N}(\text{C}_4\text{H}_9)_4][\text{Ru}(\text{N})(\text{S}_2\text{C}_6\text{H}_4)_2]$. The ruthenium complex anion has the two 1,2-benzenedithiolate ligands (4) at the base of a rectangular pyramid and the nitrido ligand at the apex. Compute the mass density of the compound given that it crystallizes into an orthorhombic unit cell with $a = 3.6881 \text{ nm}$, $b = 0.9402 \text{ nm}$, and $c = 1.7652 \text{ nm}$ and eight formula units per cell. Replacing the ruthenium with an osmium results in a compound with the same crystal structure and a unit cell with a volume less than 1 per cent larger. Estimate the mass density of the osmium analogue.



21.18 P.G. Radaelli, M. Marezio, M. Perroux, S. de Brion, J.L. Tholence, Q. Huang, and A. Santoro (*Science* 265, 380 (1994)) report the synthesis and structure of a material that becomes superconducting at temperatures below 45 K. The compound is based on a layered compound $\text{Hg}_2\text{Ba}_2\text{YCu}_2\text{O}_{8-\delta}$, which has a tetragonal unit cell with $a = 0.38606 \text{ nm}$ and $c = 2.8915 \text{ nm}$; each unit cell contains two formula units. The compound is made superconducting by partially replacing Y by Ca, accompanied by a change in unit cell volume by less than 1 per cent. Estimate the Ca content x in superconducting $\text{Hg}_2\text{Ba}_2\text{Y}_{1-x}\text{Ca}_x\text{Cu}_2\text{O}_{7.55}$ given that the mass density of the compound is 7.651 g cm^{-3} .

21.19 The scattering factor of an atom is given by eqn 7. In general this expression is difficult to evaluate as it requires knowledge of $\rho(r)$, which in turn requires knowledge of the wavefunction of the atom. The latter is not generally available in simple analytical form except for a hydrogenic atom. Derive an expression for the scattering factor of a hydrogenic atom of atomic number Z in its ground state.


21.20 Diamond forms a face-centred cubic lattice with eight atoms per unit cell. There are atoms at each lattice point and at points displaced by $\frac{1}{4}, \frac{1}{4}, \frac{1}{4}$ from each lattice point. Calculate the structure factor, F_{hkl} , for diamond. *Hint.* See Example 21.4.

21.21 Determine the relative intensities of the (100), (110), and (200) reflections in CsCl by calculating their structure factors. Assume that the atomic scattering factors are given by the number of electrons in the ions.



22

The electric and magnetic properties of molecules



Electric properties

- 22.1 Permanent and induced electric dipole moments
- 22.2 Refractive index

Intermolecular forces

- 22.3 Interactions between dipoles
- 22.4 Repulsive and total interactions
- 22.5 Molecular interactions in beams

Magnetic properties

- 22.6 Magnetic susceptibility
- 22.7 The permanent magnetic moment
- 22.8 Induced magnetic moments

Checklist of key ideas

Further reading

Exercises

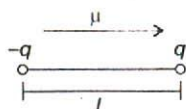
Problems

In this chapter we examine some of the electric and magnetic properties of molecules and interpret them in terms of electronic structure. The properties we consider include the electric dipole moments and polarizabilities of molecules and some related properties that include refractive index, optical activity, and intermolecular forces. All these properties reflect the degree to which the nuclei of atoms exert control over the electrons in a molecule, either by causing electrons to accumulate in particular regions, or by permitting them to respond more or less strongly to the effects of external fields. We also discuss the analogous magnetic properties, particularly the magnetizabilities and magnetic susceptibilities of molecules, and see the origins of the distinction between paramagnetic and diamagnetic substances.

The electric properties, and to a smaller extent the magnetic properties, of molecules are responsible for many of the properties of bulk matter. The small imbalances of charge distributions in molecules allow them to interact with one another and with externally applied fields. One result of this interaction is the cohesion of molecules to form the bulk phases of matter. These interactions are also important for understanding the shapes adopted by biological and synthetic macromolecules, as we shall see in Chapter 23.

Electric properties

Many of the electrical properties of molecules can be traced to the competing influences of nuclei with different charges or the competition between the control exercised by a nucleus and the influence of an externally applied field. The former competition may result in an electric dipole moment. The latter may result in properties such as refractive index and optical activity.



1 Electric dipole

22.1 Permanent and induced electric dipole moments

An electric dipole consists of two electric charges q and $-q$ separated by a distance R . This arrangement of charges is represented by a vector, the electric dipole moment, μ , that points from the negative charge to the positive charge (1).¹ The magnitude of μ is $\mu = qR$. The magnitudes of dipole moments are still commonly reported in the non-SI unit debye, D, where²

$$1 \text{ D} = 3.33564 \times 10^{-30} \text{ C m} \quad (1)$$

The dipole moment of a pair of charges $+e$ and $-e$ separated by 100 pm is $1.6 \times 10^{-29} \text{ C m}$, corresponding to 4.8 D. Dipole moments of small molecules are typically about 1 D.

(a) Classes of substance

A polar molecule is a molecule with a permanent electric dipole moment. The permanent dipole moment stems from the partial charges on the atoms in the molecule that arise from differences in electronegativity or other features of bonding (Section 14.7). Nonpolar molecules acquire an induced dipole moment in an electric field on account of the distortion the field causes in their electronic distributions and nuclear positions; however, this induced moment is only temporary, and disappears as soon as the perturbing field is removed. Polar molecules also have their existing dipole moments temporarily modified by an applied field.

The polarization, P , of a sample is the electric dipole moment density, the mean electric dipole moment of the molecules, $\langle \mu \rangle$, multiplied by the number density, \mathcal{N} :

$$P = \langle \mu \rangle \mathcal{N} \quad [2]$$

In the following pages we refer to the sample as a dielectric, by which is meant a polarizable, nonconducting medium.

The polarization of an isotropic fluid sample is zero in the absence of an applied field because the molecules adopt random orientations, so $\langle \mu \rangle = 0$. In the presence of a field, the dipoles become partially aligned because some orientations have lower energies than others. As a result, the electric dipole moment density is nonzero. Moreover, as we shall see, there is an additional contribution from the dipole moment induced by the field.

A ferroelectric solid is a solid that has a permanent polarization on account of a cooperative shift of some of its atoms in a given direction. For example, above 120°C , barium titanate, BaTiO_3 , is electrically a normal solid, and the Ti ion is symmetrically placed inside an octahedron of O atoms. However, below 120°C , the Ti ion moves from the centre of the octahedron by about 10 pm and every unit cell over a large domain acquires an electric dipole moment that persists even in the absence of an applied field.

(b) Polar molecules

The Stark effect (Section 16.5) is used to measure the electric dipole moments of molecules for which a rotational spectrum can be observed. In many cases microwave spectroscopy cannot be used because the sample is not volatile, decomposes on vaporization, or consists of molecules that are so complex that their rotational spectra cannot be interpreted. In such cases the dipole moment may be obtained by measurements on a liquid or solid bulk sample using a method explained later.

1 In elementary chemistry, an electric dipole moment is represented by the arrow \rightarrow added to the Lewis structure for the molecule, with the $+$ marking the positive end. Note that the direction of the arrow is opposite to that of μ .

2 The conversion factor stems from the original definition of the debye in terms of c.g.s. units: 1 D is the dipole moment of two equal and opposite charges of magnitude 1 e.s.u. separated by 1 Å. The debye is named after Peter Debye, a pioneer in the study of dipole moments of molecules.

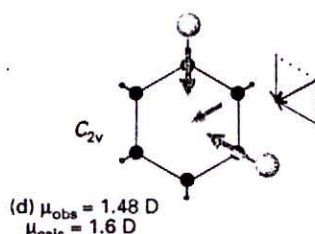
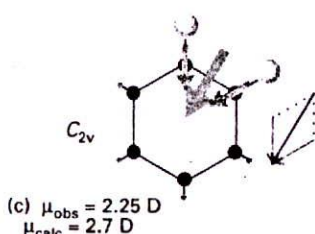
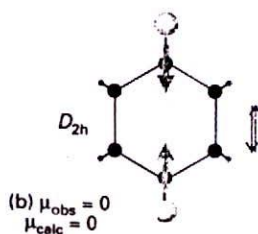
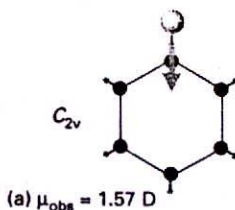
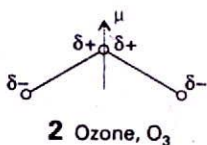
Table 22.1* Dipole moments (μ) and polarizability volumes (α')

	μ/D	$\alpha'/(10^{-30} \text{ m}^3)$
CCl_4	0	10.5
H_2	0	0.819
H_2O	1.85	1.48
HCl	1.08	2.63
HI	0.42	5.45

* More values are given in the Data section at the end of this volume.



22.1 One of the contributions to the dipole moment of a molecule is the imbalance of charge arising from the overlap of orbitals of different radii. This diagram shows how the charge accumulation leads to a region of negative charge closer to the smaller atom.



22.2 The resultant dipole moments (grey) of the dichlorobenzene isomers (b to d) can be obtained approximately by vectorial addition of two chlorobenzene dipole moments (1.57 D).

All heteronuclear diatomic molecules are polar, and typical values of μ include 1.08 D for HCl and 0.42 D for HI (Table 22.1). A very approximate relation between the dipole moment and the difference in electronegativities of the two atoms, $\Delta\chi$, is

$$\mu/\text{D} \approx \Delta\chi \quad (3)$$

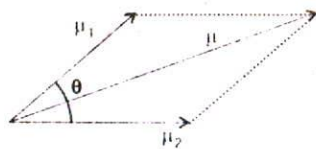
The more electronegative atom is normally the negative end of the dipole, but there are exceptions, particularly when antibonding orbitals are occupied.³ Thus the dipole moment of CO is very small (0.12 D), but the negative end of the dipole is on the C atom even though oxygen is more electronegative than carbon.

The interpretation and prediction of electric dipole moments is made even more complicated by the fact that a difference in atomic radii can result in an imbalance of electron density because the enhanced charge density associated with the overlap region lies closer to the nucleus of the smaller atom (Fig. 22.1). Such a homopolar contribution to the total dipole moment can arise even in the absence of a difference in electronegativity between the two atoms.

A polyatomic molecule is nonpolar if it fulfils certain symmetry criteria. We saw in Section 15.3a that a molecule is nonpolar if it belongs to a D point group or to one of the cubic or icosahedral point groups. We also saw that the dipole moment of a polar molecule with a symmetry axis cannot lie perpendicular to that axis (the dipole moment of NH_3 , for instance, lies parallel to the molecular C_3 axis). The symmetry criterion is more important than the question of whether or not the atoms in the molecule are the same. Thus the homonuclear triatomic molecule O_3 (which is angular, with C_{2v} symmetry) is allowed to be polar by symmetry considerations, and in fact is polar because the electron density on the central O atom differs from that on the two outer O atoms. The dipole moment of the molecule lies parallel to the C_2 axis of the molecule (2). The heteronuclear triatomic molecule CO_2 (which is linear, with $D_{\infty h}$ symmetry) is strictly nonpolar by symmetry even though the C and O atoms have different electronegativities. The dipole moments associated with each CO bond point in opposite directions in CO_2 , and cancel.

To a first approximation, the dipole moment of a polyatomic molecule can be resolved into contributions from various components (Fig. 22.2). Thus, 1,4-dichlorobenzene is nonpolar on account of the cancellation of the two equal but opposing moments associated with the presence of Cl atoms on opposite sides of the ring (the molecule has D_{2h} symmetry, so it is necessarily nonpolar). The isomer 1,2-dichlorobenzene (which has C_{2v} symmetry, with the C_2 axis lying along the bisector of the angle between the two CCl bonds) has a dipole moment that is approximately the resultant of two monochlorobenzene dipole moments arranged at 60° . The technique of vector addition can be applied with fair success

3 We remarked in Section 14.7 that the major contribution to an antibonding orbital is made by the atomic orbitals of the less electronegative atom. Therefore, if an antibonding orbital is occupied there may be so much electron density on the less electronegative atom that that atom has a partial negative charge.



3 Addition of dipoles

to other series of related molecules, and the resultant of two dipole moments that make an angle θ to each other (3) is obtained from

$$\mu^2 = \mu_1^2 + \mu_2^2 + 2\mu_1\mu_2 \cos \theta \quad (4a)$$

When the two dipole moments are equal, this equation simplifies to

$$\mu = 2\mu_1 \cos \frac{1}{2}\theta \quad (4b)$$

The mean dipole moment of the molecules of a fluid sample is zero in the absence of an orientating electric field. In the presence of a field and at a temperature T the mean moment is nonzero, and we show in the *Justification* below that

$$\langle \mu_z \rangle = \frac{\mu^2 \mathcal{E}}{3kT} \quad (5)$$

where z is the direction of the applied field. This nonzero value stems from the fact that some orientations of the dipole moment are energetically more favourable than others.

Justification 22.1

The probability dp that a dipole has an orientation in the range θ to $\theta + d\theta$ is given by the Boltzmann distribution (Section 19.1c), which in this case is

$$dp = \frac{e^{-E(\theta)/kT} \sin \theta d\theta}{\int_0^\pi e^{-E(\theta)/kT} \sin \theta d\theta}$$

where $E(\theta)$ is the energy of the dipole in the field: $E(\theta) = -\mu\mathcal{E} \cos \theta$, with $0 \leq \theta \leq \pi$. The average value of the component of the dipole moment parallel to the applied electric field is therefore

$$\langle \mu_z \rangle = \int \mu \cos \theta dp = \mu \int \cos \theta dp = \frac{\mu \int_0^\pi e^{x \cos \theta} \cos \theta \sin \theta d\theta}{\int_0^\pi e^{x \cos \theta} \sin \theta d\theta}$$

with $x = \mu\mathcal{E}/kT$. The integral takes on a simpler appearance when we write $y = \cos \theta$ and note that $dy = -\sin \theta d\theta$:

$$\langle \mu_z \rangle = \frac{\mu \int_{-1}^1 y e^{xy} dy}{\int_{-1}^1 e^{xy} dy}$$

At this point we use

$$\int_{-1}^1 e^{xy} dy = \frac{e^x - e^{-x}}{x} \quad \int_{-1}^1 y e^{xy} dy = \frac{e^x + e^{-x}}{x} - \frac{e^x - e^{-x}}{x^2}$$

It is now straightforward algebra to combine these two results and to obtain

$$\langle \mu_z \rangle = \mu \mathcal{L}(x) \quad \mathcal{L}(x) = \frac{e^x + e^{-x}}{e^x - e^{-x}} - \frac{1}{x} \quad x = \frac{\mu\mathcal{E}}{kT} \quad (6)$$

The function $\mathcal{L}(x)$ is called the **Langevin function**.

Under most circumstances, x is very small (for example, if $\mu = 1$ D and $T = 300$ K, then x exceeds 0.01 only if the field strength exceeds 100 kV cm^{-1} , and most measurements are done at much lower strengths). When $x \ll 1$, the exponentials in the Langevin function can be expanded, and the largest term that survives is

$$\mathcal{L}(x) = \frac{1}{3}x + \dots \quad (7)$$

Therefore, the average molecular dipole moment is given by eqn 5.

(c) Induced dipole moments

An applied electric field can distort a molecule as well as aligning its permanent electric dipole moment. The induced dipole moment, μ^* , is proportional to the field strength, \mathcal{E} , and we write⁴

$$\mu^* = \alpha \mathcal{E} \quad (8)$$

The constant of proportionality α is the polarizability of the molecule. The greater the polarizability, the larger is the induced dipole moment for a given applied field. When the applied field is very strong (as in laser beams), the induced moment is not strictly linear in the strength of the field, and we write

$$\mu^* = \alpha \mathcal{E} + \frac{1}{2} \beta \mathcal{E}^2 + \dots \quad (9)$$

The coefficient β is the hyperpolarizability of the molecule.

Polarizability has the units (coulomb-metre)² per joule, C² m² J⁻¹. That collection of units is awkward, so α is often expressed as a polarizability volume, α' , by using the relation

$$\alpha' = \frac{\alpha}{4\pi\epsilon_0} \quad [10]$$

where ϵ_0 is the vacuum permittivity. Because the units of $4\pi\epsilon_0$ are coulomb-squared per joule per metre (C² J⁻¹ m⁻¹), it follows that α' has the dimensions of volume (hence its name).⁵ Polarizability volumes are similar in magnitude to actual molecular volumes (of the order of 10⁻³⁰ m³, 1 Å³).

Some experimental polarizability volumes of molecules are given in Table 22.1. As shown in the *Justification* below, there is a correlation between the HOMO-LUMO separation in atoms and molecules. The electron distribution can be distorted readily if the LUMO lies close to the HOMO in energy, so the polarizability is then large. If the LUMO lies high above the HOMO, an applied field can perturb the electron distribution significantly, and the polarizability is low. Molecules with small HOMO-LUMO gaps are typically large, with numerous electrons.

Justification 22.2

The quantum mechanical expression for the mean polarizability is

$$\alpha = \frac{2}{3} \sum_n \frac{|\mu_{0n}|^2}{E_n - E_0} \quad (11)$$

where μ_{0n} is the magnitude of the transition dipole moment, the integral

$$\mu_{0n} = \int \psi_0^* \mu \psi_n \, d\tau$$

with μ the electric dipole moment operator. This integral is a measure of the extent to which electric charge is shifted when an electron migrates from a wavefunction ψ_0 to an excited-state wavefunction ψ_n . The sum is over the excited states, with energies E_n . The content of the expression for the polarizability can be appreciated by approximating the excitation energies by a mean value ΔE (an indication of the HOMO-LUMO separation),

⁴ We should use vector quantities and allow for the possibility that the induced dipole moment might not lie parallel to the applied field; for simplicity we discuss polarizabilities in terms of (scalar) magnitudes.

⁵ When using older compilations of data, it is useful to note that polarizability volumes have the same numerical values as the 'polarizabilities' reported using c.g.s. electrical units, so the tabulated values previously called 'polarizabilities' can be used directly.

and supposing that the most important transition dipole moment is approximately equal to the charge of an electron multiplied by the radius, R , of the molecule. Then

$$\alpha \approx \frac{2e^2R^2}{3\Delta E}$$

This expression shows that α increases with the size of the molecule and with the ease with which it can be excited (the smaller the value of ΔE).

If the excitation energy is approximated by the energy needed to remove an electron to infinity from a distance R from a single positive charge, we can write $\Delta E \approx e^2/4\pi\epsilon_0R$. When this expression is substituted into the equation above, both sides are divided by $4\pi\epsilon_0$, and the factor of $\frac{2}{3}$ ignored in this approximation, we obtain $\alpha \approx R^3$, which is of the same order of magnitude as the molecular volume.

For all molecules other than those belonging to one of the cubic or icosahedral groups, the polarizability depends on the orientation of the molecule relative to the field. The polarizability volume of benzene when the field is applied perpendicular to the ring is $12.3 \times 10^{-30} \text{ m}^3$ and is $6.7 \times 10^{-30} \text{ m}^3$ when the field is applied in the plane of the ring. The anisotropy of the polarizability determines whether a molecule is rotationally Raman active (Section 16.7).

(d) Polarization at high frequencies

When the applied field changes direction slowly, the permanent dipole moment has time to reorientate—the whole molecule rotates into a new direction—and follow the field. However, when the frequency of the field is high, a molecule cannot change direction fast enough to follow the change in direction of the applied field and the dipole moment then makes no contribution to the polarization of the sample. Because a molecule takes about 1 ps to turn through about 1 radian in a fluid, the loss of this contribution to the polarization occurs when measurements are made at frequencies greater than about 10^{11} Hz (in the microwave region). We say that the **orientation polarization**, the polarization arising from the permanent dipole moments, is lost at such high frequencies.

The next contribution to the polarization to be lost as the frequency is raised is the **distortion polarization**, the polarization that arises from the distortion of the positions of the nuclei by the applied field. The molecule is bent and stretched by the applied field, and the molecular dipole moment changes accordingly. The time taken for a molecule to bend is approximately the inverse of the molecular vibrational frequency, so the distortion polarization disappears when the frequency of the radiation is increased through the infrared. The disappearance of polarization occurs in stages: as shown in the *Justification* below, each successive stage occurs as the incident frequency rises above the frequency of a particular mode of vibration.

Justification 22.3

The quantum mechanical expression for the polarizability of a molecule in the presence of an electric field that is oscillating at a frequency ω is

$$\alpha(\omega) = \frac{2}{3\hbar} \sum_n \frac{\omega_{n0} |\mu_{0n}|^2}{\omega_{n0}^2 - \omega^2} \quad (12)$$

The quantities in this expression (which is valid provided that ω is not close to ω_{n0}) are the same as those in the previous *Justification*, with $\hbar\omega_{n0} = E_n - E_0$. As $\omega \rightarrow 0$, the equation reduces to eqn 11 for the static polarizability. As ω becomes very high (and much higher than any excitation frequency of the molecule), the polarizability becomes

$$\alpha(\omega) = -\frac{2}{3\hbar\omega^2} \sum_n \omega_{n0} |\mu_{0n}|^2 \rightarrow 0 \text{ as } \omega \rightarrow \infty$$

That is, when the incident frequency is higher than any excitation frequency, the polarizability becomes zero. The argument applies to each type of excitation, vibrational as well as electronic, and accounts for the successive decreases in polarizability as the frequency is increased.

At even higher frequencies, in the visible region, only the electrons are mobile enough to respond to the rapidly changing direction of the applied field. The polarization that remains is now due entirely to the distortion of the electron distribution, and the surviving contribution to the molecular polarizability is called the **electronic polarizability**.

(e) Relative permittivities

When two charges q_1 and q_2 are separated by a distance r in a vacuum, the potential energy of their interaction is

$$V = \frac{q_1 q_2}{4\pi\epsilon_0 r} \quad (13a)$$

When the same two charges are immersed in a medium (such as air or a liquid), their potential energy is reduced to

$$V = \frac{q_1 q_2}{4\pi\epsilon r} \quad (13b)$$

where ϵ is the permittivity of the medium. The permittivity is normally expressed in terms of the dimensionless relative permittivity, ϵ_r , (which is also called the dielectric constant) of the medium:⁶

$$\epsilon_r = \frac{\epsilon}{\epsilon_0} \quad [14]$$

The relative permittivity can have a very significant effect on the strength of the interactions between ions in solution. For instance, water has a relative permittivity of 78 at 25°C, so the interionic Coulombic interaction energy is reduced by nearly two orders of magnitude from its vacuum value. Some of the consequences of this reduction for electrolyte solutions were explored in Chapter 10.

The relative permittivity of a substance is large if its molecules are polar or highly polarizable. The quantitative relation between the relative permittivity and the electric

⁶ The relative permittivity of a substance is measured by comparing the capacitance of a capacitor with and without the sample present (C and C_0 , respectively) and using $\epsilon_r = C/C_0$.

properties of the molecules is obtained by considering the polarization of a medium, and is expressed by the Debye equation:

$$\frac{\epsilon_r - 1}{\epsilon_r + 2} = \frac{\rho P_m}{M} \quad (15)$$

where ρ is the mass density of the sample, M is the molar mass of the molecules, and P_m is the molar polarization,⁷ which is defined as

$$P_m = \frac{N_A}{3\epsilon_0} \left(\alpha + \frac{\mu^2}{3kT} \right) \quad (16)$$

The term $\mu^2/3kT$ stems from the thermal averaging of the electric dipole moment in the presence of the applied field (eqn 5). The corresponding expression without the contribution from the permanent dipole moment is called the Clausius–Mossotti equation:

$$\frac{\epsilon_r - 1}{\epsilon_r + 2} = \frac{\rho N_A \alpha}{3M\epsilon_0} \quad (17)$$

The Clausius–Mossotti equation is used when there is no contribution from permanent electric dipole moments to the polarization, either because the molecules are nonpolar or because the frequency of the applied field is so high that the molecules cannot orientate quickly enough to follow the change in direction of the field.

Equation 16 implies that the polarizability and permanent dipole moment of the molecules in a sample can be determined by measuring ϵ_r at a series of temperatures, calculating P_m , and plotting it against $1/T$. The slope of the graph is $N_A \mu^2/9\epsilon_0 k$ and its intercept at $1/T = 0$ is $N_A \alpha/3\epsilon_0$.



4 Camphor

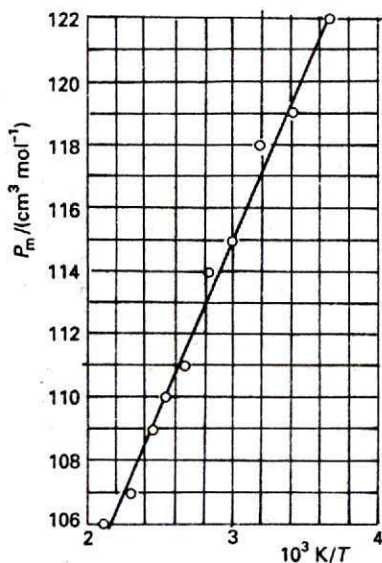
Example 22.1 Determining dipole moment and polarizability

The relative permittivity of camphor (4) was measured at a series of temperatures with the results given below. Determine the dipole moment and the polarizability volume of the molecule.

$\theta/^\circ\text{C}$	$\rho/(\text{g cm}^{-3})$	ϵ_r
0	0.99	12.5
20	0.99	11.4
40	0.99	10.8
60	0.99	10.0
80	0.99	9.50
100	0.99	8.90
120	0.97	8.10
140	0.96	7.60
160	0.95	7.11
200	0.91	6.21

Method According to eqn 15, we need to calculate $(\epsilon_r - 1)/(\epsilon_r + 2)$ at each temperature, and then multiply by M/ρ to form P_m . Next, from eqn 16, we should plot P_m against $1/T$ and expect a straight line. The intercept at $1/T = 0$ is $N_A \alpha/3\epsilon_0 = (4\pi N_A/3)\alpha'$ and the slope is $N_A \mu^2/9\epsilon_0 k$.

⁷ Molar polarization is an unhappy but traditional name for P_m , which has the dimensions of volume per mole. H. Looyenga (*Mol. Phys.* 9, 501 (1965)) has argued that a better description is obtained if $(\epsilon - 1)/(\epsilon + 2)$ is replaced by $e^{1/2} - 1$ in eqns 15 and 17.



22.3 The plot of $P_m / (\text{cm}^3 \text{mol}^{-1})$ against $(10^3 \text{ K})/T$ used in Example 22.1 for the determination of the polarizability and dipole moment of camphor.

Answer For camphor, $M = 152.23 \text{ g mol}^{-1}$. We can therefore use the data to draw up the following table:

$\theta / ^\circ\text{C}$	$(10^3 \text{ K})/T$	ϵ_r	$(\epsilon_r - 1)/(\epsilon_r + 2)$	$P_m / (\text{cm}^3 \text{mol}^{-1})$
0	3.66	12.5	0.793	122
20	3.41	11.4	0.776	119
40	3.19	10.8	0.766	118
60	3.00	10.0	0.750	115
80	2.83	9.50	0.739	114
100	2.68	8.90	0.725	111
120	2.54	8.10	0.703	110
140	2.42	7.60	0.688	109
160	2.31	7.11	0.670	107
200	2.11	6.21	0.634	106

The points are plotted in Fig. 22.3. The intercept lies at 82.7, so $\alpha' = 3.3 \times 10^{-23} \text{ cm}^3$. The slope is 10.9, so $\mu = 4.46 \times 10^{-30} \text{ C m}$, corresponding to 1.34 D.

Comment Because the Debye equation describes molecules that are free to rotate, the data show that camphor, which does not melt until 175°C , is rotating even in the solid. It is an approximately spherical molecule.

Self-test 22.1 The relative permittivity of chlorobenzene is 5.71 at 20°C and 5.62 at 25°C . Assuming a constant density (1.11 g cm^{-3}), estimate its polarizability volume and dipole moment.

[$1.4 \times 10^{-23} \text{ cm}^3$, 1.2 D]

22.2 Refractive index

One of the optical properties of matter that we are almost in a position to explain is the ability of a prism to separate light into its component colours. This effect depends on the refractive index, n_r , of the medium, the ratio of the speed of light in a vacuum, c , to its speed c' in the medium:

$$n_r = \frac{c}{c'} \quad [18]$$

It follows from the Maxwell equations⁸ that the refractive index at a (visible or ultraviolet) specified frequency is related to the relative permittivity at that frequency by

$$n_r = \epsilon_r^{1/2} \quad (19)$$

The molar polarization, P_m , and hence the molecular polarizability, α , can therefore be measured at frequencies typical of visible light (about 10^{15} to 10^{16} Hz) by measuring the refractive index of the sample (Table 22.2) and using the Clausius–Mossotti equation.

The refractive index is related to the molecular polarizability because the propagation of light through a medium can be imagined to occur by the incident light inducing an oscillating dipole moment, which then radiates light of the same frequency. The newly generated radiation is delayed slightly by this process, so it propagates more slowly through the medium than through a vacuum. Because photons of high-frequency light carry more energy than those of low-frequency light, they can distort the electronic distributions of the

Table 22.2* Refractive indices (at different wavelengths of light) relative to air at 20°C

	434 nm	589 nm	656 nm
$\text{C}_6\text{H}_6(\text{l})$	1.524	1.501	1.497
$\text{CS}_2(\text{l})$	1.675	1.628	1.618
$\text{H}_2\text{O}(\text{l})$	1.340	1.333	1.331
$\text{KI}(\text{s})$	1.704	1.666	1.658

*More values are given in the Data section.

⁸ The Maxwell equations describe the properties of electromagnetic radiation; they are not discussed in this text: see Further reading.

molecules in their path more effectively. Therefore, after allowing for the loss of contributions from low-frequency modes of motion, we can expect the electronic polarizabilities of molecules, and hence the refractive index, to increase as the incident frequency rises towards an absorption frequency. This dependence on frequency is the origin of the dispersion of white light by a prism: the refractive index is greater for blue light than for red, and therefore the blue rays are bent more than the red. The term *dispersion* is a term carried over from this phenomenon to mean the variation of the refractive index, or of any property, with frequency. Figure 22.4 shows the typical dispersion of the polarizability of a sample.

The concept of refractive index is closely related to the property of optical activity. An optically active substance is a substance that rotates the plane of polarization of plane-polarized light. As shown in the *Justification* below, the rotation arises from the difference in the refractive indices for right- and left-circularly polarized light, n_R and n_L , respectively. By convention, in right-handed circularly polarized light the electric vector rotates clockwise as seen by an observer facing the oncoming beam (Fig. 22.5). A sample in which these two refractive indices are different is said to be circularly birefringent.

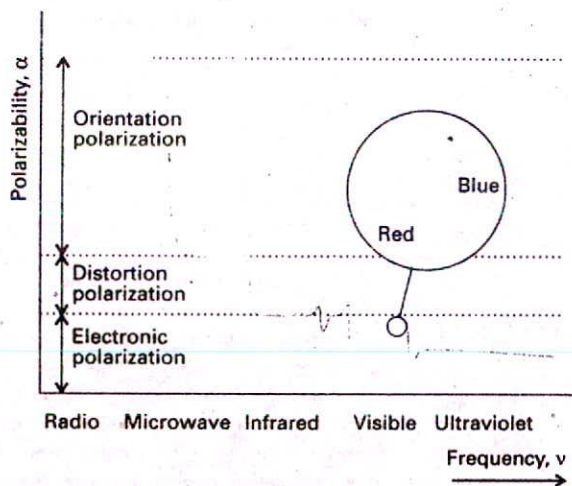
Justification 22.4

Before entering the medium, the beam is plane-polarized (that is, the electric field oscillates in a plane containing the propagation direction). This beam may be regarded as a superposition of two oppositely rotating, circularly polarized components (Fig. 22.6). On entering the medium, one component propagates faster than the other if their refractive indices are different. If the sample is of length l , the difference in the times of passage is

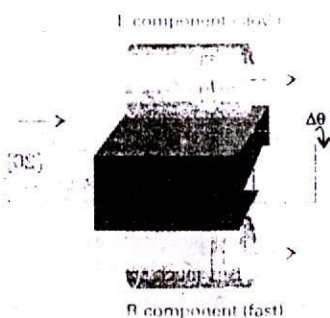
$$\Delta t = \frac{l}{c_R} - \frac{l}{c_L}$$

where c_R and c_L are the speeds of the two components in the medium. In terms of the refractive indices, the difference is

$$\Delta t = (n_R - n_L) \frac{l}{c}$$



22.4 The general form of the variation of the polarizability with the frequency of the applied field. Note the considerable reduction in polarizability when the field is reversing direction so rapidly that the polar molecules cannot reorientate quickly enough to follow it. The inset shows the variation of the electronic polarizability in the visible region near an electronic excitation of the molecule.



22.5 Linearly polarized light entering a sample (from the left) can be regarded as the superposition of two counter-rotating circularly polarized components (represented by the two cylindrical objects, which are actually superimposed inside the sample) with a definite phase relation. If one component propagates more rapidly than the other in the medium, when they emerge the phase relation is changed, and the resultant is plane-polarized light rotated through an angle $\Delta\theta$ to its original orientation.

The phase difference between the two components when they emerge from the sample is therefore

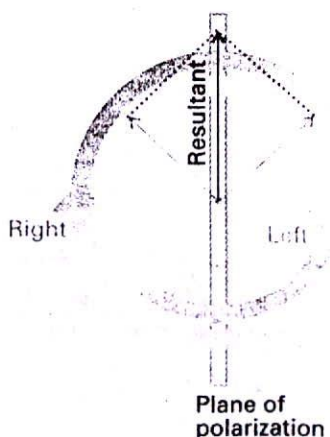
$$\Delta\theta = 2\pi\nu\Delta t = \frac{2\pi c\Delta t}{\lambda} = (n_R - n_L) \times \frac{2\pi l}{\lambda}$$

where λ is the wavelength of the light. The two rotating electric vectors have a different phase when they leave the sample from the value they had initially, so their superposition gives rise to a plane-polarized beam rotated through an angle $\Delta\theta$ relative to the plane of the incoming beam. It follows that the angle of optical rotation is proportional to the difference in refractive index, $n_R - n_L$.

To explain why the refractive indices depend on the handedness of the light, we must examine why the polarizabilities depend on the handedness. One interpretation is that, if a molecule has a helical structure (including, if the molecule is small, a structure that can be regarded as being a fragment of a helix), its polarizability depends on whether or not the electric field of the incident radiation rotates in the same sense as the helix. Molecules having a helical structure are chiral, which is the criterion for optical activity discussed in Section 15.3b.

The angle of optical rotation varies with the frequency of the radiation. This variation is called **optical rotatory dispersion (ORD)**. It arises from the individual dispersions of the polarizabilities (and refractive indices) for left- and right-circularly polarized radiation. The effect can be used to investigate the stereochemistry of molecules.

Associated with the differences in the two refractive indices (the circular birefringence of the medium) is a difference in absorption intensities \mathcal{I}_R and \mathcal{I}_L for right- and left-circularly polarized radiation. This difference is known as **circular dichroism (CD)**. The CD spectrum of a sample is a plot of the variation of $\mathcal{I}_L - \mathcal{I}_R$ with frequency of the radiation. Circular dichroism is particularly useful for determining the absolute configurations of *d*-metal complexes, because complexes with similar geometries have CD spectra with similar features.



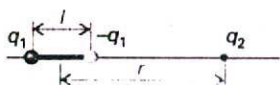
22.6 The superposition shown in Fig. 22.5 as viewed by an observer facing the oncoming beam.

Intermolecular forces

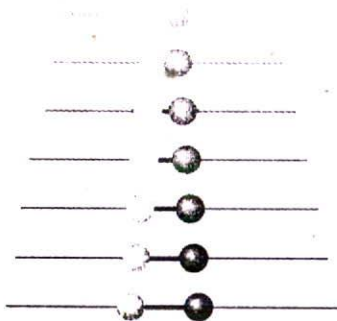
Van der Waals forces are the interactions between molecules that leave their chemical identities essentially unchanged. They include the interactions between the partial charges of polar molecules. There are also repulsive interactions that prevent the complete collapse of matter to nuclear densities. The repulsive interactions arise from Coulombic repulsions and, indirectly, from the Pauli principle and the exclusion of electrons from regions of space where the orbitals of neighbouring species overlap. In this section we consider the attractive forces between molecules, and see how they are related to the electrical properties treated in Section 22.1.

22.3 Interactions between dipoles

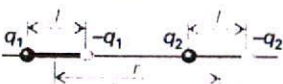
Most of the discussion in this section is based on the Coulombic potential energy of interaction between two charges (eqn 13a). It is easy to adapt this expression to obtain the potential energy of a charge and a dipole and to extend it to the interaction between two dipoles.



22.7 The potential energy of interaction between a dipole and a point charge is the sum of the repulsion of like charges and the attraction of opposite charges. For a point dipole, $l \ll r$.



22.8 There are two contributions to the diminishing field of an electric dipole with distance (here seen from the side). The potential of the charges decreases (shown here by a fading intensity) and the two charges appear to merge, so their combined effect approaches zero more rapidly than by the distance effect alone.



22.9 The potential energy of interaction between two dipoles is the sum of the repulsions of like charges and the attractions of opposite charges. This illustration shows a collinear arrangement of dipoles.

(a) The potential energy of interaction

We show in the *Justification* below that the potential energy of interaction between a point dipole $\mu_1 = q_1 l$ and the point charge q_2 in the arrangement shown in Fig. 22.7 is

$$V = -\frac{\mu_1 q_2}{4\pi\epsilon_0 r^2} \quad (20)$$

With μ in coulomb-metres, q_2 in coulombs, and r in metres, V is obtained in joules. A point dipole is a dipole in which the separation between the charges is much smaller than the distance at which the dipole is being observed, $l \ll r$. This expression should be multiplied by $\cos \theta$ when the point charge lies at an angle θ to the axis of the dipole. The potential energy rises towards zero (the value at infinite separation of the charge and the dipole) more rapidly (as $1/r^2$) than that between two point charges (which varies as $1/r$) because, from the viewpoint of the point charge, the partial charges of the dipole seem to merge and cancel as the distance r increases (Fig. 22.8).

Justification 22.5

The sum of the potential energies of repulsion between like charges and attraction between opposite charges in the orientation shown in Fig. 22.7 is

$$V = \frac{1}{4\pi\epsilon_0} \left(-\frac{q_1 q_2}{r - \frac{1}{2}l} + \frac{q_1 q_2}{r + \frac{1}{2}l} \right)$$

Because $l \ll r$ for a point dipole, this expression can be simplified by writing

$$V = \frac{q_1 q_2}{4\pi\epsilon_0 r} \left(-\frac{1}{1-x} + \frac{1}{1+x} \right)$$

where $x = l/2r$, and then expanding the terms in x by using

$$\frac{1}{1+x} = 1 - x + x^2 - \dots \quad \frac{1}{1-x} = 1 + x + x^2 + \dots$$

and retaining only the leading term:

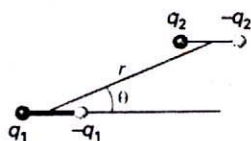
$$\begin{aligned} V &= \frac{q_1 q_2}{4\pi\epsilon_0 r} \{ -(1+x+\dots) + (1-x+\dots) \} \\ &\approx -\frac{2xq_1 q_2}{4\pi\epsilon_0 r} = -\frac{q_1 q_2 l}{4\pi\epsilon_0 r^2} \end{aligned}$$

With $\mu_1 = q_1 l$, this expression becomes eqn 20.

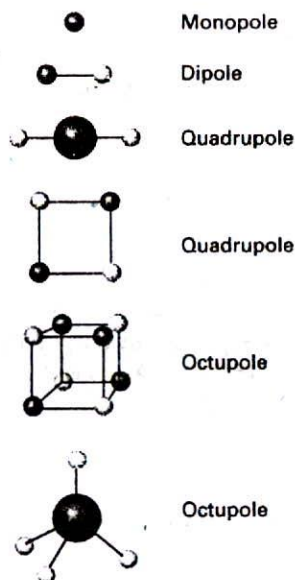
Example 22.2 Calculating the interaction energy of two dipoles

Calculate the potential energy of interaction of two dipoles in the arrangement shown in Fig. 22.9 when their separation is r .

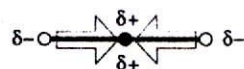
Method We proceed in exactly the same way as in the *Justification*, but now the total interaction energy is the sum of four pairwise terms: two attractions between opposite charges, which contribute negative terms to the potential energy, and two repulsions between like charges, which contribute positive terms.



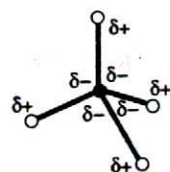
22.10 A parallel arrangement of electric dipoles.



22.11 Typical charge arrays corresponding to electric multipoles. The field arising from an arbitrary finite charge distribution can be expressed as the superposition of the fields arising from a superposition of multipoles.



5 Carbon dioxide



6 Methane

Answer The sum of the four contributions is

$$V = \frac{1}{4\pi\epsilon_0} \left(-\frac{q_1q_2}{r+l} + \frac{q_1q_2}{r} + \frac{q_1q_2}{r} - \frac{q_1q_2}{r-l} \right)$$

$$= -\frac{q_1q_2}{4\pi\epsilon_0 r} \left(\frac{1}{1+x} - 2 + \frac{1}{1-x} \right)$$

with $x = l/r$. As before, we expand the two terms in x and retain only the first surviving term, which is equal to $2x^2$. This step results in the expression

$$V = -\frac{2x^2q_1q_2}{4\pi\epsilon_0 r}$$

Therefore, because $\mu_1 = q_1l$ and $\mu_2 = q_2l$, the potential energy of interaction in the alignment shown in Fig. 22.9 is

$$V = -\frac{2\mu_1\mu_2}{4\pi\epsilon_0 r^3}$$

Comment Notice that the interaction energy approaches zero more rapidly (as $1/r^3$) than for the previous case: now both interacting entities appear neutral to each other at large separations.

Self-test 22.2 Derive an expression for the potential energy when the dipoles are in the arrangement shown in Fig. 22.10.

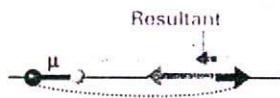
$$[V = (\mu_1\mu_2/4\pi\epsilon_0 r^3)(1 - 3\cos^2\theta)]$$

The various expressions for the interaction of charges and dipoles are summarized in Table 22.3. It is quite easy to extend the formulas given there to obtain expressions for the energy of interaction of higher multipoles, or arrays of point charges (Fig. 22.11). Specifically, an n -pole is an array of point charges with an n -pole moment but no lower moment. Thus, a monopole is a point charge, and the monopole moment is what we normally call the overall charge. A dipole, as we have seen, is an array of charges that has no monopole moment (no net charge). A quadrupole consists of an array of point charges that has neither net charge nor dipole moment (as for CO_2 molecules (5)). An octupole consists of an array of point charges that sum to zero and which has neither a dipole moment nor a quadrupole moment (as for CH_4 molecules (6)). The feature to remember is that the

Table 22.3 Multipole interaction potential energies

Interaction type	Distance dependence of potential energy	Typical energy/ (kJ mol ⁻¹)	Comment
Ion-ion	$1/r$	250	Only between ions
Ion-dipole	$1/r^2$	15	
Dipole-dipole	$1/r^3$	2	Between stationary polar molecules
	$1/r^6$	0.6	Between rotating polar molecules
London (dispersion)	$1/r^6$	2	Between all types of molecules

The energy of a hydrogen bond $\text{A-H}\cdots\text{B}$ is typically 20 kJ mol^{-1} and occurs on contact for $\text{A, B} = \text{N, O, or F}$.



22.12 The electric field of a dipole is the sum of the opposing fields from the positive and negative charges, each of which is proportional to $1/r^2$. The difference, the net field, is proportional to $1/r^3$.

interaction energy falls off more rapidly the higher the order of the multipole. For the interaction of an n -pole with an m -pole, the potential energy varies with distance as

$$V \propto \frac{1}{r^{n+m-1}} \quad (21)$$

The reason for the even steeper decrease with distance is the same as before: the array of charges appears to blend together into neutrality more rapidly with distance the higher the number of individual charges that contribute to the multipole. Note that a given molecule may have a charge distribution that corresponds to a superposition of several different multipoles.

(b) The electric field

The same kind of argument as that used to derive expressions for the potential energy can be used to establish the distance dependence of the strength of the electric field generated by a dipole. We shall need this expression when we calculate the dipole moment induced in one molecule by another.

The starting point for the calculation is the strength of the electric field⁹ generated by a point electric charge:

$$\mathcal{E} = \frac{q}{4\pi\epsilon_0 r^2} \quad (22)$$

The field generated by a dipole is the sum of the fields generated by each partial charge. For the point-dipole arrangement shown in Fig. 22.12, the same procedure that was used to derive the potential energy gives

$$\mathcal{E} = \frac{2\mu}{4\pi\epsilon_0 r^3} \quad (23)$$

The electric field of a multipole (in this case a dipole) decreases more rapidly with distance (as $1/r^3$ for a dipole) than that of a monopole (a point charge).

(c) Dipole-dipole interactions

The potential energy of interaction between two polar molecules is a complicated function of their relative orientation. When the two dipoles are parallel (as in Fig. 22.10), the potential energy is simply

$$V = \frac{\mu_1 \mu_2 f(\theta)}{4\pi\epsilon_0 r^3} \quad f(\theta) = 1 - 3 \cos^2 \theta \quad (24)$$

This expression applies to polar molecules in a fixed, parallel orientation in a solid.

In a fluid of freely rotating molecules, the interaction between dipoles averages to zero because f changes sign as the orientation changes, and its average value is zero. Physically, the like partial charges of two freely rotating molecules are close together as much as the two opposite charges, and the repulsion of the former is cancelled by the attraction of the latter.

The interaction energy of two freely rotating dipoles is zero. However, because their mutual potential energy depends on their relative orientation, the molecules do not in fact rotate completely freely, even in a gas. In fact, the lower energy orientations are marginally favoured, so there is a nonzero average interaction between polar molecules. We show in the

⁹ The electric field is actually a vector, and we cannot simply add and subtract magnitudes without taking into account the directions of the fields. In the cases we consider, this will not be a complication because the two charges of the dipoles will be collinear and give rise to fields in the same direction. Be careful, though, with more general arrangements of charges.

following *Justification* that the average potential energy of two rotating molecules that are separated by a distance r is

$$\langle V \rangle = -\frac{C}{r^6} \quad C = \frac{2\mu_1^2\mu_2^2}{3(4\pi\epsilon_0)^2 kT} \quad (25)$$

This expression describes the Keesom interaction.

Justification 22.6

The detailed calculation of the Keesom interaction energy is quite complicated, but the form of the final answer can be constructed quite simply. First, we note that the average interaction energy of two polar molecules rotating at a fixed separation r is given by

$$\langle V \rangle = \frac{\mu_1\mu_2\langle f \rangle}{4\pi\epsilon_0 r^3}$$

where $\langle f \rangle$ now includes a weighting factor in the averaging that is equal to the probability that a particular orientation will be adopted. This probability is given by the Boltzmann distribution $p \propto e^{-E/kT}$, with E interpreted as the potential energy of interaction of the two dipoles in that orientation. That is,

$$p \propto e^{-V/kT} \quad V = \frac{\mu_1\mu_2 f}{4\pi\epsilon_0 r^3}$$

When the potential energy of interaction of the two dipoles is very small compared with the energy of thermal motion, we can use $V \ll kT$, expand the exponential function in p , and retain only the first two terms:

$$p \propto 1 - \frac{V}{kT} + \dots$$

The weighted average of f is therefore

$$\langle f \rangle \propto \langle f \rangle_0 - \frac{\mu_1\mu_2}{4\pi\epsilon_0 kT r^3} \langle f^2 \rangle_0 \dots$$

where $\langle \dots \rangle_0$ denotes an unweighted spherical average. The average value of f is zero, so the first term vanishes. However, the average value of f^2 is nonzero because f^2 is positive at all orientations, so we can write

$$\langle V \rangle = -\frac{\mu_1^2\mu_2^2\langle f^2 \rangle_0}{(4\pi\epsilon_0)^2 kT r^6}$$

The average value $\langle f^2 \rangle_0$ is a number that we can expect to be close to 1 (because f^2 ranges from 0 to 4) and in fact turns out to be $\frac{2}{3}$ when the calculation is carried through in detail. The final result is that quoted in eqn 25.

The important features of eqn 25 are its negative sign (the average interaction is attractive), the dependence of the average interaction energy on the inverse sixth power of the separation, and its inverse dependence on the temperature. The last feature reflects the way that the greater thermal motion overcomes the mutual orientating effects of the dipoles at higher temperatures. The inverse sixth power arises from the inverse third power of the interaction potential energy that is weighted by the energy in the Boltzmann term, which is also proportional to the inverse third power of the separation.

At 25°C the average interaction energy for pairs of molecules with $\mu = 1$ D is about -0.07 kJ mol⁻¹ when the separation is 0.5 nm. This energy should be compared with the average molar kinetic energy of $\frac{3}{2}RT = 3.7$ kJ mol⁻¹ at the same temperature. The

interaction energy is much smaller than the energies involved in the making and breaking of chemical bonds.

(d) Dipole-induced-dipole interactions

A polar molecule with dipole moment μ_1 can induce a dipole μ_2^* in a neighbouring polarizable molecule. The induced dipole interacts with the permanent dipole of the first molecule, and the two are attracted together. It is shown in the *Justification* below that the average interaction energy when the separation of the molecules is r is¹⁰

$$V = -\frac{C}{r^6} \quad C = \frac{\mu_1^2 \alpha_2'}{\pi \epsilon_0} \quad (26)$$

where α_2' is the polarizability volume of molecule 2 and μ_1 is the permanent dipole moment of molecule 1.

Justification 22.7

The energy of interaction between a permanent dipole, μ_1 , and an induced dipole, μ_2^* , is given in Example 22.2:

$$V = -\frac{2\mu_1\mu_2^*}{4\pi\epsilon_0 r^3}$$

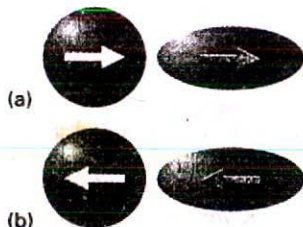
The induced dipole moment depends on the field generated by the polar molecule, and hence on the separation of the two molecules. Because we can write $\mu_2^* = \alpha_2 \mathcal{E}$, where α_2 is the polarizability of molecule 2 and \mathcal{E} is the field generated by molecule 1 (the polar molecule), the potential energy, is:

$$V = -\frac{2\mu_1\alpha_2\mathcal{E}}{4\pi\epsilon_0 r^3}$$

The electric field generated by the polar molecule is given by eqn 23, so:

$$V = -\left(\frac{2\mu_1\alpha_2}{4\pi\epsilon_0 r^3}\right)\left(\frac{2\mu_1}{4\pi\epsilon_0 r^3}\right) = -\frac{4\mu_1^2\alpha_2}{(4\pi\epsilon_0)^2 r^6}$$

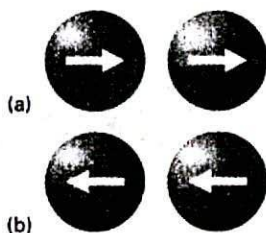
As the induced dipole follows the direction of the inducing dipole (Fig. 22.13), we do not need to take account of the effects of thermal motion: both dipoles remain aligned however fast the molecules tumble. Therefore, the interaction energy has approximately this value at all relative orientations. This expression rearranges into eqn 26 by noting that $\alpha_2' = \alpha_2/4\pi\epsilon_0$.



22.13 (a) A polar molecule (green arrow) can induce a dipole (white arrow) in a nonpolar molecule, and (b) the latter's orientation follows the former's, so the interaction does not average to zero.

The dipole-induced-dipole interaction energy is independent of the temperature because thermal motion has no effect on the averaging process. Moreover, like the dipole-dipole interaction, the potential energy depends on $1/r^6$: this distance dependence stems from the $1/r^3$ dependence of the field (and hence the magnitude of the induced dipole) and the $1/r^3$ dependence of the potential energy of interaction between the permanent and induced dipoles. For a molecule with $\mu = 1$ D (such as HCl) near a molecule of polarizability volume $\alpha' = 10 \times 10^{-30} \text{ m}^3$ (such as benzene, Table 22.1), the average interaction energy is about -0.8 kJ mol^{-1} when the separation is 0.3 nm.

10 Note that the C in this expression is different from the C in eqn 25 and other expressions below: we are using the same symbol in C/r^6 to emphasize the similarity of form of each expression.



22.14 (a) In the dispersion interaction, an instantaneous dipole on one molecule induces a dipole on another molecule, and the two dipoles then interact to lower the energy. (b) The two instantaneous dipoles are correlated and, although they occur in different orientations at different instants, the interaction does not average to zero.

(e) Induced-dipole–induced-dipole interactions

Nonpolar molecules (including closed-shell atoms, such as Ar) attract one another even though neither has a permanent dipole moment. The abundant evidence for the existence of interactions between them is the formation of condensed phases of nonpolar substances, such as the condensation of hydrogen or argon to a liquid at low temperatures and the fact that benzene is a liquid at normal temperatures.

The interaction between nonpolar molecules arises from the transient dipoles that all molecules possess as a result of fluctuations in the instantaneous positions of electrons. To appreciate the origin of the interaction, suppose that the electrons in one molecule flicker into an arrangement that gives the molecule an instantaneous dipole moment μ_1^* . This dipole generates an electric field that polarizes the other molecule, and induces in that molecule an instantaneous dipole moment μ_2^* . The two dipoles attract each other and the potential energy of the pair is lowered. Although the first molecule will go on to change the size and direction of its instantaneous dipole, the electron distribution of the second molecule will follow, that is, the two dipoles are correlated in direction (Fig. 22.14). Because of this correlation, the attraction between the two instantaneous dipoles does not average to zero, and gives rise to an induced-dipole–induced-dipole interaction. This interaction is called either the dispersion interaction or the London interaction (for Fritz London, who first described it).

Polar molecules also interact by a dispersion interaction: such molecules also possess instantaneous dipoles, the only difference being that the time average of each fluctuating dipole does not vanish, but corresponds to the permanent dipole. Such molecules therefore interact both through their permanent dipoles and through the correlated, instantaneous fluctuations in these dipoles.

The strength of the dispersion interaction depends on the polarizability of the first molecule because the instantaneous dipole moment μ_1^* depends on the looseness of the control that the nuclear charge exercises over the outer electrons. The strength of the interaction also depends on the polarizability of the second molecule, for that polarizability determines how readily a dipole can be induced by another molecule. The actual calculation of the dispersion interaction is quite involved, but a reasonable approximation to the interaction energy is given by the **London formula**:

$$V = -\frac{C}{r^6} \quad C = \frac{2}{3} \alpha_1' \alpha_2' \frac{I_1 I_2}{I_1 + I_2} \quad (27)$$

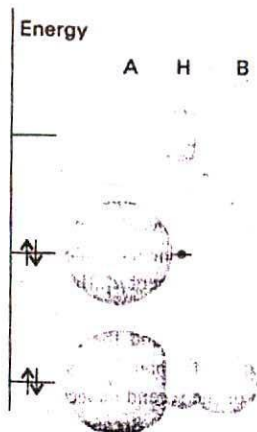
where I_1 and I_2 are the ionization energies of the two molecules (Table 13.4). This interaction energy is also proportional to the inverse sixth power of the separation of the molecules. The dispersion interaction generally dominates all the interactions between molecules other than hydrogen bonds.

Illustration

For two CH_4 molecules, we can substitute $\alpha' = 2.6 \times 10^{-30} \text{ m}^3$ and $I \approx 700 \text{ kJ mol}^{-1}$ to obtain $V = -2 \text{ kJ mol}^{-1}$ for $r = 0.3 \text{ nm}$. A very rough check on this figure is the enthalpy of vaporization of methane, which is 8.2 kJ mol^{-1} . However, this comparison is insecure, partly because the enthalpy of vaporization is a many-body quantity and partly because the long-distance assumption breaks down.

(f) Hydrogen bonding

The interactions described so far are universal in the sense that they are possessed by all molecules independent of their specific identity. However, there is a type of interaction



22.15 The molecular orbital interpretation of the formation of an $A-H \cdots B$ hydrogen bond. From the three A, H, and B orbitals, three molecular orbitals can be formed (their relative contributions are represented by the sizes of the spheres). Only the two lower energy orbitals are occupied, and there may therefore be a net lowering of energy compared with the separate AH and B species.

possessed by molecules that have a particular constitution. A hydrogen bond is an attractive interaction between two species that arises from a link of the form $A-H \cdots B$, where A and B are highly electronegative elements and B possesses a lone pair of electrons. Hydrogen bonding is conventionally regarded as being limited to N, O, and F but, if B is an anionic species (such as Cl^-), it may also participate in hydrogen bonding. There is no strict cut-off for an ability to participate in hydrogen bonding, but N, O, and F participate most effectively.

The formation of a hydrogen bond can be regarded as a particular example of delocalized molecular orbital formation in which A, H, and B each supply one atomic orbital from which three molecular orbitals are constructed (Fig. 22.15).¹¹ The A and H $1s$ orbitals are those used to form the $A-H$ bond in the AH molecule and the B orbital originally accommodates the lone pair on B. In the combined species, there are four electrons to accommodate (two from the $A-H$ bond, two from the lone pair of B), and they occupy the two lowest molecular orbitals of the AHB fragment. Because the uppermost (most antibonding) orbital is vacant, it is feasible for the net effect to be a lowering of energy, and hence the formation of a hydrogen bond.

In practice, the strength of the bond is found to be about 20 kJ mol^{-1} . Because the bonding depends on orbital overlap, it is virtually a contact-like interaction that is turned on when AH touches B and is zero as soon as the contact is broken. If hydrogen bonding is present, it dominates the other intermolecular interactions. The properties of liquid and solid water, for example, are dominated by the hydrogen bonding between H_2O molecules.

(g) The total attractive interaction

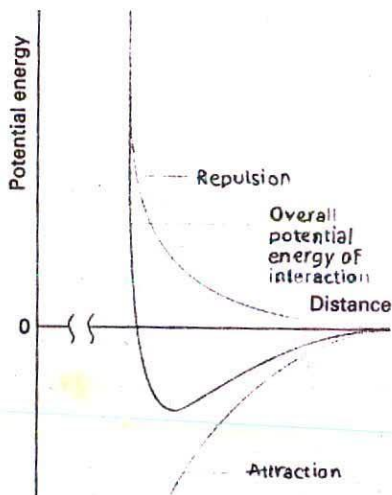
We shall consider molecules that are unable to participate in hydrogen bond formation. The total attractive interaction energy between rotating molecules is then the sum of the three van der Waals contributions discussed above. (Only the dispersion interaction contributes if both molecules are nonpolar.) In a fluid phase, all three contributions to the potential energy vary as the inverse sixth power of the separation of the molecules, so we may write

$$V = -\frac{C_6}{r^6} \quad (28)$$

where C_6 is a coefficient that depends on the identity of the molecules.

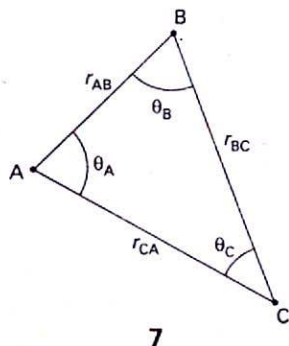
Although attractive interactions between molecules are often expressed as in eqn 28, we must remember that this equation has only limited validity. First, we have taken into account only dipolar interactions of various kinds, for they have the longest range and are dominant if the average separation of the molecules is large. However, in a complete treatment we should also consider quadrupolar and higher-order multipole interactions, particularly if the molecules do not have permanent electric dipole moments. Secondly, the expressions have been derived by assuming that the molecules can rotate reasonably freely. That is not the case in most solids, and in rigid media the dipole-dipole interaction is proportional to $1/r^3$ because the Boltzmann averaging procedure is irrelevant when the molecules are trapped into a fixed orientation.

A different kind of limitation is that eqn 28 relates to the interactions of pairs of molecules. There is no reason to suppose that the energy of interaction of three (or more) molecules is the sum of the pairwise interaction energies alone. The total dispersion energy



22.16 The general form of an intermolecular potential energy curve. At long range the interaction is attractive, but at close range the repulsions dominate.

¹¹ A purely electrostatic description, in which the partial positive charge of H interacts Coulombically with the partial negative charge of B, is an alternative model of hydrogen bonding.



of three closed-shell atoms, for instance, is given approximately by the Axilrod-Teller formula:

$$V = -\frac{C_6}{r_{AB}^6} - \frac{C_6}{r_{BC}^6} - \frac{C_6}{r_{CA}^6} + \frac{C'}{(r_{AB}r_{BC}r_{CA})^3} \quad (29a)$$

where

$$C' = a(3 \cos \theta_A \cos \theta_B \cos \theta_C + 1) \quad (29b)$$

The parameter a is approximately equal to $\frac{3}{4}\alpha' C_6$; the angles θ are the internal angles of the triangle formed by the three atoms (7). The term in C' (which represents the non-additivity of the pairwise interactions) is negative for a linear arrangement of atoms (so that arrangement is stabilized) and positive for an equilateral triangular cluster. It is found that the three-body term contributes about 10 per cent of the total interaction energy in liquid argon.

22.4 Repulsive and total interactions

When molecules are squeezed together, the nuclear and electronic repulsions and the rising electronic kinetic energy begin to dominate the attractive forces. The repulsions increase steeply with decreasing separation in a way that can be deduced only by very extensive, complicated molecular structure calculations of the kind described in Chapter 14 (Fig. 22.16).

In many cases, however, progress can be made by using a greatly simplified representation of the potential energy, where the details are ignored and the general features expressed by a few adjustable parameters. One such approximation is the **hard-sphere potential**, in which it is assumed that the potential energy rises abruptly to infinity as soon as the particles come within a separation d :

$$V = \infty \text{ for } r \leq d \quad V = 0 \text{ for } r > d \quad (30)$$

This very simple potential is surprisingly useful for assessing a number of properties. Another widely used approximation is the **Mie potential**:

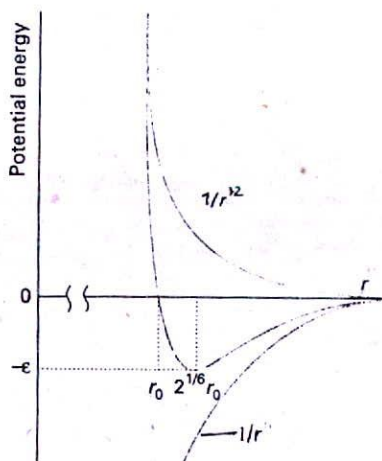
$$V = \frac{C_n}{r^n} - \frac{C_m}{r^m} \quad (31)$$

with $n > m$. The first term represents repulsions and the second term attractions. The **Lennard-Jones potential** is a special case of the Mie potential with $n = 12$ and $m = 6$ (Fig. 22.17); it is often written in the form

$$V = 4\epsilon \left\{ \left(\frac{r_0}{r} \right)^{12} - \left(\frac{r_0}{r} \right)^6 \right\} \quad (32)$$

The two parameters are ϵ , the depth of the well, and r_0 , the separation at which $V = 0$ (Table 22.4). The well minimum occurs at $r_e = 2^{1/6}r_0$. Although the Lennard-Jones potential has been used in many calculations, there is plenty of evidence to show that $1/r^{12}$ is a very poor representation of the repulsive potential, and that an exponential form, e^{-r/r_0} , is greatly superior. An exponential function is more faithful to the exponential decay of atomic wavefunctions at large distances, and hence to the overlap that is responsible for repulsion. The potential with an exponential repulsive term and a $1/r^6$ attractive term is known as an **exp-6 potential**. These potentials can be used to calculate the virial coefficients of gases, as explained in Section 20.5, and through them various properties of real gases, such as the Joule-Thompson coefficient. The potentials are also used to model the structures of condensed fluids.

Until recently, the potential energy of interaction of molecules was of primary interest. However, with the advent of atomic force microscopy (AFM), in which the force between a



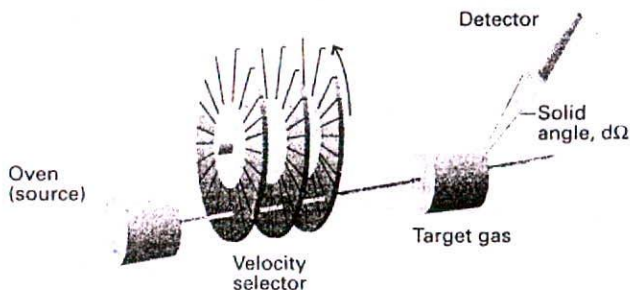
22.17 The Lennard-Jones potential, the relation of the parameters to the features of the curve, and the two contributions. Note that $2^{1/6} = 1.122\dots$

Table 22.4* Lennard-Jones (12, 6) parameters

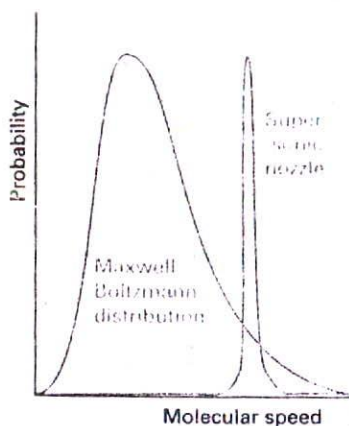
	$(\epsilon/k)/\text{K}$	r_0/pm
Ar	111.84	362.3
CCl ₄	376.86	624.1
N ₂	91.85	391.9
Xe	213.96	426.0

*More values are given in the Data section.

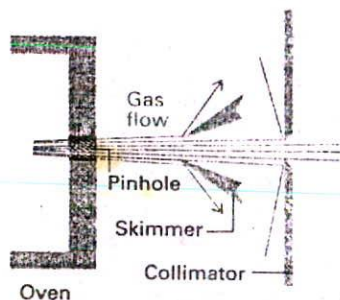
† ϵ is expressed as an effective temperature on division by Boltzmann's constant k .



22.18 The basic arrangement of a molecular beam apparatus. The atoms or molecules emerge from a heated source, and pass through the velocity selector, a train of rotating disks. The scattering occurs from the target gas (which might take the form of another beam), and the flux of particles entering the detector set at some angle is recorded.



22.19 The shift in the mean speed and the width of the distribution brought about by use of a supersonic nozzle.



22.20 A supersonic nozzle skims off some of the molecules of the jet and leads to a beam with well-defined velocity.

molecular sized probe and a surface is monitored (see Section 28.2f), force is moving back into the centre of attention. As force, F , is the negative slope of potential, for a Lennard-Jones potential between individual molecules

$$F = -\frac{dV}{dr} = \frac{24\varepsilon}{r_0} \left\{ 2\left(\frac{r_0}{r}\right)^{13} - \left(\frac{r_0}{r}\right)^7 \right\} \quad (33)$$

The net attractive force is greatest at $r = (26/7)^{1/6}r_0$, or $1.244r_0$, and at that distance is equal to $-144(7/26)^{7/6}\varepsilon/13r_0$, or $-2.397\varepsilon/r_0$. For typical parameters, the magnitude of this force is about 10 pN.

22.5 Molecular interactions in beams

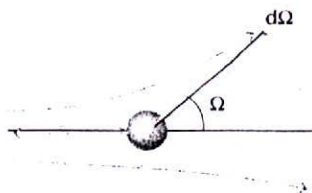
Intermolecular forces can be studied in **molecular beams**, which consist of a collimated, narrow stream of molecules travelling through an evacuated vessel. The beam is directed towards other molecules, and the scattering that occurs on impact is related to the intermolecular interactions.

(a) The basic principles

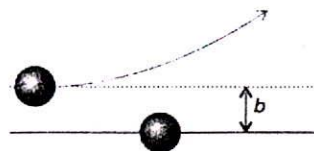
The basic arrangement for a molecular beam experiment is shown in Fig. 22.18. If the pressure of vapour in the source is increased so that the mean free path of the molecules in the emerging beam is much shorter than the diameter of the pinhole, many collisions take place even outside the source. The net effect of these collisions, which give rise to **hydrodynamic flow**, is to transfer momentum into the direction of the beam. The molecules in the beam then travel with very similar speeds, so further downstream few collisions take place between them. This condition is called **molecular flow**. Because the spread in speeds is so small, the molecules are **effectively** in a state of very low translational temperature (Fig. 22.19). The translational temperature may reach as low as 1 K. Such jets are called **supersonic** because the average speed of the molecules in the jet is much greater than the speed of sound for the molecules that are not part of the jet.

A supersonic jet can be converted into a more parallel supersonic beam if it is 'skimmed' in the region of hydrodynamic flow and the excess gas pumped away. A skimmer consists of a conical nozzle shaped to avoid any supersonic shock waves spreading back into the gas and so increasing the translational temperature (Fig. 22.20). A jet or beam may also be formed by using helium or neon as the principal gas, and injecting molecules of interest into it in the hydrodynamic region of flow.

The low translational temperature of the molecules is reflected in the low rotational and vibrational temperatures of the molecules. In this context, a rotational or vibrational



22.21 The definition of the solid angle, $d\Omega$, for scattering.

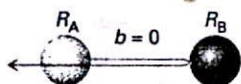


22.22 The definition of the impact parameter, b , as the perpendicular separation of the initial paths of the particles.

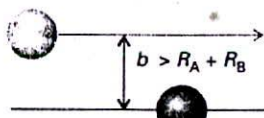
temperature means the temperature that should be used in the Boltzmann distribution to reproduce the observed populations of the states. However, as rotational modes equilibrate more slowly, and vibrational modes equilibrate even more slowly, the rotational and vibrational populations of the species correspond to somewhat higher temperatures, of the order of 10 K for rotation and 100 K for vibrations.

The target gas may be either a bulk sample or another molecular beam. The latter crossed beam technique gives a lot of information because the states of both the target and projectile molecules may be controlled. The intensity of the incident beam is measured by the incident beam flux, \mathcal{I} , which is the number of particles passing through a given area in a given interval divided by the area and the duration of the interval.

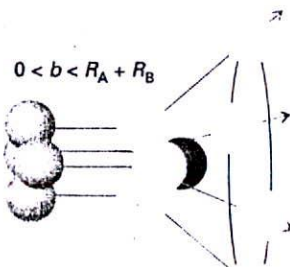
The detectors may consist of a chamber fitted with a sensitive pressure gauge, a bolometer, or an ionization detector, in which the incoming molecule is first ionized and then detected electronically. The state of the scattered molecules may also be determined spectroscopically, and is of interest when the collisions change their vibrational or rotational states.



(a)



(b)



(c)

22.23 Three typical cases for the collisions of two hard spheres: (a) $b = 0$, giving backward scattering; (b) $b > R_A + R_B$, giving forward scattering; (c) $0 < b < R_A + R_B$, leading to scattering into one direction on a ring of possibilities. (The target molecule is taken to be so heavy that it remains virtually stationary.)

(b) The experimental observations

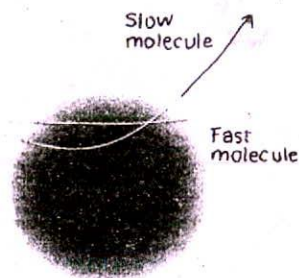
The primary experimental information from a molecular beam experiment is the fraction of the molecules in the incident beam that are scattered into a particular direction. The fraction is normally expressed in terms of $d\mathcal{I}$, the rate at which molecules are scattered into a cone that represents the area covered by the 'eye' of the detector (Fig. 22.21). This rate is reported as the differential scattering cross-section, σ , the constant of proportionality between the value of $d\mathcal{I}$ and the intensity, \mathcal{I} , of the incident beam, the number density of target molecules, \mathcal{N} , and the infinitesimal path length dx through the sample:

$$d\mathcal{I} = \sigma \mathcal{I} \mathcal{N} dx \quad (34)$$

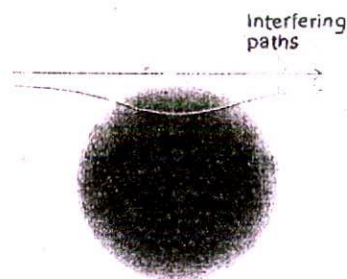
The value of σ (which has the dimensions of area) depends on the impact parameter, b , the initial perpendicular separation of the paths of the colliding molecules (Fig. 22.22), and the details of the intermolecular potential. The role of the impact parameter is most easily seen by considering the impact of two hard spheres (Fig. 22.23). If $b = 0$, the lighter projectile is on a trajectory that leads to a head-on collision, so the only scattering intensity is detected when the detector is at $\theta = \pi$. When the impact parameter is so great that the spheres do not make contact ($b > R_A + R_B$), there is no scattering and the scattering cross-section is zero at all angles except $\theta = 0$. Glancing blows, with $0 < b \leq R_A + R_B$, lead to scattering intensity in cones around the forward direction.

(c) Scattering effects

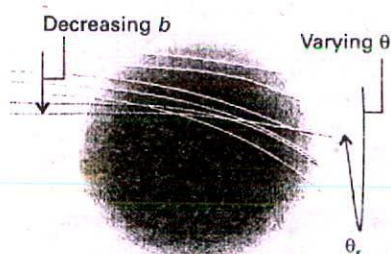
The scattering pattern of real molecules, which are not hard spheres, depends on the details of the intermolecular potential, including the anisotropy that is present when the molecules are non-spherical. The scattering also depends on the relative speed of approach of the two



22.24 The extent of scattering may depend on the relative speed of approach as well as the impact parameter. The dark central zone represents the repulsive core; the fuzzy outer zone represents the long-range attractive potential.



22.25 Two paths leading to the same destination will interfere quantum mechanically; in this case they give rise to quantum oscillations in the forward direction.



22.26 The interference of paths leading to rainbow scattering. The rainbow angle, θ_r , is the maximum scattering angle reached as b is decreased. Interference between the numerous paths at that angle modifies the scattering intensity markedly.

particles: a very fast particle might pass through the interaction region without much deflection, whereas a slower one on the same path might be temporarily captured and undergo considerable deflection (Fig. 22.24). The variation of the scattering cross-section with the relative speed of approach should therefore give information about the strength and range of the intermolecular potential.

A further point is that the outcome of collisions is determined by quantum, not classical, mechanics. The wave nature of the particles can be taken into account, at least to some extent, by drawing all classical trajectories that take the projectile particle from source to detector, and then considering the effects of interference between them.

Two quantum mechanical effects are of great importance. A particle with a certain impact parameter might approach the attractive region of the potential in such a way that the particle is deflected towards the repulsive core (Fig. 22.25), which then repels it out through the attractive region to continue its flight in the forward direction. Some molecules, however, also travel in the forward direction because they have impact parameters so large that they are undeflected. The wavefunctions of the particles that take the two types of path interfere, and the intensity in the forward direction is modified. The effect is called **quantum oscillation**. The same phenomenon accounts for the optical 'glory effect', in which a bright halo can sometimes be seen surrounding an illuminated object. (The coloured rings around the shadow of an aircraft cast on clouds by the sun, and often seen in flight, is an example of an optical glory.)

The second quantum effect we need consider is the observation of a strongly enhanced scattering in a nonforward direction. This effect is called **rainbow scattering** because the same mechanism accounts for the appearance of an optical rainbow. The origin of the phenomenon is illustrated in Fig. 22.26. As the impact parameter decreases, there comes a stage at which the scattering angle passes through a maximum and the interference between the paths results in a strongly scattered beam. The rainbow angle, θ_r , is the angle for which $d\theta/db = 0$ and the scattering is strong.

Another phenomenon that can occur in certain beams is the capturing of one species by another. The vibrational temperature in supersonic beams is so low that **van der Waals molecules** may be formed, which are complexes of the form AB in which A and B are held together by van der Waals forces or hydrogen bonds. Large numbers of such molecules have been studied spectroscopically, including ArHCl , $(\text{HCl})_2$, ArCO_2 , and $(\text{H}_2\text{O})_2$. More recently, van der Waals clusters of water molecules have been pursued as far as $(\text{H}_2\text{O})_6$. The study of their spectroscopic properties gives detailed information about the intermolecular potentials involved.

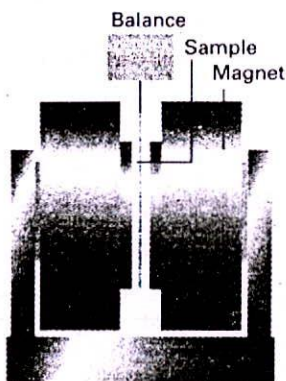
Magnetic properties

The magnetic and electric properties of molecules are analogous. For instance, some molecules possess permanent magnetic dipole moments, and an applied magnetic field can induce a magnetic moment.

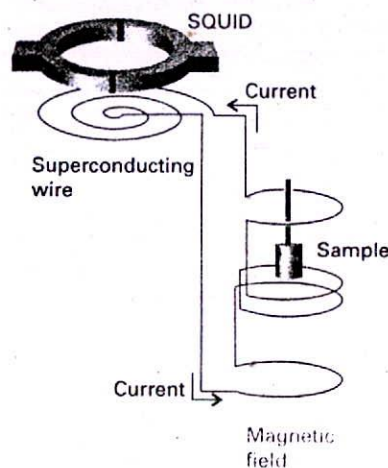
22.6 Magnetic susceptibility

The analogue of the electric polarization, P , is the magnetization, M , the average molecular magnetic dipole moment multiplied by the number density of molecules in the sample. The magnetization induced by a field of strength \mathcal{H} is proportional to \mathcal{H} , and we write

$$M = \chi\mathcal{H}$$



22.27 The arrangement of the Gouy balance for measuring magnetic susceptibilities. A paramagnetic sample appears to weigh more and a diamagnetic sample appears to weigh less, when the magnetic field is on. In a modern alternative version (not shown), a sensitive balance is used to measure the force exerted by the sample on a suspended permanent magnet.



22.28 The arrangement used to measure magnetic susceptibility by using a SQUID. The sample is moved upwards in small increments and the potential difference across the SQUID is monitored.

Table 22.5* Magnetic susceptibilities at 289 K

	$\chi/10^{-6}$	$\chi_m/(10^{-5} \text{ cm}^3 \text{ mol}^{-1})$
H ₂ O(l)	-90	-160
NaCl(s)	-13.9	-38
Cu(s)	-9.6	-6.8
CuSO ₄ ·5H ₂ O(s)	+176	+1930

* More values are given in the Data section.

where χ is the dimensionless volume magnetic susceptibility. A closely related quantity is the molar magnetic susceptibility, χ_m :

$$\chi_m = \chi V_m \quad [36]$$

where V_m is the molar volume of the substance (we shall soon see why it is sensible to introduce this quantity). The magnetic flux density, B , is related to the applied field strength and the magnetization by

$$B = \mu_0(\mathcal{H} + M) = \mu_0(1 + \chi)H \quad [37]$$

where μ_0 is the vacuum permeability:

$$\mu_0 = 4\pi \times 10^{-7} \text{ J C}^{-2} \text{ m}^{-1} \text{ s}^2 \quad [38]$$

The magnetic flux density can be thought of as the density of magnetic lines of force permeating the medium. This density is increased if M adds to \mathcal{H} (when $\chi > 0$), but the density is decreased if M opposes \mathcal{H} (when $\chi < 0$). Materials for which χ is positive are called paramagnetic. Those for which χ is negative are called diamagnetic.

Just as polar molecules contribute a term proportional to $\mu^2/3kT$ to the electric polarization of a medium, so molecules with a permanent magnetic dipole moment of magnitude m contribute to the magnetization an amount proportional to $m^2/3kT$. An applied field can also induce a magnetic moment to an extent determined by the magnetizability, ξ (xi), of the molecules, and the magnetic analogue of eqn 16 is

$$\chi = \mathcal{N}\mu_0 \left(\xi + \frac{m^2}{3kT} \right) \quad [39]$$

We can now see why it is convenient to introduce χ_m , for the product of the number density \mathcal{N} and the molar volume is the Avogadro constant, N_A :

$$\mathcal{N}V_m = \frac{NV_m}{V} = \frac{nN_A V_m}{nV_m} = N_A \quad [40]$$

Hence

$$\chi_m = N_A \mu_0 \left(\xi + \frac{m^2}{3kT} \right) \quad [41]$$

and the density dependence of the susceptibility (which occurs in eqn 39 via $\mathcal{N} = N_A \rho/M$) has been eliminated. The expression for χ_m is in agreement with the empirical Curie law:

$$\chi_m = A + \frac{C}{T} \quad [42]$$

with $A = N_A \mu_0 \xi$ and $C = N_A \mu_0 m^2/3k$.

The magnetic susceptibility is traditionally measured with a Gouy balance. This instrument consists of a sensitive balance from which the sample hangs in the form of a narrow cylinder (Fig. 22.27) and lies between the poles of a magnet. If the sample is paramagnetic, it is drawn into the field, and its apparent weight is greater than when the field is off. A diamagnetic sample tends to be expelled from the field and appears to weigh less when the field is turned on. The balance is normally calibrated against a sample of known susceptibility. The modern version of the determination makes use of a superconducting quantum interference device (SQUID, Fig. 22.28).

Some experimental values are listed in Table 22.5; a typical paramagnetic volume susceptibility is about 10^{-3} , and a typical diamagnetic volume susceptibility is about $(-1)10^{-5}$. The permanent magnetic moment can be extracted from susceptibility measurements by plotting χ against $1/T$.

22.7 The permanent magnetic moment

The permanent magnetic moment of a molecule arises from any unpaired electron spins in the molecule. We saw in Section 13.10a that the magnitude of the magnetic moment of an electron is proportional to the magnitude of the spin angular momentum, $\{s(s+1)\}^{1/2}\hbar$.

$$m = g_e \{s(s+1)\}^{1/2} \mu_B \quad \mu_B = \frac{e\hbar}{2m_e} \quad (43)$$

where $g_e = 2.0023$. If there are several electron spins in each molecule, they combine to a total spin S , and then $s(s+1)$ should be replaced by $S(S+1)$. It follows that the spin contribution to the molar magnetic susceptibility is

$$\chi_m = \frac{N_A g_e^2 \mu_0 \mu_B^2 S(S+1)}{3kT} \quad (44)$$

This expression shows that the susceptibility is positive, so the spin magnetic moments contribute to the paramagnetic susceptibilities of materials. The contribution decreases with increasing temperature because the thermal motion randomizes the spin orientations. In practice, a contribution to the paramagnetism also arises from the orbital angular momenta of electrons: we have discussed the spin-only contribution.

Illustration

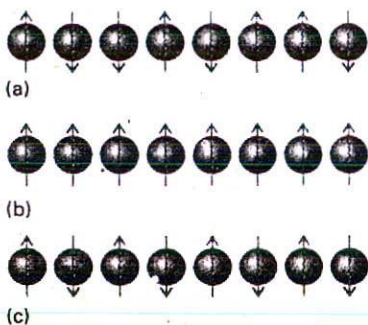
Consider a complex salt with three unpaired electrons per complex cation at 298 K, of mass density 3.24 g cm^{-3} , and molar mass 200 g mol^{-1} . First note that

$$\frac{N_A g_e^2 \mu_0 \mu_B^2}{3k} = 6.3001 \text{ cm}^3 \text{ K}^{-1} \text{ mol}^{-1}$$

Consequently,

$$\chi_m = 6.3001 \times \frac{S(S+1)}{T/\text{K}} \text{ cm}^3 \text{ mol}^{-1}$$

Substitution of the data with $S = \frac{3}{2}$ gives $\chi_m = 7.9 \times 10^{-2} \text{ cm}^3 \text{ mol}^{-1}$. Note that the density is not needed at this stage. To obtain the volume magnetic susceptibility, the molar susceptibility is divided by the molar volume $V_m = M/\rho$, where ρ is the mass density. In this illustration, $V_m = 61.7 \text{ cm}^3 \text{ mol}^{-1}$, so $\chi = 1.3 \times 10^{-3}$.



22.29 (a) In a paramagnetic material, the electron spins are aligned at random in the absence of an applied magnetic field. (b) In a ferromagnetic material, the electron spins are locked into a parallel alignment over large domains. (c) In an antiferromagnetic material, the electron spins are locked into an antiparallel arrangement. The latter two arrangements survive even in the absence of an applied field.

At low temperatures, some paramagnetic solids make a phase transition to a state in which large domains of spins align with parallel orientations. This cooperative alignment gives rise to a very strong magnetization and is called **ferromagnetism** (Fig. 22.29). In other cases, the cooperative effect leads to alternating spin orientations: the spins are locked into a low-magnetization arrangement to give an **antiferromagnetic phase**. The ferromagnetic phase has a nonzero magnetization in the absence of an applied field, but the antiferromagnetic phase has a zero magnetization because the spin magnetic moments cancel. The ferromagnetic transition occurs at the **Curie temperature**, and the antiferromagnetic transition occurs at the **Néel temperature**.

22.8 Induced magnetic moments

An applied magnetic field induces the circulation of electronic currents. These currents give rise to a magnetic field which usually opposes the applied field, so the substance is diamagnetic. In a few cases the induced field augments the applied field, and the substance is then paramagnetic.

The great majority of molecules with no unpaired electron spins are diamagnetic. In these cases, the induced electron currents occur within the orbitals of the molecule that are

occupied in its ground state. In the few cases in which molecules are paramagnetic despite having no unpaired electrons, the induced electron currents flow in the opposite direction because they can make use of unoccupied orbitals that lie close to the HOMO in energy. This orbital paramagnetism can be distinguished from spin paramagnetism by the fact that it is temperature-independent: this is why the property is called temperature-independent paramagnetism (TIP).

We can summarize these remarks as follows. All molecules have a diamagnetic component to their susceptibility, but it is dominated by spin paramagnetism if the molecules have unpaired electrons. In a few cases (where there are low-lying excited states) TIP is strong enough to make the molecules paramagnetic even though their electrons are paired.

Checklist of key ideas

Electric properties

22.1 Permanent and induced electric dipole moments

- electric dipole
- electric dipole moment
- polar molecule
- polarization
- dielectric
- ferroelectric solid
- homopolar contribution
- Langevin function (6)
- induced dipole moment
- polarizability
- hyperpolarizability
- polarizability volume (10)
- orientation polarization
- distortion polarization
- electronic polarizability
- permittivity
- relative permittivity
- Debye equation (15)
- molar polarization (16)
- Clausius-Mossotti equation (17)

22.2 Refractive index

- refractive index (18)
- dispersion
- optically active
- circularly birefringent
- optical rotatory dispersion (ORD)
- circular dichroism (CD)

Intermolecular forces

- van der Waals forces

22.3 Interactions between dipoles

- point dipole
- multipole
- n -pole
- Keesom interaction (25)
- dispersion interaction
- London interaction
- London formula (27)
- hydrogen bond
- Axilrod-Teller formula (29)

22.4 Repulsive and total interactions

- hard-sphere potential (30)

- Mie potential (31)
- Lennard-Jones potential (32)
- exp-6 potential
- atomic force microscopy (AFM)

22.5 Molecular interactions in beams

- molecular beam
- hydrodynamic flow
- molecular flow
- supersonic jet
- supersonic beam
- crossed beam technique
- incident beam flux
- differential scattering cross-section
- impact parameter
- quantum oscillation
- rainbow scattering
- rainbow angle
- van der Waals molecule

Magnetic properties

- 22.6 Magnetic susceptibility
- magnetization

- volume magnetic susceptibility
- molar magnetic susceptibility
- magnetic flux density
- vacuum permeability (38)
- paramagnetic
- diamagnetic
- magnetizability
- Curie law (42)
- Gouy balance
- superconducting quantum interference device (SQUID)

22.7 The permanent magnetic moment

- spin-only contribution
- ferromagnetism
- antiferromagnetic phase
- Curie temperature
- Néel temperature

22.8 Induced magnetic moments

- temperature-independent paramagnetism (TIP)

Further reading

Articles of general interest

C.E. Dykstra, Electrical polarization in diatomic molecules. *J. Chem. Educ.* **65**, 198 (1988).

P. Hobza and R. Zahradnik, Intermolecular interactions between medium-sized systems. Nonempirical and empirical calculations of interaction energies: successes and failures. *Chem. Rev.* **88**, 871 (1988).

G. Chalasinski and M. Gutowski, Weak interactions between small systems. Models for studying the nature of intermolecular forces and challenging problems for *ab initio* calculations. *Chem. Rev.* **88**, 943 (1988).

A.D. Buckingham, P.W. Fowler, and J.M. Hutson, Theoretical studies of van der Waals molecules and intermolecular forces. *Chem. Rev.* **88**, 963 (1988).

- F. Caudros, I. Cachadiña, and W. Ahamuda, Determination of Lennard-Jones interaction parameters using a new procedure. *Molec. Engineering* 6, 319 (1996).
- F. Cuadros, A. Mulero, and P. Rubio, The perturbative theories of fluids as a modern version of van der Waals theory. *J. Chem. Educ.* 71, 956 (1994).
- H. Guerin, Influence of the well width on the third virial coefficient of the square-well intermolecular potential. *J. Chem. Educ.* 69, 203 (1992).
- J.-L. Barrat and M.L. Klein, Molecular dynamics simulations of supercooled liquids near the glass transition. *Ann. Rev. Phys. Chem.* 42, 23 (1991).
- A. Gelessus, W. Thiel, and W. Weber, Multipoles and symmetry. *J. Chem. Educ.* 72, 505 (1995).
- L.N. Mulay and I.L. Mulay, Static magnetic techniques and applications. In *Techniques of chemistry* (ed. B.W. Rossiter and J.E. Hamilton), IIB, 133 (1989).
- W.E. Hatfield, Magnetic measurements. In *Solid-state chemistry: techniques* (ed. A.K. Cheetham and P. Day). Clarendon Press, Oxford (1987).
- C.E. Dykstra, Intermolecular electrical interaction: a key ingredient in hydrogen bonding. *Acc. Chem. Res.* 21, 355 (1988).
- J. Israelachvili, Solvation forces and liquid structure, as probed by direct force measurements. *Acc. Chem. Res.* 20, 415 (1987).
- J.M. Hunter and M.F. Jarrold, Molecular and atomic clusters. In *Encyclopedia of applied physics* (ed. G.L. Trigg), 10, 411. VCH, New York (1994).
- C.D. Graham, Jr., Magnetic materials. In *Encyclopedia of applied physics* (ed. G.L. Trigg), 9, 1. VCH, New York (1994).
- LM. Falicov, Diamagnetism. In *Encyclopedia of applied physics* (ed. G.L. Trigg), 4, 557. VCH, New York (1992).
- Y. Yafet, Paramagnetism. In *Encyclopedia of applied physics* (ed. G.L. Trigg), 13, 101. VCH, New York (1995).
- S. Foner, Measurement of magnetic properties and quantities. In *Encyclopedia of applied physics* (ed. G.L. Trigg), 9, 463. VCH, New York (1994).

Texts and sources of data and information

- J. Israelachvili, *Intermolecular and surface forces*. Academic Press, New York (1985).
- C.P. Smyth, Determination of dipole moments. In *Techniques of chemistry* (ed. A. Weissberger and B.W. Rossiter), 4, 351. Wiley-Interscience, New York (1972).
- M. Rigby, E.B. Smith, W.A. Wakeham, and G.C. Maitland, *The forces between molecules*. Oxford University Press (1986).
- G.C. Maitland, M. Rigby, E.B. Smith, and W.A. Wakeham, *Intermolecular forces: their origin and determination*. Clarendon Press, Oxford (1981).
- M.A.D. Fluendy and K.P. Lawley, *Molecular beams in chemistry*. Chapman & Hall, London (1973).
- E.A.V. Ebsworth, D.W.H. Rankin, and S. Craddock, *Structural methods in inorganic chemistry*. Blackwell Scientific, Oxford (1991).
- R. Drago, *Physical methods for chemists*. Saunders, Philadelphia (1992).

Exercises

- 22.1 (a) Which of the following molecules may be polar: ClF_3 , O_3 , H_2O_2 ?
- 22.1 (b) Which of the following molecules may be polar: SO_3 , XeF_4 , SF_4 ?
- 22.2 (a) The molar polarization of fluorobenzene vapour varies linearly with T^{-1} , and is $70.62 \text{ cm}^3 \text{ mol}^{-1}$ at 351.0 K and $62.47 \text{ cm}^3 \text{ mol}^{-1}$ at 423.2 K . Calculate the polarizability and dipole moment of the molecule.
- 22.2 (b) The molar polarization of the vapour of a compound was found to vary linearly with T^{-1} , and is $75.74 \text{ cm}^3 \text{ mol}^{-1}$ at 320.0 K and $71.43 \text{ cm}^3 \text{ mol}^{-1}$ at 421.7 K . Calculate the polarizability and dipole moment of the molecule.
- 22.3 (a) At 0°C , the molar polarization of liquid chlorine trifluoride is $27.18 \text{ cm}^3 \text{ mol}^{-1}$ and its density is 1.89 g cm^{-3} . Calculate the relative permittivity of the liquid.
- 22.3 (b) At 0°C , the molar polarization of a liquid is $32.16 \text{ cm}^3 \text{ mol}^{-1}$ and its density is 1.92 g cm^{-3} . Calculate the relative permittivity of the liquid. Take $M = 85.0 \text{ g mol}^{-1}$.
- 22.4 (a) The refractive index of CH_2I_2 is 1.732 for 656 nm light. Its density at 20°C is 3.32 g cm^{-3} . Calculate the polarizability of the molecule at this wavelength.
- 22.4 (b) The refractive index of a compound is 1.622 for 643 nm light. Its density at 20°C is 2.99 g cm^{-3} . Calculate the polarizability of the molecule at this wavelength. Take $M = 65.5 \text{ g mol}^{-1}$.
- 22.5 (a) The dipole moments of the bonds $\text{C}-\text{O}$ and $\text{C}=\text{O}$ are 1.2 and 2.7 D, respectively. The bond lengths are 143 and 122 pm, respectively. Estimate the percentage ionic character of the bonds. How well do the results correlate with the electronegativity differences of the atoms in the bonds?
- 22.5 (b) The dipole moments of the bonds $\text{C}-\text{F}$ and $\text{C}-\text{O}$ are 1.4 and 1.2 D, respectively. The bond lengths are 141 and 143 pm,

respectively. Estimate the percentage ionic character of the bonds. How well do the results correlate with the electronegativity differences of the atoms in the bonds?

22.6 (a) The electric dipole moment of toluene (methylbenzene) is 0.4 D. Estimate the dipole moments of the three xylenes (dimethylbenzene). Which answer can you be sure about?

22.6 (b) Calculate the resultant of two dipole moments of magnitude 1.5 D and 0.80 D that make an angle of 109.5° to each other.

22.7 (a) Calculate the magnitude and direction of the dipole moment of the following arrangement of charges in the xy -plane: $3e$ at (0, 0), $-e$ at (0.32 nm, 0), and $-2e$ at an angle of 20° from the x -axis and a distance of 0.23 nm from the origin.

22.7 (b) Calculate the magnitude and direction of the dipole moment of the following arrangement of charges in the xy -plane: $4e$ at (0, 0), $-2e$ at (162 pm, 0), and $-2e$ at an angle of 30° from the x -axis and a distance of 143 pm from the origin.

22.8 (a) The polarizability volume of H_2O is $1.48 \times 10^{-24} \text{ cm}^3$; calculate the dipole moment of the molecule (in addition to the permanent dipole moment) induced by an applied electric field of strength 1.0 kV m^{-1} .

22.8 (b) The polarizability volume of NH_3 is $2.22 \times 10^{-30} \text{ m}^3$; calculate the dipole moment of the molecule (in addition to the permanent dipole moment) induced by an applied electric field of strength 15.0 kV m^{-1} .

22.9 (a) The polarizability volume of H_2O at optical frequencies is $1.5 \times 10^{-24} \text{ cm}^3$; estimate the refractive index of water. The experimental value is 1.33; what may be the origin of the discrepancy?

22.9 (b) The polarizability volume of a liquid of molar mass 72.3 g mol^{-1} and density 865 kg mol^{-1} at optical frequencies is $2.2 \times 10^{-30} \text{ m}^3$; estimate the refractive index of the liquid.

22.10 (a) The dipole moment of chlorobenzene is 1.57 D and its polarizability volume is $1.23 \times 10^{-23} \text{ cm}^3$. Estimate its relative permittivity at 25°C , when its density is 1.173 g cm^{-3} .

22.10 (b) The dipole moment of bromobenzene is $5.17 \times 10^{-30} \text{ C m}$ and its polarizability volume is approximately $1.5 \times 10^{-29} \text{ m}^3$. Estimate its relative permittivity at 25°C , when its density is 1491 kg m^{-3} .

22.11 (a) A solution of an optically active substance shows an optical rotation of 250° in a cell of length 10 cm at 500 nm. What is the difference of the refractive indices of left and right circularly polarized light through this substance?

22.11 (b) A solution of an optically active substance shows an optical rotation of 192° in a cell of length 15 cm at 450 nm. What is the difference of the refractive indices of left and right circularly polarized light through this substance?

22.12 (a) The magnetic moment of CrCl_3 is $3.81 \mu_B$. How many unpaired electrons does the Cr possess?

22.12 (b) The magnetic moment of Mn^{2+} in its complexes is typically $5.3 \mu_B$. How many unpaired electrons does the ion possess?

22.13 (a) Calculate the molar susceptibility of benzene given that its volume susceptibility is -7.2×10^{-7} and its density 0.879 g cm^{-3} at 25°C .

22.13 (b) Calculate the molar susceptibility of cyclohexane given that its volume susceptibility is -7.9×10^{-7} and its density 811 kg m^{-3} at 25°C .

22.14 (a) According to Lewis theory, an O_2 molecule should be diamagnetic. However, experimentally it is found that $\chi_m/(\text{m}^3 \text{ mol}^{-1}) = (1.22 \times 10^{-5} \text{ K})/T$. Determine the number of unpaired spins in O_2 . How is the problem of the Lewis structure resolved?

22.14 (b) Predict the molar susceptibility of nitrogen dioxide at 298 K. Why does the molar susceptibility of a sample of nitrogen dioxide gas decrease as it is compressed?

22.15 (a) Data on a single crystal of MnF_2 give $\chi_m = 0.1463 \text{ cm}^3 \text{ mol}^{-1}$ at 294.53 K. Determine the effective number of unpaired electrons in this compound and compare your result with the theoretical value.

22.15 (b) Data on a single crystal of $\text{NiSO}_4 \cdot 7H_2O$ give $\chi_m = 6.00 \times 10^{-8} \text{ m}^3 \text{ mol}^{-1}$ at 298 K. Determine the effective number of unpaired electrons in this compound and compare your result with the theoretical value.

22.16 (a) Estimate the spin-only molar susceptibility of $\text{CuSO}_4 \cdot 5H_2O$ at 25°C .

22.16 (b) Estimate the spin-only molar susceptibility of $\text{MnSO}_4 \cdot 4H_2O$ at 298 K.

22.17 (a) Approximately how large must the magnetic induction, B , be for the orientational energy of an $S = 1$ system to be comparable to kT at 298 K?

22.17 (b) Estimate the ratio of populations of the M_S states of a system with $S = 1$ in 15.0 T at 298 K.

Problems

Numerical problems

22.1 Suppose an H_2O molecule ($\mu = 1.85 \text{ D}$) approaches an anion. What is the favourable orientation of the molecule? Calculate the electric field (in volts per metre) experienced by the anion when the water dipole is (a) 1.0 nm, (b) 0.3 nm, (c) 30 nm from the ion.

22.2 An H_2O molecule is aligned by an external electric field of strength 1.0 kV m^{-1} and an Ar atom ($\alpha' = 1.66 \times 10^{-24} \text{ cm}^3$) is brought up slowly from one side. At what separation is it energetically favourable for the H_2O molecule to flip over and point towards the approaching Ar atom?

22.3 The relative permittivity of chloroform was measured over a range of temperatures with the following results:

$\theta/^\circ\text{C}$	-80	-70	-60	-40	-20	0	20
ϵ_r	3.1	3.1	7.0	6.5	6.0	5.5	5.0
$\rho/(\text{g cm}^{-3})$	1.65	1.64	1.64	1.61	1.57	1.53	1.50

The freezing point of chloroform is -64°C . Account for these results and calculate the dipole moment and polarizability volume of the molecule.

22.4 The relative permittivities of methanol (m.p. -95°C) corrected for density variation are given below. What molecular information can be deduced from these values? Take $\rho = 0.791 \text{ g cm}^{-3}$ at 20°C .

$\theta/^\circ\text{C}$	-185	-170	-150	-140	-110	-80	-50	-20	0	20
ϵ_r	3.2	3.6	4.0	5.1	67	57	49	43	38	34

22.5 In his classic book *Polar molecules*, Debye reports some early measurements of the polarizability of ammonia. From the selection below, determine the dipole moment and the polarizability volume of the molecule.

T/K	292.2	309.0	333.0	387.0	413.0	446.0
$P_m/(\text{cm}^3 \text{ mol}^{-1})$	57.57	55.01	51.22	44.99	42.51	39.59

The refractive index of ammonia at 273 K and 100 kPa is 1.000379 (for yellow sodium light). Calculate the molar polarizability of the gas at this temperature and at 292.2 K. Combine the value calculated with the static molar polarizability at 292.2 K and deduce from this information alone the molecular dipole moment.

22.6 Values of the molar polarization of gaseous water at 100 kPa as determined from capacitance measurements are given below as a function of temperature.

T/K	384.3	420.1	444.7	484.1	522.0
$P_m/(\text{cm}^3 \text{ mol}^{-1})$	57.4	53.5	50.1	46.8	43.1

Calculate the dipole moment of H_2O and its polarizability volume.

Theoretical problems

22.7 Calculate the potential energy of the interaction between two linear quadrupoles when they are (a) collinear, (b) parallel and separated by a distance r .

22.8 Show that, in a gas (for which the refractive index is close to 1), the refractive index depends on the pressure as $n_r = 1 + \text{const} \times p$, and find the constant of proportionality. Go on to show how to deduce the polarizability volume of a molecule from measurements of the refractive index of a gaseous sample.

22.9 The refractive index of benzene is constant (at 1.51) from 0.4 GHz up to 0.55 GHz (in the microwave region of the spectrum), but then shows a series of oscillations between 1.47 and 1.54. Throughout the same frequency range, methylbenzene shows a higher refractive index (about 1.55), the same oscillations as in benzene, and additional oscillations between 1.52 and 1.56 near 0.4 GHz. Account for these observations.

22.10 Acetic acid vapour contains a proportion of planar, hydrogen-bonded dimers. The relative permittivity of pure liquid acetic acid is 7.14 at 290 K and increases with increasing temperature. Suggest an interpretation of the latter observation. What effect should

isothermal dilution have on the relative permittivity of solutions of acetic acid in benzene?

22.11 Show that the mean interaction energy of N atoms of diameter d interacting with a potential energy of the form C_6/R^6 is given by $U = -2N^2C_6/3Vd^3$, where V is the volume in which the molecules are confined and all effects of clustering are ignored. Hence, find a connection between the van der Waals parameter a and C_6 from $n^2a/V^2 = (\partial U/\partial V)_T$.

22.12 Suppose the repulsive term in a Lennard-Jones (12,6) potential is replaced by an exponential function of the form $e^{-r/d}$. Sketch the form of the potential energy and locate the distance at which it is a minimum.

22.13 The cohesive energy density, \mathcal{U} , is defined as \bar{U}/V , where \bar{U} is the mean potential energy of attraction within the sample and V its volume. Show that $\mathcal{U} = -\frac{1}{2}N^2 \int V(R) dr$, where N is the number density of the molecules and $V(R)$ is their attractive potential energy and where the integration ranges from d to infinity and over all angles. Go on to show that the cohesive energy density of a uniform distribution of molecules that interact by a van der Waals attraction of the form $-C_6/R^6$ is equal to $(2\pi/3)(N_A^2/d^3M^2)\rho^2C_6$, where ρ is the mass density of the solid sample and M is the molar mass of the molecules.

22.14 Consider the collision between a hard-sphere molecule of radius R_1 and mass m , and an infinitely massive impenetrable sphere of radius R_2 . Plot the scattering angle θ as a function of the impact parameter b . Carry out the calculation using simple geometrical considerations.

22.15 The dependence of the scattering characteristics of atoms on the energy of the collision can be modelled as follows. We suppose that the two colliding atoms behave as impenetrable spheres, as in Problem 22.14, but that the effective radius of the heavy atom depends on the speed v of the light atom. Suppose its effective radius depends on v as R_2e^{-v/v^*} , where v^* is a constant. Take $R_1 = \frac{1}{2}R_2$ for simplicity and an impact parameter $b = \frac{1}{2}R_2$, and plot the scattering angle as a function of (a) speed, (b) kinetic energy of approach.

22.16 The magnetizability, ξ , and the volume and molar magnetic susceptibilities can be calculated from the wavefunctions of molecules. For instance, the magnetizability of a hydrogenic atom is given by the expression $\xi = -(e^2/6m_e)\langle r^2 \rangle$, where $\langle r^2 \rangle$ is the (expectation) mean value of r^2 in the atom. Calculate ξ and χ_m for the ground state of a hydrogenic atom.

22.17 Nitrogen dioxide, a paramagnetic compound, is in equilibrium with its dimer, dinitrogen tetroxide, a diamagnetic compound. Derive an expression in terms of the equilibrium constant, K , for the dimerization to show how the molar susceptibility varies with the pressure of the sample. Suggest how the susceptibility might be expected to vary as the temperature is changed at constant pressure.

22.18 An NO molecule has thermally accessible electronically excited states. It also has an unpaired electron, and so may be expected to be paramagnetic. However, its ground state is not paramagnetic because the magnetic moment of the orbital motion of the unpaired electron almost exactly cancels the spin magnetic moment. The first excited state (at 121 cm^{-1}) is paramagnetic because the orbital magnetic

moment adds to, rather than cancels, the spin magnetic moment. The upper state has a magnetic moment of $2\mu_B$. Because the upper state is thermally accessible, the paramagnetic susceptibility of NO shows a pronounced temperature dependence even near room temperature. Calculate the molar paramagnetic susceptibility of NO and plot it as a function of temperature.

Additional problems supplied by Carmen Giunta and Charles Trapp

22.19 The notion of group additivity of thermodynamic properties was introduced in Chapter 2. Results of a computational study of the polarizabilities of the homologous series of linear saturated silanes $\text{Si}_2\text{N}_4\text{H}_{4N+2}$ raise the possibility of group additivity of polarizability. B. Champagne, E.A. Perpète, and J.-M. André (*J. Molec. Structure (Theochem)* **391**, 67 (1997)) report the following values for the electronic contribution to the polarizability, α , of $\text{Si}_2\text{N}_4\text{H}_{4N+2}$ based on *ab initio* quantum mechanical calculations):

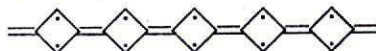
N	1	2	3	4	5
$\alpha/(10^{-40} \text{ J}^{-1} \text{ C m}^2)$	3.495	7.766	12.40	17.18	22.04
N	6	7	8	9	
$\alpha/(10^{-40} \text{ J}^{-1} \text{ C m}^2)$	26.92	31.82	36.74	41.63	

Determine the average contribution to this quantity per additional Si_2H_4 group, and report the root mean square deviation between the reported values and the best group-additivity fit.

22.20 F. Luo, G.C. McBane, G. Kim, C.F. Giese, and W.R. Gentry (*J. Chem. Phys.* **98**, 3564 (1993)) reported experimental observation of the He_2 complex, a species which had escaped detection for a long time. The fact that the observation required temperatures in the neighbourhood of 1 mK is consistent with computational studies which suggest that hcD_e for He_2 is about $1.51 \times 10^{-23} \text{ J}$, hcD_0 about $2 \times 10^{-26} \text{ J}$, and R_e about 297 pm. (a) Determine the Lennard-Jones parameters r_0 and ϵ and plot the Lennard-Jones potential for He-He

interactions. (b) Plot the Morse potential given that $a = 5.79 \times 10^{10} \text{ m}^{-1}$.

22.21 J.J. Dannenberg, D. Liotard, P. Halvick, and J.C. Rayez (*J. Phys. Chem.* **100**, 9631 (1996)) carried out theoretical studies of organic molecules consisting of chains of unsaturated four-membered rings. The calculations suggest that such compounds have large numbers of unpaired spins, and that they should therefore have unusual magnetic properties. For example, the lowest-energy state of the five-ring compound $\text{C}_{22}\text{H}_{14}$ (**8**) is computed to have $S = 3$, but the energies of $S = 2$ and $S = 4$ structures are each predicted to be 50 kJ mol^{-1} higher in energy. Compute the molar magnetic susceptibility of these three low-lying levels at 298 K. Estimate the molar susceptibility at 298 K if each level is present in proportion to its Boltzmann factor (effectively assuming that the degeneracy is the same for all three of these levels).



8

22.22 D.D. Nelson, G.T. Fraser, and W. Klemperer (*Science* **238**, 1670 (1987)) examined several weakly bound gas-phase complexes of ammonia in search of examples in which the H atoms in NH_3 formed hydrogen bonds, but found none. For example, they found that the complex of NH_3 and CO_2 has the carbon atom nearest the nitrogen (299 pm away): the CO_2 molecule is at right angles to the C-N 'bond', and the H atoms of NH_3 are pointing away from the CO_2 . The permanent dipole moment of this complex is reported as 1.77 D. If the N and C atoms are the centres of the negative and positive charge distributions, respectively, what is the magnitude of those partial charges (as multiples of e)?

22.23 From data in Table 22.1 calculate the molar polarization, relative permittivity, and refractive index of methanol at 20°C . Its density at that temperature is 0.7914 g cm^{-3} .



23

Macromolecules and colloids



Size and shape

- 23.1 Mean molar masses
- 23.2 Colligative properties
- 23.3 Sedimentation
- 23.4 Viscosity
- 23.5 Light scattering

Conformation and configuration

- 23.6 Random coils
- 23.7 Helices and sheets
- 23.8 Higher-order structures

Colloids and surfactants

- 23.9 The properties of colloids
- 23.10 Surface films

Checklist of key ideas

Further reading

Exercises

Problems

Macromolecules exhibit a range of properties and problems that illustrate a wide variety of physical-chemical principles. They need to be characterized in terms of their molar mass, their size, and their shape. However, the molecules are so large that the solutions they form depart strongly from ideality, so techniques for accommodating these departures need to be developed. Although the shapes of large biomolecules can be determined by X-ray diffraction, synthetic polymers have less regular shapes in solution, and only their general shape can be inferred. Another major problem concerns the influences that determine the shapes of the molecules. We consider a range of influences in this chapter, beginning with the structureless random coil and ending with the structurally precise forces that operate in polypeptides.

Colloids, and other aggregates of molecules that are not chemically bonded together, exhibit some of the properties of molecules but have their own characteristic features arising from the very large surface-to-volume ratios of their constituent particles.

There are macromolecules everywhere, inside us and outside us. Some are natural: they include polysaccharides such as cellulose, polypeptides such as enzymes, and nucleic acids such as DNA. Others are synthetic: they include polymers such as nylon and polystyrene that are manufactured by stringing together and (in some cases) cross-linking smaller units known as monomers. Life in all its forms, from its intrinsic nature to its technological interaction with its environment, is the chemistry of macromolecules.

Macromolecules give rise to special problems that include the determination of their sizes, the shapes and the lengths of polymer chains, and the large deviations from ideality of their solutions. We concentrate on these special characteristics here.

Size and shape

X-ray diffraction (Chapter 21) can reveal the position of almost every atom even in highly complex molecules. However, there are several reasons why other techniques must also be

used. In the first place, the sample might be a mixture of molecules with different chain lengths and extents of cross-linking, in which case sharp X-ray images are unobtainable. Even if all the molecules in the sample are identical, it might prove impossible to obtain a single crystal. Furthermore, although the work on enzymes, proteins, and DNA has shown how immensely stimulating the data can be, the information is incomplete. For instance, what can be said about the shape of the molecule in its natural environment, a biological cell? What can be said about the response of its shape to changes in its environment?

23.1 Mean molar masses

A pure protein is **monodisperse**, meaning that it has a single, definite molar mass. (There may be small variations, such as one amino acid replacing another, depending on the source of the sample.) A synthetic polymer, however, is **polydisperse** in the sense that a sample is a mixture of molecules with various chain lengths and molar masses. The various techniques that are used to measure molar masses result in different types of mean values of polydisperse systems. The mean obtained from the determination of molar mass by osmometry (Section 7.5e) gives the **number-average molar mass**, \bar{M}_n , which is the value obtained by weighting each molar mass by the number of molecules of that mass present in the sample:

$$\bar{M}_n = \frac{1}{N} \sum_i N_i M_i \quad [1]$$

where N_i is the number of molecules with molar mass M_i and there are N molecules in all. Viscosity measurements give the **viscosity-average molar mass**, \bar{M}_v , light-scattering experiments give the **weight-average molar mass**, \bar{M}_w , and sedimentation experiments give the **Z-average molar mass**, \bar{M}_z . Although such averages are often best left as empirical quantities, some may be interpreted in terms of the composition of the sample. Thus, the weight-average molar mass is the average calculated by weighting the molar masses of the molecules by the mass of each one present in the sample:

$$\bar{M}_w = \frac{1}{m} \sum_i m_i M_i \quad [2]$$

In this expression, m_i is the total mass of molecules of molar mass M_i and m is the total mass of the sample. Because $m_i = N_i M_i / N_A$, we can also express this average as

$$\bar{M}_w = \frac{\sum_i N_i M_i^2}{\sum_i N_i M_i} \quad (3)$$

Hence, the weight-average molar mass is proportional to the mean square molar mass. Similarly, the Z-average molar mass can be interpreted in terms of the mean cubic molar mass:

$$\bar{M}_z = \frac{\sum_i N_i M_i^3}{\sum_i N_i M_i^2} \quad (4)$$

Example 2.3.1 Calculating number and mass averages

Determine the number-average and the weight-average molar masses for a sample of poly(vinyl chloride) from the following data:

Molar mass interval/(kg mol ⁻¹)	Average molar mass within interval/(kg mol ⁻¹)	Mass of sample within interval/g
5-10	7.5	9.6
10-15	12.5	8.7
15-20	17.5	8.9
20-25	22.5	5.6
25-30	27.5	3.1
30-35	32.5	1.7

Method The relevant equations are eqns 1 and 2. The two averages are obtained by weighting the molar mass within each interval by the number and mass, respectively, of the molecule in each interval. The numbers in each interval are obtained by dividing the mass of the sample in each interval by the average molar mass for that interval. Because number of molecules is proportional to amount of substance (the number of moles), the number-weighted average can be obtained directly from the amounts in each interval.

Answer The amounts in each interval are as follows:

Interval	5-10	10-15	15-20	20-25	25-30	30-35
Molar mass/(kg mol ⁻¹)	7.50	12.5	17.5	22.5	27.5	32.5
Amount/mmol	1.30	0.70	0.51	0.25	0.11	0.052
					Total:	2.92

The number-average molar mass is therefore

$$\begin{aligned}\bar{M}_n/(\text{kg mol}^{-1}) &= \frac{1}{2.92} (1.3 \times 7.5 + 0.70 \times 12.5 + 0.51 \times 17.5 \\ &\quad + 0.25 \times 22.5 + 0.11 \times 27.5 + 0.052 \times 32.5) \\ &= 13\end{aligned}$$

The weight-average molar mass is calculated directly from the data after noting that the total mass of the sample is 37.6 g:

$$\begin{aligned}\bar{M}_w/(\text{kg mol}^{-1}) &= \frac{1}{37.6} (9.6 \times 7.5 + 8.7 \times 12.5 \\ &\quad + 8.9 \times 17.5 + 5.6 \times 22.5 + 3.1 \times 27.5 + 1.7 \times 32.5) \\ &= 16\end{aligned}$$

Comment Note the significantly different values of the two averages. In this instance, $\bar{M}_w/\bar{M}_n = 1.2$.

Self-test 23.1 Evaluate the Z-average molar mass of the sample.

[19 kg mol⁻¹]

Whereas at first sight it might appear troublesome to have several types of average, the observation that they have different values gives additional information about the range of molar masses in the sample: the ratio \bar{M}_w/\bar{M}_n is called the **heterogeneity index** (or 'polydispersity index'). In the determination of protein molar masses we expect the various averages to be the same because the sample is monodisperse (unless there has been degradation). In samples of synthetic polymers there is normally a range of molar masses and the different averages are expected to yield different values. Typical synthetic materials have $\bar{M}_w/\bar{M}_n \approx 4$. The term 'monodisperse' is conventionally applied to synthetic polymers in which this index is less than 1.1; commercial polyethylene samples might be much more

heterogeneous, with a ratio close to 30. One consequence of a narrow molar mass distribution for synthetic polymers is often a higher crystallinity, and therefore density and melting point. The spread of values is controlled by the choice of catalyst and reaction conditions (Section 26.1).

The most direct method for measuring molar masses is by mass spectrometry. However, until recently this technique was thwarted by the difficulty of vaporizing the sample. That problem has been solved by embedding the macromolecules in a substrate; the substrate is vaporized, and carries the macromolecules into the vapour with it.

23.2 Colligative properties

The classical methods of determining molar mass utilize colligative properties (Section 7.5). For macromolecules, where the number of molecules in solution may be very small even though the mass of the solute may be appreciable, only osmometry is sufficiently sensitive; this procedure was described and illustrated in Section 7.5e. Osmometry can be used for molar masses up to about 100 kg mol^{-1} . Its lower limit of about 8 kg mol^{-1} is due to the use of membrane materials that allow these relatively small molecules to pass through.

Macromolecules give strongly nonideal solutions: being so large, they displace a large quantity of solvent instead of replacing individual solvent molecules with negligible disturbance. In thermodynamic terms, the displacement of solvent molecules implies that the entropy change is especially important when a macromolecule dissolves. Furthermore, its great bulk means that a macromolecule is unable to move freely through the solution because the molecule is excluded from the regions occupied by other solute molecules. There are also significant contributions to the Gibbs energy from the enthalpy of solution, largely because solvent-solvent interactions are more favourable than the macromolecule-solvent interactions that replace them.

The osmotic virial coefficient, B (see eqn 7.38), arises largely from the effect of excluded volume. If we imagine a solution of a macromolecule being built by the successive addition of macromolecules to the solvent, each one being excluded by the ones that preceded it, then the value of B turns out to be

$$B = \frac{1}{2}N_A v_p \quad (5)$$

where v_p is the excluded volume due to a single molecule.

Example 23.2 Estimating the volume of polymer molecules

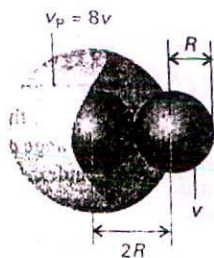
Use the information in Example 7.5 to estimate the volume of the polymer molecules regarded as impenetrable spheres.

Method The excluded volume of spherical molecules of volume v is $v_p = 8v$ because the minimum separation of the centres of two spheres is the sum of their radii (Fig. 23.1). Estimate v_p from B by using eqn 5, and find B from the slope of the graph plotted in Fig. 7.25. To do so use (as in Example 7.5):

$$\frac{h}{c} = \frac{RT}{\rho g \bar{M}_n} \left(1 + \frac{B}{\bar{M}_n} c \right)$$

Answer The intercept $RT/\rho g \bar{M}_n$ was found in Example 7.5 to be $0.21 \text{ cm}^3/(\text{g L}^{-1})$. The slope of the straight line in Fig. 7.25, which is equal to $(RT/\rho g \bar{M}_n) \times B/\bar{M}_n$, is $0.073 \text{ (cm}^3 \text{ g}^{-1} \text{ L)} / (\text{g L}^{-1})$. It follows that

$$\frac{\text{slope}}{\text{intercept}} = \frac{B}{\bar{M}_n} = \frac{0.073 \text{ (cm}^3 \text{ g}^{-1} \text{ L)} / (\text{g L}^{-1})}{0.21 \text{ cm}^3 \text{ g}^{-1} \text{ L}} = \frac{0.35}{\text{g L}^{-1}}$$



23.1 The excluded volume into which the centre of a molecule cannot penetrate is $8v$, where v is the volume of the molecule itself.

Therefore

$$B = (0.35/\text{g L}^{-1}) \times (123 \times 10^3 \text{ g mol}^{-1}) = 4.3 \times 10^4 \text{ L mol}^{-1}$$

Equation 5 then implies that

$$v_p = \frac{2B}{N_A} = 1.4 \times 10^{-22} \text{ m}^3$$

From this value of v_p it follows that the molecular volume is approximately $1.8 \times 10^4 \text{ nm}^3$.

Comment The radius of the molecule is approximately 16 nm.

Self-test 23.2 Another sample in the same solvent resulted in the following heights of solution at the same temperature: 0.22, 0.53, 1.39, 3.32, 5.02 cm. Calculate the molar mass and the molecular volume of the solute.

$$[14 \text{ kg mol}^{-1}, 9 \times 10^{-23} \text{ m}^3]$$

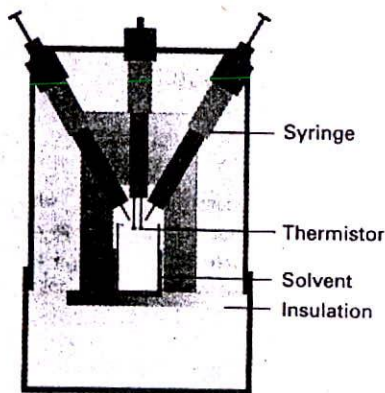
In broad terms, the excluded volume contributes to the excess entropy of solution (the entropy change in excess of the ideal value, Section 7.4), and the attractions and repulsions between macromolecules contribute to the excess enthalpy. For most solute-solvent systems there is a unique temperature (which is not always experimentally attainable) at which these effects cancel and the solution is virtually ideal. This temperature (the analogue of the Boyle temperature for real gases) is called the Flory theta temperature, θ . At this temperature, the osmotic virial coefficient B is zero. As an example, for polystyrene in cyclohexane $\theta \approx 306 \text{ K}$, the exact value depending on the average molar mass of the polymer. A solution at its Flory theta temperature is called a θ solution. Because a θ solution behaves nearly ideally, its thermodynamic and structural properties are easier to describe even though the molar concentration is not low. In molecular terms, in a θ solution the molecules are in an unperturbed condition, whereas in other solutions expansion or contraction of the coiled molecule takes place as a result of interactions with the solvent.

(a) Vapour-phase osmometry

In the technique of vapour-phase osmometry, a droplet of solution is placed on one thermistor (a semiconductor temperature probe) and a droplet of pure solvent is placed on another thermistor (Fig. 23.2). The two droplets are surrounded by an atmosphere of solvent vapour. Because the vapour pressure of a solvent in a solution is lower than when it is pure, the net rate of condensation of solvent on to a droplet of solution is greater than the rate of condensation on to a droplet of pure solvent. It follows that more heat is liberated in the solution droplet, and the rise in temperature is greater there than in the droplet of pure solvent. The difference in temperature is measured for a series of concentrations and extrapolated to zero concentration. After calibration by using samples of known molar mass, the molar mass of the sample can be inferred from the temperature difference between the two thermistors. The method is not particularly sensitive, and is confined to samples of low molar mass.

(b) Polyelectrolytes and dialysis

Some polymers are strings of acid groups, as in poly(acrylic acid), $-(\text{CH}_2\text{CHCOOH})_n-$, or strings of bases, as in nylon, $-\text{[NH}(\text{CH}_2)_6\text{NHCO}(\text{CH}_2)_4\text{CO}]_n-$; proteins have both acid and base groups. Macromolecules may therefore be polyelectrolytes, and, depending on their state of ionization, polyanions or polycations. A macromolecule with mixed cation and anion character is known as a polyampholyte.



23.2 A vapour-phase osmometer. The syringes introduce droplets of solvent and solution on to the thermistors, and the difference in temperature (arising from the different rates of vaporization) is noted.

One consequence of dealing with polyelectrolytes is that it is necessary to know the extent of ionization before osmotic data can be interpreted. For example, suppose the sodium salt of a polyelectrolyte is present in solution as ν Na^+ ions and a single polyanion $\text{P}^{\nu-}$; then if it is fully dissociated in solution it gives rise to $\nu + 1$ particles for each formula unit of salt that dissolves. If we guess that $\nu = 1$ when in fact $\nu = 10$, then the estimate of the molar mass will be wrong by an order of magnitude. We can find a way out of this difficulty by considering another feature of charged macromolecules.

Suppose the solution of the polyelectrolyte Na_νP also contains added NaCl , and that it is in contact through a semipermeable membrane with another salt solution. Furthermore, suppose the membrane is permeable to the solvent and to the salt ions, but not to the polyanion. This arrangement is one that actually occurs in living systems, where osmosis is an important feature of cell operation. The presence of the salt affects the osmotic pressure because the anions and cations cannot migrate through the membrane to an arbitrary extent. Apart from small imbalances of charge close to the membrane and which give rise to transmembrane potentials, electrical neutrality must be preserved in the bulk on both sides of the membrane: if an anion migrates, a cation must accompany it.

The presence of a high concentration of added salt on each side of a semipermeable membrane ensures that the effective difference in concentrations is due solely to the presence of the polyanion P on one side of the membrane, for the number of cations the polymer provides is insignificant in comparison with the number supplied by the additional salt. Hence, under such circumstances we can expect the osmotic pressure to be given by $\Pi = RT[\text{P}]$, independent of the value of ν (a result confirmed in the *Justification* below). Therefore, if we measure the osmotic pressure in the presence of high concentrations of salt, the molar mass may be obtained unambiguously.

Justification 23.1

Suppose that Na_νP is at a molar concentration $[\text{P}]$ on one side of the membrane, and that NaCl is added to each side. On the left (L) there are $\text{P}^{\nu-}$, Na^+ , and Cl^- ions. On the right (R) there are Na^+ and Cl^- ions. The condition for equilibrium is that the Gibbs energy of NaCl in solution is the same on both sides of the membrane, so a net flow of Na^+ and Cl^- ions occurs until $G_m(\text{NaCl}, \text{L}) = G_m(\text{NaCl}, \text{R})$. This equality occurs when

$$\mu^\circ(\text{NaCl}) + RT \ln a_L(\text{Na}^+) + RT \ln a_L(\text{Cl}^-) = \mu^\circ(\text{NaCl}) + RT \ln a_R(\text{Na}^+) + RT \ln a_R(\text{Cl}^-)$$

or

$$RT \ln a_L(\text{Na}^+) a_L(\text{Cl}^-) = RT \ln a_R(\text{Na}^+) a_R(\text{Cl}^-)$$

If we ignore activity coefficients, the two expressions are equal when $[\text{Na}^+]_L [\text{Cl}^-]_L = [\text{Na}^+]_R [\text{Cl}^-]_R$. As the Na^+ ions are supplied by the polyelectrolyte as well as the added salt, the conditions for bulk electrical neutrality are $[\text{Na}^+]_L = [\text{Cl}^-]_L + \nu[\text{P}]$ and $[\text{Na}^+]_R = [\text{Cl}^-]_R$. We can now combine these three conditions to obtain expressions for the differences in ion concentrations across the membrane:

$$\begin{aligned} [\text{Na}^+]_L - [\text{Na}^+]_R &= \frac{\nu[\text{P}][\text{Na}^+]_L}{[\text{Na}^+]_L + [\text{Na}^+]_R} = \frac{\nu[\text{P}][\text{Na}^+]_L}{2[\text{Cl}^-] + \nu[\text{P}]} \\ [\text{Cl}^-]_L - [\text{Cl}^-]_R &= -\frac{\nu[\text{P}][\text{Cl}^-]_L}{[\text{Cl}^-]_L + [\text{Cl}^-]_R} = -\frac{\nu[\text{P}][\text{Cl}^-]_L}{2[\text{Cl}^-]} \end{aligned} \quad (6)$$

where $[\text{Cl}^-] = \frac{1}{2}([\text{Cl}^-]_L + [\text{Cl}^-]_R)$. The quantity $[\text{Cl}^-]$ is the average concentration of Cl^- ions on each side of the membrane.

The final step is to note that the osmotic pressure depends on the difference in the numbers of solute particles on each side of the membrane. That being so, the van't Hoff equation, $\Pi = RT[\text{Solute}]$, becomes

$$\begin{aligned}\Pi &= RT\{([P] + [\text{Na}^+]_L + [\text{Cl}^-]_L) - ([\text{Na}^+]_R + [\text{Cl}^-]_R)\} \\ &= RT[P](1 + B[P]) \quad B = \frac{\nu^2[\text{Cl}^-]_R}{4[\text{Cl}^-]^2 + 2\nu[\text{Cl}^-]_L[P]}\end{aligned}\quad (7)$$

When the concentration of added salt is so great that $[\text{Cl}^-]_L$ and $[\text{Cl}^-]_R$ are both much larger than $[P]$, it follows that $B[P] \ll 1$ and this expression reduces to the one quoted in the text.

A second point arises from the effect of added salt. There is often interest in the extent to which ions are bound to macromolecules, especially when a membrane (such as a cell wall) separates two solutions. The equations

$$\begin{aligned}[\text{Na}^+]_L - [\text{Na}^+]_R &= \frac{\nu[P][\text{Na}^+]_L}{2[\text{Cl}^-] + \nu[P]} \\ [\text{Cl}^-]_L - [\text{Cl}^-]_R &= -\frac{\nu[P][\text{Cl}^-]_L}{2[\text{Cl}^-]}\end{aligned}\quad (8)$$

which are derived in the *Justification*, show that cations will dominate the anions in the compartment containing the polyanion (because the concentration difference is positive for Na^+ and negative for Cl^-) as a result of the equilibrium and electroneutrality conditions. The equilibrium distribution of ions in two compartments in contact through a semipermeable membrane, in one of which there is a polyelectrolyte, is called a **Donnan equilibrium**.

Example 23.3 Analysing a Donnan equilibrium

Suppose that two equal volumes of 0.200 M NaCl(aq) are separated by a membrane and that a macromolecule of molar mass 55 kg mol^{-1} , which cannot pass through the membrane, is added as its sodium salt Na_6P to a concentration of 50 g L^{-1} to the left-hand compartment. Calculate the molar concentrations of Na^+ and Cl^- in each compartment.

Method The sums of the equilibrium concentrations of Na^+ and Cl^- in each compartment are

$$[\text{Na}^+]_L + [\text{Na}^+]_R = [\text{Cl}^-]_L + [\text{Cl}^-]_R + \nu[P] = 2[\text{Cl}^-] + \nu[P]$$

Then use $[\text{Cl}^-] = 0.200 \text{ mol L}^{-1}$.

Answer As $[P] = 9.1 \times 10^{-4} \text{ mol L}^{-1}$, we find

$$[\text{Na}^+]_L - [\text{Na}^+]_R = \frac{6 \times (9.1 \times 10^{-4} \text{ mol L}^{-1}) \times [\text{Na}^+]_L}{2 \times (0.200 \text{ mol L}^{-1}) + 6 \times (9.1 \times 10^{-4} \text{ mol L}^{-1})}$$

and the sum above gives

$$\begin{aligned}[\text{Na}^+]_L + [\text{Na}^+]_R &= 2 \times (0.200 \text{ mol L}^{-1}) + 6 \times (9.1 \times 10^{-4} \text{ mol L}^{-1}) \\ &= 0.405 \text{ mol L}^{-1}\end{aligned}$$

The solutions of these two equations are

$$[\text{Na}^+]_L = 0.204 \text{ mol L}^{-1} \quad [\text{Na}^+]_R = 0.201 \text{ mol L}^{-1}$$

Then

$$[\text{Cl}^-]_{\text{R}} = [\text{Na}^+]_{\text{R}} = 0.201 \text{ mol L}^{-1}$$

$$[\text{Cl}^-]_{\text{L}} = [\text{Na}^+]_{\text{L}} - 6[\text{P}] = 0.199 \text{ mol L}^{-1}$$

Comment The Na^+ ions accumulate slightly in the compartment containing the macromolecule.

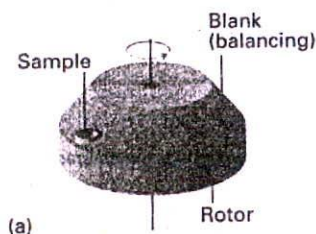
Self-test 23.3 Repeat the calculation for 0.300 M NaCl(aq), a polyelectrolyte Na_{10}P of molar mass 33 kg mol^{-1} at a mass concentration of 50.0 g L^{-1} .

$$[\text{Na}^+]_{\text{R}}: 0.311 \text{ mol L}^{-1}, 0.304 \text{ mol L}^{-1}$$

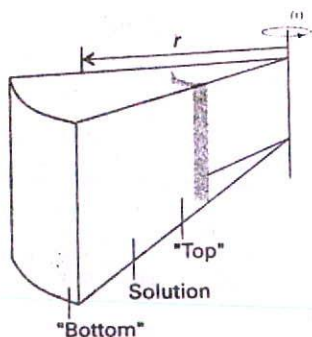
23.3 Sedimentation

In a gravitational field, heavy particles settle towards the foot of a column of solution by the process called sedimentation. The rate of sedimentation depends on the strength of the field and on the masses and shapes of the particles. Spherical molecules (and compact molecules in general) sediment faster than rod-like or extended molecules. For example, DNA helices sediment much faster when they are denatured to a random coil, so sedimentation rates can be used to study denaturation. When the sample is at equilibrium, the particles are dispersed over a range of heights in accord with the Boltzmann distribution (because the gravitational field competes with the stirring effect of thermal motion). The spread of heights depends on the masses of the molecules, so the equilibrium distribution is another way of determining molar mass.

Sedimentation is normally very slow, but it can be accelerated by replacing the gravitational field by a centrifugal field. The latter can be achieved in an ultracentrifuge, which is essentially a cylinder that can be rotated at high speed about its axis with a sample in a cell near its periphery (Fig. 23.3). Modern ultracentrifuges can produce accelerations equivalent to about 10^5 that of gravity ($10^5 g$). Initially the sample is uniform, but the 'top' (innermost) boundary of the solute moves outwards as sedimentation proceeds.



(a)



(b)

23.3 (a) An ultracentrifuge head. The sample on one side is balanced by a blank diametrically opposite. (b) Detail of the sample cavity: the 'top' surface is the inner surface, and the centrifugal force causes sedimentation towards the outer surface; a particle at a radius r experiences a force of magnitude $m\omega^2 r$.

(a) The rate of sedimentation

A solute particle of mass m has an effective mass $m_{\text{eff}} = bm$ on account of the buoyancy of the medium, with

$$b = 1 - \rho v_s \quad (9)$$

where ρ is the solution density, v_s is the solute's partial specific volume ($v_s = (\partial V / \partial m_B)_T$, where m_B is the total mass of the solute), and ρv_s is the mass of solvent displaced per gram of solute. The solute particles at a distance r from the axis of a rotor spinning at an angular velocity ω experience a centrifugal force of magnitude $m_{\text{eff}} r \omega^2$. The acceleration outwards is countered by a frictional force proportional to the speed, s , of the particles through the medium. This force is written fs , where f is the frictional coefficient. The particles therefore adopt a drift speed, a steady speed through the medium, which is found by equating the two forces $m_{\text{eff}} r \omega^2$ and fs . The forces are equal when

$$s = \frac{m_{\text{eff}} r \omega^2}{f} = \frac{b m r \omega^2}{f} \quad (10)$$

The drift speed depends on the angular velocity and the radius, and it is convenient to focus on the sedimentation constant, S , which is defined as

$$S = \frac{s}{r\omega^2} \quad [11]$$

Then, because the average molecular mass is related to the average molar mass \overline{M}_n through $m = \overline{M}_n/N_A$,

$$S = \frac{b\overline{M}_n}{fN_A} \quad (12)$$

Example 23.4 Determining a sedimentation constant

The sedimentation of bovine serum albumin (BSA) was monitored at 25°C. The initial location of the solute surface was at 5.50 cm from the axis of rotation, and during centrifugation at 56 850 r.p.m. it receded as follows:

t/s	0	500	1000	2000	3000	4000	5000
r/cm	5.50	5.55	5.60	5.70	5.80	5.91	6.01

Calculate the sedimentation coefficient.

Method Equation 11 can be interpreted as a differential equation for $s = dr/dt$ in terms of r , so integrate it to obtain a formula for r in terms of t . The integrated expression, an expression for r as a function of t , will suggest how to plot the data and obtain from it the sedimentation constant.

Answer Equation 11 may be written

$$\frac{dr}{dt} = r\omega^2 S$$

This equation integrates to

$$\ln \frac{r}{r_0} = \omega^2 S t$$

It follows that a plot of $\ln(r/r_0)$ against t should be a straight line of slope $\omega^2 S$. Use $\omega = 2\pi\nu$, where ν is in cycles per second, and draw up the following table:

t/s	0	500	1000	2000	3000	4000	5000
$100 \ln(r/r_0)$	0	0.900	1.80	3.57	5.31	7.19	8.87

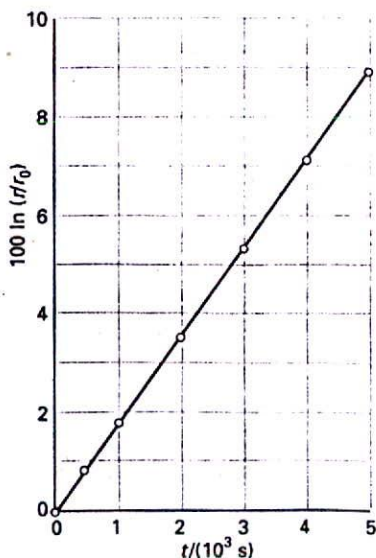
The straight-line graph (Fig. 23.4) has slope 1.78×10^{-5} , so $\omega^2 S = 1.79 \times 10^{-5} \text{ s}^{-1}$. Because $\omega = 2\pi \times (56\,850/60) \text{ s}^{-1} = 5.95 \times 10^3 \text{ s}^{-1}$, it follows that $S = 5.02 \times 10^{-13} \text{ s}$.

Comment We develop this result below. The unit 10^{-13} s is sometimes called a 'svedberg' and denoted Sv; in this case $S = 5.02 \text{ Sv}$. Accurate results are obtained by extrapolating to zero concentration.

Self-test 23.4 Calculate the sedimentation constant given the following data (the other conditions being the same as above):

t/s	0	500	1000	2000	3000	4000	5000
r/cm	5.65	5.68	5.71	5.77	5.84	5.90	5.97

[3.11 Sv]



23.4 A plot of the data in Example 23.4.

Table 23.1* Frictional coefficients and molecular geometry†

a/b	Prolate	Oblate
2	1.04	1.04
4	1.18	1.17
6	1.31	1.28
8	1.43	1.37
10	1.54	1.46

* More values and analytical expressions are given in the *Data section* at the end of this volume.

† Entries are the ratio f/f_0 where $f_0 = 6\pi\eta c$ with $c = (ab^2)^{1/3}$ for prolate ellipsoids and $c = (a^2b)^{1/3}$ for oblate ellipsoids; $2a$ is the major axis and $2b$ is the minor axis.

Table 23.2* Diffusion coefficients in water at 20°C

	$M/(\text{kg mol}^{-1})$	$D/(\text{m}^2 \text{s}^{-1})$
Sucrose	0.342	4.59×10^{-10}
Lysozyme	14.1	1.04×10^{-10}
Haemoglobin	68	6.9×10^{-11}
Collagen	345	6.9×10^{-12}

To make progress we need to know the frictional constant, f . For a spherical particle of radius a in a solvent of viscosity η , and for solute molecules that are not small compared with the solvent molecules, f is given by Stokes' relation

$$f = 6\pi a\eta \quad (13)$$

Therefore, for spherical molecules,

$$S = \frac{b\bar{M}_n}{6\pi a\eta N_A} \quad (14)$$

and S may be used to determine either \bar{M}_n or a . If the molecules are not spherical, we use the appropriate value of f given in Table 23.1. As always when dealing with macromolecules, the measurements must be carried out at a series of concentrations and then extrapolated to zero concentration to avoid the complications that arise from the interference between bulky molecules.

At this stage, it appears that we need to know the molecular radius a (and in general the frictional coefficient f) to obtain the molar mass from the value of S . Fortunately, this requirement can be avoided by drawing on the Stokes-Einstein relation between f and the diffusion coefficient, D :

$$f = \frac{kT}{D} \quad (15)$$

The diffusion coefficient is a measure of the rate at which molecules spread down a concentration gradient (it is treated in detail in Section 24.11); this coefficient can be measured by observing the rate at which a concentration boundary spreads or the rate at which a more concentrated solution diffuses into a less concentrated one. Some typical values are given in Table 23.2. The diffusion coefficient can also be measured by using light scattering (Section 23.5). It follows from eqns 12 and 15 that

$$\bar{M}_n = \frac{SRT}{bD} \quad (16)$$

This result is independent of the shape of the solute molecules. It follows that we can find the molar mass by combining measurements of sedimentation and diffusion rates (for S and D , respectively).

(b) Sedimentation equilibria

The difficulty with using sedimentation rates to measure molar masses lies in the inaccuracies inherent in the determination of diffusion coefficients, such as the blurring of the boundary by convection currents. This problem can be avoided by allowing the system to reach equilibrium, for the transport property D is then no longer relevant. As we show in the *Justification* below, the weight-average molar mass can be obtained from the ratio of concentrations of the macromolecules at two different radii in a centrifuge operating at angular frequency ω :

$$\bar{M}_w = \frac{2RT}{(r_2^2 - r_1^2)b\omega^2} \ln \frac{c_2}{c_1} \quad (17)$$

An alternative treatment of the data leads to the Z -average molar mass. The centrifuge is run more slowly in this technique than in the sedimentation rate method to avoid having all the solute pressed in a thin film against the bottom of the cell. At these slower speeds, several days may be needed for equilibrium to be reached.

Justification 23.2

The distribution of particles is the outcome of the balance between the effect of the centrifugal force and the dispersing effect of diffusion down a concentration gradient. The kinetic energy of a particle of effective mass m at a radius r in a rotor spinning at a frequency ω is $\frac{1}{2}m\omega^2r^2$, so the total chemical potential at a radius r is $\bar{\mu}(r) = \mu(r) - \frac{1}{2}M\omega^2r^2$, where $\mu(r)$ is the contribution that depends on the concentration of solute. The condition for equilibrium is that the chemical potential is uniform, so

$$\left(\frac{\partial \bar{\mu}}{\partial r}\right)_T = \left(\frac{\partial \mu}{\partial r}\right)_T - M\omega^2r = 0$$

To evaluate the partial derivative of μ , we write

$$\begin{aligned} \left(\frac{\partial \mu}{\partial r}\right)_T &= \left(\frac{\partial \mu}{\partial p}\right)_{T,c} \left(\frac{\partial p}{\partial r}\right)_{T,c} + \left(\frac{\partial \mu}{\partial c}\right)_{T,p} \left(\frac{\partial c}{\partial r}\right)_{T,p} \\ &= Mv\omega^2r\rho + RT \left(\frac{\partial \ln c}{\partial r}\right)_{T,p} \end{aligned}$$

The first result follows from the fact that $(\partial\mu/\partial p)_T = V_m$, the partial molar volume, and $V_m = Mv$. It also makes use of the fact that the hydrostatic pressure at r is $p(r) = p(r_0) + \frac{1}{2}\rho\omega^2(r^2 - r_0^2)$, where r_0 is the radius of the surface of the liquid in the sample holder (that is, the location of its meniscus), with ρ the density of the solution. The concentration term stems from the expression $\mu = \mu^\ominus + RT \ln c$. The condition for equilibrium is therefore

$$Mr\omega^2(1 - v\rho) - RT \left(\frac{\partial \ln c}{\partial r}\right)_{T,p} = 0$$

and therefore, at constant temperature,

$$d \ln c = \frac{Mr\omega^2(1 - v\rho)dr}{RT}$$

This expression integrates to eqn 17.

(c) Electrophoresis

Many macromolecules are charged and move in response to an electric field: this motion is called **electrophoresis**. In gel electrophoresis the migration takes place through a cross-linked polyacrylamide gel. The mobilities of macromolecules depend on their masses and their shapes, and a constant drift speed is reached when the driving force $ez\mathcal{E}$ (where z is the charge number and \mathcal{E} is the field strength) is matched by the viscous retarding force f_s .

One way to avoid the problem of knowing neither the hydrodynamic shape of the molecules nor their charge is to denature them in a controlled way. Sodium dodecylsulfate has been found to be very useful in this respect: it denatures proteins, whatever their initial shapes, into rods by forming a complex with them. Moreover, most proteins bind a constant amount of the anion to a given mass, so the charge per protein molecule is well regulated. The molar mass of the protein is determined by comparing its mobility in its rod-like complexed form with standard samples.

The charge on a protein depends on the pH, and hence the rate of migration varies with pH. This apparent difficulty can be used to distinguish proteins. For example, at a given pH the rate of migration of haemoglobin from people with sickle-cell anaemia is different from that of a sample taken from people without the disease. This difference is an indication that

there are different charges on the protein molecule, which in turn is ascribed to the presence of a different amino acid residue in the polypeptide chain.

(d) Size-exclusion chromatography

All the techniques discussed so far have certain drawbacks, including the time needed to obtain data, and the often awkward interpretation of the data. Much of this difficulty has been swept away by a technique that makes use of beads of porous polymeric material about 0.1 mm in diameter that capture molecules selectively, according to their size. In the technique of size-exclusion chromatography (SEC), or gel permeation chromatography (GPC), which is now the most widely used technique for molar mass determinations of polymers, a solution of the polymer sample is filtered through a column. The small molecules, which can permeate into the porous structure of the gel, require a long elution time, or time to pass through a particular length of column, whereas the larger ones, which are not captured, pass through rapidly. The average molar mass of a macromolecule may therefore be determined by observing its elution time in a column calibrated against standard samples.

The range of molar masses that can be determined by SEC can be altered by selecting columns made from polymers with different degrees of cross-linking and different materials. The elution time depends on shape in a complicated way and the technique works best if the molecules are spherical. Polystyrene gels are used for investigations of nonpolar polymers in nonpolar solvents, and porous glass gels are used for more polar systems. Because elution is performed under pressure, molar mass determinations may be completed within a few minutes, in striking contrast to the time required for more classical techniques. Moreover, only a few milligrams of material are needed for highly reliable measurements.

23.4 Viscosity

The presence of a macromolecular solute increases the viscosity of a solution. The effect is large even at low concentrations, because big molecules affect the fluid flow over an extensive region surrounding them. At low concentrations the viscosity, η , of the solution is related to the viscosity of the pure solvent, η_0 , by

$$\eta = \eta_0(1 + [\eta]c + \dots) \quad (18)$$

The intrinsic viscosity, $[\eta]$, is the analogue of a virial coefficient (and has the dimensions of l/concentration). It follows from eqn 18 that

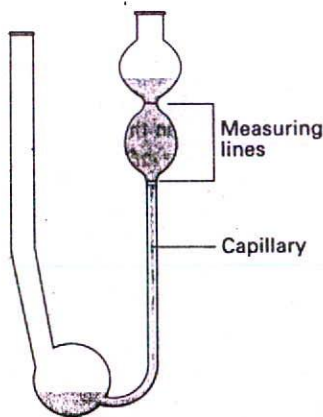
$$[\eta] = \lim_{c \rightarrow 0} \left(\frac{\eta - \eta_0}{c\eta_0} \right) = \lim_{c \rightarrow 0} \left(\frac{\eta/\eta_0 - 1}{c} \right) \quad (19)$$

Viscosities are measured in several ways. In the Ostwald viscometer shown in Fig. 23.5, the time taken for a solution to flow through the capillary is noted, and compared with a standard sample. The method is well suited to the determination of $[\eta]$ because the ratio of the viscosities of the solution and the pure solvent is proportional to the drainage times t and t_0 after correcting for different densities ρ and ρ_0 :

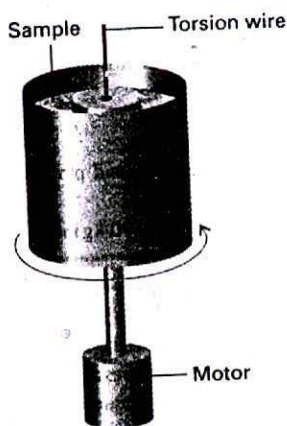
$$\frac{\eta}{\eta_0} = \frac{t}{t_0} \times \frac{\rho}{\rho_0} \quad (20)$$

(In practice, the two densities are only rarely significantly different.) This ratio can be used directly in eqn 19. Viscometers in the form of rotating concentric cylinders are also used (Fig. 23.6), and the torque on the inner cylinder is monitored while the outer one is rotated.

Such rotating drum viscometers have the advantage over the Ostwald type that the shear gradient between the cylinders is simpler than in the capillary, and effects of the kind discussed shortly can be studied more easily.



23.5 An Ostwald viscometer. The viscosity is measured by noting the time required for the liquid to drain between the two marks.



23.6 A rotating drum viscometer. The torque on the inner drum is observed when the outer container is rotated.

Table 23.3* Intrinsic viscosity

Macromolecule	Solvent	$\theta/^\circ\text{C}$	$K/(\text{cm}^3\text{g}^{-1})$	a
Polystyrene	Benzene	25	9.5×10^{-3}	0.74
Polyisobutylene	Benzene	23	8.3×10^{-2}	0.50
Various proteins	Guanidine hydrochloride + $\text{HSCH}_2\text{CH}_2\text{OH}$		7.2×10^{-3}	0.66

*More values are given in the Data section.

There are many complications in the interpretation of viscosity measurements. Much of the work is based on empirical observations, and the determination of molar mass is usually based on comparisons with standard, nearly monodisperse samples. Some regularities are observed that help in the determination. For example, it is found that θ solutions of macromolecules often fit the Mark-Kuhn-Houwink-Sakurada equation:

$$[\eta] = K\bar{M}_v^a \quad (21)$$

where K and a are constants that depend on the solvent and type of macromolecule (Table 23.3); the viscosity-average molar mass, \bar{M}_v , appears in this expression. As an example, solutions of poly(γ -benzyl-L-glutamate) in its rod-like form have an intrinsic viscosity about four times greater than when it is denatured and the rods collapse into random coils. Conversely, solutions of natural ribonuclease are less viscous than solutions of the denatured form: this observation indicates that the natural protein is more compact than the denatured form.

Example 23.5 Using intrinsic viscosity to measure molar mass

The viscosities of a series of solutions of polystyrene in toluene were measured at 25°C with the following results:

$c/(\text{g L}^{-1})$	0	2.0	4.0	6.0	8.0	10.0
$\eta/(10^{-4} \text{ kg m}^{-1} \text{ s}^{-1})$	5.58	6.15	6.74	7.35	7.98	8.64

Calculate the intrinsic viscosity and estimate the molar mass of the polymer by using eqn 21 with $K = 3.80 \times 10^{-5} \text{ L g}^{-1}$ and $a = 0.63$.

Method The intrinsic viscosity is defined in eqn 19; therefore, form this ratio at the series of data points and extrapolate to $c = 0$. Interpret \bar{M}_v as $\bar{M}_v/(\text{g mol}^{-1})$ in eqn 21.

Answer We draw up the following table:

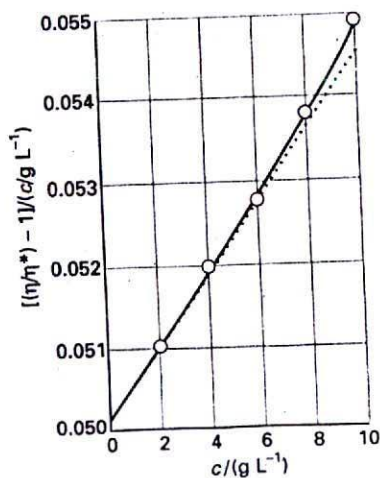
$c/(\text{g L}^{-1})$	0	2.0	4.0	6.0	8.0	10.0
η/η_0	1	1.102	1.208	1.317	1.430	1.549
$100[(\eta/\eta_0) - 1]/(c/\text{g L}^{-1})$		5.11	5.20	5.28	5.38	5.49

The points are plotted in Fig. 23.7. The extrapolated intercept at $c = 0$ is 0.0504, so $[\eta] = 0.0504 \text{ L g}^{-1}$. Therefore,

$$\bar{M}_v = \left(\frac{[\eta]}{K}\right)^{1/a} = 9.0 \times 10^4 \text{ g mol}^{-1}$$

Comment When $\eta \approx \eta_0$,

$$\ln \frac{\eta}{\eta_0} = \ln \left(1 + \frac{\eta - \eta_0}{\eta_0}\right) \approx \frac{\eta - \eta_0}{\eta_0} = \frac{\eta}{\eta_0} - 1$$



23.7 The plot used for the determination of intrinsic viscosity, which is taken from the intercept at $c = 0$; see Example 23.5.

This relation is exact in the limit that η coincides with η_0 , which is true when $c = 0$. Hence, $[\eta]$ can also be defined as the limit of $(1/c) \ln(\eta/\eta_0)$ as $c \rightarrow 0$. The intercept is identified more precisely by plotting both functions.

Self-test 23.5 Evaluate the viscosity-average molar mass by using the second plotting technique.

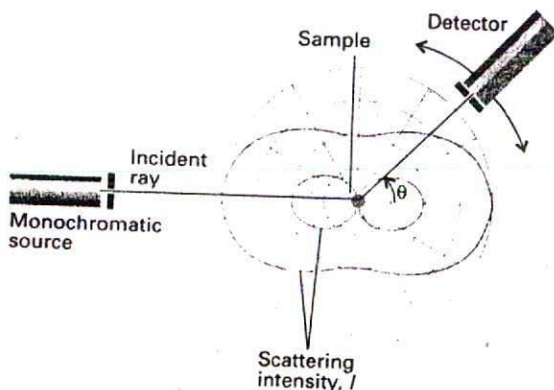
[90 kg mol⁻¹]

In some cases, it is found that the flow is non-Newtonian in the sense that the viscosity of the solution changes as the rate of flow increases. A decrease in viscosity with increasing rate of flow indicates the presence of long rod-like molecules that are orientated by the flow and hence slide past each other more freely. In some somewhat rare cases the stresses set up by the flow are so great that long molecules are broken up, with further consequences for the viscosity.

23.5 Light scattering

When electromagnetic radiation falls on an object, it forces the electron distribution in the object to oscillate and hence to radiate. If the medium is perfectly homogeneous (for example, a perfect crystal or a completely random collection of molecules that is homogeneous on the scale of the wavelength of the radiation, like a sample of water), the secondary waves interfere destructively except in the original propagation direction. Therefore, an observer sees the beam only when looking towards the source along the initial direction. If the medium is inhomogeneous (an imperfect crystal or a solution containing foreign bodies, such as macromolecules in a solvent or smoke in air), radiation is scattered into other directions too. A familiar example is light scattered by specks of dust in a sunbeam (and in advertisers' photographs of laser beams).

Scattering by particles with diameters much smaller than the wavelength of the incident radiation is called Rayleigh scattering. The intensity of Rayleigh scattered radiation depends on $1/\lambda^4$, so shorter wavelength radiation is scattered more intensely than longer wavelengths. The blue of the sky arises from the more intense scattering of the blue component of white sunlight by the molecules of the atmosphere. The intensity also depends on the scattering angle θ , and is proportional to $1 + \cos^2 \theta$ when the light is unpolarized and to $\cos^2 \theta$ when it is polarized (Fig. 23.8). In practice it turns out to be easier to make observations at an angle to the incident beam. The intensity also depends on the strength of



23.8 Rayleigh scattering from a sample of point-like particles follows a $1 + \cos^2 \theta$ dependence (outer trace on the polar plot) when unpolarized light is used, but a $\cos^2 \theta$ dependence (inner trace) when plane-polarized light is used.

the interaction of the light with the molecules: the interaction is strong when the polarizability of the molecules is large.

When these remarks are combined into a quantitative theory, it turns out that the scattering intensity, $\mathcal{I}(\theta)$, at the angle θ is

$$\mathcal{I} = A\mathcal{I}_0\bar{M}_w[P]g(\theta) \quad g(\theta) = \begin{cases} 1 + \cos^2 \theta & \text{for unpolarized light} \\ \cos^2 \theta & \text{for polarized light} \end{cases} \quad (22)$$

In this expression, \mathcal{I}_0 is the incident intensity, $[P]$ is the molar concentration of the solute, \bar{M}_w its weight-average molar mass, and A is a constant that depends on the refractive index of the solution, the wavelength, and the distance of the detector from the sample. Equation 22 is an 'ideal' result in the sense that it ignores the complications that arise from the interactions between solute particles, and in an actual experiment it is important to extrapolate to zero concentration.

(a) Large-particle scattering

When the wavelength of the incident radiation is comparable to the size of the scattering particles, scattering may occur from different sites of the same molecule and the interference between different rays is important.¹ As a result, the scattering intensity is distorted from the form characteristic of small-particle, Rayleigh scattering of light given in eqn 22. A measure of the distortion is the ratio

$$P = \frac{\mathcal{I}_{\text{observed}}}{\mathcal{I}_{\text{Rayleigh}}} \quad (23)$$

measured at several angles, where $\mathcal{I}_{\text{observed}}$ is the observed intensity at each angle and $\mathcal{I}_{\text{Rayleigh}}$ is the intensity predicted for Rayleigh scattering at that angle.

If the molecule is regarded as composed of a number of atoms i at distances R_i from a convenient point, interference occurs between the radiation scattered by each pair. The scattering from all the particles is then calculated by allowing for contributions from all possible orientations of each pair of atoms in each molecule. This description is very much like the one used in the discussion of electron diffraction (Section 21.10), so we can expect the intensity pattern to be described by a kind of Wierl equation. This turns out to be so and, if there are N atoms in the macromolecule, and if all are assumed to have the same scattering power, then

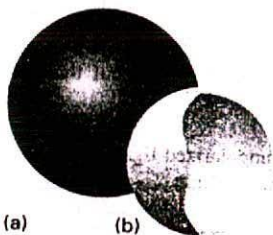
$$P = \frac{1}{N^2} \sum_{ij} \frac{\sin sR_{ij}}{sR_{ij}} \quad s = \frac{4\pi}{\lambda} \sin \frac{1}{2}\theta \quad (24)$$

In this expression, R_{ij} is the separation of atoms i and j , and λ is the wavelength of the incident radiation. The observed intensity is equal to $P\mathcal{I}_{\text{Rayleigh}}$, with $\mathcal{I}_{\text{Rayleigh}}$ given by eqn 22.

(b) Small-particle scattering

When the molecule is much smaller than the wavelength of the incident radiation in the sense that $sR_{ij} \ll 1$ (for example, if $R = 5$ nm, and $\lambda = 500$ nm, all the sR_{ij} are about 0.1),

¹ The effect accounts for the appearance of clouds, which, although we see them by scattered light, look white, not blue like the sky. The water molecules group together into droplets of a size comparable to the wavelength of light, and scatter cooperatively. Although blue light scatters more strongly, more molecules can contribute cooperatively when the wavelength is longer (as for red light), so the net result is uniform scattering for all wavelengths: white light scatters as white light. This paper looks white for the same reason. Cigarette smoke is blue before it is inhaled, but brownish after it is exhaled because the particles aggregate in the lungs.



23.9 (a) A spherical molecule and (b) the hollow spherical shell that has the same rotational characteristics. The radius of the hollow shell is the radius of gyration of the molecule. The radius of gyration of a solid sphere of radius R is $0.77R$.

then we show in the *Justification* below that the deviation from Rayleigh scattering is proportional to the square of the radius of gyration, R_g , of the molecule:

$$P - 1 \propto R_g^2 \quad (25)$$

The radius of gyration is the radius of a thin hollow spherical shell of the same mass and moment of inertia as the molecule (Fig. 23.9), and is calculated formally from the expression:²

$$R_g = \frac{1}{N} \left(\frac{1}{2} \sum_{ij} R_{ij}^2 \right)^{1/2} \quad [26]$$

Justification 23.3

When $sR_{ij} \ll 1$ we can use the expansion $\sin x = x - \frac{1}{6}x^3 + \dots$ to write

$$\sin sR_{ij} = sR_{ij} - \frac{1}{6}(sR_{ij})^3 + \dots$$

and then

$$P(\theta) = \frac{1}{N^2} \sum_{ij} \left\{ 1 - \frac{1}{6}(sR_{ij})^2 + \dots \right\} = 1 - \frac{s^2}{6N^2} \sum_{ij} R_{ij}^2 + \dots$$

The sum over the squares of the separations gives the radius of gyration of the molecule (through eqn 26). Therefore

$$P(\theta) \approx 1 - \frac{1}{3}s^2 R_g^2 = 1 - \frac{16\pi^2 \sin^2 \frac{1}{2}\theta}{3\lambda^2} R_g^2$$

shows that $P - 1$ is proportional to R_g^2 .

Because the deviation from Rayleigh scattering depends on R_g , an analysis of the scattering intensity should give the value of R_g for the molecule in solution. This quantity in turn can be interpreted in terms of the size of the molecule. For example, a solid sphere of radius R has $R_g = (3/5)^{1/2}R$, and a long thin rod of length l has $R_g = l/2(3)^{1/2}$ for rotation about an axis perpendicular to the long axis. Once again, it must be emphasized that the analysis must be performed on data obtained by extrapolation to zero concentration. Some experimental values are listed in Table 23.4.

The use of laser light has led to further refinements in the application and interpretation of light scattering. There has been a shift of emphasis towards the investigation of the time dependence of the positions of atoms and the orientation of macromolecules in solution. These aspects of polymer dynamics can be studied by measuring the shift of frequency that occurs when monochromatic light is scattered by a moving target in the technique called **dynamic light scattering**. In particular, laser light scattering can be used for the direct determination of the diffusional characteristics of macromolecules, and provides a fast, direct, and reliable method for the measurement of diffusion coefficients, even of macromolecules of low stability. Polymer dynamics are also studied by inelastic neutron scattering, and are a target of computer simulation algorithms.*

Table 23.4* Radius of gyration

	$M/(\text{kg mol}^{-1})$	R_g/nm
Serum albumin	66	2.98
Polystyrene	3.2×10^3	50†
DNA	4×10^3	117

*More values are given in the *Data section*.
†In a poor solvent.

2 In Problem 23.25, this definition is shown to be equivalent to another and more easily visualized one in the case of a chain of identical atoms: the radius of gyration is the root mean square distance of the atoms from the centre of mass.

Conformation and configuration

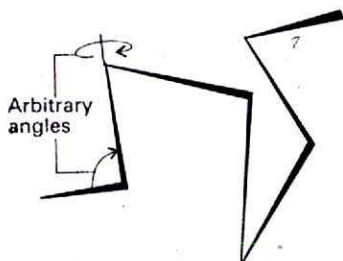
The **primary structure** of a macromolecule is the sequence of small molecular residues making up the chain (or network if there is cross-linking). In the case of a synthetic polymer, virtually all the residues are identical, and it is sufficient to name the monomer used in the synthesis. Thus, the repeating unit of polyethylene is $-\text{CH}_2\text{CH}_2-$, and the primary structure of the chain is specified by denoting it as $-(\text{CH}_2\text{CH}_2)_n-$.

The concept of primary structure ceases to be trivial in the case of synthetic copolymers and biological macromolecules, for in general these substances are chains formed from different molecules. Proteins, for example, are **polypeptides**, the name signifying chains formed from different amino acids (about twenty occur naturally) strung together by the peptide link, $-\text{CONH}-$. The determination of the primary structure is then a highly complex problem of chemical analysis called *sequencing*. The degradation of a polymer is a disruption of its primary structure, when the chain breaks into shorter components.

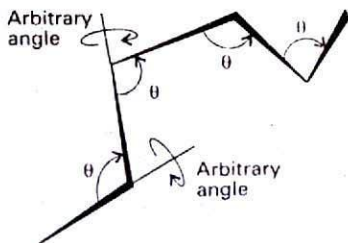
The **secondary structure** of macromolecules refers to the (often local) spatially well-characterized arrangement of the basic structural units. The secondary structure of an isolated molecule of polyethylene is a random coil, whereas that of a protein is a highly organized arrangement determined largely by hydrogen bonds, and taking the form of helices or sheets in various segments of the molecule. The loss of secondary structure is called **denaturation**. When the hydrogen bonds in a protein are destroyed (for instance, by heating, as when cooking an egg) the structure denatures into a random coil.

The difference between primary and secondary structure is closely related to the difference between the 'configuration' and the 'conformation' of a chain. The term **configuration** refers to the structural features that can be changed only by breaking chemical bonds and forming new ones. Thus, the chains $-\text{A}-\text{B}-\text{C}-$ and $-\text{A}-\text{C}-\text{B}-$ have different configurations. The term **conformation** refers to the spatial arrangement of the different parts of a chain, and one conformation can be changed into another by rotating one part of a chain around a bond.

By **tertiary structure** is meant the overall three-dimensional structure of the molecule. For instance, many proteins have a helical secondary structure, but in many proteins the helix is so bent and distorted that the molecule has a globular tertiary structure. The term **quaternary structure** refers to the manner in which some molecules are formed by the aggregation of others. Haemoglobin is a famous example: each molecule consists of four subunits of two types (the α and the β chains).



23.10 A freely jointed chain is like a three-dimensional random walk, each step being in an arbitrary direction but of the same length.



23.11 A better description is obtained by fixing the bond angle (for example, at the tetrahedral angle) and allowing free rotation about a bond direction.

23.6 Random coils

As the first step in unravelling the various aspects of structure, we consider the most likely conformation of a chain of identical units that are incapable of forming hydrogen bonds or any other type of specific bond. Polyethylene is a simple example, but the general idea applies to a denatured protein too. The simplest model is a **freely jointed chain**, in which any bond is free to make any angle with respect to the preceding one (Fig. 23.10); the residues are assumed to occupy zero volume, so different parts of the chain can occupy the same region of space. The model is obviously an oversimplification, because a bond is actually constrained to a cone of angles around a direction defined by its neighbour (Fig. 23.11).

The **random coil** is the least structured conformation of a polymer chain and corresponds to the state of greatest entropy. Any stretching of the coil introduces order and reduces the entropy. Conversely, the formation of a random coil from a more extended form is a spontaneous process (provided enthalpy contributions do not interfere). The random coil model is a helpful starting point for estimating the orders of magnitude of the

hydrodynamic properties (such as sedimentation rates) of polymers and denatured proteins in solution.

The elasticity of a perfect elastomer, a flexible polymer in which the internal energy is independent of the extension, may also be discussed in terms of the properties of a random coil. The strategy is to set up an expression for the conformational entropy, the statistical entropy arising from the arrangement of bonds, and then to use various thermodynamic relations to establish an expression for the force needed to stretch the coil. The first part of the calculation leads to the result that the change in conformational entropy is

$$\Delta S = -\frac{1}{2}kN \ln\{(1+\nu)^{1+\nu}(1-\nu)^{1-\nu}\} \quad \nu = n/N \quad (27)$$

when a polymer containing N bonds of length l is stretched or compressed by nl .

Justification 23.4

Consider a one-dimensional freely jointed polymer. The conformation of a molecule can be expressed in terms of the number of bonds pointing to the right (N_R) and the number pointing to the left (N_L). The distance between the ends of the chain is $(N_R - N_L)l$, where l is the length of an individual bond. We write $n = N_R - N_L$ and the total number of bonds as $N = N_R + N_L$.

The number of ways of forming a chain with a given end-to-end distance nl is the number of ways of having N_R right-pointing and N_L left-pointing bonds, and is given by the binomial coefficient

$$W = \frac{N!}{N_L!N_R!} = \frac{N!}{\{\frac{1}{2}(N+n)\}!\{\frac{1}{2}(N-n)\}!}$$

The conformational entropy of the chain, $S = k \ln W$, is therefore

$$S/k = \ln N! - \ln \{\frac{1}{2}(N+n)\}! - \ln \{\frac{1}{2}(N-n)\}!$$

Because the factorials are large (except for large extensions), we can use Stirling's approximation (Section 19.1a) in the form

$$\ln x! \approx \ln(2\pi)^{1/2} + (x + \frac{1}{2}) \ln x - x$$

to obtain

$$S/k = -\ln(2\pi)^{1/2} + (N+1) \ln 2 + (N + \frac{1}{2}) \ln N - \frac{1}{2} \ln \{(N+n)^{N+n+1} (N-n)^{N-n+1}\}$$

The most probable conformation of the chain is the one with the ends close together ($n = 0$), as may be confirmed by differentiation. Therefore, the maximum entropy is

$$S/k = -\ln(2\pi)^{1/2} + (N+1) \ln 2 - \frac{1}{2} \ln N$$

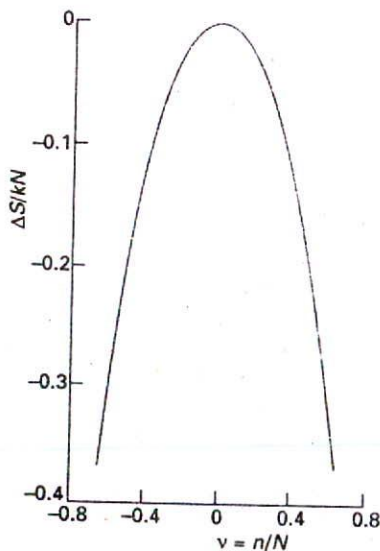
The change in entropy when the chain is stretched or compressed by nl is therefore the difference of these two quantities, and the resulting expression is eqn 27 (Fig. 23.12).

Now for the thermodynamic part of the calculation. The work done on an elastomer when it is extended through a distance dx is $F dx$, where F is the restoring force. The change in internal energy is therefore

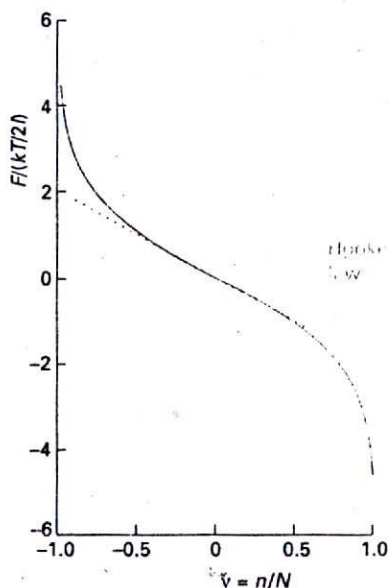
$$dU = T dS - p dV + F dx \quad (28)$$

It follows that

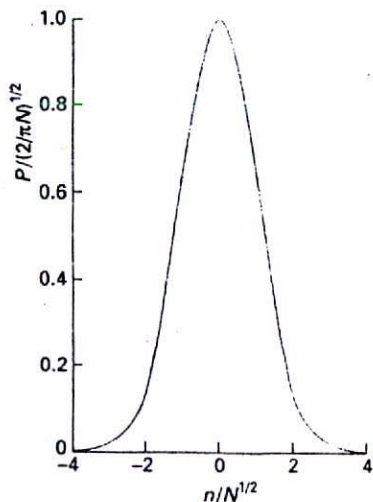
$$\left(\frac{\partial U}{\partial x}\right)_{T,V} = T \left(\frac{\partial S}{\partial x}\right)_{T,V} + F \quad (29)$$



23.12 The change in molar entropy of a perfect rubber as its extension changes: $\nu = 1$ corresponds to complete extension; $\nu = 0$, the conformation of highest entropy, corresponds to the random coil.



23.13 The restoring force, F , of a one-dimensional perfect rubber. For small deflections, F is linearly proportional to extension, corresponding to Hooke's law.



23.14 The probability distribution for the separation of the ends of a one-dimensional random coil. The separation of the ends is nl , where l is the bond length.

In a perfect elastomer, as in a perfect gas, the internal energy is independent of the dimensions (at constant temperature), so $(\partial U/\partial x)_{T,V} = 0$. The restoring force is therefore

$$F = -T \left(\frac{\partial S}{\partial v} \right)_{T,V} \quad (30)^\circ$$

If eqn 27 is now substituted into this expression (we evade problems arising from the constraint of constant volume by supposing that the sample contracts laterally as it is stretched), we obtain

$$F = -\frac{T}{l} \left(\frac{\partial S}{\partial n} \right)_{T,V} = -\frac{T}{Nl} \left(\frac{\partial S}{\partial v} \right)_{T,V} = \frac{kT}{2l} \ln \left(\frac{1+\nu}{1-\nu} \right) \quad (31)^\circ$$

This function is plotted in Fig. 23.13. At low extensions, when $\nu \ll 1$,

$$F \approx \frac{\nu kT}{l} = \frac{nkT}{Nl} \quad (32)^\circ$$

and the sample obeys Hooke's law (that the restoring force is proportional to the displacement). For small displacements, therefore, the whole coil shakes with simple harmonic motion.

(a) The radial distribution

As shown in the *Justification* below, the same model used to discuss the elasticity of a polymer can be used to calculate the probability that the ends of a one-dimensional random coil are a distance nl apart:

$$P = \left(\frac{2}{\pi N} \right)^{1/2} e^{-n^2/N} \quad (33)$$

This function is plotted in Fig. 23.14.

Justification 23.3

The probability of the separation being nl is

$$P = \frac{\text{number of polymers with } N_R \text{ bonds to the right}}{\text{total number of arrangements of bonds}} \\ = \frac{N!/N_R!(N-N_R)!}{2^N} = \frac{N!}{\left\{ \frac{1}{2}(N+n) \right\}! \left\{ \frac{1}{2}(N-n) \right\}! 2^N}$$

At this point, the development follows the same route as in the previous *Justification*, and the use of Stirling's approximation gives (after quite a lot of algebra)

$$\ln P = \ln \left(\frac{2}{\pi N} \right)^{1/2} - \frac{1}{2}(N+n+1) \ln(1+\nu) - \frac{1}{2}(N-n+1) \ln(1-\nu)$$

For small extensions ($\nu \ll 1$) we can use the approximation $\ln(1 \pm \nu) \approx \pm \nu - \frac{1}{2}\nu^2$, and so obtain

$$\ln P \approx \ln \left(\frac{2}{\pi N} \right)^{1/2} - \frac{1}{2}N\nu^2$$

which rearranges into eqn 33.

Equation 33 can be used to calculate the probability that in a three-dimensional coil the ends of the chain lie in the infinitesimal range R to $R + dR$. We write this probability as $f dR$, where

$$f = 4\pi \left(\frac{a}{\pi^{1/2}}\right)^3 R^2 e^{-a^2 R^2} \quad a = \left(\frac{3}{2Nl^2}\right)^{1/2} \quad (34)$$

As usual, N is the number of bonds and l is the bond length.³ Equation 34 shows that, in some coils (the proportion being given by the value of f with R large), the ends may be far apart, whereas in others their separation is small. An alternative interpretation is to regard each coil as ceaselessly writhing from one conformation to another; then $f dR$ is the probability that at any instant the chain will be found with the separation of its ends between R and $R + dR$.

(b) Measures of size

There are several measures of the geometrical size of a random coil. The **contour length**, R_c , is the length of the macromolecule measured along its backbone from atom to atom (the maximum distance that the random walker could walk). For a polymer of N monomer units each of length l , the contour length is

$$R_c = Nl \quad (35)$$

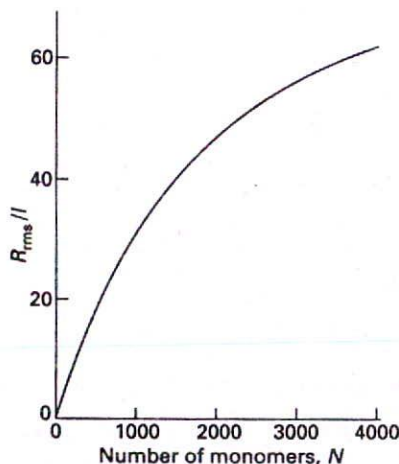
The **root mean square separation**, R_{rms} , is a measure of the average separation of the ends of a random coil: it is the square root of the mean value of R^2 , calculated by weighting each possible value of R^2 with the probability that R occurs:

$$R_{\text{rms}} = \left(\int_0^\infty R^2 f dR \right)^{1/2} = N^{1/2} l \quad (36)$$

We see that, as the number of monomer units increases, the root mean square separation of its ends increases as $N^{1/2}$ (Fig. 23.15), and consequently its volume increases as $N^{3/2}$. Similarly, the radius of gyration of the coil is

$$R_g = \left(\frac{N}{6}\right)^{1/2} l \quad (37)$$

The radius of gyration also increases as $N^{1/2}$.



23.15 The variation of the root mean square separation of the ends of a three-dimensional random coil, R_{rms} , with the number of monomers.

Example 23.6 Calculating the dimensions of a random coil

Calculate the mean separation of the ends of a freely jointed polymer chain of N bonds of length l .

Method The general expression for the mean n th power of the end-to-end separation is

$$\langle R^n \rangle = \int_0^\infty R^n f dR$$

which should be used with $n = 1$ and f from eqn 34.

Answer The mean separation is

$$\langle R \rangle = 4\pi \left(\frac{a}{\pi^{1/2}}\right)^3 \int_0^\infty R^3 e^{-a^2 R^2} dR = \frac{2}{a\pi^{1/2}} = \left(\frac{8N}{3\pi}\right)^{1/2} l$$

³ Here and elsewhere we are ignoring the fact that the chain cannot be longer than Nl . Although eqn 34 gives a nonzero probability for $R > Nl$, the values are so small that the errors in pretending that R can range up to infinity are negligible.

The standard integral we have used is

$$\int_0^{\infty} x^3 e^{-a^2 x^2} dx = \frac{1}{2a^4}$$

Comment The result must be multiplied by a factor when the chain is not freely jointed: see below.

Self-test 23.6 Evaluate the root mean square separation of the ends of the chain.

$[N^{1/2}l]$

(c) Constrained chains

Before making use of these conclusions we must remove the freedom for bond angles to take any value. This adjustment is simple for long chains, for we can take groups of neighbouring bonds and consider the direction of their resultant. Although the individual bonds are constrained to a single cone of angle θ , the resultant of several bonds lies in a random direction. By concentrating on such groups rather than individuals, it turns out that for long chains the average values given above should be multiplied by

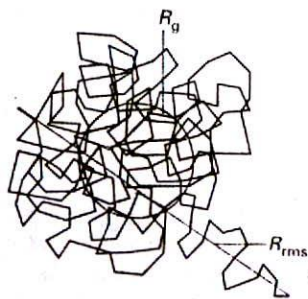
$$F = \left(\frac{1 - \cos \theta}{1 + \cos \theta} \right)^{1/2} \quad (38)$$

For tetrahedral bonds, for which $\cos \theta = -\frac{1}{3}$ (that is, $\theta = 109.5^\circ$), $F = 2^{1/2}$. Therefore:

$$R_{\text{rms}} = (2N)^{1/2}l \quad R_g = \left(\frac{N}{3} \right)^{1/2} l \quad (39)$$

Illustration

For a polyethylene chain with $M = 56 \text{ kg mol}^{-1}$, corresponding to $N = 4000$, because $l = 154 \text{ pm}$ for a C—C bond, we find $R_{\text{rms}} = 14 \text{ nm}$ and $R_g = 5.6 \text{ nm}$ (Fig. 23.16). This value of R_g means that, on average, the coils rotate like hollow spheres of radius 5.6 nm and mass equal to the molecular mass.



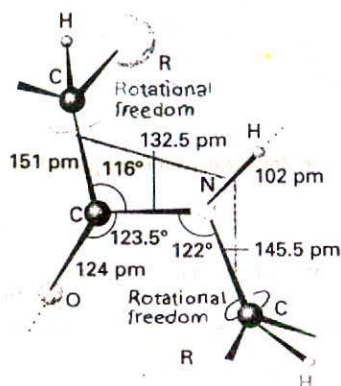
23.16 A random coil in three dimensions. This one contains about 200 units. The root mean square distance between the ends (R_{rms}) and the radius of gyration (R_g) are indicated.

46—A

The model of a randomly coiled molecule is still an approximation, even after the bond angles have been restricted, because it does not take into account the impossibility of two or more atoms occupying the same place. Such self-avoidance tends to swell the coil, so it is better to regard R_{rms} and R_g as lower bounds to the actual values. The model also ignores the role of the solvent: a poor solvent will tend to cause the coil to tighten so that solute-solvent contacts are minimized; a good solvent does the opposite. A θ solvent leaves the coil in its natural state.

23.7 Helices and sheets

Natural macromolecules need a precisely maintained conformation to function. The achievement of a specific conformation is the major remaining problem in protein synthesis for, although primary structures can be built, the product is inactive because the correct secondary structure is not adopted.



23.17 The dimensions that characterize the peptide link. The C—CO—NH—C atoms define a plane (the C—N bond has partial double-bond character), but there is rotational freedom around the C—CO and N—C bonds.

(a) The Corey–Pauling rules

The origin of the secondary structures of proteins is found in the rules formulated by Linus Pauling and Robert Corey in 1951. The essential feature is the stabilization of structures by hydrogen bonds involving the peptide link. The latter can act both as a donor of the H atom (the NH part of the link) and as an acceptor (the CO part). The Corey–Pauling rules are as follows (Fig. 23.17):

1. The atoms of the peptide link lie in a plane.
2. The N, H, and O atoms of a hydrogen bond lie in a straight line (with displacements of H tolerated up to not more than 30° from the N—O vector).
3. All NH and CO groups are engaged in hydrogen bonding.

The rules are satisfied by two structures. One, in which hydrogen bonding occurs between peptide links of the same chain, is the α helix. The other, in which hydrogen bonding links different chains, is the β -pleated sheet; this form is the secondary structure of the protein fibroin, the constituent of silk.

The α helix is illustrated in Fig. 23.18. Each turn of the helix contains 3.6 amino acid residues, so the period of the helix corresponds to 5 turns (18 residues). The pitch of a single turn (the distance between points separated by 360°) is 544 pm. The N—H...O bonds lie parallel to the axis and residue i is linked to residues $i - 4$ and $i + 4$. There is freedom for the helix to be arranged as either a right- or a left-handed screw, but the overwhelming majority of natural polypeptides are right-handed on account of the preponderance of the L-configuration of the naturally occurring amino acids, as we explain below. The reason for their preponderance is uncertain, but it may be related to the symmetries of fundamental particles and the nonconservation of parity (the fact that this universe behaves differently from its hypothetical mirror image).

(b) Conformational energy

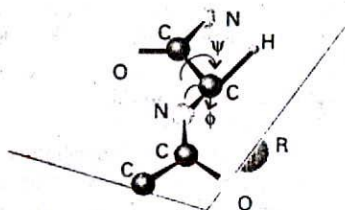
The stabilities of different polypeptide geometries can be investigated by calculating the total potential energy of all the interactions between nonbonded atoms, and looking for a minimum. It turns out, in agreement with experience, that a right-handed α helix of L-amino acids is marginally more stable than a left-handed helix of the same acids.

The geometry of the chain can be specified by two angles, ϕ (the torsional angle for the N—C bond) and ψ (the torsional angle for the C—C bond). The illustration in Fig. 23.19 defines these angles. The sign convention is that a positive angle means that the front atom must be rotated clockwise to bring it into an eclipsed position relative to the rear atom. The illustration shows the all-*trans* form of the chain, in which all ϕ and ψ are 180° . A helix is obtained when all the ϕ are equal and when all the ψ are equal. For a right-handed α helix, all $\phi = -57^\circ$ and all $\psi = -47^\circ$. For a left-handed α helix, both angles are positive. Because only two angles are needed to specify the conformation of a helix, and they range from -180° to $+180^\circ$, the potential energy of the entire molecule can be represented on a Ramachandran plot, a contour diagram in which one axis represents ϕ and the other represents ψ .

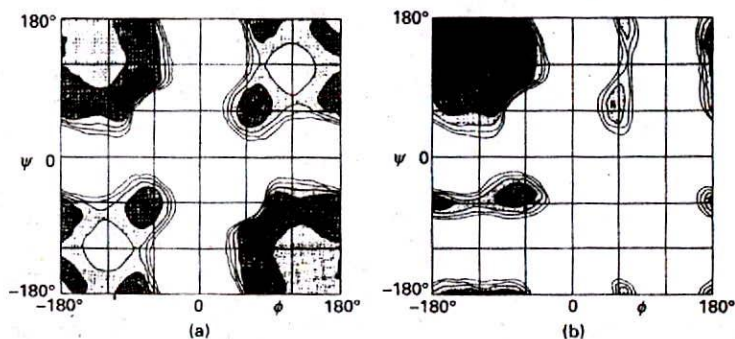
The potential energy of a given conformation (ϕ, ψ) can be calculated by using the expressions developed in Sections 22.3 and 22.4; the procedure is now widely automated in commercially available molecular modelling software. For example, the interaction energy of two atoms separated by a distance R (which we know once ϕ and ψ are specified) can be given the Lennard–Jones (12, 6) form. If the partial charges on the atoms (arising from ionic character in the bonds) are known, a Coulombic contribution of the form $1/R$ can be included. The inclusion of Coulombic interactions is sometimes accomplished by ascribing charges $-0.28e$ and $+0.28e$ to N and H, respectively, and $-0.39e$ and $+0.39e$ to O and C,



23.18 The polypeptide α helix. There are 3.6 residues per turn, and a translation along the helix of 150 pm per residue, giving a pitch of 540 pm. The diameter (ignoring side chains) is about 600 pm.



23.19 The definition of the torsional angles ψ and ϕ between two peptide units. In this case (an α -L-polypeptide) the chain has been drawn in its all-trans form, with $\psi = \phi = 180^\circ$.



23.20 Ramachandran diagrams for (a) a glycyl residue of a polypeptide chain and (b) an alanyl residue. The darker the shading is, the lower the potential energy. The glycyl diagram is symmetrical, but regions I and II in the alanine diagram, which correspond to right- and left-handed helices, are unsymmetrical, and the minimum in region I lies lower than that in region II. (After D.A. Brant and P.J. Flory, *J. Mol. Biol.* 23, 47 (1967).)

respectively. There is also a torsional contribution arising from the barrier to internal rotation of one bond relative to another (just like the barrier to internal rotation in ethane), and which is normally expressed as

$$V = A(1 + \cos 3\phi) + B(1 + \cos 3\psi) \quad (40)$$

in which A and B are constants of the order of 1 kJ mol^{-1} .

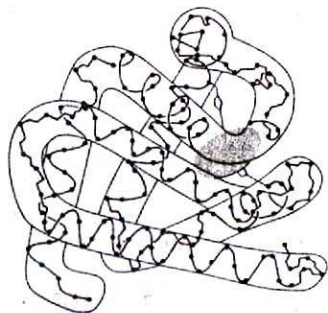
The potential energy contours for the helical form of polypeptide chains formed from the nonchiral amino acid glycine ($R = H$) and the chiral amino acid L-alanine are shown in Fig. 23.20. They were computed by summing all the contributions described above for each choice of angles, and then plotting contours of equal potential energy. The glycine map is symmetrical, with minima of equal depth at $\phi = -80^\circ$, $\psi = +90^\circ$ and at $\phi = +80^\circ$, $\psi = -90^\circ$. In contrast, the map for L-alanine is unsymmetrical, and there are three distinct low-energy conformations (marked I, II, III). The minima of regions I and II lie close to the angles typical of right- and left-handed α helices, but the former has a lower minimum, which is consistent with the formation of right-handed helices from the naturally occurring L-amino acids.

23.8 Higher-order structures

Helical polypeptide chains are folded into a tertiary structure if there are other bonding influences between the residues of the chain that are strong enough to overcome the interactions responsible for the secondary structure. The folding influences include disulfide ($-S-S-$) links, ionic interactions (which depend on the pH), and strong hydrogen bonds (such as $O-H \cdots O-$), and is illustrated by the structure of myoglobin (Fig. 23.21), the full structure (of 2600 atoms) having been determined by X-ray diffraction. The folding of the basic α helix caused by disulfide links can be seen in the structure: about 77 per cent of the structure is α helix, the rest being involved in the folds.

Proteins with $M > 50 \text{ kg mol}^{-1}$ are often found to be aggregates of two or more polypeptide chains. The possibility of such a quaternary structure often confuses the determination of their molar masses, for different techniques might give values differing by factors of 2 or more. Haemoglobin, which consists of four myoglobin-like chains, is an example.

Protein denaturation can be caused by several means, and different aspects of structure may be affected. The 'permanent waving' of hair, for example, is reorganization at the



23.21 The structure of myoglobin. Only the α -carbon atom positions are shown. The haem group, the oxygen binding group, is shown as a shaded region. (Based on M.F. Perutz, copyright *Scientific American*, 1964; with permission.)

quaternary level. Hair is a form of the protein keratin, and its quaternary structure is thought to be a multiple helix, with the α helices bound together by disulfide links and hydrogen bonds (although there is some dispute about its precise structure). The process of permanent waving consists of disrupting these links, unravelling the keratin quaternary structure, and then reforming it into a more fashionable disposition. The 'permanence' is only temporary, however, because the structure of newly formed hair is genetically controlled. Incidentally, normal hair grows at a rate that requires at least 10 twists of the keratin helix to be produced each second, so very close inspection of the human scalp would show it to be literally writhing with activity.

Denaturation at the secondary level is brought about by agents that destroy hydrogen bonds. Thermal motion may be sufficient, in which case denaturation is a kind of intramolecular melting. When eggs are cooked, the albumin is denatured irreversibly, and the protein collapses into a structure resembling a random coil. This **helix-coil transition** is sharp, like ordinary melting, because it is a cooperative process: when one hydrogen bond has been broken it is easier to break the bonds to its neighbours, and then even easier to break their bonds, and so on. The disruption cascades down the helix, and the transition occurs sharply. Denaturation may also be brought about chemically. For instance, a solvent that forms stronger hydrogen bonds than those within the helix will compete successfully for the NH and CO groups. Acids and bases can cause denaturation by protonation or deprotonation of groups involved in hydrogen bonding.

Colloids and surfactants

Much of the material discussed in this chapter also applies to aggregates of particles, either in the form of small particles or of extended sheets, like those forming biological cell walls. However, these systems present a number of specific properties, and we concentrate on them.

23.9 The properties of colloids

A colloid, or disperse phase, is a dispersion of small particles of one material in another. In this context, 'small' means something less than about 500 nm in diameter (about the wavelength of visible light). In general, colloidal particles are aggregates of numerous atoms or molecules, but are too small to be seen with an ordinary optical microscope. They pass through most filter papers, but can be detected by light-scattering, sedimentation, and osmosis.

(a) Classification and preparation

The name given to the disperse phase depends on the two phases involved. A sol is a dispersion of a solid in a liquid (such as clusters of gold atoms in water) or of a solid in a solid (such as ruby glass, which is a gold-in-glass sol, and achieves its colour by scattering). An aerosol is a dispersion of a liquid in a gas (like fog and many sprays) or a solid in a gas (such as smoke): the particles are often large enough to be seen with a microscope. An emulsion is a dispersion of a liquid in a liquid (such as milk).

A further classification of colloids is as **lyophilic**, or solvent-attracting, and **lyophobic**, solvent-repelling. If the solvent is water, the terms **hydrophilic** and **hydrophobic**, respectively, are used instead. Lyophobic colloids include the metal sols. Lyophilic colloids generally have some chemical similarity to the solvent, such as -OH groups able to form hydrogen bonds. A gel is a semirigid mass of a lyophilic sol in which all the dispersion medium has penetrated into the sol particles.

The preparation of aerosols can be as simple as sneezing (which produces an imperfect aerosol). Laboratory and commercial methods make use of several techniques. Material (for example, quartz) may be ground in the presence of the dispersion medium. Passing a heavy electric current through a cell may lead to the sputtering (crumbling) of an electrode into colloidal particles. Arcing between electrodes immersed in the support medium also produces a colloid. Chemical precipitation sometimes results in a colloid. A precipitate (for example, silver iodide) already formed may be dispersed by the addition of a peptizing agent (for example, potassium iodide). Clays may be peptized by alkalis, the OH^- ion being the active agent.

Emulsions are normally prepared by shaking the two components together vigorously, although some kind of emulsifying agent usually has to be added to stabilize the product. This emulsifying agent may be a soap (the salt of a long-chain carboxylic acid) or other surfactant (surface active) species, or a lyophilic sol that forms a protective film around the dispersed phase. In milk, which is an emulsion of fats in water, the emulsifying agent is casein, a protein containing phosphate groups. It is clear from the formation of cream on the surface of milk that casein is not completely successful in stabilizing milk: the dispersed fats coalesce into oily droplets which float to the surface. This coagulation may be prevented by ensuring that the emulsion is dispersed very finely initially: intense agitation with ultrasonics brings this dispersion about, the product being 'homogenized' milk.

One way to form an aerosol is to tear apart a spray of liquid with a jet of gas. The dispersal is aided if a charge is applied to the liquid, for then electrostatic repulsions help to blast it apart into droplets. This procedure may also be used to produce emulsions, for the charged liquid phase may be directed into another liquid.

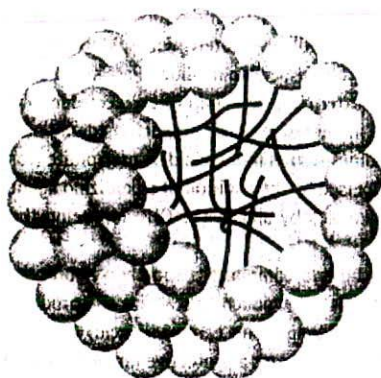
Colloids are often purified by dialysis. The aim is to remove much (but not all, for reasons explained later) of the ionic material that may have accompanied their formation. As in the discussion of the Donnan effect in Section 23.2b, a membrane (for example, cellulose) is selected that is permeable to solvent and ions, but not to the colloid particles. Dialysis is very slow, and is normally accelerated by applying an electric field and making use of the charges carried by many colloid particles; the technique is then called *electrodialysis*.

(b) Structure and stability

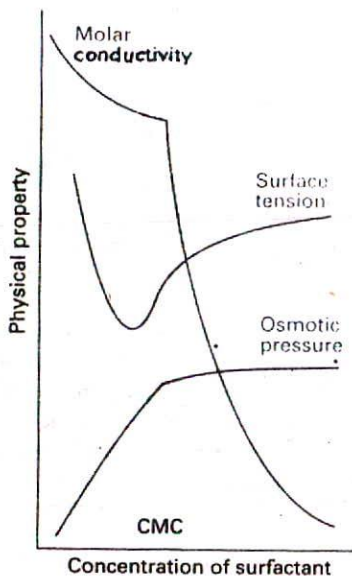
A disperse phase is thermodynamically unstable with respect to the bulk. This instability can be expressed thermodynamically by noting that, because the change in Gibbs energy, dG , when the surface area of the sample changes by $d\sigma$ at constant temperature and pressure is $dG = \gamma d\sigma$, where γ is the interfacial surface tension (Section 6.10), it follows that $dG < 0$ if $d\sigma < 0$. The survival of colloids must therefore be a consequence of the kinetics of collapse: colloids are thermodynamically unstable but kinetically nonlabile.

At first sight, even the kinetic argument seems to fail: colloidal particles attract each other over large distances, so there is a long-range force that tends to condense them into a single blob. The reasoning behind this remark is as follows. The energy of attraction between two individual atoms i and j separated by a distance R_{ij} , one in each colloidal particle, varies as their separation as $1/R_{ij}^6$ (Section 22.4). The sum of all these pairwise interactions, however, decreases only as approximately $1/R^2$ (the precise variation depending on the shape of the particles and their closeness), where R is the separation of the centres of the particles. The sum has a much longer range than the $1/R^6$ dependence characteristic of individual particles and small molecules.

Several factors oppose the long-range dispersion attraction. For example, there may be a protective film at the surface of the colloid particles that stabilizes the interface and cannot be penetrated when two particles touch. Thus the surface atoms of a platinum sol in water react chemically and are turned into $-\text{Pt}(\text{OH})_3\text{H}_3$, and this layer encases the particle like a shell. A fat can be emulsified by a soap because the long hydrocarbon tails penetrate the oil



23.22 A schematic version of a spherical micelle. The hydrophilic groups are represented by spheres and the hydrophobic hydrocarbon chains are represented by the stalks; these stalks are mobile.



23.23 The typical variation of some physical properties of an aqueous solution of sodium dodecylsulfate close to the critical micelle concentration (CMC).

droplet but the carboxylate head groups (or other hydrophilic groups in synthetic detergents) surround the surface, form hydrogen bonds with water, and give rise to a shell of negative charge that repels a possible approach from another similarly charged particle.

(c) Micelle formation and the hydrophobic interaction

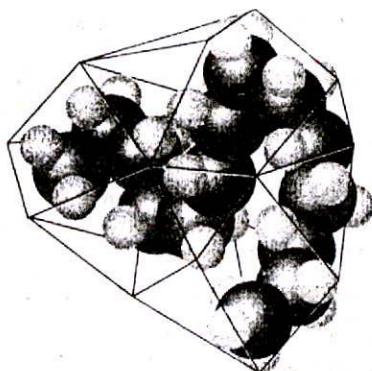
Surfactant molecules or ions can cluster together as micelles, which are colloid-sized clusters of molecules, for their hydrophobic tails tend to congregate, and their hydrophilic heads provide protection (Fig. 23.22). Micelles form only above the critical micelle concentration (CMC) and above the Krafft temperature. The CMC is detected by noting a pronounced discontinuity in physical properties of the solution, particularly the molar conductivity (Fig. 23.23). The hydrocarbon interior of a micelle is like a droplet of oil. Nuclear magnetic resonance shows that the hydrocarbon tails are mobile, but slightly more restricted than in the bulk. Micelles are important in industry and biology on account of their solubilizing function: matter can be transported by water after it has been dissolved in their hydrocarbon interiors. For this reason, micellar systems are used as detergents and drug carriers, and for organic synthesis, froth flotation, and petroleum recovery.

Nonionic surfactant molecules may cluster together in clumps of 1000 or more, but ionic species tend to be disrupted by the electrostatic repulsions between head groups and are normally limited to groups of less than about 100. The micelle population is often polydisperse, and the shapes of the individual micelles vary with concentration. Spherical micelles do occur, but micelles are more commonly flattened spheres close to the CMC. Some micelles at concentrations well above the CMC form extended parallel sheets, called lamellar micelles, two molecules thick. The individual molecules lie perpendicular to the sheets, with hydrophilic groups on the outside in aqueous solution and on the inside in nonpolar media. Such lamellar micelles show a close resemblance to biological membranes, and are often a useful model on which to base investigations of biological structures. In concentrated solutions micelles formed from surfactant molecules may take the form of long cylinders and stack together in reasonably close-packed (hexagonal) arrays. These orderly arrangements of micelles are called lyotropic mesomorphs, and more colloquially 'liquid crystalline phases' (Section 24.5e).

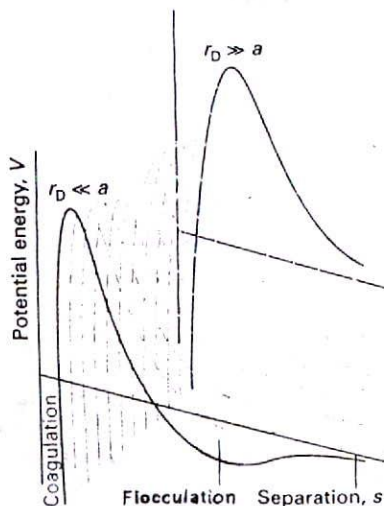
Micelle formation in aqueous systems is commonly endothermic, with $\Delta H \approx 1-2$ kJ per mole of surfactant. That micelles do form above the CMC indicates that the entropy change accompanying their formation must then be positive, and measurements suggest a value of about $+140 \text{ J K}^{-1} \text{ mol}^{-1}$ at room temperature. The fact that the entropy change is positive even though the molecules are clustering together shows that there must be a contribution to the entropy from the solvent, and that solvent molecules must be more free to move once the solute molecules have herded into small clusters. This interpretation is plausible, because each individual solute molecule is held in an organized solvent cage (Fig. 23.24), but once the micelle has formed the solvent molecules need form only a single (admittedly larger) cage. The increase in energy when hydrophobic groups cluster together and reduce their structural demands on the solvent is the origin of the hydrophobic interaction, which tends to stabilize groupings of hydrophobic groups in biological macromolecules. The hydrophobic interaction is an example of an ordering process that is stabilized by a tendency toward greater disorder of the solvent.

(d) The electrical double layer

A major source of kinetic stability of colloids is the existence of an electric charge on the surfaces of the particles. On account of this charge, ions of opposite charge tend to cluster nearby, and an ionic atmosphere is formed, just as for ions (Section 10.2c).



23.24 When a hydrocarbon molecule is surrounded by water, the H_2O molecules form a clathrate cage. As a result of this acquisition of structure, the entropy of the water decreases, so the dispersal of the hydrocarbon into the water is entropy-opposed; its coalescence is entropy-favoured.



23.25 The potential energy of interaction as a function of the separation of the centres of the two particles and its variation with the ratio of the particle size to the thickness a of the electrical double layer r_D . The regions labelled coagulation and flocculation show the dips in the potential energy curves where these processes occur.

Two regions of charge must be distinguished. First, there is a fairly immobile layer of ions that adhere tightly to the surface of the colloidal particle, and which may include water molecules (if that is the support medium). The radius of the sphere that captures this rigid layer is called the **radius of shear**, and is the major factor determining the mobility of the particles. The electric potential at the radius of shear relative to its value in the distant, bulk medium is called the **zeta potential**, ζ , or the **electrokinetic potential**. Second, the charged unit attracts an oppositely charged atmosphere of mobile ions. The inner shell of charge and the outer ionic atmosphere is called the **electrical double layer**.

The theory of the stability of lyophobic dispersions was developed by B. Derjaguin and L. Landau and independently by E. Verwey and J.T.G. Overbeek, and is known as the **DLVO theory**. It assumes that there is a balance between the repulsive interaction between the charges of the electrical double layers on neighbouring particles and the attractive interactions arising from van der Waals interactions between the molecules in the particles. The potential energy arising from the repulsion of double layers on particles of radius a has the form

$$V_{\text{repulsion}} = + \frac{Aa^2\zeta^2}{R} e^{-s/r_D} \quad (41)$$

where A is a constant, ζ is the zeta potential,⁴ R is the separation of centres, s is the separation of the surfaces of the two particles ($s = R - 2a$ for spherical particles of radius a), and r_D is the thickness of the double layer. This expression is valid for small particles with a thick double layer ($a \ll r_D$). When the double layer is thin ($a \gg r_D$), the expression is replaced by

$$V_{\text{repulsion}} = + \frac{1}{2} Aa\zeta^2 \ln(1 + e^{-s/r_D}) \quad (42)$$

In each case, the thickness of the double layer can be estimated from an expression like that derived for the thickness of the ionic atmosphere in the Debye-Hückel theory (eqn 10.33):

$$r_D = \left(\frac{\epsilon RT}{2\rho F^2 I b^{\ominus}} \right)^{1/2} \quad (43)$$

where I is the ionic strength of the solution, ρ its mass density, and $b^{\ominus} = 1 \text{ mol kg}^{-1}$. The potential energy arising from the attractive interaction has the form

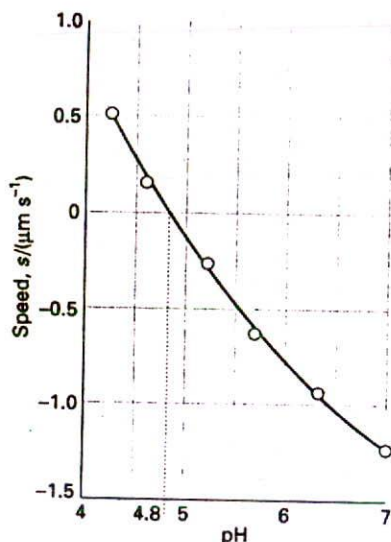
$$V_{\text{attraction}} = - \frac{B}{s} \quad (44)$$

where B is another constant. The variation of the total potential energy with separation is shown in Fig. 23.25.

At high ionic strengths, the ionic atmosphere is dense and the potential shows a secondary minimum at large separations. Aggregation of the particles arising from the stabilizing effect of this secondary minimum is called **flocculation**. The flocculated material can often be redispersed by agitation because the well is so shallow. **Coagulation**, the irreversible blending together of distinct particles into large particles, occurs when the separation of the particles is so small that they enter the primary minimum of the potential energy curve and van der Waals forces are dominant.

The ionic strength is increased by the addition of ions, particularly those of high charge type, so such ions act as flocculating agents. This increase is the basis of the empirical **Schulze-Hardy rule**, that hydrophobic colloids are flocculated most efficiently by ions of opposite charge type and high charge number. The Al^{3+} ions in alum are very effective, and are used to induce the congealing of blood. When river water containing colloidal clay flows

⁴ The actual potential is that of the surface of the particles; there is some danger in identifying it with the zeta potential. See the references in *Further reading*.



23.26 The plot of drift speed against pH by which the isoelectric point of a macromolecule can be determined: it corresponds to the pH at which the drift speed in the presence of an electric field is zero.

into the sea, the salt water induces flocculation and coagulation, and is a major cause of silting in estuaries.

Metal oxide sols tend to be positively charged whereas sulfur and the noble metals tend to be negatively charged. Naturally occurring macromolecules also acquire a charge when dispersed in water, and an important feature of proteins and other natural macromolecules is that their overall charge depends on the pH of the medium. For instance, in acidic environments protons attach to basic groups, and the net charge of the macromolecule is positive; in basic media the net charge is negative as a result of proton loss. At the isoelectric point the pH is such that there is no net charge on the macromolecule.

Example 23.7 Determining the isoelectric point

The drift speed of bovine serum albumin (BSA) under the influence of an electric field in aqueous solution was monitored at several values of pH, and the data are listed below (opposite signs indicate opposite directions of travel). What is the isoelectric point of the protein?

pH	4.20	4.56	5.20	5.65	6.30	7.00
Speed/($\mu\text{m s}^{-1}$)	+0.50	+0.18	-0.25	-0.65	-0.90	-1.25

Method The macromolecule has zero electrophoretic mobility when it is uncharged. Therefore, the isoelectric point is the pH at which it does not migrate in an electric field. We should therefore plot speed against pH and find by interpolation the pH of zero mobility.

Answer The data are plotted in Fig. 23.26. The drift speed is zero at pH = 4.8; hence pH = 4.8 is the isoelectric point.

Comment For some species, the isoelectric point must be obtained by extrapolation because the macromolecule might not be stable over the whole pH range.

Self-test 23.7 The following data were obtained for another protein:

pH	4.5	5.0	5.5	6.0
Speed/($\mu\text{m s}^{-1}$)	-0.10	-0.20	-0.30	-0.35

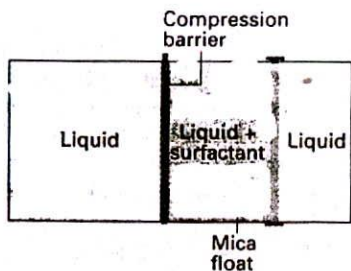
Estimate the pH of the isoelectric point.

[4.3]

The primary role of the electrical double layer is to confer kinetic stability. Colliding colloidal particles break through the double layer and coalesce only if the collision is sufficiently energetic to disrupt the layers of ions and solvating molecules, or if thermal motion has stirred away the surface accumulation of charge. This disruption may occur at high temperatures, which is one reason why sols precipitate when they are heated. The protective role of the double layer is the reason why it is important not to remove all the ions when a colloid is being purified by dialysis, and why proteins coagulate most readily at their isoelectric point.

23.10 Surface films

The compositions of surface layers have been investigated by the simple (but technically elegant) procedure of slicing thin layers off the surfaces of solutions and analysing their compositions. The physical properties of surface films have also been investigated. Surface films one molecule thick, such as that formed by a surfactant, are called monolayers. When a



23.27 A schematic diagram of the apparatus used to measure the surface pressure and other characteristics of a surface film. The surfactant is spread on the surface of the liquid in the trough, and then compressed horizontally by moving the compression barrier towards the mica float. The latter is connected to a torsion wire, so the difference in force on either side of the float can be monitored.

monolayer has been transferred to a solid support, it is called a Langmuir–Blodgett film, after Irving Langmuir and Katherine Blodgett, who developed experimental techniques for studying them.

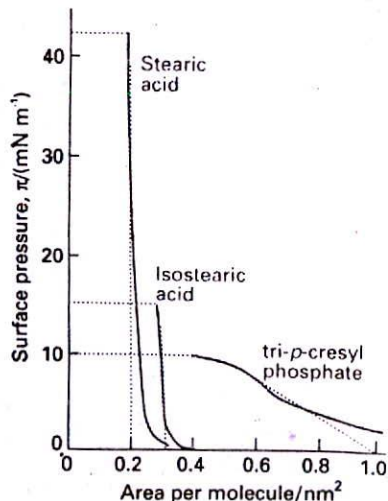
(a) Surface pressure

The principal apparatus used for the study of surface monolayers is a surface film balance, Fig. 23.27. This device consists of a shallow trough and a barrier that can be moved along the surface of the liquid in the trough, and hence compress any monolayer on the surface. The surface pressure, π , the difference between the surface tension of the pure solvent and the solution ($\pi = \gamma^* - \gamma$) is measured by using a torsion wire attached to a strip of mica that rests on the surface and against which one edge of the monolayer is pressed. The parts of the apparatus that are in touch with liquids are coated in polytetrafluoroethylene to eliminate effects arising from the liquid–solid interface. In an actual experiment, a small amount (about 0.01 mg) of the surfactant under investigation is dissolved in a volatile solvent and then poured on to the surface of the water; the compression barrier is then moved across the surface and the surface pressure exerted on the mica bar is monitored.

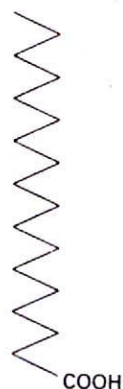
Some typical results are shown in Fig. 23.28. One parameter obtained from the isotherms is the area occupied by the molecules when the monolayer is closely packed. This quantity is obtained from the extrapolation of the steepest part of the isotherm to the horizontal axis. As can be seen from the illustration, even though stearic acid (1) and isostearic acid (2) are chemically very similar (they differ only in the location of a methyl group at the end of a long hydrocarbon chain), they occupy significantly different areas in the monolayer. Neither, though, occupies as much area as the tri-*p*-cresyl phosphate molecule (3), which is like a wide bush rather than a lanky tree.

The second feature to note from Fig. 23.28 is that the tri-*p*-cresyl phosphate isotherm is much less steep than the stearic acid isotherms. This difference indicates that the tri-*p*-cresyl phosphate film is more compressible than the stearic acid films, which is consistent with their different molecular structures.

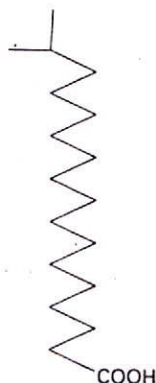
A third feature of the isotherms is the collapse pressure, the highest surface pressure. When the monolayer is compressed beyond the point represented by the collapse pressure, the monolayer buckles and collapses into a film several molecules thick. As can be seen from the isotherms in Fig. 23.28, stearic acid has a high collapse pressure, but that of tri-*p*-cresyl phosphate is significantly smaller, indicating a much weaker film.



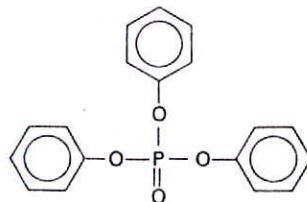
23.28 The variation of surface pressure with the area occupied by each surfactant molecule. The collapse pressures are indicated by the horizontal dotted lines.



1 Stearic acid



2 Isostearic acid



3 Tri-*p*-cresylphosphate

(b) The thermodynamics of surface layers

A surfactant is active at the interface between two phases, such as at the interface between hydrophilic and hydrophobic phases. A surfactant accumulates at the interface, and modifies its surface tension and hence the surface pressure. To establish the relation between the concentration of surfactant at a surface and the change in surface tension it brings about, we consider two phases α and β in contact and suppose that the system consists of several components J , each one present in an overall amount n_J . If the components were distributed uniformly through the two phases right up to the interface, which is taken to be a plane of surface area σ , the total Gibbs energy, G , would be the sum of the Gibbs energies of both phases, $G = G(\alpha) + G(\beta)$. However, the components are not uniformly distributed because one may accumulate at the interface. As a result, the sum of the two Gibbs energies differs from G by an amount called the surface Gibbs energy, $G(\sigma)$:

$$G(\sigma) = G - \{G(\alpha) + G(\beta)\} \quad [45]$$

Similarly, if it is supposed that the concentration of a species J is uniform right up to the interface, then from its volume we would conclude that it contains an amount $n_J(\alpha)$ of J in phase α and an amount $n_J(\beta)$ in phase β . However, because a species may accumulate at the interface, the total amount of J differs from the sum of these two amounts by $n_J(\sigma) = n_J - \{n_J(\alpha) + n_J(\beta)\}$. This difference is expressed in terms of the surface excess, Γ_J :

$$\Gamma_J = \frac{n_J(\sigma)}{\sigma} \quad [46]$$

The surface excess may be either positive (an accumulation of J at the interface) or negative (a deficiency there).

The relation between the change in surface tension and the composition of a surface (as expressed by the surface excess) was derived by Gibbs. In the following *Justification* we derive the Gibbs isotherm, between the changes in the chemical potentials of the substances present in the interface and the change in surface tension:

$$d\gamma = - \sum_J \Gamma_J d\mu_J \quad (47)$$

Justification 23.6

A general change in G is brought about by changes in T , p , and the n_J :

$$dG = -SdT + Vdp + \gamma d\sigma + \sum_J \mu_J dn_J$$

When this relation is applied to G , $G(\alpha)$, and $G(\beta)$ we find

$$dG(\sigma) = -S(\sigma)dT + \gamma d\sigma + \sum_J \mu_J dn_J(\sigma)$$

because at equilibrium the chemical potential of each component is the same in every phase, $\mu_J(\alpha) = \mu_J(\beta) = \mu_J(\sigma)$. Just as in the discussion of partial molar quantities (Section 7.1), the last equation integrates at constant temperature to

$$G(\sigma) = \gamma\sigma + \sum_J \mu_J n_J(\sigma)$$

We are seeking a connection between the change of surface tension $\mathrm{d}\gamma$ and the change of composition at the interface. Therefore, we use the argument which in Section 7.1d led to the Gibbs-Duhem equation (eqn 7.12), but this time we compare the expression

$$\mathrm{d}G(\sigma) = \gamma \mathrm{d}\sigma + \sum_{\mathrm{J}} \mu_{\mathrm{J}} \mathrm{d}n_{\mathrm{J}}(\sigma)$$

(which is valid at constant temperature) with the expression for the same quantity but derived from the preceding equation:

$$\mathrm{d}G(\sigma) = \gamma \mathrm{d}\sigma + \sigma \mathrm{d}\gamma + \sum_{\mathrm{J}} \mu_{\mathrm{J}} \mathrm{d}n_{\mathrm{J}} + \sum_{\mathrm{J}} n_{\mathrm{J}}(\sigma) \mathrm{d}\mu_{\mathrm{J}}$$

The comparison implies that, at constant temperature,

$$\sigma \mathrm{d}\gamma + \sum_{\mathrm{J}} n_{\mathrm{J}} \mathrm{d}\mu_{\mathrm{J}} = 0$$

Division by σ then gives eqn 47.

Now consider a simplified model of the interface in which the 'oil' and 'water' phases are separated by a geometrically flat surface. This approximation implies that only the surfactant, S, accumulates at the surface, and hence that Γ_{Oil} and Γ_{Water} are both zero. Then the Gibbs equation becomes

$$\mathrm{d}\gamma = -\Gamma_{\text{S}} \mathrm{d}\mu_{\text{S}} \quad (48)$$

For dilute solutions,

$$\mathrm{d}\mu_{\text{S}} = RT \mathrm{d} \ln c \quad (49)^{\circ}$$

where c is the molar concentration of the surfactant. It follows that

$$\mathrm{d}\gamma = -RT\Gamma_{\text{S}} \frac{\mathrm{d}c}{c}$$

at constant temperature, or

$$\left(\frac{\partial\gamma}{\partial c}\right)_T = -\frac{RT\Gamma_{\text{S}}}{c} \quad (50)^{\circ}$$

If the surfactant accumulates at the interface, its surface excess is positive and eqn 50 implies that $(\partial\gamma/\partial c)_T < 0$. That is, the surface tension decreases when a solute accumulates at a surface. Conversely, if the concentration dependence of γ is known, the surface excess may be predicted and used to infer the area occupied by each surfactant molecule on the surface.

Checklist of key ideas

- polymers
- monomers

Size and shape

23.1 Mean molar masses

- monodisperse
- polydisperse
- number-average molar mass (1)

- viscosity-average molar mass (3)
- weight-average molar mass (2)
- Z-average molar mass (4)
- heterogeneity index

23.2 Colligative properties

- Flory theta temperature
- θ solution
- vapour-phase osmometry
- polyelectrolyte

- polyanion
- polycation
- polyampholyte
- Donnan equilibrium

23.3 Sedimentation

- sedimentation
- frictional coefficient
- drift speed
- sedimentation constant (11)
- Stokes' relation (13)
- Stokes-Einstein relation (15)

- electrophoresis
- gel electrophoresis
- size-exclusion chromatography (SEC)
- gel permeation chromatography (GPC)

23.4 Viscosity

- intrinsic viscosity (19)
- Ostwald viscometer
- rotating drum viscometer

- Mark-Kuhn-Houwink-Sakurada equation (21)

23.5 Light scattering

- Rayleigh scattering
 radius of gyration (26)
 polymer dynamics
 dynamic light scattering

Conformation and configuration

- primary structure
 polypeptides
 secondary structure
 denaturation
 configuration
 conformation
 tertiary structure
 quaternary structure

23.6 Random coils

- freely jointed chain
 random coil
 perfect elastomer
 conformational entropy (27)
 radial distribution (34)
 contour length (35)
 root mean square separation (36)

23.7 Helices and sheets

- Corey-Pauling rules
 Ramachandran plot
 α helix
 β -pleated sheet

23.8 Higher-order structures

- helix-coil transition

Colloids and surfactants

23.9 The properties of colloids

- colloid
 disperse phase
 sol
 aerosol
 emulsion
 lyophilic
 lyophobic
 hydrophilic
 hydrophobic
 gel
 surfactant
 electro dialysis
 micelle
 critical micelle concentration (CMC)
 Krafft temperature
 lamellar micelle

- lyotropic mesomorph
 hydrophobic interaction
 radius of shear
 zeta potential
 electrokinetic potential
 electrical double layer
 DLVO theory
 flocculation
 coagulation
 Schulze-Hardy rule
 isoelectric point

23.10 Surface films

- monolayer
 Langmuir-Blodgett film
 surface film balance
 surface pressure
 collapse pressure
 surface Gibbs energy (45)
 surface excess (46)
 Gibbs isotherm (47)

Further reading

Articles of general interest

- J.P. Queslel and J.E. Mark, Advances in rubber elasticity and characterization of elastomeric networks. *J. Chem. Educ.* **64**, 491 (1987).
- H. Bisswanger, Proteins and enzymes. In *Encyclopedia of applied physics* (ed. G.L. Trigg), **15**, 185. VCH, New York (1996).
- C.M. Guttman and B. Fanconi, Molecular properties of polymers. In *Encyclopedia of applied physics* (ed. G.L. Trigg), **16**, 549. VCH, New York (1996).
- R.H. Barth, Dialysis. In *Encyclopedia of applied physics* (ed. G.L. Trigg), **4**, 533. VCH, New York (1992).
- B.Y.H. Liu and D.Y.H. Pui, Aerosols. In *Encyclopedia of applied physics* (ed. G.L. Trigg), **1**, 415. VCH, New York (1991).
- R.J. Hunter, *Foundations of colloid science*, Vols 1 and 2. Oxford University Press (1987, 1989).
- B. Dobiáš, *Coagulation and flocculation*. Marcel Dekker, New York (1993).
- Y. Morai, *Micelles*. Plenum, New York (1982).
- M. Takeo, Disperse systems. In *Encyclopedia of applied physics* (ed. G.L. Trigg), **5**, 87. VCH, New York (1993).

Texts and sources of data and information

- F.W. Billmeyer, *Textbook of polymer science*. Wiley, New York (1984).
- I.M. Ward and D.W. Hedley, *Mechanical properties of solid polymers*. Wiley, New York (1993).
- H.R. Allcock and F.W. Lampe, *Contemporary polymer chemistry*. Prentice-Hall, Englewood Cliffs (1981).
- E.G. Richards, *An introduction to physical properties of large molecules in solution*. Cambridge University Press (1980).
- L.H. Sperling, *Physical polymer science*. Wiley-Interscience, New York (1986).
- D. Freifelder, *Physical biochemistry*. W.H. Freeman & Co, New York (1982).
- P. Flory, *Principles of polymer chemistry*. Cornell University Press, Ithaca (1953).
- A.R. Leach, *Molecular modelling: principles and applications*. Longman, Harlow (1996).
- D. Frenkel and B. Smit, *Understanding molecular simulation*. Academic Press, San Diego (1996).

Exercises

- 23.1 (a)** Calculate the number-average molar mass and the mass-average molar mass of a mixture of equal amounts of two polymers, one having $M = 62 \text{ kg mol}^{-1}$ and the other $M = 78 \text{ kg mol}^{-1}$.
- 23.1 (b)** Calculate the number-average molar mass and the mass-average molar mass of a mixture of two polymers, one having $M = 62 \text{ kg mol}^{-1}$ and the other $M = 78 \text{ kg mol}^{-1}$, with their amounts (numbers of moles) in the ratio 3 : 2.
- 23.2 (a)** A polymer chain consists of 700 segments, each 0.90 nm long. If the chain were ideally flexible, what would be the r.m.s. separation of the ends of the chain?
- 23.2 (b)** A polymer chain consists of 1200 segments, each 1.125 nm long. If the chain were ideally flexible, what would be the r.m.s. separation of the ends of the chain?
- 23.3 (a)** The radius of gyration of a long chain molecule is found to be 7.3 nm. The chain consists of C-C links. Assume the chain is randomly coiled and estimate the number of links in the chain.
- 23.3 (b)** The radius of gyration of a long chain molecule is found to be 18.9 nm. The chain consists of links of length 450 pm. Assume the chain is randomly coiled and estimate the number of links in the chain.
- 23.4 (a)** Calculate the contour length (the length of the extended chain) and the root mean square separation (the end-to-end distance) for polyethylene with a molar mass of 280 kg mol^{-1} .
- 23.4 (b)** Calculate the contour length (the length of the extended chain) and the root mean square separation (the end-to-end distance) for polypropylene of molar mass 174 kg mol^{-1} .
- 23.5 (a)** What is the relative rate of sedimentation for two spherical particles of the same density, but which differ in radius by a factor of 10?
- 23.5 (b)** What is the relative rate of sedimentation for two spherical particles with densities 1.10 g cm^{-3} and 1.18 g cm^{-3} and which differ in radius by a factor of 8.4, the former being the larger?
- 23.6 (a)** Find the drift speed of a particle of radius $20 \text{ }\mu\text{m}$ and density 1750 kg m^{-3} which is settling from suspension in water (density 1000 kg m^{-3}) under the influence of gravity alone. The viscosity of water is $8.9 \times 10^{-4} \text{ kg m}^{-1} \text{ s}^{-1}$.
- 23.6 (b)** Find the drift speed of a particle of radius $15.5 \text{ }\mu\text{m}$ and density 1250 kg m^{-3} which is settling from suspension in water (density 1000 kg m^{-3}) under the influence of gravity alone. The viscosity of water is $8.9 \times 10^{-4} \text{ kg m}^{-1} \text{ s}^{-1}$.
- 23.7 (a)** Human haemoglobin has a specific volume of $0.749 \times 10^{-3} \text{ m}^3 \text{ kg}^{-1}$, a sedimentation constant of 4.48 Sv, and a diffusion coefficient of $6.9 \times 10^{-11} \text{ m}^2 \text{ s}^{-1}$. Determine its molar mass from this information.
- 23.7 (b)** A synthetic polymer has a specific volume of $8.01 \times 10^{-4} \text{ m}^3 \text{ kg}^{-1}$, a sedimentation constant of 7.46 Sv, and a diffusion coefficient of $7.72 \times 10^{-11} \text{ m}^2 \text{ s}^{-1}$. Determine its molar mass from this information.
- 23.8 (a)** At 20°C the diffusion coefficient of a macromolecule is found to be $8.3 \times 10^{-11} \text{ m}^2 \text{ s}^{-1}$. Its sedimentation constant is 3.2 Sv in a solution of density 1.06 g cm^{-3} . The specific volume of the macromolecule is $0.656 \text{ cm}^3 \text{ g}^{-1}$. Determine the molar mass of the macromolecule.
- 23.8 (b)** At 20°C the diffusion coefficient of a macromolecule is found to be $7.9 \times 10^{-11} \text{ m}^2 \text{ s}^{-1}$. Its sedimentation constant is 5.1 Sv in a solution of density 997 kg m^{-3} . The specific volume of the macromolecule is $0.721 \text{ cm}^3 \text{ g}^{-1}$. Determine the molar mass of the macromolecule.
- 23.9 (a)** A solution consists of solvent, 30 per cent by mass of a dimer with $M = 30 \text{ kg mol}^{-1}$ and its monomer. What average molar mass would be obtained from measurement of: (a) osmotic pressure, (b) light scattering?
- 23.9 (b)** A solution consists of 25 per cent by mass of a trimer with $M = 22 \text{ kg mol}^{-1}$ and its monomer. What average molar mass would be obtained by measurement of: (a) osmotic pressure, (b) light scattering?
- 23.10 (a)** A polyelectrolyte Na_{20}P with $M = 100 \text{ kg mol}^{-1}$ at a concentration $1.00 \text{ g}/(100 \text{ cm}^3)$ was equilibrated in the presence of $0.0010 \text{ M NaCl(aq)}$ (that is, $[\text{Na}^+]_{\text{R}} = 0.0010 \text{ mol L}^{-1}$). What is the value of $[\text{Na}^+]_{\text{L}}$ at equilibrium?
- 23.10 (b)** A polyelectrolyte K_{15}P with $M = 98.0 \text{ kg mol}^{-1}$ at a concentration $2.00 \text{ g}/(100 \text{ cm}^3)$ was equilibrated in the presence of 0.0015 M KCl(aq) (that is, $[\text{K}^+]_{\text{R}} = 0.0015 \text{ mol L}^{-1}$). What is the value of $[\text{K}^+]_{\text{L}}$ at equilibrium?
- 23.11 (a)** At the start of a membrane equilibrium experiment, the first compartment contains 1.00 L of solution with an NaX concentration of 0.100 mol L^{-1} , where X^- cannot pass through the membrane. The second compartment has 2.00 L of 0.030 M NaCl(aq) . Find the concentration of Cl^- ions in the first compartment after equilibrium is established.
- 23.11 (b)** At the start of a membrane equilibrium experiment, the first compartment contains 1.00 L of solution with a KX concentration of 0.150 mol L^{-1} , where X^- cannot pass through the membrane. The second compartment has 2.00 L of 0.045 M KCl(aq) . Find the concentration of Cl^- ions in the first compartment after equilibrium is established.
- 23.12 (a)** The data from a sedimentation equilibrium experiment performed at 300 K on a macromolecular solute in aqueous solution show that a graph of $\ln c$ against r^2 is a straight line with a slope of 729 cm^{-2} . The rotational rate of the centrifuge was 50 000 r.p.m. The specific volume of the solute is $0.61 \text{ cm}^3 \text{ g}^{-1}$. Calculate the molar mass of the solute.
- 23.12 (b)** The data from a sedimentation equilibrium experiment performed at 293 K on a macromolecular solute in aqueous solution show that a graph of $\ln c$ against $(r/\text{cm})^2$ is a straight line with a slope of 821. The rotation rate of the centrifuge was 1080 Hz. The specific volume of the solute is $7.2 \times 10^{-4} \text{ m}^3 \text{ kg}^{-1}$. Calculate the molar mass of the solute.

23.13 (a) Calculate the radial acceleration (as so many g) in a cell placed at 6.0 cm from the centre of rotation in an ultracentrifuge operating at 80 000 r.p.m.

23.13 (b) Calculate the radial acceleration (as so many g) in a cell placed at 5.50 cm from the centre of rotation in an ultracentrifuge operating at 1.32 kHz.

23.14 (a) Cotton consists of the polymer cellulose, which is a linear chain of glucose molecules. The chains are held together by hydrogen

bonding. When a cotton shirt is ironed, it is first moistened, then heated under pressure. Explain this process.

23.14 (b) Sections of the solid fuel rocket boosters of the space shuttle *Challenger* were sealed together with O-ring rubber seals of circumference 11 m. These seals failed at 0°C, a temperature well above the crystallization temperature of the rubber. Speculate on why the failure occurred.

Problems

Numerical problems

23.1 The concentration dependence of the osmotic pressure of solutions of a macromolecule at 20°C was found to be as follows:

$c/(\text{g L}^{-1})$	1.21	2.72	5.08	6.60
Π/Pa	134	321	655	898

Determine the molar mass of the macromolecule and the osmotic virial coefficient.

23.2 The osmotic pressure of a fraction of poly(vinyl chloride) in a ketone solvent was measured at 25°C. The density of the solvent (which is virtually equal to the density of the solution) was 0.798 g cm^{-3} . Calculate the molar mass and the osmotic virial coefficient, B , of the fraction from the following data:

$c/(\text{g}/10^2 \text{ cm}^3)$	0.200	0.400	0.600	0.088	1.000
h/cm	0.48	1.2	1.86	2.76	3.88

23.3 The concentration dependence of the viscosity of a polymer solution is found to be as follows:

$c/(\text{g L}^{-1})$	1.32	2.89	5.73	9.17
$\eta/(\text{g m}^{-1} \text{ s}^{-1})$	1.08	1.20	1.42	1.73

The viscosity of the solvent is $0.985 \text{ g m}^{-1} \text{ s}^{-1}$. What is the intrinsic viscosity of the polymer?

23.4 In a sedimentation experiment the position of the boundary as a function of time was found to be as follows:

t/min	15.5	29.1	36.4	58.2
r/cm	5.05	5.09	5.12	5.19

The rotation rate of the centrifuge was 45 000 r.p.m. Calculate the sedimentation constant of the solute.

23.5 In an ultracentrifuge experiment at 20°C on bovine serum albumin the following data were obtained: $\rho = 1.001 \text{ g cm}^{-3}$, $v_s = 1.112 \text{ cm}^3 \text{ g}^{-1}$, $\omega/2\pi = 322 \text{ Hz}$,

r/cm	5.0	5.1	5.2	5.3	5.4
$c/(\text{mg cm}^{-3})$	0.536	0.284	0.148	0.077	0.039

Evaluate the molar mass of the sample.

23.6 Calculate the speed of operation (in r.p.m.) of an ultracentrifuge needed to obtain a readily measurable concentration gradient in a sedimentation equilibrium experiment. Take that gradient to be a concentration at the bottom of the cell about five times greater that

at the top. Use $r_{\text{top}} = 5.0 \text{ cm}$, $r_{\text{bottom}} = 7.0 \text{ cm}$, $M \approx 10^5 \text{ g mol}^{-1}$, $\rho v_s \approx 0.75$, $T = 298 \text{ K}$.

23.7 At the start of a Donnan equilibrium experiment, the first compartment contains 2.00 L of solution which is 0.015 M in the polyelectrolyte $\text{Na}_2\text{P}(\text{aq})$ and 0.010 M in $\text{NaCl}(\text{aq})$. The second compartment has 2.00 L of solution which is 0.0050 M in $\text{NaCl}(\text{aq})$. What is the potential difference across the membrane arising from the Na^+ ion concentration difference at 300 K?

23.8 Investigation of the composition of the solutions used to study the osmotic pressure due to a polyelectrolyte with $\nu = 20$ showed that at equilibrium the concentrations corresponded to $[\text{Cl}^-] \approx 0.020 \text{ mol L}^{-1}$. Calculate the osmotic virial coefficient for $\nu = 20$. Does it dominate the effect of excluded volume?

23.9 Sedimentation studies on haemoglobin in water gave a sedimentation constant $S = 4.5 \text{ Sv}$ at 20°C. The diffusion coefficient is $6.3 \times 10^{-11} \text{ m}^2 \text{ s}^{-1}$ at the same temperature. Calculate the molar mass of haemoglobin using $v_s = 0.75 \text{ cm}^3 \text{ g}^{-1}$ for its partial specific volume and $\rho = 0.998 \text{ g cm}^{-3}$ for the density of the solution. Estimate the effective radius of the haemoglobin molecule given that the viscosity of the solution is $1.00 \times 10^{-3} \text{ kg m}^{-1} \text{ s}^{-1}$.

23.10 The times of flow of dilute solutions of polystyrene in benzene through a viscometer at 25°C are given in the table below. From these data, calculate the molar mass of the polystyrene samples. Since the solutions are dilute, assume that the densities of the solutions are the same as those of pure benzene. $\eta(\text{benzene}) = 0.601 \times 10^{-3} \text{ kg m}^{-1} \text{ s}^{-1}$ (0.601 cP) at 25°C.

$c/(\text{g L}^{-1})$	0.000	2.22	5.00	8.00	10.00
t/s	208.2	248.1	303.4	371.8	421.3

23.11 The rate of sedimentation of a recently isolated protein was monitored at 20°C and with a rotor speed of 50 000 r.p.m. The boundary receded as follows:

t/s	0	300	600	900	1200	1500	1800
r/cm	6.127	6.153	6.179	6.206	6.232	6.258	6.284

Calculate the sedimentation constant and the molar mass of the protein on the basis that its partial specific volume is $0.728 \text{ cm}^3 \text{ g}^{-1}$ and its diffusion coefficient is $7.62 \times 10^{-11} \text{ m}^2 \text{ s}^{-1}$ at 20°C, the density of the solution then being 0.9981 g cm^{-3} . Suggest a shape

for the protein given that the viscosity of the solution is $1.00 \times 10^{-3} \text{ kg m}^{-1} \text{ s}^{-1}$ at 20°C .

23.12 The viscosities of solutions of polyisobutylene in benzene were measured at 24°C (the θ temperature for the system) with the following results:

$c/(\text{g}/10^2 \text{ cm}^3)$	0	0.2	0.4	0.6	0.8	1.0
$\eta/(\text{g}/10^{-3} \text{ kg m}^{-1} \text{ s}^{-1})$	0.647	0.690	0.733	0.777	0.821	0.865

Use the information in Table 23.3 to deduce the molar mass of the polymer.

23.13 Evaluate the radius of gyration, R_g , of (a) a solid sphere of radius a , (b) a long straight rod of radius a and length l . Show that, in the case of a solid sphere of specific volume v_s ,

$$R_g/\text{nm} \approx 0.056902 \times \{(v_s/\text{cm}^3 \text{ g}^{-1})(M/\text{g mol}^{-1})\}^{1/3}$$

Evaluate R_g for a species with $M = 100 \text{ kg mol}^{-1}$, $v_s = 0.750 \text{ cm}^3 \text{ g}^{-1}$, and, in the case of the rod, of radius 0.50 nm .

23.14 Use the information below and the expression for R_g of a solid sphere quoted in the previous problem, to classify the species below as globular or rod-like.

	$M/(\text{g mol}^{-1})$	$v_s/(\text{cm}^3 \text{ g}^{-1})$	R_g/nm
Serum albumin	66×10^3	0.752	2.98
Bushy stunt virus	10.6×10^6	0.741	12.0
DNA	4×10^6	0.556	117.0

23.15 In formamide as solvent, poly(γ -benzyl-L-glutamate) is found by light scattering experiments to have a radius of gyration proportional to M ; in contrast, polystyrene in butanone has R_g proportional to $M^{1/2}$. Present arguments to show that the first polymer is a rigid rod, while the second is a random coil.

23.16 The structures of crystalline macromolecules may be determined by X-ray diffraction techniques by methods similar to those for smaller molecules. Fully crystalline polyethylene has its chains aligned in an orthorhombic unit cell of dimensions $740 \text{ pm} \times 493 \text{ pm} \times 253 \text{ pm}$. There are two repeating CH_2CH_2 units per unit cell. Calculate the theoretical density of fully crystalline polyethylene. The actual density ranges from 0.92 to 0.95 g cm^{-3} .

Theoretical problems

23.17 A polymerization process produced a Gaussian distribution of polymers in the sense that the proportion of molecules having a molar mass in the range M to $M + dM$ was proportional to $e^{-(M-M^0)^2/2\sigma^2} dM$. What is the number-average molar mass when the distribution is narrow?

23.18 Consider the thermodynamic description of stretching rubber. The observables are the tension, t , and length, l (the analogues of p and V for gases). Because $dw = tdl$, the basic equation is $dU = TdS + tdl$. (The term $p dV$ is supposed negligible throughout.) If $G = U - TS - tl$, find expressions for dG and dA , and deduce the Maxwell relations

$$\left(\frac{\partial S}{\partial l}\right)_T = -\left(\frac{\partial t}{\partial T}\right)_l, \quad \left(\frac{\partial S}{\partial T}\right)_T = \left(\frac{\partial l}{\partial T}\right)_l$$

Go on to deduce the equation of state for rubber,

$$\left(\frac{\partial U}{\partial l}\right)_T = t - \left(\frac{\partial t}{\partial T}\right)_l$$

23.19 On the assumption that the tension required to keep a sample at a constant length is proportional to the temperature ($t = aT$, the analogue of $p \propto T$), show that the tension can be ascribed to the dependence of the entropy on the length of the sample. Account for this result in terms of the molecular nature of the sample.

23.20 Radius of gyration is defined in eqn 26. Show that an equivalent definition is that R_g is the average root mean square distance of the atoms or groups (all assumed to be of the same mass), that is, that $R_g^2 = (1/N) \sum_j R_j^2$, where R_j is the distance of atom j from the centre of mass.

23.21 Use eqn 34 to deduce expressions for (a) the root mean square separation of the ends of the chain, (b) the mean separation of the ends, and (c) their most probable separation. Evaluate these three quantities for a fully flexible chain with $N = 4000$ and $l = 154 \text{ pm}$.

Additional problems supplied by Carmen Giunta and Charles Trapp

23.22 Polystyrene in cyclohexane at 34.5°C forms a θ solution, with an intrinsic viscosity related to the molar mass by $[\eta] = KM^a$. The following data on polystyrene in cyclohexane are taken from L.J. Fetters, N. Hadjichristidis, J.S. Lindner, and J.W. Mays (*J. Phys. Chem. Ref. Data* 23, 619 (1994)).

$M/(\text{kg mol}^{-1})$	10.0	19.8	106	249	359
$[\eta]/(\text{cm}^3 \text{ g}^{-1})$	8.90	11.9	28.1	44.0	51.2
$M/(\text{kg mol}^{-1})$	860	1800	5470	9720	56 800
$[\eta]/(\text{cm}^3 \text{ g}^{-1})$	77.6	113.9	195	275	667

Determine the parameters K and a . What is the molar mass of a polystyrene that forms a θ solution in cyclohexane with $[\eta] = 100 \text{ cm}^3 \text{ g}^{-1}$?

23.23 Polymer scientists often report their data in rather strange units. For example, in the determination of molar masses of polymers in solution by osmometry, osmotic pressures are often reported in grams per square centimetre (g cm^{-2}) and concentrations in grams per cubic centimetre (g cm^{-3}). (a) With these choices of units, what would be the units of R in the van't Hoff equation? (b) The data in the table below on the concentration dependence of the osmotic pressure of polyisobutene in chlorobenzene at 25°C have been adapted from J. Leonard and H. Daoust (*J. Polymer Sci.* 57, 53 (1962)). From these data, determine the number average molar mass of polyisobutene by plotting Π/c against c . (c) Theta solvents are solvents for which the second osmotic virial coefficient is zero; for 'poor' solvents the plot is linear and for good solvents the plot is nonlinear. From your plot, how would you classify chlorobenzene as a solvent for polyisobutene? Rationalize the result in terms of the molecular structure of polymer and solvent. (d) Determine the second and third osmotic virial coefficients by fitting the curve to the virial form of the osmotic

pressure equation. (e) Experimentally, it is often found that the virial expansion can be represented as

$$\frac{\Pi}{c} = \frac{RT}{M} (1 + B'c + gB'^2c^2 + \dots)$$

and in good solvents, the parameter g is often about 0.25. With terms beyond the second power ignored, obtain an equation for $(\Pi/c)^{1/2}$ and plot this quantity against c . Determine the second and third virial coefficients from this plot and compare to the values from the first plot. Does this plot confirm the assumed value of g ?

$10^{-2}(\Pi/c)/$ ($\text{g cm}^{-2}/\text{g cm}^{-3}$)	2.6	2.9	3.6	4.3	6.0	12.0
$c/(\text{g cm}^{-3})$	0.0050	0.010	0.020	0.033	0.057	0.10
$10^{-2}(\Pi/c)/$ ($\text{g cm}^{-2}/\text{g cm}^{-3}$)	19.0	31.0	38.0	52	63	
$c/(\text{g cm}^{-3})$	0.145	0.195	0.245	0.27	0.29	

23.24 A manufacturer of polystyrene beads claims that they have an average molar mass of 250 kg mol^{-1} . Solutions of these beads are studied by a physical chemistry student by dilute solution viscometry with an Ostwald viscometer in both the 'good' solvent toluene and the theta solvent cyclohexane. The drainage times, t_D , as a function of concentration for the two solvents are given in the table below. (a) Fit the data to the virial equation for viscosity,

$$\eta = \eta^* (1 + [\eta]c + k'[\eta]^2c^2 + \dots)$$

where k' is called the *Huggins constant* and is typically in the range 0.35–0.40. From the fit, determine the intrinsic viscosity and the Huggins constant. (b) Use the empirical Mark–Kuhn–Houwink–Sakurada equation (eqn 21) to determine the molar mass of polystyrene in the two solvents. For theta solvents, $a = 0.5$ and $K = 8.2 \times 10^{-5} \text{ L g}^{-1}$ for cyclohexane; for the good solvent toluene $a = 0.72$ and $K = 1.15 \times 10^{-5} \text{ L g}^{-1}$. (c) According to a general theory proposed by Kirkwood and Riseman, the root mean square end-to-end distance of a polymer chain in solution is related to $[\eta]$ by $[\eta] = \Phi \langle r^2 \rangle^{3/2} / M$, where Φ is a universal constant with the value 2.84×10^{26} when $[\eta]$ is expressed in litres per gram and the distance is in metres. Calculate this quantity for each solvent. (d) From the molar masses calculate the average number of styrene ($\text{C}_6\text{H}_5\text{CH}=\text{CH}_2$) monomer units, $\langle n \rangle$. (e) Calculate the length of a fully stretched, planar zigzag configuration, taking the C–C distance as 154 pm and the CCC bond angle to be 109° . (f) Use eqn 39 to calculate the radius of gyration, R_g . Also calculate $\langle r^2 \rangle^{1/2} = n^{1/2}$. Compare this result with that predicted by the Kirkwood–Riseman theory: which gives the better fit? (g) Compare your values for M to the results of Problem 23.23. Is there any reason why they should or should not agree? Is the manufacturer's claim valid?

$c/(\text{g L}^{-1} \text{ toluene})$	0	1.0	3.0	5.0
t_D/s	8.37	9.11	10.72	12.52
$c/(\text{g L}^{-1} \text{ cyclohexane})$	0	1.0	1.5	2.0
t_D/s	8.32	8.67	8.85	9.03

23.25 K. Sato, F.R. Eirich, and J.E. Mark (*J. Polym. Sci., Polym. Phys.* **14**, 619 (1976)) have reported the data in the table below for the osmotic pressures of polychloroprene ($\rho = 1.25 \text{ g cm}^{-3}$) in toluene ($\rho = 0.858 \text{ g cm}^{-3}$) at 30°C . Determine the molar mass of polychloroprene and its second osmotic virial coefficient.

$c/(\text{mg cm}^{-3})$	1.33	2.10	4.52	7.18	9.87
$\Pi/(\text{N m}^{-2})$	30	51	132	246	390

23.26 Standard polystyrene solutions of known average molar masses continue to be used for the calibration of many methods of characterizing polymer solutions. M. Kolinsky and J. Janca (*J. Polym. Sci., Polym. Chem.* **12**, 1181 (1974)) studied polystyrene in tetrahydrofuran (THF) for use in calibrating a gel permeation chromatograph. Their results for the intrinsic viscosity, $[\eta]$, as a function of average molar mass at 25°C are given in the table below. (a) Obtain the Mark–Houwink constants that fit these data. (b) Compare your values to those in Table 23.3 and Example 23.5. How might you explain the differences?

$M_w/(10^3 \text{ g mol}^{-1})$	5.0	10.3	19.85	51	98.2	173	411	867
$[\eta]/(\text{cm}^3 \text{ g}^{-1})$	5.2	8.8	14.0	21.6	43.6	67.0	125.0	206.7

23.27 There is much recent interest in electronically conducting polymers and the determination of their average molar masses is an important part of their characterization. S. Holdcroft (*J. Polym. Sci., Polym. Phys.* **29**, 1585 (1991)) has determined the molar masses and Mark–Houwink constants for the electronically conducting polymer, poly(3-hexylthiophene) (P3HT) in tetrahydrofuran (THF) at 25°C by methods similar to those used for nonconducting polymers. The values for molar mass and intrinsic viscosity in the table below are adapted from their data. Determine the constants in the Mark–Kuhn–Houwink–Sakurada equation from these results and compare to the values obtained in your solution to Problem 23.26.

$M_w/(10^3 \text{ g mol}^{-1})$	3.8	11.1	15.3	58.8
$[\eta]/(\text{cm}^3 \text{ g}^{-1})$	6.23	17.44	23.73	85.28

23.28 A problem arises in the use of the Svedberg equation (eqn 16) for the determination of the molar masses of macromolecules due to the fact that values of S and D depend upon concentration. Consequently, accurate values for M_w must be obtained by extrapolation of the data to infinite dilution by using a virial expansion in the form

$$\frac{bD}{SRT} = \frac{1}{M_w} (1 + 2B'c + 3gB'^2c^2 + \dots)$$

where g is the parameter introduced in Problem 23.23. W.J. Closs, B.R. Jennings, and H.G. Gerrard (*Eur. Polymer J.* **4**, 639 (1968)) reported the data in the table below for polystyrene in cyclohexane at 35°C . The density of cyclohexane at this temperature, which can also be assumed to be that of the solution, is 0.765 g cm^{-3} , and the partial specific volume of polystyrene is $0.93 \text{ cm}^3 \text{ g}^{-1}$. The dependence of the diffusion constant for these solutions has been determined empirically by T.A. King, A. Knox, W.I. Lee, and J.D.G. McAdam (*Polymer* **14**, 151 (1973)) to be given by the relation $D/(\text{cm}^2 \text{ s}^{-1}) = 1.3 \times 10^{-4} (M_w/(\text{g mol}^{-1}))^{-0.497}$. Determine the molar mass of polystyrene in cyclohexane and the second virial coefficient, B' . Compare the molar mass obtained here to that calculated in Problem 23.24. Is there any reason for them to be the same?

$c/(\text{mg cm}^{-3})$	2.0	3.0	4.0	5.0	6.0	7.0
$S/(10^{-13} \text{ s})$	14.8	13.9	13.1	12.4	11.8	11.2

MicroProjects Part 2:

Prepared by M. Cady and C. A. Trapp

2.1 Black-body radiation and the greenhouse effect

The experimentally observed average temperature of the Earth's surface is 288.16 K. This temperature is maintained in a steady state through an energy balance between solar radiation absorbed by the Earth and black-body radiation which is emitted by the Earth and lost to space. Energy balances of this type are often discussed in terms of energy flux, J , the energy passing through an area in an interval divided by the area and the duration of the interval and expressed in watts per square metre (W m^{-2}).

(a) Prove that $J = \frac{1}{4}c\mathcal{E}$, where \mathcal{E} is the isotropic black-body energy density (eqn 11.5). *Hint.* Examine the radiation passing through area A in the time; use spherical coordinates centred on A and recognize that only volume elements within the hemisphere of radius c contribute to the flux through A . Also, determine $f(\tilde{\nu})$, where $dJ = f(\tilde{\nu})d\tilde{\nu}$ and prove that the Stefan-Boltzmann constant is given by eqn 11.6. Use $f(\tilde{\nu})$ to demonstrate graphically that the Earth's black-body emissions are in the infrared.

(b) Consider an atmospheric model consisting of atmospheric nitrogen and oxygen only. Can these gases absorb any of Earth's black-body emissions? Why? Determine the value of the Earth's surface temperature that is predicted by this model. It is found experimentally that the solar energy flux at the edge of the Earth's atmosphere is 0.1353 W cm^{-2} and that the fraction of the solar radiation scattered by gases and clouds of the atmosphere (the albedo) is 0.29. Consider that the magnitude of the solar radiation absorbed by the Earth equals the disk area of the Earth times the fraction of unscattered solar radiation times the solar radiation flux. The difference between the experimental value of the Earth's temperature and the temperature predicted by this model is due to the so-called greenhouse effect.

(c) Now, consider an atmospheric model consisting of nitrogen, oxygen, some water vapour, and some carbon dioxide. Why is it that water and carbon dioxide are able to absorb some of the Earth's black-body radiation? Which vibrational modes are responsible for this absorption? Water vapour shows strong absorption between 1300 cm^{-1} and 1900 cm^{-1} and also between 3550 cm^{-1} and 3900 cm^{-1} . Carbon dioxide shows strong absorption between 500 cm^{-1} and 725 cm^{-1} and also between 2250 cm^{-1} and 2400 cm^{-1} . Why are these bands so broad? Assume that these gases absorb all radiation falling within these bands and calculate the average surface temperature predicted by this atmospheric model. What percentage of the greenhouse effect is explained by the presence of atmospheric water and carbon dioxide?

2.2 One-dimensional tunnelling

Consider the one-dimensional space in which a particle can experience one of three potentials depending upon its position. They are: $V = 0$ for $-\infty < x \leq 0$, $V = V_2$ for $0 \leq x \leq L$, and $V = V_3$ for $L \leq x < \infty$.

The particle wavefunction is to have both a component e^{ik_1x} that is incident upon the barrier V_2 and a reflected component e^{-ik_1x} in region 1 ($-\infty < x \leq 0$). In region 3 the wavefunction has only a forward component, e^{ik_3x} , which represents a particle which has traversed the barrier. The energy of the particle, E , is somewhere in the range of the $V_2 > E > V_3$. The transmission probability, T , is the ratio of the square modulus of the region 3 amplitude to the square modulus of the incident amplitude.

(a) Base your calculation on the continuity of the amplitudes and the slope of the wavefunction at the locations of the zone boundaries and derive a general equation for T .

(b) Show that the general equation for T reduces to eqn 12.27 in the high, wide barrier limit when $V_1 = V_3 = 0$.

(c) Draw graphs of the probability of proton tunnelling when $V_3 = 0$, $L = 50 \text{ pm}$, and $E = 10 \text{ kJ mol}^{-1}$ in the barrier range $E < V_2 < 2E$.

2.3 Hydrogenic orbitals

Explicit expressions for hydrogenic orbitals are given in Tables 13.1 and 13.2.

(a) Verify both that the $3p_x$ orbital is normalized (to 1) and that $3p_x$ and $3d_{xy}$ are mutually orthogonal.

(b) Determine the positions of both the radial nodes and nodal planes of the $3s$, $3p_x$, and $3d_{xy}$ orbitals.

(c) Determine the mean radius of the $3s$ orbital.

(d) Draw a graph of the radial distribution function for the three orbitals (of part (b)) and discuss the significance of the graphs for interpreting the properties of many-electron atoms.

(e) Create both xy -plane polar plots and boundary surface plots for these orbitals. Construct the boundary plots so that the distance from the origin to the surface is the absolute value of the angular part of the wavefunction. Compare the s , p , and d boundary surface plots with that of an f -orbital, for example, $\psi_f \propto x(5z^2 - r^2) \propto \sin \theta(5 \cos^2 \theta - 1) \cos \phi$.

2.4 A partition function paradox

Consider the electronic partition function of a perfect atomic hydrogen gas at a density of $1.99 \times 10^{-4} \text{ kg m}^{-3}$ and 5780 K. These are the mean conditions within the Sun's photosphere, the surface layer of the Sun that is about 190 km thick.

(a) Show that this partition function, which involves a sum over an infinite number of quantum states that are solutions for the isolated atomic hydrogen atom, is infinite.

(b) Develop a theoretical argument for truncating the sum and estimate the maximum number of quantum states that contribute to the sum.

Structure

(c) Calculate the equilibrium probability that an atomic hydrogen electron is in each quantum state. Are there any general implications concerning electronic states that will be observed for other atoms and molecules? Is it wise to apply these calculations in the study of the Sun's photosphere?

2.5 Ammonia inversion

(a) Use quantum mechanical concepts to explain both the origin of ammonia microwave absorptions at 0.8 cm^{-1} and 36 cm^{-1} and an infrared absorption at 1000 cm^{-1} . All are associated with the umbrella-like inversion of ammonia (see the illustration); the absorption at 1000 cm^{-1} is the lowest-energy infrared transition associated with the inversion.

(b) Prove that

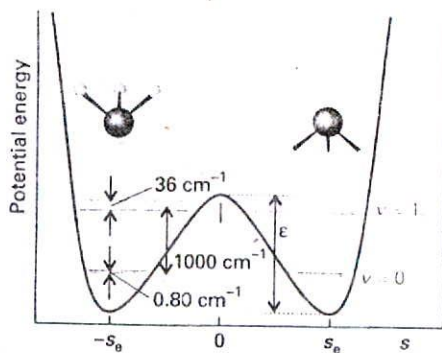
$$C = 2B^{1/2} \quad D = \frac{s_e}{\text{arccosh } B^{1/4}}$$

for an assumed inversion potential of the form

$$V(s) = A\{1 + B \text{sech}^4(s/D) - C \text{sech}^2(s/D)\}$$

where s is the perpendicular distance of the nitrogen from the plane of the three hydrogens. At $s = s_e$ the potential has a minimum value equal to zero and the parameters A , B , C , and D are all positive.

(c) Use the absorption lines and $s_e = 38.1\text{ pm}$ to determine both the potential parameters and the value of the inversion potential barrier height, ϵ . Simplify the computations by assuming that the inversion mode vibrational wavefunctions are adequately described by harmonic oscillator wavefunctions. Also assume that the distances between hydrogen atoms remain constant during inversion. This approximation simplifies the effective mass to: $m_{\text{eff}} = 3m_{\text{H}}m_{\text{N}}/(3m_{\text{H}} + m_{\text{N}})$.



2.6 Vibration-rotation spectra and molecular constants

High-resolution absorption lines of three infrared vibrational bands of carbon monoxide are summarized in Table 1.

(a) Make the J and m assignments for each line, using J to represent the initial rotational state and defining $m = -J$ for P branches and $m = J + 1$ for R branches. Derive an equation for the dependence of the spectral lines upon m including terms for anharmonicity, centrifugal distortion, and rotation-vibration coupling. The rotation-vibration perturbation of the energy of the state (v, J) is equal to $-a(v + \frac{1}{2})J(J + 1)$, where a is the molecular rotation-vibration coupling constant.

(b) Determine all molecular constants associated with the absorption lines by performing an appropriate regression analysis of Table 1 data.

Table 1 Wavenumbers ($\bar{\nu}/\text{cm}^{-1}$) of the infrared absorption lines for vibrational bands of carbon monoxide. (From N. Mina-Camilde, C.I. Manzariates, and J.F. Caballero, *J. Chem. Educ.* 73, 804 (1996).)

	1←0	2←0	3←0		
2059.6	2146.9	4169.8	4263.2	6253.1	6353.8
2063.9	2150.7	4174.6	4267.2	6259.3	6357.2
2068.8	2154.1	4180.0	4270.6	6264.6	6361.0
2073.1	2158.0	4184.8	4274.4	6270.4	6364.4
2077.4	2161.8	4190.1	4277.8	6276.2	6367.8
2081.8	2165.2	4194.9	4281.2	6281.5	6370.7
2086.1	2169.0	4199.7	4284.6	6286.8	6374.1
2090.5	2172.4	4204.1	4287.9	6291.6	6377.0
2094.3	2175.8	4208.9	4290.8	6296.9	6379.9
2098.7	2179.2	4213.7	4294.2	6303.7	6382.7
2103.0	2183.0	4218.0	4297.1	6307.1	6385.2
2106.8	2186.4	4222.4	4300.5	6311.4	6388.0
2111.2	2189.8	4226.7	4303.4	6316.2	6390.5
2115.5	2193.1	4231.1	4306.6	6321.0	6392.9
2119.4	2196.5	4235.4	4308.7	6325.4	6394.8
2123.2	2199.4	4239.7	4311.6	6329.7	6397.2
2127.1	2202.8	4244.1	4314.0	6334.0	6399.1
2131.4	2206.2	4247.9	4316.9	6337.9	6401.1
2135.3	2209.1	4251.8	4319.3	6342.2	6403.0
2139.2	2212.4	4255.6	4321.7	6346.1	6404.6

(c) Determine each of the following: the moment of inertia and bond length defined by the harmonic oscillator and rigid rotor models, I_e and R_e ; the moments of inertia and bond lengths for the $v = 0, 1, 2, 3$ vibration states (define these by analogy to the harmonic oscillator and rigid rotor models); the depth of the Morse potential; D_e (the 'spectroscopic dissociation energy'); and D_0 (the bond dissociation energy).

2.7 An IR absorption band of carbon dioxide

A mixture of carbon dioxide (2.1 per cent) and helium, at 1.00 bar and 298 K in a gas cell of length 10 cm has an IR absorption band centred at 2349 cm^{-1} with absorbances, $A(\bar{\nu})$, described by:

$$A(\bar{\nu}) = \frac{a_1}{1 + a_2(\bar{\nu} - a_3)^2} + \frac{a_4}{1 + a_5(\bar{\nu} - a_6)^2}$$

where the coefficients are $a_1 = 0.932$, $a_2 = 0.005050 \text{ cm}^2$, $a_3 = 2333 \text{ cm}^{-1}$, $a_4 = 1.504$, $a_5 = 0.01521 \text{ cm}^2$, $a_6 = 2362 \text{ cm}^{-1}$.

(a) Draw graphs of $A(\bar{\nu})$ and $\epsilon(\bar{\nu})$. What is the origin of both the band and the band width? What are the allowed and forbidden transitions of this band?

(b) Calculate the transition wavenumbers and absorbances of the band with a simple harmonic oscillator-rigid rotor model and compare the result with the experimental spectra. The CO bond length is 116.2 pm.

(c) Within what height, h , is basically all the IR emission from the Earth in this band absorbed by atmospheric carbon dioxide? The mole fraction of CO_2 in the atmosphere is 3.3×10^{-4} and $T/\text{K} = 288 - 0.0065(h/\text{m})$ below 10 km. Draw a surface plot of the atmospheric transmittance of the band as a function of both height and wavenumber.

2.8 σ and π bonding

Use the $2p_x$ and $2p_z$ hydrogenic atomic orbitals to construct simple LCAO descriptions of $2p\sigma$ and $2p\pi$ molecular orbitals.

(a) Make a probability density plot, and both surface and contour plots of the xz -plane amplitudes of the $2p_x\sigma$ and $2p_z\sigma^*$ molecular orbitals.

(b) Make surface and contour plots of the xz -plane amplitudes of the $2p_x\pi$ and $2p_x\pi^*$ molecular orbitals. Include plots for both of internuclear distances, R , of $10a_0$ and $3a_0$. Interpret the graphs, and describe why scientists are so interested in this graphical information.

2.9 Numerical analysis of the simple LCAO-MO description of H_2^+

The LCAO-MO constructed from normalized $1s$ hydrogenic wavefunctions centred on nuclei that are a distance R apart, and having g symmetry, does not describe the molecular hydrogen ion ground state accurately. It does provide insight into functional characteristics of wavefunctions, bonding, and numerical methods needed in quantum chemistry. The overlap, Coulomb, and resonance integrals of this LCAO-MO can be analytically evaluated to give the result in eqns 14.12 and 14.13. In this problem we evaluate the integrals numerically for S, j , and k and compare the results with the values determined from the analytically integrated forms of eqn 14.13.

(a) Use the LCAO-MO wavefunction and the H_2^+ hamiltonian to derive equations for the Coulomb and resonance integrals in terms of j and k ; do not integrate j and k analytically. Evaluate the overlap, Coulomb, and resonance integrals numerically, and the total energy for the $1s\sigma_g$ MO in the range $a_0 < R < 4a_0$. Compare the results obtained through numerical integration with results obtained with the analytical equations.

(b) Use the results of the numerical integrations to draw a graph of the total energy, $E(R)$, and determine the minimum of total energy, the equilibrium internuclear distance, and the spectroscopic dissociation energy (D_e).

2.10 The variation method and H_2^+

A highly accurate description of the molecular hydrogen ion bond length, R_e , is provided by an MO constructed with the variation parameter η , within the LCAO-MO ground state consisting of two $1s$ hydrogenic orbitals centred upon nuclei A and B. With the nuclear separation R , the MO is

$$\psi = N \left(e^{-\eta r_A/a_0} + e^{-\eta r_B/a_0} \right) \quad N = \left(\frac{\eta^3}{2\pi a_0^3(1+S)} \right)^{1/2}$$

(a) Use this wavefunction and the variation principle to determine η , R_e , the electronic energy (E_{el}), the minimum total energy (E), and D_e . The electronic Hamiltonian does not contain the nuclear repulsion term. Draw graphs of $\eta(R)$, $E_{el}(R)$, and $E(R)$. With this MO it is found that the electronic energy is the sum of the expectation value for kinetic energy ($\eta^2 F_1$) and the expectation value for electron potential energy (ηF_2):

$$E_{el} = \frac{e^2 \{ \eta^2 F_1(\omega) + \eta F_2(\omega) \}}{4\pi\epsilon_0 a_0} \quad \omega = \eta R/a_0$$

$$F_1(\omega) = \frac{1 + (1 + \omega - \frac{1}{3}\omega^2)e^{-\omega}}{2\{1 + S(\omega)\}}$$

$$F_2(\omega) = \frac{(1 + \omega)e^{-2\omega} - 1 - \omega - 2\omega(1 + \omega)e^{-\omega}}{\omega\{1 + S(\omega)\}}$$

$$S(\omega) = (1 + \omega + \frac{1}{3}\omega^2)e^{-\omega}$$

(b) Check numerically to determine whether or not the virial theorem is satisfied by this solution.

(c) Prove that the overlap integral, S , is correctly described by the above expression. The integration is facilitated by the ellipsoidal coordinates (μ, ν, ϕ) defined by the following relations:

$$R\mu = r_A + r_B \quad r\nu = r_A - r_B \quad d\tau = \frac{1}{8}R^3(\mu^2 - \nu^2) d\mu d\nu d\phi$$

with $1 \leq \mu \leq \infty$, $-1 \leq \nu \leq 1$, and $0 \leq \phi \leq 2\pi$.

2.11 Simple Hückel molecular orbitals

Solve the following in the context of simple Hückel theory.

(a) Prove that for an open chain of N conjugated carbons the characteristic polynomial of the secular determinant, $P_N(x)$, where $x = (\alpha - \beta)/\beta$, obeys the recurrence relation $P_N = xP_{N-1} - P_{N-2}$, with $P_1 = x$ and $P_0 = 1$.

(b) Determine a reasonable empirical estimate of the resonance integral for the homologous series consisting of ethene, butadiene, hexatriene, and octatetraene given that the $\pi^* \leftarrow \pi$ ultraviolet absorptions are at 61 500, 46 080, 39 750, and 32 900 cm^{-1} , respectively.

(c) Calculate the π -electron delocalization energy, E_{deloc} , of octatetraene where $E_{\text{deloc}} = E_{\pi} - n(\alpha + \beta)$, where E_{π} is the total π -electron binding energy and n is the total number of π -electrons.

2.12 Equilibrium statistical thermodynamics

Treat carbon monoxide as a perfect gas and apply equilibrium statistical thermodynamics to the study of its properties, as specified below, in the temperature range 100–1000 K at 1 bar. $\nu = 2169.8 \text{ cm}^{-1}$,

$B = 1.931 \text{ cm}^{-1}$, and $D_0 = 11.09 \text{ eV}$; neglect anharmonicity and centrifugal distortion.

(a) Examine the probability distribution of molecules over available rotational and vibrational states.

(b) Explore numerically the differences, if any, between the rotational molecular partition function as calculated with the discrete energy distribution and that calculated with the classical, continuous energy distribution.

(c) Calculate the individual contributions to $U_{\text{m}}(T) - U_{\text{m}}(100 \text{ K})$, $C_{V,\text{m}}(T)$, and $S_{\text{m}}(T) - S_{\text{m}}(100 \text{ K})$ made by the translational, rotational, and vibrational degrees of freedom.



Part 3 Change

- 24 Molecules in motion
- 25 The rates of chemical reactions
- 26 The kinetics of complex reactions
- 27 Molecular reaction dynamics
- 28 Processes at solid surfaces
- 29 Dynamic electrochemistry
- MicroProjects

Part 3 considers the processes by which change occurs. We prepare the ground for a discussion of the rates of reactions by considering the motion of molecules in gases and in liquids. Then we establish the precise meaning of reaction rate, and see how the overall rate, and the complex behaviour of some reactions, may be expressed in terms of elementary steps and the atomic events that take place when molecules meet. Characteristic physical and chemical events take place at surfaces, including catalysis, and we see how to describe them. A special type of surface is that of an electrode, and we shall see how to describe and understand the rate at which electrons are transferred between an electrode and species in solution.



24

Molecules in motion



Molecular motion in gases

- 24.1 Collisions with walls and surfaces
- 24.2 The rate of effusion
- 24.3 Migration down gradients
- 24.4 Transport properties of a perfect gas

Motion in liquids

- 24.5 The structures of liquids
- 24.6 Molecular motion in liquids
- 24.7 The conductivities of electrolyte solutions
- 24.8 The mobilities of ions
- 24.9 Conductivities and ion-ion interactions

Diffusion

- 24.10 The thermodynamic view
- 24.11 The diffusion equation
- 24.12 Diffusion probabilities
- 24.13 The statistical view

Checklist of key ideas

Further reading

Exercises

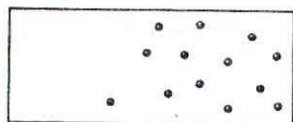
Problems

One of the simplest types of molecular motion to describe is the random motion of molecules of a perfect gas. We see that the kinetic theory can be used to account for the rates at which molecules and energy migrate through gases and that simple expressions for the rates can be derived. Molecular mobility is particularly important in liquids, and we shall see a little of the structure of this phase and the motion of molecules in it. Another simple kind of motion is the largely uniform motion of ions in solution in the presence of an electric field. Molecular and ionic motion have common features and, by considering them from a more general viewpoint, we derive expressions that govern the migration of properties through matter. One of the most useful consequences of this general approach is the formulation of the diffusion equation, which is an equation that shows how matter and energy spread through media of various kinds. Finally, we build a simple model for all types of molecular motion, in which the molecules migrate in a series of small steps, and see that it accounts for many of the properties of migrating molecules in both gases and condensed phases.

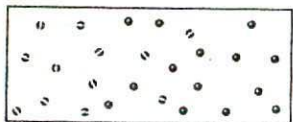
The general approach we describe in this chapter provides techniques for discussing the motion of all kinds of particles in all kinds of fluids. We set the scene by considering a simple type of motion, that of molecules in a perfect gas, and go on to see that molecular motion in liquids shows a number of similarities.

Molecular motion in gases

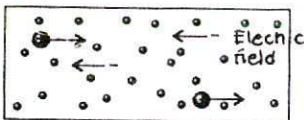
In Section 1.3 we saw that the equilibrium properties of a gas can be understood in terms of the kinetic theory, which is based on a model of a gas in which the molecules are in ceaseless, random motion. Here we develop the kinetic theory to deal with gases that are not at internal equilibrium. In particular, we concentrate on the transport properties of a substance, its ability to transfer matter, energy, or some other property from one place to another. Four examples of transport properties are:



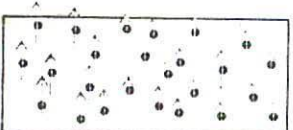
(a)



(b)



(c)



(d)

24.1 Four types of transport process: (a) diffusion, the spreading of one species into another; (b) thermal conduction, when molecules with different energies of thermal motion (represented by the arrows) spread into each others' regions; (c) electrical conduction, when ions migrate under the influence of an electric field; (d) viscosity, when molecules with different linear momenta (represented by the arrows) migrate.

Diffusion, the migration of matter down a concentration gradient.

Thermal conduction, the migration of energy down a temperature gradient.

Electric conduction, the migration of electric charge along a potential gradient.

Viscosity, the migration of linear momentum down a velocity gradient.

These processes are illustrated in Fig. 24.1. It is convenient to include effusion, the emergence of a gas from a container through a small hole, in the discussion.

We shall use two expressions derived in Chapter 1. One is for the mean free path, λ , of molecules in a gas:

$$\lambda = \frac{kT}{2^{1/2}\sigma p} \quad (1)^\circ$$

where σ is the collision cross-section (this is eqn 1.33). The mean free path is independent of temperature in a container of constant volume because p is proportional to the temperature ($p = nRT/V$) and its variation cancels the T in the numerator. The second property is the mean speed, \bar{c} , of molecules of mass m and molar mass M :

$$\bar{c} = \left(\frac{8kT}{\pi m}\right)^{1/2} = \left(\frac{8RT}{\pi M}\right)^{1/2} \quad (2)^\circ$$

This expression was derived in Example 1.6. The mean speed is proportional to $T^{1/2}$ and inversely proportional to $M^{1/2}$.

24.1 Collisions with walls and surfaces

The key to accounting for transport in the gas phase is the rate at which molecules strike an area (which may be an imaginary area embedded in the gas, or part of a real wall). The collision flux, Z_w , is the number of collisions with the area in a given time interval divided by the area and the duration of the interval. The collision frequency, the number of hits per second, is obtained by multiplication of the collision flux by the area of interest. We show in the *Justification* below that

$$Z_w = \frac{p}{(2\pi mkT)^{1/2}} \quad (3)^\circ$$

When $p = 100$ kPa (1.00 bar) and $T = 300$ K, $Z_w \approx 3 \times 10^{23}$ cm⁻²s⁻¹.

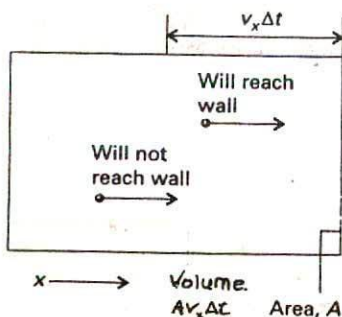
Justification 24.1

Consider a wall of area A perpendicular to the x -axis (Fig. 24.2). If a molecule has $v_x > 0$ (that is, it is travelling in the direction of positive x), then it will strike the wall within an interval Δt if it lies within a distance $v_x \Delta t$ of the wall. Therefore, all molecules in the volume $Av_x \Delta t$, and with positive x -component of velocities, will strike the wall in the interval Δt . The total number of collisions in this interval is therefore the volume $Av_x \Delta t$ multiplied by the number density, \mathcal{N} , of molecules. However, to take account of the presence of a range of velocities in the sample, we must sum the result over all the positive values of v_x weighted by the probability distribution of velocities (eqn 1.25):

$$\text{Number of collisions} = \mathcal{N}A\Delta t \int_0^\infty v_x f(v_x) dx$$

The collision flux is the number of collisions divided by A and Δt , so

$$Z_w = \mathcal{N} \int_0^\infty v_x f(v_x) dx$$



24.2 Only molecules within a distance $v_x \Delta t$ with $v_x > 0$ can reach the wall on the right in an interval Δt .

Then, using the velocity distribution in eqn 1.25,

$$\int_0^{\infty} v_x f(v_x) dv_x = \left(\frac{m}{2\pi kT}\right)^{1/2} \int_0^{\infty} v_x e^{-mv_x^2/2kT} dv_x = \left(\frac{kT}{2\pi m}\right)^{1/2}$$

Therefore,

$$Z_w = \mathcal{N} \left(\frac{kT}{2\pi m}\right)^{1/2} = \frac{1}{4} \bar{c} \mathcal{N} \quad (4)^\circ$$

Substitution of $\mathcal{N} = nN_A/V = p/kT$ gives eqn 3.

24.2 The rate of effusion

The essential empirical observations on effusion are summarized by **Graham's law of effusion**, which states that the rate of effusion is inversely proportional to the square root of the molar mass. The basis of this result is that, as remarked above, the mean speed of molecules is inversely proportional to $M^{1/2}$, so the rate at which they strike the area of the hole is similarly inversely proportional to $M^{1/2}$. However, by using the expression for the rate of collisions, we can obtain a more detailed expression for the rate of effusion and hence use effusion data more effectively.

When a gas at a pressure p and temperature T is separated from a vacuum by a small hole, the rate of escape of its molecules is equal to the rate at which they strike the area of the hole (which is given by eqn 3). Therefore, for a hole of area A_0 ,

$$\text{Rate of effusion} = Z_w A_0 = \frac{pA_0}{(2\pi mkT)^{1/2}} = \frac{pA_0 N_A}{(2\pi MRT)^{1/2}} \quad (5)^\circ$$

(In the last step we have used $R = N_A k$ and $M = mN_A$.) This rate is inversely proportional to $M^{1/2}$, in accord with Graham's law.

Example 24.1 Deducing the time dependence of the pressure inside an effusion oven

Derive an expression that shows how the pressure of a gas inside an effusion oven (a heated chamber with a small hole in one wall) varies with time if the oven is not replenished as the gas escapes.

Method The rate of effusion is proportional to the pressure of the gas in the container so, as gas effuses and the pressure falls, the rate of effusion will decrease. To find the explicit expression, set up a differential equation relating dp/dt to p , and then integrate it. The rate of effusion, as given by eqn 5, is the number of molecules that leave the container in a given interval divided by the duration of the interval. The first step is to relate the rate of change of pressure to the rate of change of number of molecules by using the perfect gas law in the form $pV = NkT$.

Answer The rate of change of pressure of a gas in a container at constant pressure and temperature is related to the rate of change of the number of molecules present by

$$\frac{dp}{dt} = \frac{kT}{V} \frac{dN}{dt}$$

The rate of change of the number of molecules is equal to the collision frequency with the hole, and that in turn is equal to the collision flux multiplied by the area of the hole:

$$\frac{dN}{dt} = -Z_w A_0 = -\frac{pA_0}{(2\pi mkT)^{1/2}}$$

Substitution of this expression into the one above gives

$$\frac{dp}{dt} = -\left(\frac{kT}{2\pi m}\right)^{1/2} \frac{pA_0}{V}$$

This expression integrates to

$$p = p_0 e^{-t/\tau} \quad \tau = \left(\frac{2\pi m}{kT}\right)^{1/2} \frac{V}{A_0}$$

Comment The pressure falls exponentially towards zero; the decrease is faster the higher the temperature; the bigger the hole, and the lower the mass of the molecules.

Self-test 24.1 Show that $t_{1/2}$, the time required for the pressure to decrease to half its initial value, is independent of the initial pressure.

$$[t_{1/2} = \tau \ln 2]$$

Equation 5 is the basis of the Knudsen method for the determination of the vapour pressures of liquids and solids, particularly of substances with very low vapour pressures. Thus, if the vapour pressure of a sample is p , and it is enclosed in a cavity with a small hole, then the rate of loss of mass from the container is proportional to p .

Example 24.2 Calculating the vapour pressure from a mass loss

Caesium (m.p. 29°C, b.p. 686°C) was introduced into a container and heated to 500°C. When a hole of diameter 0.50 mm was opened in the container for 100 s, a mass loss of 385 mg was measured. Calculate the vapour pressure of liquid caesium at 500°C.

Method The pressure of vapour is constant inside the container despite the effusion of atoms because the hot liquid metal replenishes the vapour. The rate of effusion is therefore constant, and given by eqn 5. To express the rate in terms of mass, the number of atoms that escape is multiplied by the mass of each atom.

Answer The mass loss Δm in an interval Δt is related to the collision flux by

$$\Delta m = Z_w A_0 m \Delta t$$

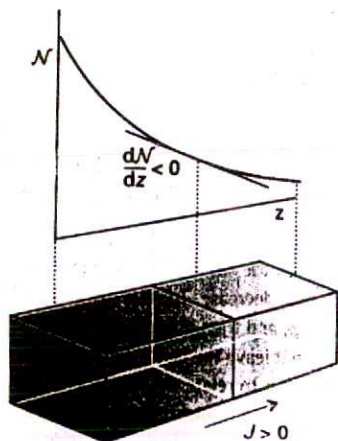
where A_0 is the area of the hole and m is the mass of one atom. It follows that

$$Z_w = \frac{\Delta m}{A_0 m \Delta t}$$

Because Z_w is related to the pressure by eqn 3, we can write

$$p = \left(\frac{2\pi RT}{M}\right)^{1/2} \frac{\Delta m}{A_0 \Delta t}$$

Because $M = 132.9 \text{ g mol}^{-1}$, substitution of the data gives $p = 11 \text{ kPa}$ (using $1 \text{ Pa} = 1 \text{ N m}^{-2} = 1 \text{ J m}^{-1}$), or 83 Torr.



24.3 The flux of particles down a concentration gradient. Fick's first law states that the flux of matter (the number of particles passing through an imaginary window in a given interval divided by the area of the window and the length of the interval) is proportional to the density gradient at that point.

Self-test 24.2 How long would it take 1.0 g of Cs atoms to effuse out of the oven under the same conditions?

[260 s]

24.3 Migration down gradients

The rate of migration of a property is measured by its *flux*, J , the quantity of that property passing through a given area in a given time interval divided by the area and the duration of the interval. If matter is flowing (as in diffusion), we speak of a *matter flux* of so many molecules per square metre per second; if the property is energy (as in thermal conduction), then we speak of the *energy flux* and express it in joules per square metre per second, and so on.

Experimental observations on transport properties show that the flux of a property is usually proportional to the first derivative of some other related property. For example, the flux of matter diffusing parallel to the z -axis of a container is found to be proportional to the first derivative of the concentration:

$$J(\text{matter}) \propto \frac{dN}{dz} \quad (6)$$

where N is the number density of particles with units number per metre cubed (m^{-3}). The SI units of J are number per metre squared per second ($\text{m}^{-2} \text{s}^{-1}$). The proportionality of the flux of matter to the concentration gradient is sometimes called *Fick's first law of diffusion*: the law implies that, if the concentration varies steeply with position, then diffusion will be fast. There is no net flux if the concentration is uniform ($dN/dz = 0$). Similarly, the rate of thermal conduction (the flux of the energy associated with thermal motion) is found to be proportional to the temperature gradient:

$$J(\text{energy}) \propto \frac{dT}{dz} \quad (7)$$

The SI units of this flux are joules per metre squared per second ($\text{J m}^{-2} \text{s}^{-1}$).

A positive value of J signifies a flux towards positive z ; a negative value of J signifies a flux towards negative z . Because matter flows down a concentration gradient, from high concentration to low concentration, J is positive if dN/dz is negative (Fig. 24.3). Therefore, the coefficient of proportionality in eqn 7 must be negative, and we write it $-D$:

$$J(\text{matter}) = -D \frac{dN}{dz} \quad (8)$$

The constant D is called the *diffusion coefficient*; its SI units are metre squared per second ($\text{m}^2 \text{s}^{-1}$). Energy migrates down a temperature gradient, and the same reasoning leads to

$$J(\text{energy}) = -\kappa \frac{dT}{dz} \quad (9)$$

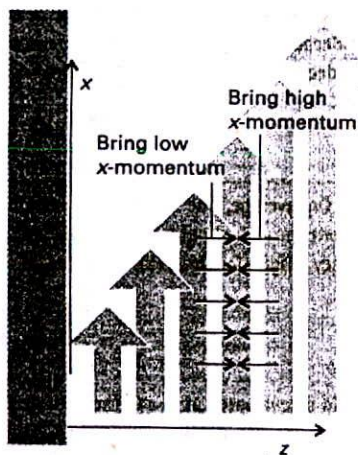
where κ is the coefficient of thermal conductivity. The SI units of κ are joules per kelvin per metre per second ($\text{J K}^{-1} \text{m}^{-1} \text{s}^{-1}$). Some experimental values are given in Table 24.1.

To see the connection between the flux of momentum and the viscosity, consider a fluid in a state of *Newtonian flow*, which can be imagined as occurring by a series of layers moving past one another (Fig. 24.4). The layer next to the wall of the vessel is stationary, and the velocity of successive layers varies linearly with distance, z , from the wall. Molecules ceaselessly move between the layers and bring with them the x -component of linear momentum they possessed in their original layer. A layer is retarded by molecules arriving from a more slowly moving layer because they have a low momentum in the x -direction. A

Table 24.1* Transport properties of gases at 1 atm

	$\kappa/(\text{JK}^{-1} \text{m}^{-1} \text{s}^{-1})$	$\eta/\mu\text{P}\dagger$	
	273 K	273 K	293 K
Ar	0.0163	210	223
CO ₂	0.0145	136	147
He	0.1442	187	196
N ₂	0.0240	166	176

* More values are given in the *Data* section at the end of this volume.



24.4 The viscosity of a gas arises from the transport of linear momentum. In this illustration the liquid is undergoing laminar flow, and particles bring their initial momentum when they enter a new layer. If they arrive with a high x -component of momentum they accelerate the layer; if they arrive with a low x -component of momentum they retard the layer.

layer is accelerated by molecules arriving from a more rapidly moving layer. We interpret the net retarding effect as the fluid's viscosity.

Because the retarding effect depends on the transfer of the x -component of linear momentum into the layer of interest, the viscosity depends on the flux of this x -component in the z -direction. The flux of the x -component of momentum is proportional to dv_x/dz because there is no net flux when all the layers move at the same velocity. We can therefore write

$$J(x\text{-component of momentum}) = -\eta \frac{dv_x}{dz} \quad (10)$$

The constant of proportionality, η , is the coefficient of viscosity (or simply 'the viscosity'). Its units are kilogram per metre per second ($\text{kg m}^{-1} \text{s}^{-1}$). Viscosities are often reported in poise (P), where $1 \text{ P} = 10^{-1} \text{ kg m}^{-1} \text{ s}^{-1}$. Some experimental values are given in Table 24.1.

24.4 Transport properties of a perfect gas

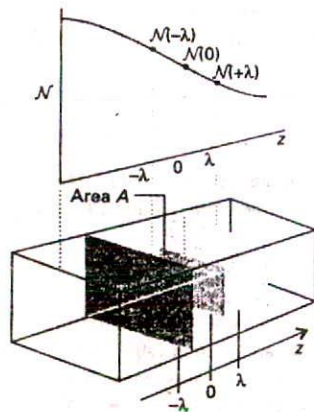
We shall now see how the kinetic theory can be used to justify Fick's law, and deduce the values of the transport coefficients of a perfect gas. These expressions show how transport properties vary with the conditions.

(a) Diffusion

As shown in the *Justification* below and summarized in Table 24.2, the kinetic theory leads to the result that, for a perfect gas,

$$D = \frac{1}{3} \lambda \bar{c} \quad (11)^\circ$$

The mean free path, λ , decreases as the pressure is increased (Section 1.3c), so D decreases with increasing pressure and, as a result, the gas molecules diffuse more slowly. The mean speed, \bar{c} , increases with the temperature (Section 1.3a), so D also increases with temperature. As a result, molecules in a hot sample diffuse more quickly than those in a cool sample (for a given concentration gradient). Because the mean free path increases when the collision cross-section of the molecules decreases, the diffusion coefficient is greater for small molecules than for large molecules.



24.5 The calculation of the rate of diffusion of a gas considers the net flux of molecules through a plane of area A as a result of arrivals from on average a distance λ away in each direction, where λ is the mean free path.

Justification 24.2

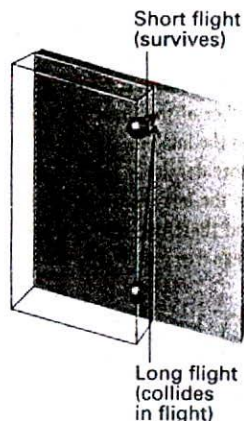
Consider the arrangement depicted in Fig. 24.5. On average, the molecules passing through the area A at $z = 0$ have travelled about one mean free path λ since their last collision. Therefore, the number density where they originated is $\mathcal{N}(z)$ evaluated at $z = -\lambda$. This number density is approximately¹

$$\mathcal{N}(-\lambda) = \mathcal{N}(0) - \lambda \left(\frac{d\mathcal{N}}{dz} \right)_0 \quad (12)$$

where the subscript 0 indicates that the slope should be evaluated at $z = 0$. The average number of impacts on the imaginary window of area A_0 during an interval Δt is $Z_w A_0 \Delta t$, with $Z_w = \frac{1}{4} \mathcal{N} \bar{c}$ (eqn 4). Therefore, the flux from left to right, $J(L \rightarrow R)$, arising from the supply of molecules on the left, is

$$J(L \rightarrow R) = \frac{\frac{1}{4} A_0 \mathcal{N}(-\lambda) \bar{c} \Delta t}{A_0 \Delta t} = \frac{1}{4} \mathcal{N}(-\lambda) \bar{c} \quad (13a)$$

¹ This relation, and others like it that follow, is based on the Taylor expansion of a function, $f(x) = f(0) + (df/dx)_0 x + \dots$, truncated after the second term.



24.6 One approximation ignored in the simple treatment is that some particles might make a long flight to the plane even though they are only a short perpendicular distance away, and therefore they have a higher chance of colliding during their journey.

Table 24.2 Transport properties of perfect gases

Property	Transported quantity	Simple kinetic theory	Units
Diffusion	Matter	$D = \frac{1}{3} \lambda \bar{c}$	$\text{m}^2 \text{s}^{-1}$
Thermal conductivity	Energy	$\kappa = \frac{1}{3} \lambda \bar{c} C_{V,m} [A]$ $= \frac{\bar{c} C_{V,m}}{(3\sqrt{2}) \sigma N_A}$	$\text{JK}^{-1} \text{m}^{-1} \text{s}^{-1}$
Viscosity	Momentum	$\eta = \frac{1}{3} \lambda \bar{c} m \mathcal{N}$ $= \frac{m \bar{c}}{(3\sqrt{2}) \sigma}$	$\text{kg m}^{-1} \text{s}^{-1}$

There is also a flux of molecules from right to left. On average, the molecules making the journey have originated from $z = +\lambda$ where the number density is $\mathcal{N}(\lambda)$. Therefore,

$$J(L \leftarrow R) = -\frac{1}{4} \mathcal{N}(\lambda) \bar{c} \quad (13b)$$

The average number density at $z = +\lambda$ is approximately

$$\mathcal{N}(\lambda) = \mathcal{N}(0) + \lambda \left(\frac{d\mathcal{N}}{dz} \right)_0 \quad (14)$$

The net flux is

$$\begin{aligned} J_z &= J(L \rightarrow R) + J(L \leftarrow R) \\ &= \frac{1}{4} \bar{c} \left\{ \left[\mathcal{N}(0) - \lambda \left(\frac{d\mathcal{N}}{dz} \right)_0 \right] - \left[\mathcal{N}(0) + \lambda \left(\frac{d\mathcal{N}}{dz} \right)_0 \right] \right\} \\ &= -\frac{1}{2} \bar{c} \lambda \left(\frac{d\mathcal{N}}{dz} \right)_0 \end{aligned} \quad (15)$$

This equation shows that the flux is proportional to the first derivative of the concentration, in agreement with Fick's law.

At this stage it looks as though we can pick out a value of the diffusion coefficient by comparing eqns 8 and 15, so obtaining $D = \frac{1}{2} \lambda \bar{c}$. It must be remembered, however, that the calculation is quite crude, and is little more than an assessment of the order of magnitude of D . One aspect that has not been taken into account is illustrated in Fig. 24.6, which shows that, although a molecule may have begun its journey very close to the window, it could have a long flight before it gets there. Because the path is long, the molecule is likely to collide before reaching the window, so it ought to be added to the graveyard of other molecules that have collided. To take this effect into account involves a lot of work, but the end result is the appearance of a factor of $\frac{2}{3}$ representing the lower flux. The modification results in eqn 11.

(b) Thermal conduction

According to the kinetic theory of gases, and as shown in the *Justification* below, the coefficient of thermal conductivity of a perfect gas A having molar concentration [A] is given by the expression

$$\kappa = \frac{1}{3} \lambda \bar{c} C_{V,m} [A] \quad (16)^\circ$$

where $C_{V,m}$ is the molar heat capacity at constant volume.

Justification 24.3

According to the equipartition theorem (Section 20.3 and the *Introduction*), each molecule carries an average energy $\varepsilon = \nu kT$, where ν is a number of the order of 1. For monatomic particles, $\nu = \frac{3}{2}$. When one molecule passes through the imaginary window, it transports that energy on average. We suppose that the number density is uniform but that the temperature is not. On average, molecules arrive from the left after travelling a mean free path from their last collision in a hotter region, and therefore with a higher energy. Molecules also arrive from the right after travelling a mean free path from a cooler region. The two opposing energy fluxes are therefore

$$\begin{aligned} J(L \rightarrow R) &= \frac{1}{4} \bar{c} \mathcal{N} \varepsilon(-\lambda) & \varepsilon(-\lambda) &= \nu k \left\{ T - \lambda \left(\frac{dT}{dz} \right)_0 \right\} \\ J(L \leftarrow R) &= -\frac{1}{4} \bar{c} \mathcal{N} \varepsilon(\lambda) & \varepsilon(\lambda) &= \nu k \left\{ T + \lambda \left(\frac{dT}{dz} \right)_0 \right\} \end{aligned} \quad (17)$$

and the net flux is

$$J_z = J(L \rightarrow R) + J(L \leftarrow R) = -\frac{1}{2} \nu k \lambda \bar{c} \mathcal{N} \left(\frac{dT}{dz} \right)_0 \quad (18)$$

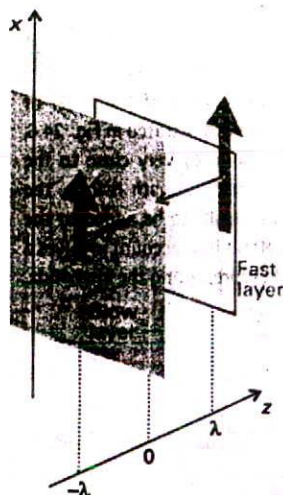
As before, we multiply by $\frac{2}{3}$ to take long flight paths into account, and so arrive at

$$J_z = -\frac{1}{3} \nu k \lambda \bar{c} \mathcal{N} \left(\frac{dT}{dz} \right)_0 \quad (19)$$

The energy flux is proportional to the temperature gradient, as we wanted to show. Comparison of this equation with eqn 9 shows that

$$\kappa = \frac{1}{3} \nu k \lambda \bar{c} \mathcal{N} \quad (20)$$

Equation 16 then follows from $C_{v,m} = \nu k N_A$ for a perfect gas, where $[A]$ is the molar concentration of A . For this step, we use $\mathcal{N} = N/V = n N_A/V = N_A [A]$.



24.7 The calculation of the viscosity of a gas examines the net x -component of momentum brought to a plane from faster and slower layers on average a mean free path away in each direction.

Because λ is inversely proportional to the pressure, and hence inversely proportional to the molar concentration of the gas, it follows from eqn 16 that the thermal conductivity is independent of the pressure. The physical reason for this independence is that the thermal conductivity can be expected to be large when many molecules are available to transport the energy, but the presence of so many molecules limits their mean free path and they cannot carry the energy over a great distance. These two effects balance. The thermal conductivity is indeed found experimentally to be independent of the pressure, except when the pressure is very low, when $\kappa \propto p$. At low pressures λ exceeds the dimensions of the apparatus, and the distance over which the energy is transported is determined by the size of the container and not by the other molecules present. The flux is still proportional to the number of carriers, but the length of the journey no longer depends on λ , so $\kappa \propto [A]$, which implies that $\kappa \propto p$.

(c) The viscosity of a perfect gas

We have seen that viscosity is related to the flux of momentum. As shown in the *Justification* below, the expression obtained from the kinetic theory of gases is

$$\eta = \frac{1}{3} M \lambda \bar{c} [A] \quad (21)^\circ$$

where $[A]$ is the molar concentration of the gas molecules and M is their molar mass.

Justification 24.4

Molecules travelling from the right in Fig. 24.7 (from a fast layer to a slower one) transport a momentum $mw_x(\lambda)$ to their new layer at $z = 0$; those travelling from the left transport $mw_x(-\lambda)$ to it. If it is assumed that the density is uniform, the collision flux is $\frac{1}{2}N\bar{c}$. Those arriving from the right on average carry a momentum

$$mw_x(\lambda) = mw_x(0) + m\lambda\left(\frac{dv_x}{dz}\right)_0$$

Those arriving from the left bring a momentum

$$mw_x(-\lambda) = mw_x(0) - m\lambda\left(\frac{dv_x}{dz}\right)_0$$

The net flux of x -momentum in the z -direction is therefore

$$\begin{aligned} J &= \frac{1}{2}N\bar{c}\left\{\left[mw_x(0) - m\lambda\left(\frac{dv_x}{dz}\right)_0\right] - \left[mw_x(0) + m\lambda\left(\frac{dv_x}{dz}\right)_0\right]\right\} \\ &= -\frac{1}{2}N\bar{c}m\lambda\left(\frac{dv_x}{dz}\right)_0 \end{aligned}$$

The flux is proportional to the velocity gradient, as we wished to show. Comparison of this expression with eqn 10, and multiplication by $\frac{2}{3}$ in the normal way, leads to

$$\eta = \frac{1}{3}N\bar{c}m\lambda\bar{c} \quad (22)$$

which can easily be converted into eqn 21.

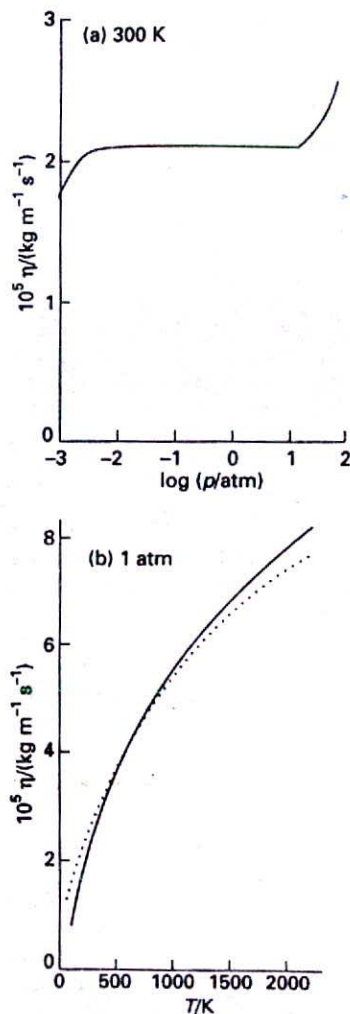
The viscosity is independent of the pressure: $\lambda \propto 1/p$ and $[A] \propto p$, implying that $\eta \propto \bar{c}$, independent of p . The physical reason is the same as for the thermal conductivity: more molecules are available to transport the momentum, but they carry it less far on account of the decrease in mean free path. An unexpected result is that, because $\bar{c} \propto T^{1/2}$, the viscosity coefficient is proportional to $T^{1/2}$. That is, the viscosity of a gas increases with temperature. This conclusion is explained when we remember that at high temperatures the molecules travel more quickly, so the flux of momentum is greater.²

There are two main techniques for measuring viscosities of gases. One technique depends on the rate of damping of the torsional oscillations of a disk hanging in the gas. The half-life of the decay of the oscillation depends on the viscosity and the design of the apparatus, and the apparatus needs to be calibrated. The other method is based on Poiseuille's formula for the rate of flow of a fluid through a tube of radius r :

$$\frac{dV}{dt} = \frac{(p_1^2 - p_2^2)\pi r^4}{16l\eta p_0} \quad (23)$$

where V is the volume flowing, p_1 and p_2 are the pressures at each end of the tube of length l , and p_0 is the pressure at which the volume is measured.

Such measurements confirm that the viscosities of gases are independent of pressure over a wide range. For instance, the results for argon from 10^{-3} atm to 10^2 atm are shown in Fig. 24.8, and we see that η is constant from about 0.01 atm to 20 atm. The measurements also confirm (to a lesser extent) the $T^{1/2}$ dependence. The dotted line in the illustration shows the calculated values using $\sigma = 22 \times 10^{-20}$ m², implying a collision diameter of 260 pm, in contrast to the van der Waals diameter of 335 pm obtained from the density of



24.8 The experimental results for (a) the pressure dependence of the viscosity of argon, and (b) its temperature dependence. The dotted line in the latter is the calculated value. Fitting the observed and calculated curves is one way of determining the collision cross-section.

² As we shall see in Section 24.6, the viscosity of a liquid decreases with increase in temperature because intermolecular interactions must be overcome.

the solid. The agreement is not too bad, considering the simplicity of the model, especially the neglect of intermolecular forces.

Example 24.3 Using the Poiseuille formula to measure a viscosity

In a Poiseuille flow experiment to measure the viscosity of air at 298 K, the sample was allowed to flow through a tube of length 100 cm and internal diameter 1.00 mm. The high-pressure end was at 765 Torr and the low-pressure end was at 760 Torr. The volume was measured at the latter pressure. In 100 s, 90.2 cm³ of air passed through the tube. What is the viscosity of air at 298 K?

Method The data can be used in the Poiseuille formula, eqn 23, reorganized into

$$\eta = \frac{(p_1^2 - p_2^2)\pi r^4}{16lp_0(dV/dt)}$$

To use this formula, convert the pressures to pascals by using 1 Torr = 133.3 Pa.

Answer The rate of flow is

$$\frac{dV}{dt} = \frac{9.02 \times 10^{-5} \text{ m}^3}{100 \text{ s}} = 9.02 \times 10^{-7} \text{ m}^3 \text{ s}^{-1}$$

Therefore, because

$$p_1^2 - p_2^2 = 1.355 \times 10^8 \text{ Pa}^2$$

and

$$\frac{\pi r^4}{16lp_0} = 1.94 \times 10^{-18} \text{ N}^{-1} \text{ m}^5$$

it follows that $\eta = 2.91 \times 10^{-4} \text{ kg m}^{-1} \text{ s}^{-1}$.

Comment The kinetic theory expression gives $\eta = 1.4 \times 10^{-5} \text{ kg m}^{-1} \text{ s}^{-1}$, so the agreement is quite good. Viscosities are commonly expressed in centipoise (cP) or (for gases) micropoise (μP), the conversion being 1 cP = $10^{-3} \text{ kg m}^{-1} \text{ s}^{-1}$; the viscosity of air at 20°C is about 180 μP .

Self-test 24.3 What volume would be collected if the pressure gradient were doubled, other conditions remaining constant?

[180 cm³]

Motion in liquids

As a first step in dealing with the much more difficult problem of motion in liquids, we outline what is currently known about the structure of a simple liquid. Then we consider a particularly simple type of motion through a liquid, that of an ion, and see that the information that motion provides can be used to infer the behaviour of uncharged species too.

24.5 The structures of liquids

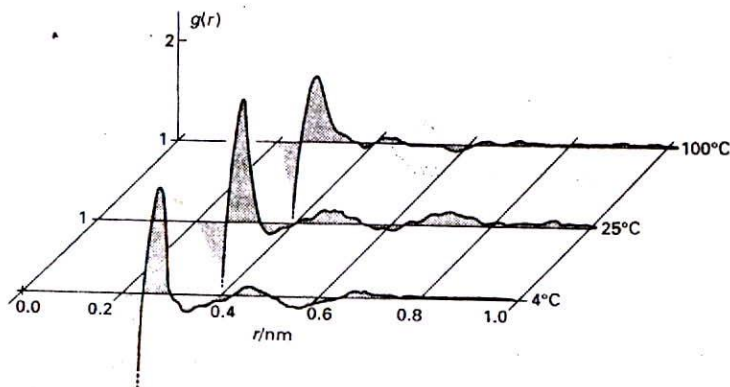
The starting point for the discussion of solids is the well-ordered structure of perfect crystals. The starting point for the discussion of gases is the completely disordered distribution of the molecules of a perfect gas. Liquids lie between these two extremes.

(a) The radial distribution function

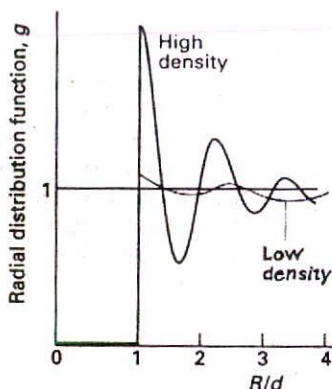
The average relative locations of the particles of a liquid are expressed in terms of the radial distribution function, $g(r)$. This function is defined so that $g(r)r^2 dr$ is the probability that a molecule will be found in the range dr at a distance r from another molecule. In a perfect crystal, $g(r)$ is a periodic array of sharp spikes, representing the certainty (in the absence of defects and thermal motion) that molecules (or ions) lie at definite locations. This regularity continues out to the edges of the crystal, so we say that crystals have long-range order. When the crystal melts, the long-range order is lost and, wherever we look at long distances from a given molecule, there is equal probability of finding a second molecule. Close to the first molecule, though, the nearest neighbours might still adopt approximately their original relative positions and, even if they are displaced by newcomers, the new particles might adopt their vacated positions. It is still possible to detect a sphere of nearest neighbours at a distance r_1 , and perhaps beyond them a sphere of next-nearest neighbours at r_2 . The existence of this short-range order means that the radial distribution function can be expected to oscillate at short distances, with a peak at r_1 , a smaller peak at r_2 , and perhaps some more structure beyond that.

The radial distribution function can be determined experimentally by X-ray diffraction, for $g(r)$ can be extracted from the diffuse diffraction pattern characteristic of liquid samples in much the same way as a crystal structure is obtained from X-ray diffraction of crystals. The shells of local structure shown in the example in Fig. 24.9 (for water) are unmistakable. Closer analysis shows that any given H_2O molecule is surrounded by other molecules at the corners of a tetrahedron, similar to the arrangement in ice (Fig. 21.33). The form of $g(r)$ at 100°C shows that the intermolecular forces (in this case, principally by hydrogen bonds) are strong enough to affect the local structure right up to the boiling point. Raman spectra and molecular dynamics calculations indicate that in liquid water most molecules participate in either three or four hydrogen bonds. Infrared spectra show that about 90 per cent of hydrogen bonds are intact at the melting point of ice, falling to about 20 per cent at the boiling point.

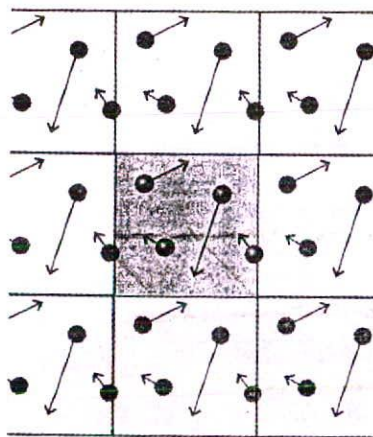
Despite its uniquely extensive hydrogen bonding, water has only a modest viscosity (much less than that of glycerol, for example). Indeed, water is a conundrum and a severe testing ground for theories of the liquid state. Water is a simple liquid when examined in the context of dynamic characteristics, and the challenge is to reconcile its extensive hydrogen-bonded structure with its dynamical simplicity.



24.9 The radial distribution function of the oxygen atoms in liquid water at three temperatures. Note the expansion as the temperature is raised. (A.H. Narten, M.D. Danford, and H.A. Levy, *Discuss. Faraday Soc.* 43, 97 (1967).)



24.10 The radial distribution function for a simulation of a liquid using impenetrable hard spheres (ball-bearings).



24.11 In a two-dimensional molecular dynamics simulation that uses periodic boundary conditions, when one particle leaves the cell its mirror image enters through the opposite face.

(b) The calculation of $g(r)$

Because the radial distribution function can be calculated by making assumptions about the intermolecular forces, it can be used to test theories of liquid structure. However, even a fluid of hard spheres without attractive interactions (a collection of ball-bearings in a container) gives a function that oscillates near the origin (Fig. 24.10), and one of the factors influencing, and sometimes dominating, the structure of a liquid is the geometrical problem of stacking together reasonably hard spheres. Indeed, the radial distribution function of a liquid of hard spheres shows more pronounced oscillations at a given temperature than that of any other type of liquid. The attractive part of the potential modifies this basic structure, but sometimes only quite weakly. One of the reasons behind the difficulty of describing liquids theoretically is the similar importance of both the attractive and repulsive (hard core) components of the potential.

The formal expression for the radial distribution function for molecules 1 and 2 in a fluid consisting of N particles is the somewhat fearsome equation

$$g(r_{12}) = \frac{\int \int \dots \int e^{-\beta V_N} dr_3 dr_4 \dots dr_N}{N^2 \int \int \dots \int e^{-\beta V_N} dr_1 dr_2 \dots dr_N} \quad (24)$$

where $\beta = 1/kT$ and V_N is the N -particle potential energy. There are several ways of building the intermolecular potential into the calculation of $g(r)$. Numerical methods take a box of about 10^3 particles (the number increases as computers grow more powerful), and the rest of the liquid is simulated by surrounding the box with replications of the original box (Fig. 24.11). Then, whenever a particle leaves the box through one of its faces, its image arrives through the opposite face. When calculating the interactions of a molecule in a box, it interacts with all the molecules in the box and all the periodic replications of those molecules and itself in the other boxes.

Once $g(r)$ is known it can be used to calculate the thermodynamic properties of liquids. For example, the contribution of the pairwise additive intermolecular potential, V_2 , to the internal energy is given by the integral

$$U = \frac{2\pi N^2}{V} \int_0^\infty g V_2 r^2 dr \quad (25)$$

That is, U is essentially the average two-particle potential energy weighted by $g(r)r^2 dr$, which is the probability that the pair of particles have a separation between r and $r + dr$. Likewise, the contribution that pairwise interactions make to the pressure is

$$\frac{pV}{nRT} = 1 - \frac{2\pi N}{kTV} \int_0^\infty g v_2 r^2 dr \quad v_2 = r \left(\frac{dV_2}{dr} \right) \quad (26)$$

The quantity v_2 is called the virial (hence the term 'virial equation of state').

(c) Monte Carlo methods

In the Monte Carlo method, the particles in the box are moved through small but otherwise random distances, and the change in total potential energy of the N particles in the box, ΔV_N , is calculated using one of the intermolecular potentials discussed in Chapter 22. Whether or not this new configuration is accepted is then judged from the following rules:

1. If the potential energy is not greater than before the change, then the configuration is accepted.
2. If the potential energy is greater than before the change, the factor $e^{-\Delta V_N/kT}$ is compared with a random number between 0 and 1: if the factor is larger than the random number, the configuration is accepted; if the factor is not larger, the configuration is rejected.

This procedure ensures that at equilibrium the probability of occurrence of any configuration is proportional to the Boltzmann factor $e^{-V_w/kT}$. The configurations generated in this way can then be used to construct $g(r)$ simply by counting the number of pairs of particles with a separation r and averaging the result over the whole collection of configurations.

(d) Molecular dynamics

In the molecular dynamics approach, the history of an initial arrangement is followed by calculating the trajectories of all the particles under the influence of the intermolecular potentials. Newton's laws are used to predict where each particle will be after a short time interval (about 10^{-15} s, which is shorter than the average time between collisions), and then the calculation is repeated for tens of thousands of such steps. The time-consuming part of the calculation is the evaluation of the net force on the molecule arising from all the other molecules present in the system.

A molecular dynamics calculation gives a series of snapshots of the liquid, and $g(r)$ can be calculated as before. The temperature of the system is inferred by computing the mean kinetic energy of the particles and using the equipartition result that

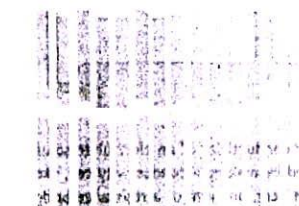
$$\langle \frac{1}{2}mv_q^2 \rangle = \frac{1}{2}kT \quad (27)$$

for each coordinate q .

(e) Liquid crystals

A feature that makes calculations even more difficult is the possibility that molecules have strongly anisotropic interactions. An important extreme case of anisotropy gives rise to a mesophase, a phase intermediate between solid and liquid. Mesophases are of great importance in biology, for they occur as lipid bilayers and in vesicular systems.

A mesophase may arise when molecules have highly anisotropic shapes, such as being long and thin, as in (1), or disk-like. When the solid melts, some aspects of the long-range order characteristic of the solid may be retained, and the new phase may be a liquid crystal, a substance having liquid-like imperfect long-range order in at least one direction in space but positional or orientational order in at least one other direction. One type of retained long-range order gives rise to a smectic phase (from the Greek word for soapy), in which the molecules align themselves in layers (Fig. 24.12a). Other materials, and some smectic liquid crystals at higher temperatures, lack the layered structure but retain a parallel alignment (Fig. 24.12b): this mesophase is called a nematic phase (from the Greek for thread, which refers to the observed defect structure of the phase). In the cholesteric phase (from the



(a)

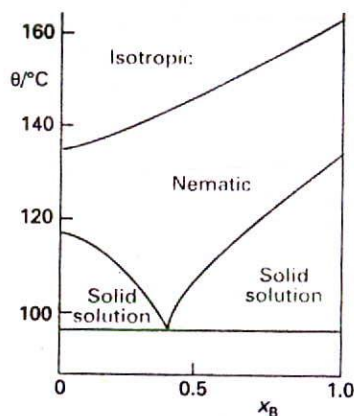


(b)



(c)

24.12 The arrangement of molecules in (a) the nematic phase, (b) the smectic phase, and (c) the cholesteric phase of liquid crystals. In the cholesteric phase, the stacking of layers continues to give a helical arrangement of molecules.



24.13 The phase diagram at 1 atm for a binary system of two liquid crystalline materials, 4,4'-dimethoxyazoxybenzene (A) and 4,4'-diethoxyazoxybenzene (B).

Table 24.3* Viscosities of liquids at 298 K, $\eta / (10^{-3} \text{ kg m}^{-1} \text{ s}^{-1})$

Benzene	0.601
Mercury	1.55
Pentane	0.224
Water†	0.891

* More values are given in the Data section.

† The viscosity of water corresponds to 0.891 cP.

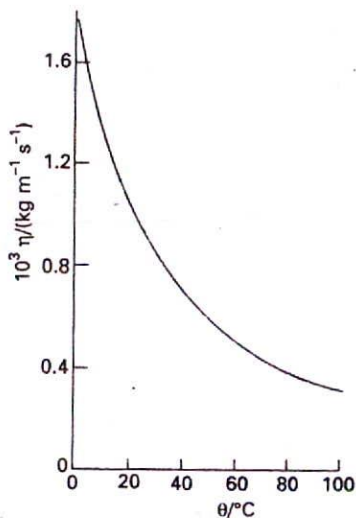
Greek for bile solid) the molecules lie in sheets at angles that change slightly between each sheet (Fig. 24.12c). That is, they form helical structures with a pitch that depends on the temperature. As a result, cholesteric liquid crystals diffract light and have colours that depend on the temperature. The strongly anisotropic optical properties of nematic liquid crystals, and their response to electric fields, is the basis of their use as data displays (LCDs).

Although there are many liquid crystalline materials, some difficulty is often experienced in achieving a technologically useful temperature range for the existence of the mesophase. To overcome this difficulty, mixtures can be used. An example of the type of phase diagram that is then obtained is shown in Fig. 24.13. As can be seen, the mesophase exists over a wider range of temperatures than either liquid crystalline material alone.

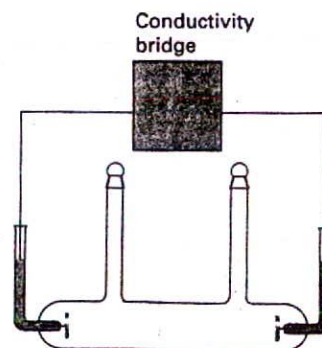
24.6 Molecular motion in liquids

The motion of molecules in liquids can be studied experimentally by a variety of methods. Relaxation time measurements in NMR and ESR (Section 18.6b) can be interpreted in terms of the mobilities of the molecules, and have been used to show that big molecules in viscous fluids typically rotate in a series of small (about 5°) steps, whereas small molecules in nonviscous fluids typically jump through about 1 radian (57°) in each step. Another important technique is inelastic neutron scattering, in which the energy neutrons collect or discard as they pass through a sample is interpreted in terms of the motion of its particles. The same technique is used to examine the internal dynamics of macromolecules.

More mundane than these experiments are viscosity measurements (Table 24.3). For a molecule to move in a liquid, it must acquire at least a minimum energy to escape from its neighbours. The probability that a molecule has at least an energy E_a is proportional to $e^{-E_a/RT}$, so the mobility of the molecules in the liquid should follow this type of temperature



24.14 The experimental temperature dependence of the viscosity of water. As the temperature is increased, more molecules are able to escape from the potential wells provided by their neighbours, and so the liquid becomes more fluid. A plot of $\ln \eta$ against $1/T$ is a straight line (over a small range) with positive slope.



24.15 The conductivity of an electrolyte solution is measured by making a conductivity cell, like the one shown here, one arm of a resistance bridge.

dependence. Because the coefficient of viscosity, η , is inversely proportional to the mobility of the particles, we should expect that

$$\eta \propto e^{E_a/RT} \quad (28)$$

(Note the positive sign of the exponent.) This expression implies that the viscosity should decrease sharply with increasing temperature. Such a variation is found experimentally, at least over reasonably small temperature ranges (Fig. 24.14). The activation energy typical of viscosity is comparable to the mean potential energy of intermolecular interactions.

One problem with the interpretation of viscosity measurements is that the change in density of the liquid as it is heated makes a pronounced contribution to the temperature variation of the viscosity. Thus, the temperature dependence of viscosity at constant volume, when the density is constant, is much less than that at constant pressure. The intermolecular forces between the molecules of the liquid govern the magnitude of E_a , but the problem of calculating it is immensely difficult and still largely unsolved. At low temperatures, the viscosity of water decreases as the pressure is increased. This behaviour is consistent with the rupture of hydrogen bonds.

24.7 The conductivities of electrolyte solutions

Further insight into the nature of molecular motion can be obtained by studying the motion of ions in solution, for they can be dragged through the solution by the application of a potential difference between two electrodes immersed in the sample. By studying the transport of charge through electrolyte solutions it is possible to build up a picture of the events that occur in them and, in some cases, to extrapolate the conclusions to species that have zero charge, that is, to neutral molecules.

(a) Conductance and conductivity

The fundamental measurement used to study the motion of ions is that of the electrical resistance, \mathcal{R} , of the solution. The standard technique is to incorporate a conductivity cell into one arm of a resistance bridge and to search for the balance point, as explained in standard texts on electricity (Fig. 24.15). The main complication is that alternating current must be used because a direct current would lead to electrolysis and to polarization, which in this context means the modification of the composition of the layers of solution in contact with the electrodes. The use of alternating current (with a frequency of about 1 kHz) may avoid polarization because the charging that occurs on one half of the cycle is undone during the second half (if the reverse reaction is kinetically feasible).

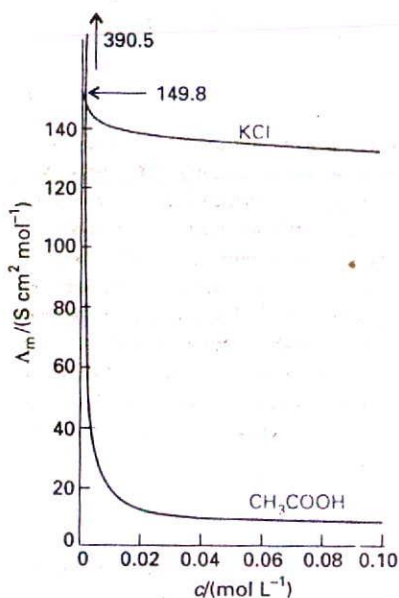
The conductance, G , of a solution is the inverse of its resistance \mathcal{R} : $G = 1/\mathcal{R}$. As resistance is expressed in ohms, Ω , the conductance of a sample is expressed in Ω^{-1} . The reciprocal ohm used to be called the mho, but its official designation is now the siemens, S, and $1 \text{ S} = 1 \Omega^{-1}$. The conductance of a sample decreases with its length l and increases with its cross-sectional area A . We therefore write

$$G = \frac{\kappa A}{l} \quad (29)$$

where κ is the conductivity. With the conductance in siemens and the dimensions in metres, it follows that the SI units of κ are siemens per metre (S m^{-1}).

The conductivity of a solution depends on the number of ions present, and it is normal to introduce the molar conductivity, Λ_m , which is defined as

$$\Lambda_m = \frac{\kappa}{c} \quad [30]$$



24.16 The concentration dependence of the molar conductivities of (a) a typical strong electrolyte (aqueous potassium chloride) and (b) a typical weak electrolyte (aqueous acetic acid).

where c is the molar concentration of the added electrolyte. The SI unit of molar conductivity is siemens metre-squared per mole ($\text{S m}^2 \text{ mol}^{-1}$), and typical values are about $10 \text{ mS m}^2 \text{ mol}^{-1}$ (where $1 \text{ mS} = 10^{-3} \text{ S}$).

The molar conductivity of an electrolyte would be independent of concentration if κ were proportional to the concentration of the electrolyte. However, in practice, the molar conductivity is found to vary with the concentration. One reason for this variation is that the number of ions in the solution might not be proportional to the concentration of the electrolyte. For instance, the concentration of ions in a solution of a weak acid depends on the concentration of the acid in a complicated way, and doubling the concentration of the acid added does not double the number of ions. Secondly, because ions interact strongly with one another, the conductivity of a solution is not exactly proportional to the number of ions present.

The concentration dependence of molar conductivities indicates that there are two classes of electrolyte. The characteristic of a **strong electrolyte** is that its molar conductivity decreases only slightly as its concentration is increased (Fig. 24.16). The characteristic of a **weak electrolyte** is that its molar conductivity is normal at concentrations close to zero, but falls sharply to low values as the concentration increases. The classification depends on the solvent employed as well as the solute: lithium chloride, for example, is a strong electrolyte in water but a weak electrolyte in propanone.

(b) Strong electrolytes

Strong electrolytes are substances that are virtually fully ionized in solution, and include ionic solids and strong acids. As a result of their complete ionization, the concentration of ions in solution is proportional to the concentration of strong electrolyte added.

In an extensive series of measurements during the nineteenth century, Friedrich Kohlrausch showed that at low concentrations the molar conductivities of strong electrolytes vary linearly with the square root of the concentration:

$$A_m = A_m^\circ - \kappa c^{1/2} \quad (31)$$

This variation is called Kohlrausch's law. The constant A_m° is the **limiting molar conductivity**, the molar conductivity in the limit of zero concentration (when the ions are effectively infinitely far apart and do not interact with one another). The constant κ is found to depend more on the stoichiometry of the electrolyte (that is, whether it is of the form MA, or M_2A , etc.) than on its specific identity.

Kohlrausch was also able to show that A_m° can be expressed as the sum of contributions from its individual ions. If the limiting molar conductivity of the cations is denoted λ_+ and that of the anions λ_- , then his **law of the independent migration of ions** states that

$$A_m^\circ = \nu_+ \lambda_+ + \nu_- \lambda_- \quad (32)^\circ$$

where ν_+ and ν_- are the numbers of cations and anions per formula unit of electrolyte (for example, $\nu_+ = \nu_- = 1$ for HCl, NaCl, and CuSO_4 , but $\nu_+ = 1$, $\nu_- = 2$ for MgCl_2). This simple result, which can be understood on the grounds that the ions migrate independently in the limit of zero concentration, lets us predict the limiting molar conductivity of any strong electrolyte from the data in Table 24.4.

Illustration

The limiting molar conductivity of BaCl_2 in water at 298 K is

$$A_m^\circ = (12.72 + 2 \times 7.63) \text{ mS m}^2 \text{ mol}^{-1} = 27.98 \text{ mS m}^2 \text{ mol}^{-1}$$

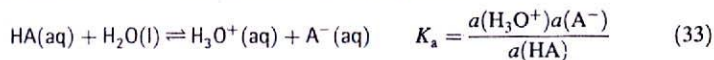
Table 24.4* Limiting ionic conductivities in water at 298 K, λ_i° ($\text{mS m}^2 \text{ mol}^{-1}$)

H^+	34.96	OH^-	19.91
Na^+	5.01	Cl^-	7.63
K^+	7.35	Br^-	7.81
Zn^{2+}	10.56	SO_4^{2-}	16.00

*More values are given in the Data section.

(c) Weak electrolytes

Weak electrolytes are not fully ionized in solution. They include weak Brønsted acids and bases, such as CH_3COOH and NH_3 . The marked concentration dependence of their molar conductivities arises from the displacement of the equilibrium



towards products at low molar concentrations.

The conductivity depends on the number of ions in the solution, and therefore on the degree of ionization, α , of the electrolyte. The degree of ionization is defined so that, for the acid HA at a molar concentration c , at equilibrium

$$[\text{H}_3\text{O}^+] = \alpha c \quad [\text{A}^-] = \alpha c \quad [\text{HA}] = (1 - \alpha)c \quad (34)$$

If we ignore activity coefficients, the acidity constant, K_a , is approximately

$$K_a = \frac{\alpha^2 c}{1 - \alpha} \quad (35)^\circ$$

from which it follows that

$$\alpha = \frac{K_a}{2c} \left\{ \left(1 + \frac{4c}{K_a} \right)^{1/2} - 1 \right\} \quad (36)^\circ$$

The electrolyte is fully ionized at infinite dilution, and its molar conductivity is then Λ_m° . Because only a fraction α is actually present as ions in the actual solution, the measured molar conductivity Λ_m is given by

$$\Lambda_m = \alpha \Lambda_m^\circ \quad (37)^\circ$$

with α given by eqn 36.

Example 24.4 Using conductivity measurements to determine $\text{p}K_a$

The molar conductivity of 0.0100 M $\text{CH}_3\text{COOH}(\text{aq})$ at 298 K was measured as $\Lambda_m = 1.65 \text{ mS m}^2 \text{ mol}^{-1}$. Determine the degree of ionization and the $\text{p}K_a$ of the acid.

Method To calculate α , use eqn 37 with Λ_m° calculated from the data in Table 24.4. Then calculate K_a by substitution of α into eqn 35 and form $\text{p}K_a = -\log K_a$.

Answer From the data in Table 24.4 we find $\Lambda_m^\circ = 39.05 \text{ mS m}^2 \text{ mol}^{-1}$. Therefore, $\alpha = 0.0423$. It follows from eqn 35 that $K_a = 1.9 \times 10^{-5}$, implying that $\text{p}K_a = 4.72$.

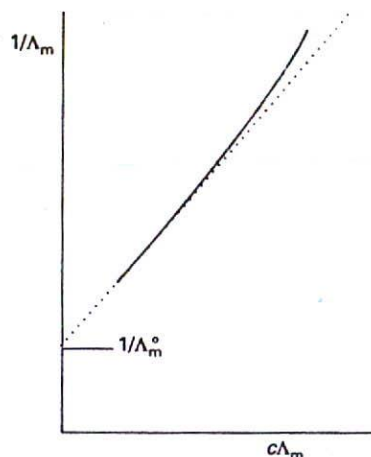
Comment The thermodynamic value of $\text{p}K_a$ is obtained by repeating the determination with different concentrations and extrapolating to zero concentration.

Self-test 24.4 The molar conductivity of 0.0250 M $\text{HCOOH}(\text{aq})$ was measured as $4.61 \text{ mS m}^2 \text{ mol}^{-1}$. Determine the $\text{p}K_a$ of the acid.

[3.44]

Once we know K_a , we can use eqns 36 and 37 to predict the concentration dependence of the molar conductivity. The result agrees quite well with the experimental curve in Fig. 24.16. More usefully, we can use the concentration dependence of Λ_m in measurements of the limiting molar conductance. First, we rearrange eqn 36 into

$$\frac{1}{\alpha} = 1 + \frac{\alpha c}{K_a} \quad (38)^\circ$$



24.17 The graph used to determine the limiting value of the molar conductivity of a solution by extrapolation to zero concentration.

Then, by using eqn 37, we obtain Ostwald's dilution law:

$$\frac{1}{\Lambda_m} = \frac{1}{\Lambda_m^0} + \frac{\Lambda_m c}{K_a (\Lambda_m^0)^2} \quad (39)^\circ$$

This equation implies that, if $1/\Lambda_m$ is plotted against $c\Lambda_m$, then the intercept at $c = 0$ will be $1/\Lambda_m^0$ (Fig. 24.17).

24.8 The mobilities of ions

To interpret conductivity measurements we need to know why ions move at different rates, why they have different molar conductivities, and why the molar conductivities of strong electrolytes decrease with the square root of the molar concentration. The central idea in this section is that, although the motion of an ion remains largely random, the presence of an electric field biases its motion, and the ion undergoes net migration through the solution.

(a) The drift speed

When the potential difference between two electrodes a distance l apart is $\Delta\phi$, the ions in the solution between them experience a uniform electric field of magnitude

$$\mathcal{E} = \frac{\Delta\phi}{l} \quad (40)$$

In such a field, an ion of charge³ ze experiences a force of magnitude

$$\mathcal{F} = ze\mathcal{E} = \frac{ze\Delta\phi}{l} \quad (41)$$

A cation responds to the application of the field by accelerating towards the negative electrode and an anion responds by accelerating towards the positive electrode. However, this acceleration is short-lived. As the ion moves through the solvent it experiences a frictional retarding force $\mathcal{F}_{\text{fric}}$ proportional to its speed. If we assume that the Stokes formula (eqn 23.13) for a sphere of radius a and speed s applies even on a microscopic scale (and independent evidence from magnetic resonance suggests that it often gives at least the right order of magnitude), then we can write this retarding force as

$$\mathcal{F}_{\text{fric}} = fs \quad f = 6\pi\eta a \quad (42)$$

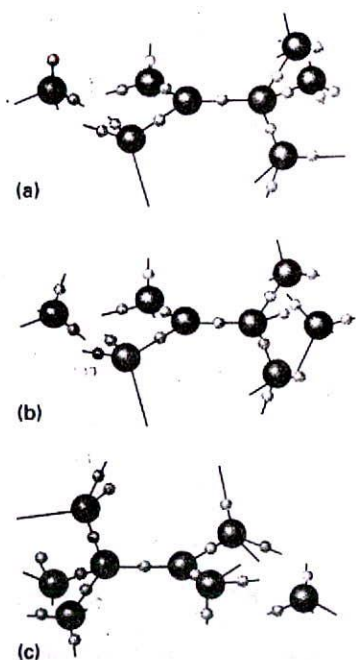
The two forces act in opposite directions, and the ions quickly reach a terminal speed, the **drift speed**, when the accelerating force is balanced by the viscous drag. The net force is zero when

$$s = \frac{ze\mathcal{E}}{f} \quad (43)$$

Because the drift speed governs the rate at which charge is transported, we might expect the conductivity to decrease with increasing solution viscosity and ion size. Experiments confirm these predictions for bulky ions (such as R_4N^+ and RCO_2^-) but not for small ions. For example, the molar conductivities of the alkali metal ions increase from Li^+ to Cs^+ (Table 24.4) even though the ionic radii increase. The paradox is resolved when we realize that the radius a in the Stokes formula is the **hydrodynamic radius** (or 'Stokes' radius') of the ion, its effective radius in the solution taking into account all the H_2O molecules it carries in its hydration sphere. Small ions give rise to stronger electric fields than large ones,⁴ so small ions are more extensively solvated than big ions. Thus, an ion of small ionic radius may have a large hydrodynamic radius because it drags many solvent molecules through the

³ In this chapter we disregard the sign of the charge number and so avoid notational complications.

⁴ The electric field at the surface of a sphere of radius r is proportional to ze/r^2 , so the smaller the radius the stronger the field.



24.18 The mechanism of conduction by water as proposed by N. Agmon (*Chem. Phys. Letts.* 244, 456 (1995)). Proton transfer between neighbouring molecules occurs when one molecule rotates into such a position that an O—H...O hydrogen bond can flip into being an O...H—O hydrogen bond. See text for a description of the steps.

solution as it migrates. The hydrating H_2O molecules are often very labile, however, and NMR and isotope studies have shown that the exchange between the coordination sphere of the ion and the bulk solvent is very rapid.

The proton, although it is very small, has a very high molar conductivity (Table 24.4)! Proton and ^{17}O -NMR show that the times characteristic of protons hopping from one molecule to the next are about 1.5 ps, which is comparable to the time that inelastic neutron scattering shows it takes a water molecule to reorientate through about 1 rad (1 to 2 ps). According to the Grotthuss mechanism,⁵ there is an effective motion of a proton that involves the rearrangement of bonds in a group of water molecules. However, the actual mechanism is still highly contentious. Attention now focuses on the H_3O_4^+ unit, in which the nearly trigonal planar H_3O^+ ion⁶ is linked to three strongly solvating H_2O molecules. This cluster of atoms is itself hydrated, but the hydrogen bonds in the secondary sphere are weaker than in the primary sphere. It is envisaged that the rate-determining step is the cleavage of one of the weaker hydrogen bonds of this secondary sphere (Fig. 24.18a). After this bond cleavage has taken place, and the released molecule has rotated through a few degrees (a process that takes about 1 ps), there is a rapid adjustment of bond lengths and angles in the remaining cluster, to form an H_5O_2^+ cation of structure $\text{H}_2\text{O}\cdots\text{H}^+\cdots\text{OH}_2$ (Fig. 24.18b). Shortly after this reorganization has occurred, a new H_3O_4^+ cluster forms as other molecules rotate into a position where they can become members of a secondary hydration sphere, but now the positive charge is located one molecule to the right of its initial location (Fig. 24.18c). According to this model, there is no coordinated motion of a proton along a chain of molecules, simply a very rapid hopping between neighbouring sites, with a low activation energy. The model is consistent with the observation that the molar conductivity of protons increases as the pressure is raised, for increasing pressure ruptures hydrogen bonds.

(b) Ion mobilities

According to eqn 43, the drift speed of an ion is proportional to the strength of the applied field. We write

$$s = u\mathcal{E} \quad [44]$$

where u is called the mobility of the ion (Table 24.5). Comparison of eqns 43 and 44 and use of eqn 42 show that

$$u = \frac{ze}{f} = \frac{ze}{6\pi\eta a} \quad (45)$$

Illustration

For an order of magnitude estimate we can take $z = 1$ and a the radius of an ion such as Cs^+ (which might be typical of a smaller ion plus its hydration sphere), which is 170 pm. For the viscosity, we use $\eta = 1.0$ cP ($1.0 \times 10^{-3} \text{ kg m}^{-1} \text{ s}^{-1}$, Table 24.3). Then $u \approx 5 \times 10^{-8} \text{ m}^2 \text{ V}^{-1} \text{ s}^{-1}$. This value means that, when there is a potential difference of 1 V across a solution of length 1 cm (so $\mathcal{E} = 100 \text{ V m}^{-1}$), the drift speed is typically about $5 \mu\text{m s}^{-1}$. That speed might seem slow, but not when expressed on a molecular scale, for it corresponds to an ion passing about 10^4 solvent molecules per second.

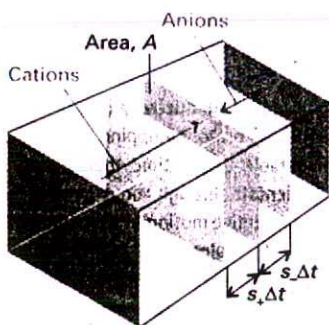
Table 24.5* Ionic mobilities in water at 298 K, $u/(10^{-8} \text{ m}^2 \text{ s}^{-1} \text{ V}^{-1})$

H^+	36.23	OH^-	20.64
Na^+	5.19	Cl^-	7.91
K^+	7.62	Br^-	8.09
Zn^{2+}	5.47	SO_4^{2-}	8.29

*More values are given in the Data section.

5 The name of the mechanism is an allusion to an early view advanced by von Grotthuss, in which it was supposed that chains of dipoles were responsible for the transport of charge in water.

6 In the gas phase, H_3O^+ is trigonal pyramidal.



24.19 In the calculation of the current, all the cations within a distance $s_+ \Delta t$ (that is, those in the volume $s_+ A \Delta t$) will pass through the area A . The anions in the corresponding volume on the other side of the window will also contribute to the current similarly.

(c) Mobility and conductivity

The usefulness of ionic mobilities is that they provide a link between measurable and theoretical quantities. As a first step we establish in the *Justification* below the following relation between an ion's mobility and its molar conductivity:

$$\lambda = zuF \quad (46)^{\circ}$$

where F is the Faraday constant ($F = N_A e$).

Justification 24.5

To keep the calculation simple, we ignore signs in the following, and concentrate on the magnitudes of quantities: the direction of ion flux can always be decided by common sense.

Consider a solution of a fully dissociated strong electrolyte at a molar concentration c . Let each formula unit give rise to ν_+ cations of charge $z_+ e$ and ν_- anions of charge $z_- e$. The molar concentration of each type of ion is therefore νc (with $\nu = \nu_+$ or ν_-), and the number density of each type is $\nu c N_A$. The number of ions of one kind that pass through an imaginary window of area A during an interval Δt is equal to the number within the distance $s \Delta t$ (Fig. 24.19), and therefore to the number in the volume $s \Delta t A$. (The same sort of argument was used in Section 1.3 in the discussion of the pressure of a gas.) The number of ions of that kind in this volume is equal to $s \Delta t A \nu c N_A$. The flux through the window (the number of this type of ion passing through the window divided by the area of the window and the duration of the interval) is therefore

$$J(\text{ions}) = \frac{s \Delta t A \nu c N_A}{A \Delta t} = \nu c N_A s$$

Each ion carries a charge ze , so the flux of charge is

$$J(\text{charge}) = z \nu c e N_A s = z \nu c F s$$

Because $s = u \mathcal{E}$, the flux is

$$J(\text{charge}) = z \nu c F u \mathcal{E}$$

The current, I , through the window due to the ions we are considering is the charge flux times the area:

$$I = JA = z \nu c F u \mathcal{E} A$$

Because the electric field is the potential gradient, $\Delta \phi / l$, we can write

$$I = \frac{z \nu c F A \Delta \phi}{l} \quad (47)$$

Current and potential difference are related by Ohm's law, that

$$I = \frac{\Delta \phi}{\mathcal{R}} = G \Delta \phi = \frac{\kappa A \Delta \phi}{l}$$

where we have used eqn 29 in the form $\kappa = Gl/A$. Comparison of the last two expressions gives $\kappa = z \nu c F$. Division by the molar concentration of ions, νc , then results in eqn 46.

Equation 46 applies to the cations and to the anions. Therefore, for the solution itself in the limit of zero concentration (when there are no interionic interactions),

$$\Lambda_m^{\circ} = (z_+ u_+ \nu_+ + z_- u_- \nu_-) F \quad (48)^{\circ}$$

For a symmetrical $z : z$ electrolyte (for example, CuSO_4 with $z = 2$), this equation simplifies to

$$\Lambda_m^\circ = z(u_+ + u_-)F \quad (49)^\circ$$

Illustration

Earlier, we estimated the typical ionic mobility as $5 \times 10^{-8} \text{ m}^2 \text{ V}^{-1} \text{ s}^{-1}$; so, with $z = 1$ for both the cation and anion, we can estimate that a typical limiting molar conductivity should be about $10 \text{ mS m}^2 \text{ mol}^{-1}$, in accord with experiment. The experimental value for KCl, for instance, is $15 \text{ mS m}^2 \text{ mol}^{-1}$.

(d) Transport numbers

The transport number, t_\pm , is defined as the fraction of total current carried by the ions of a specified type. For a solution of two kinds of ion, the transport numbers of the cations (t_+) and anions (t_-) are

$$t_\pm = \frac{I_\pm}{I} \quad [50]$$

where I_\pm is the current carried by the cation (I_+) or anion (I_-) and I is the total current through the solution. Because the total current is the sum of the cation and anion currents, it follows that

$$t_+ + t_- = 1 \quad (51)$$

The limiting transport number, t_\pm° , is defined in the same way but for the limit of zero concentration of the electrolyte solution. We shall consider only these limiting values from now on, for that avoids the problem of ionic interactions.

The current that can be ascribed to each type of ion is related to the mobility of the ion by eqn 47. Hence the relation between t_\pm° and u_\pm is

$$t_\pm^\circ = \frac{z_\pm \nu_\pm u_\pm}{z_+ \nu_+ u_+ + z_- \nu_- u_-} \quad (52)^\circ$$

Because $z_+ \nu_+ = z_- \nu_-$ for all ionic species, this equation simplifies to

$$t_\pm^\circ = \frac{u_\pm}{u_+ + u_-} \quad (53)^\circ$$

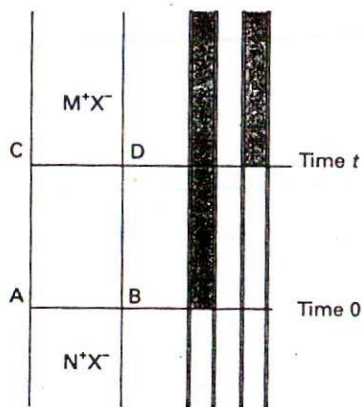
Moreover, because the ionic conductivities are related to the mobilities by eqn 46, it follows that

$$t_\pm^\circ = \frac{\nu_\pm \lambda_\pm}{\nu_+ \lambda_+ + \nu_- \lambda_-} = \frac{\nu_\pm \lambda_\pm}{\Lambda_m^\circ} \quad (54)^\circ$$

and hence, for each type of ion,

$$\nu_\pm \lambda_\pm = t_\pm^\circ \Lambda_m^\circ \quad (55)^\circ$$

Consequently, because there are independent ways of measuring transport numbers of ions, we can determine the individual ionic conductivities and (through eqn 46) the ionic mobilities.



24.20 In the moving boundary method for the measurement of transport numbers, the distance moved by the boundary is observed as a current is passed. All the M ions in the volume between AB and CD must have passed through CD if the boundary moves from AB to CD.

(e) The measurement of transport numbers

One of the most accurate methods for measuring transport numbers is the **moving boundary method**, in which the motion of a boundary between two ionic solutions having a common ion is observed as a current flows.

Let MX be the salt of interest and NX a salt giving a denser solution. The solution of NX is called the **indicator solution**; it occupies the lower part of a vertical tube of cross-sectional area A (Fig. 24.20). The MX solution, which is called the **leading solution**, occupies the upper part of the tube. There is a sharp boundary between the two solutions. The indicator solution must be denser than the leading solution, and the mobility of the M ions must be greater than that of the N ions.⁷ Thus, if any M ions diffuse into the lower solution, they will be pulled upwards more rapidly than the N ions around them, and the boundary will reform. The interpretation of the experiment makes use of the relation (see the *Justification* below) between the distance, l , moved by the boundary in the time Δt for which a current I is passed for a period Δt :

$$t_+ = \frac{z_+ c l A F}{I \Delta t} \quad (56)$$

Hence, by measuring the distance moved, the transport number and hence the conductivity and mobility of the ions can be determined.

Justification 24.6

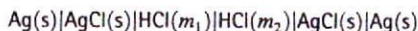
When a current I is passed for a time Δt , the boundary moves from AB to CD, so all the M ions in the volume between AB and CD must have passed through CD. That number is $c l A N_A$, so the charge that the M ions transfer through the plane is $z_+ c l A e N_A$. However, the *total* charge transferred when a current I flows for an interval Δt is $I \Delta t$. Therefore, the fraction due to the motion of the M ions, which is their transport number, is given by eqn 56.

In the **Hittorf method**, an electrolytic cell is divided into three compartments and a charge $I \Delta t$ is passed. An amount $I \Delta t / z_+ F$ of cations is discharged at the cathode, but an amount $t_+ I \Delta t / z_+ F$ of cations migrates into the cathode compartment. The net change in the amount of cations in that compartment is therefore

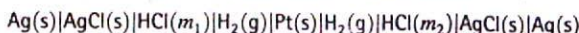
$$\text{Net change} = (t_+ - 1) \frac{I \Delta t}{z_+ F} = -t_- \frac{I \Delta t}{z_+ F} \quad (57)$$

Hence, by measuring the change of composition in the cathode compartment, the anion transport number t_- can be deduced. Likewise, the change in composition of the anode compartment is $-t_+ I \Delta t / z_+ F$, which gives the cation transport number, t_+ .

Transport numbers may also be measured by using galvanic cells. In particular, the measurement is made on a cell with **transference**, which is a galvanic cell with a liquid boundary across which ions may pass from one electrode compartment to the other. An example is the cell



for which the zero-current cell potential is E_t and the electrodes are reversible with respect to anions (Cl^-). The corresponding cell without transference is



⁷ One procedure is to add bromothymol blue indicator to a slightly alkaline solution of the ion of interest and to use a cadmium electrode at the lower end of the vertical tube. The electrode produces Cd^{2+} ions, which are slow moving and slightly acidic (the hydrated ion is a Brønsted acid), and the boundary is revealed by the colour change of the indicator.

and its zero-current potential is E . We show in the *Justification* below that the two potentials are related by

$$E_t = 2t_+E \quad (58)$$

Therefore, comparison of the two cell potentials gives the transport number of the *counterion* of the ion with respect to which the electrodes are reversible (in this case, the transport number of H^+).

Justification 24.7

The argument is similar to that used to analyse the Hittorf method. Consider the consequences of passing 1 mol of electrons through the cell with transport specified above. In the right-hand electrode compartment, 1 mol Cl^- is formed but t_- mol Cl^- migrates out of it across the junction. The net change is $(1 - t_-)$ mol = t_+ mol. At the same time, t_+ mol H^+ migrates into the compartment. In the left-hand electrode compartment 1 mol Cl^- is removed from solution (to form 1 mol $AgCl$), but t_- mol Cl^- flows in across the junction. The net change is therefore $(-1 + t_-)$ mol = $-t_+$ mol Cl^- . At the same time, t_+ mol H^+ flows out. The reaction Gibbs energy is therefore

$$\begin{aligned} \Delta_r G &= t_+ \{ \mu(Cl^-, m_2) - \mu(Cl^-, m_1) + \mu(H^+, m_2) - \mu(H^+, m_1) \} \\ &= 2t_+ RT \ln \frac{a_2}{a_1} \end{aligned}$$

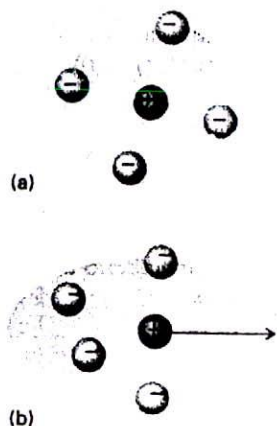
Because $\Delta_r G = -FE$, it follows that

$$E_t = -\frac{2t_+ RT}{F} \ln \frac{a_2}{a_1}$$

For the same cell without transference, the Nernst equation gives

$$E = -\frac{RT}{F} \ln \frac{a_2}{a_1}$$

and the ratio of the two cell potentials is $2t_+$.



24.21 (a) In the absence of an applied field, the ionic atmosphere is spherically symmetric, but (b) when a field is present it is distorted and the centres of negative and positive charge no longer coincide. The attraction between the opposite charges retards the motion of the central ion.

24.9 Conductivities and ion-ion interactions

The remaining problem is to account for the $c^{1/2}$ dependence of the Kohlrausch law (eqn 31). In Section 10.2c we saw something similar: the activity coefficients of ions at low concentrations also depend on $c^{1/2}$ and depend on their charge type rather than their specific identities. That $c^{1/2}$ dependence was explained in terms of the properties of the ionic atmosphere around each ion, and we can suspect that the same explanation applies here too.

To accommodate the effect of motion, we need to modify the picture of an ionic atmosphere as a spherical haze of charge. The ions forming the atmosphere do not adjust to the moving ion infinitely quickly, and the atmosphere is incompletely formed in front of the moving ion and incompletely decayed behind the ion (Fig. 24.21). The overall effect is the displacement of the centre of charge of the atmosphere a short distance behind the moving ion. Because the two charges are opposite, the result is a retardation of the moving ion. This reduction of the ions' mobility is called the relaxation effect. A confirmation of the picture is obtained by observing the conductivities of ions at high frequencies, which are greater than at low frequencies: the atmosphere does not have time to follow the rapidly changing direction of motion of the ion, and the effect of the field averages to zero.

The ionic atmosphere has another effect on the motion of the ions. We have seen that the moving ion experiences a viscous drag. When the ionic atmosphere is present this drag is enhanced because the ionic atmosphere moves in an opposite direction to the central ion.

Table 24.6* Debye-Hückel-Onsager coefficients for (1, 1)-electrolytes at 298 K

Solvent	$A/(\text{mS m}^2 \text{ mol}^{-1} / (\text{mol L}^{-1})^{1/2})$	$B/(\text{mol L}^{-1})^{-1/2}$
Methanol	15.61	0.923
Propanone	32.8	1.63
Water	6.02	0.229

* More values are given in the Data section.

The enhanced viscous drag, which is called the **electrophoretic effect**, reduces the mobility of the ions, and hence also reduces their conductivities.

The quantitative formulation of these effects is far from simple, but the Debye-Hückel-Onsager theory is an attempt to obtain quantitative expressions at about the same level of sophistication as the Debye-Hückel theory itself. The theory leads to a Kohlrausch-like expression in which

$$\kappa = A + B\Lambda_m^0 \quad (59a)$$

with

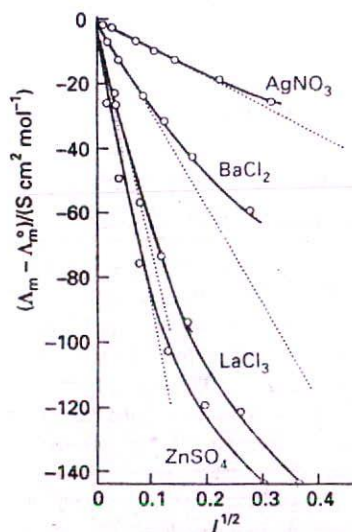
$$A = \frac{z^2 e F^2}{3\pi\eta} \left(\frac{2}{\epsilon RT}\right)^{1/2} \quad B = \frac{qz^3 e F}{24\pi\epsilon RT} \left(\frac{2}{\epsilon RT}\right)^{1/2} \quad (59b)$$

where ϵ is the electric permittivity of the solvent (Section 22.1e) and $q = 0.586$ for a 1, 1-electrolyte (Table 24.6). The slopes of the conductivity curves are predicted to depend on the charge type of the electrolyte, in accord with the Kohlrausch law, and some comparisons between theory and experiment are shown in Fig. 24.22. The agreement is quite good at very low molar concentrations (less than about 10^{-3} M, depending on the charge type).

Molecular dynamics calculations can also shed light on electric conduction. The key equation is a special case of a Green-Kubo relation, which expresses a transport property in terms of the fluctuations in microscopic properties of a system. The electrical conductivity is related to the fluctuations in the instantaneous electric current, j , in the sample that arises from variations in the velocities of the ions:

$$\kappa = \frac{1}{kTV} \int_0^\infty \langle j(0)j(t) \rangle dt \quad j = \sum_i z_i e v_i \quad (60)$$

where v_i is the velocity of the ion i at a given instant and the angular brackets denote an average over the sample. If the ions are very mobile, there will be large fluctuations in the instantaneous currents in the sample, and the conductivity of the medium will be high. If the ions are locked into position, as in an ionic solid, there will be no instantaneous currents, and the ionic conductivity will be zero. The velocities of the ions are calculated explicitly in a molecular dynamics simulation, so the correlation function, the quantity $\langle j(0)j(t) \rangle$, can be evaluated reasonably simply.



24.22 The dependence of molar conductivities on the square root of the ionic strength, and comparison (dotted lines) with the dependence predicted by the Debye-Hückel-Onsager theory.

Diffusion

We are now in a position to extend the discussion of ionic motion to cover the migration of neutral molecules and of ions in the absence of an applied electric field. We shall do this by expressing ion motion in a more general way than hitherto, and will then discover that the same equations apply even when the charge on the particles is zero.

24.10 The thermodynamic view

We saw in Part 1 that, at constant temperature and pressure, the maximum non-expansion work that can be done per mole when a substance moves from a location where its chemical potential is μ to a location where its chemical potential is $\mu + d\mu$ is $d\mu$. In a system in which the chemical potential depends on the position x ,

$$d\mu = d\mu = \left(\frac{\partial\mu}{\partial x}\right)_{p,T} dx \quad (61)$$

We also saw in Chapter 2 (Table 2.1) that in general work can always be expressed in terms of an opposing force (which here we write \mathcal{F}), and that

$$dw = -\mathcal{F} dx \quad (62)$$

By comparing these two expressions, we see that the slope of the chemical potential can be interpreted as an effective force per mole of molecules. We write this **thermodynamic force** as

$$\mathcal{F} = -\left(\frac{\partial\mu}{\partial x}\right)_{p,T} \quad (63)$$

There is not necessarily a real force pushing the particles down the slope of the chemical potential. As we shall see, the force may represent the spontaneous tendency of the molecules to disperse as a consequence of the Second Law and the hunt for maximum entropy.

(a) The thermodynamic force of a concentration gradient

In a solution in which the activity of the solute is a , the chemical potential is

$$\mu = \mu^\ominus + RT \ln a$$

If the solution is not uniform the activity depends on the position and we can write

$$\mathcal{F} = -RT \left(\frac{\partial \ln a}{\partial x}\right)_{p,T} \quad (64)$$

If the solution is ideal, a may be replaced by the molar concentration c , and then

$$\mathcal{F} = -\frac{RT}{c} \left(\frac{\partial c}{\partial x}\right)_{p,T} \quad (65)^\circ$$

because $(d \ln c/dx) = (1/c)dc/dx$.

Example 24.5 Calculating the thermodynamic force

Suppose the concentration of a solute decays exponentially along the length of a container. Calculate the thermodynamic force on the solute at 25°C given that the concentration falls to half its value in 10 cm.

Method According to eqn 65, the thermodynamic force is calculated by differentiating the concentration with respect to distance. Therefore, write an expression for the variation of the concentration with distance, and then differentiate it. Note that 1 J = 1 N m.

Answer The concentration varies with position as

$$c = c_0 e^{-x/\lambda}$$

where λ is the decay constant. Therefore,

$$\frac{dc}{dx} = -\frac{c}{\lambda}$$

Equation 65 then implies that

$$\mathcal{F} = \frac{RT}{\lambda}$$

We know that the concentration falls to $\frac{1}{2}c_0$ at $x = 10$ cm, so we can find λ from $\frac{1}{2} = e^{-(10 \text{ cm})/\lambda}$. That is, $\lambda = (10 \text{ cm}/\ln 2)$. It follows that

$$\mathcal{F} = \frac{(8.31451 \text{ J K}^{-1} \text{ mol}^{-1}) \times (298 \text{ K}) \times \ln 2}{1.0 \times 10^{-1} \text{ m}} = 17 \text{ kN mol}^{-1}$$

Self-test 24.5 Calculate the thermodynamic force on the molecules of molar mass M in a vertical tube in a gravitational field on the surface of the Earth, and evaluate \mathcal{F} for molecules of molar mass 100 g mol^{-1} . Comment on its magnitude relative to that just calculated.

[$\mathcal{F} = -Mg$, -0.98 N mol^{-1} ; the force arising from the concentration gradient greatly dominates that arising from the gravitational gradient]

(b) Fick's first law of diffusion

In Section 24.4a it was shown that Fick's first law of diffusion (that the particle flux is proportional to the concentration gradient) could be deduced from the kinetic theory of gases. We shall now show that it can be deduced more generally and that it applies to the diffusion of species in condensed phases too.

We suppose that the flux of diffusing particles is motion in response to a thermodynamic force arising from a concentration gradient. The particles reach a steady drift speed, s , when the thermodynamic force, \mathcal{F} , is matched by the viscous drag. This drift speed is proportional to the thermodynamic force, and we write $s \propto \mathcal{F}$. However, the particle flux, J , is proportional to the drift speed, and the thermodynamic force is proportional to the concentration gradient, dc/dx . The chain of proportionalities ($J \propto s$, $s \propto \mathcal{F}$, and $\mathcal{F} \propto dc/dx$) implies that $J \propto dc/dx$, which is the content of Fick's law.

(c) The Einstein relation

Fick's law can be written⁸

$$J = -D \frac{dc}{dx} \quad (66)$$

In this expression, D is the diffusion coefficient and dc/dx is the slope of the molar concentration. The flux is related to the drift speed by

$$J = sc \quad (67)$$

This relation follows from the argument that we have used several times before. Thus, all particles within a distance $s\Delta t$, and therefore in a volume $s\Delta tA$, can pass through a window of area A in an interval Δt . Hence, the amount of substance that can pass through the window in that interval is $s\Delta tAc$. Therefore,

$$sc = -D \frac{dc}{dx}$$

If now we express dc/dx in terms of \mathcal{F} by using eqn 65, we find

$$s = -\frac{D}{c} \frac{dc}{dx} = \frac{D\mathcal{F}}{RT} \quad (68)$$

⁸ This expression is derived from eqn 8 by dividing both sides by the Avogadro constant, which converts numbers into amounts (numbers of moles).

Therefore, once we know the effective force and the diffusion coefficient, D , we can calculate the drift speed of the particles (and vice versa) whatever the origin of the force.

There is one case where we already know the drift speed and the effective force acting on a particle: an ion in solution has a drift speed $s = u\mathcal{E}$ when it experiences a force $ez\mathcal{E}$ from an electric field of strength \mathcal{E} . Therefore, substituting these known values into eqn 68 gives

$$u\mathcal{E} = \frac{zF\mathcal{E}D}{RT}$$

and hence

$$u = \frac{zFD}{RT} \quad (69)$$

This equation rearranges into the very important result known as the Einstein relation between the diffusion coefficient and the ionic mobility:

$$D = \frac{uRT}{zF} \quad (70)^\circ$$

On inserting the typical value $u = 5 \times 10^{-8} \text{ m}^2 \text{ s}^{-1} \text{ V}^{-1}$, we find $D \approx 1 \times 10^{-9} \text{ m}^2 \text{ s}^{-1}$ at 25°C as a typical value of the diffusion coefficient of an ion in water.

(d) The Nernst–Einstein equation

The Einstein relation provides a link between the molar conductivity of an electrolyte and the diffusion coefficients of its ions. First, by using eqns 46 and 70 we write

$$\lambda = zuF = \frac{z^2DF^2}{RT} \quad (71)^\circ$$

for each type of ion. Then, from $A_m^\circ = \nu_+\lambda_+ + \nu_-\lambda_-$, the limiting molar conductivity is

$$A_m^\circ = (\nu_+z_+^2D_+ + \nu_-z_-^2D_-) \frac{F^2}{RT} \quad (72)^\circ$$

which is the Nernst–Einstein equation. One of its applications is to the determination of ionic diffusion coefficients from conductivity measurements; another is to the prediction of conductivities using models of ionic diffusion (see below).

(e) The Stokes–Einstein equation

Equations 45 ($u = ez/f$) and 70 relate the mobility of an ion to the frictional force and to the diffusion coefficient, respectively. The two expressions can be combined to give the Stokes–Einstein equation:

$$D = \frac{kT}{f} \quad (73)$$

If the frictional force is described by Stokes' law, then we also obtain a relation between the diffusion coefficient and the viscosity of the medium:

$$D = \frac{kT}{6\pi\eta a} \quad (74)$$

An important feature of eqn 73 (and of its special case, eqn 74) is that it makes no reference to the charge of the diffusing species. Therefore, the equation also applies in the limit of vanishingly small charge, that is, it also applies to neutral molecules. Consequently, we may use viscosity measurements to estimate the diffusion coefficients for electrically neutral molecules in solution (Table 24.7). It must not be forgotten, however, that both equations depend on the assumption that the viscous drag is proportional to the speed.

Table 24.7* Diffusion coefficients at 298 K, $D/(10^{-9} \text{ m}^2 \text{ s}^{-1})$

H^+ in water	9.31
I_2 in hexane	4.05
Na^+ in water	1.33
Sucrose in water	0.522

* More values are given in the Data section.

Example 24.6 Interpreting the mobility of an ion

Use the experimental value of the mobility to evaluate the diffusion coefficient, the limiting molar conductivity, and the hydrodynamic radius of a sulfate ion in aqueous solution.

Method The starting point is the mobility of the ion, which is given in Table 24.5. The diffusion coefficient can then be determined from the Einstein relation, eqn 70. The ionic conductivity is related to the mobility by eqn 46. To estimate the hydrodynamic radius, a , of the ion, use the Stokes–Einstein relation to find f and Stokes' law to relate f to a .

Answer From Table 24.5, the mobility of SO_4^{2-} is $8.29 \times 10^{-8} \text{ m}^2 \text{ s}^{-1} \text{ V}^{-1}$. It follows from eqn 70 that

$$D = \frac{uRT}{zF} = 1.1 \times 10^{-9} \text{ m}^2 \text{ s}^{-1}$$

From eqn 46 it follows that

$$\lambda = zuF = 16 \text{ mS m}^2 \text{ mol}^{-1}$$

Finally, from $f = 6\pi\eta a$ using 1.00 cP (or $1.00 \times 10^{-3} \text{ kg m}^{-1} \text{ s}^{-1}$) for the viscosity of water (Table 24.3):

$$a = \frac{kT}{6\pi\eta D} = 200 \text{ pm}$$

Comment The bond length in SO_4^{2-} is 144 pm , so the radius calculated here is plausible and consistent with a small degree of solvation.

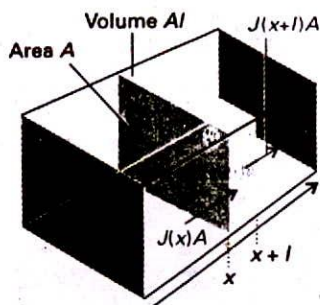
Self-test 24.6 Repeat the calculation for the NH_4^+ ion.

[$1.96 \times 10^{-9} \text{ m}^2 \text{ s}^{-1}$, $7.4 \text{ mS m}^2 \text{ mol}^{-1}$, 110 pm]

Experimental support for the relations derived above comes from conductivity measurements. In particular, Walden's rule is the empirical observation that the product $\eta\Lambda_m$ is very approximately constant for the same ions in different solvents. Because $\Lambda_m \propto D$, and we have just seen that $D \propto 1/\eta$, we do indeed predict that $\Lambda_m \propto 1/\eta$, as Walden's rule implies. The usefulness of the rule, however, is muddled by the role of solvation: different solvents solvate the same ions to different extents, so both the hydrodynamic radius and the viscosity change with the solvent.

24.11 The diffusion equation

We now turn to the discussion of time-dependent diffusion processes, where we are interested in the spreading of inhomogeneities with time. One example is the temperature of a metal bar that has been heated at one end: if the source of heat is removed, then the bar gradually settles down into a state of uniform temperature. When the source of heat is maintained and the bar can radiate, it settles down into a steady state of nonuniform temperature. Another example (and one more relevant to chemistry) is the concentration distribution in a solvent to which a solute is added. We shall focus on the description of the diffusion of particles, but similar arguments apply to the diffusion of physical properties, such as temperature. Our aim is to obtain an equation for the rate of change of the concentration of particles in an inhomogeneous region.



24.23 The net flux in a region is the difference between the flux entering from the region of high concentration (on the left) and the flux leaving to the region of low concentration (on the right).

The central equation of this section is the diffusion equation,⁹ which relates the rate of change of concentration at a point to the spatial variation of the concentration at that point:

$$\frac{\partial c}{\partial t} = D \frac{\partial^2 c}{\partial x^2} \quad (75)$$

Justification 24.8

Consider a thin slab of cross-sectional area A that extends from x to $x + l$ (Fig. 24.23). Let the concentration at x be c at the time t . The amount (number of moles) of particles that enter the slab in the infinitesimal interval dt is $JAdt$, so the rate of increase in molar concentration inside the slab (which has volume Al) on account of the flux from the left is

$$\frac{\partial c}{\partial t} = \frac{JAdt}{Al} = \frac{J}{l}$$

There is also an outflow through the right-hand window. The flux through that window is J' , and the rate of change of concentration that results is

$$\frac{\partial c}{\partial t} = -\frac{J'Adt}{Al} = -\frac{J'}{l}$$

The net rate of change of concentration is therefore

$$\frac{\partial c}{\partial t} = \frac{J - J'}{l}$$

Each flux is proportional to the concentration gradient at the window. So, by using Fick's first law, we can write

$$\begin{aligned} J - J' &= -D \frac{\partial c}{\partial x} + D \frac{\partial c'}{\partial x} = -D \frac{\partial c}{\partial x} + D \frac{\partial}{\partial x} \left\{ c + \left(\frac{\partial c}{\partial x} \right) l \right\} \\ &= D l \frac{\partial^2 c}{\partial x^2} \end{aligned}$$

When this relation is substituted into the expression for the rate of change of concentration in the slab, we get eqn 75.

(a) The significance of the diffusion equation

The diffusion equation shows that the rate of change of concentration is proportional to the curvature (more precisely, to the second derivative) of the concentration with respect to distance. If the concentration changes sharply from point to point (if the distribution is highly wrinkled), then the concentration changes rapidly with time. If the curvature is zero, then the concentration is constant in time. If the concentration decreases linearly with distance, then the concentration at any point is constant because the inflow of particles is exactly balanced by the outflow.

The diffusion equation can be regarded as a mathematical formulation of the intuitive notion that there is a natural tendency for the wrinkles in a distribution to disappear. More succinctly: Nature abhors a wrinkle.

(b) Diffusion with convection

The transport of particles arising from the motion of a streaming fluid is called convection. If for the moment we ignore diffusion, then the flux of particles through an area A in an

⁹ This equation used to be called 'Fick's second law of diffusion', but that name is now rarely used.

interval Δt when the fluid is flowing at a velocity v can be calculated in the way we have used several times before (by counting the particles within a distance $v\Delta t$), and is

$$J = \frac{cAv\Delta t}{A\Delta t} = cv \quad (76)$$

This J is called the convective flux. The rate of change of concentration in a slab of thickness l and area A is, by the same argument as before,

$$\frac{\partial c}{\partial t} = \frac{J - J'}{l} = \left\{ c - \left[c + \left(\frac{\partial c}{\partial x} \right) l \right] \right\} \frac{v}{l} = -v \frac{\partial c}{\partial x} \quad (77)$$

(We have assumed that the velocity does not depend on the position.)

When both diffusion and convection occur, the total change of concentration in a region is the sum of the two effects, and the generalized diffusion equation is

$$\frac{\partial c}{\partial t} = D \frac{\partial^2 c}{\partial x^2} - v \frac{\partial c}{\partial x} \quad (78)$$

A further refinement, which is important in chemistry, is the possibility that the concentrations of particles may change as a result of reaction. When reactions are included in eqn 78 (Section 27.3), we get a powerful differential equation for discussing the properties of reacting, diffusing, convecting systems and which is the basis of reactor design in chemical industry and of the utilization of resources in living cells.

(c) Solutions of the equation

The diffusion equation, eqn 75, is a second-order differential equation with respect to space and a first-order differential equation with respect to time. Therefore, we must specify two boundary conditions for the spatial dependence and a single initial condition for the time dependence.

As an illustration, consider a solvent in which the solute is initially coated on one surface of the container (for example, a layer of sugar on the bottom of a deep beaker of water). The single initial condition is that at $t = 0$ all N_0 particles are concentrated on the yz -plane (of area A) at $x = 0$. The two boundary conditions are derived from the requirements: (1) that the concentration must everywhere be finite and (2) that the total amount (number of moles) of particles present is n_0 (with $n_0 = N_0/N_A$) at all times. These requirements imply that the flux of particles is zero at the top and bottom surfaces of the system. Under these conditions it is found that

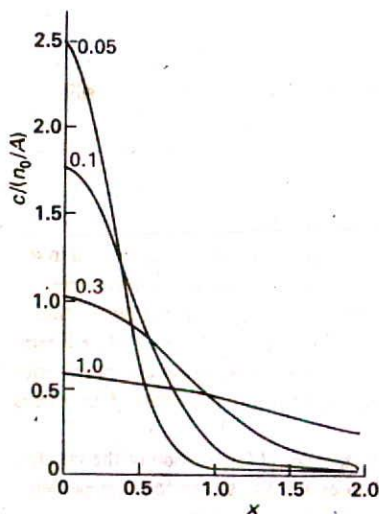
$$c(x, t) = \frac{n_0}{A(\pi Dt)^{1/2}} e^{-x^2/4Dt} \quad (79)$$

as may be verified by direct substitution. Figure 24.24 shows the shape of the concentration distribution at various times, and it is clear that the concentration spreads and tends to uniformity.

Another useful result is for a localized concentration of solute in a three-dimensional solvent (a sugar lump suspended in a large flask of water). The concentration of diffused solute is spherically symmetrical, and at a radius r is

$$c(r, t) = \frac{n_0}{8(\pi Dt)^{3/2}} e^{-r^2/4Dt} \quad (80)$$

Other chemically (and physically) interesting arrangements can be treated, but the solutions are more cumbersome.



24.24 The concentration profiles above a plane from which a solute is diffusing. The curves are plots of eqn 79. The units of Dt and x are arbitrary, but are related so that Dt/x^2 is dimensionless. For example, if x is in metres, Dt would be in metres², so, for $D = 10^{-9} \text{ m}^2 \text{ s}^{-1}$, $Dt = 0.1$ corresponds to $t = 10^4 \text{ s}$.

(d) The measurement of diffusion coefficients

The solutions of the diffusion equation are useful for experimental determinations of diffusion coefficients. In the **capillary technique**, a capillary tube, open at one end and containing a solution, is immersed in a well stirred larger quantity of solvent, and the change of concentration in the tube is measured at a series of times. The solute diffuses from the open end of the capillary at a rate that can be calculated by solving the diffusion equation with the appropriate boundary conditions, so D may be determined. In the **diaphragm technique**, the diffusion occurs through the capillary pores of a sintered glass diaphragm separating the well-stirred solution and solvent. The concentrations are monitored and then related to the solutions of the diffusion equation corresponding to this arrangement.

24.12 Diffusion probabilities

The solutions of the diffusion equation can be used to predict the concentration of particles (or the value of some other physical quantity, such as the temperature in a nonuniform system) at any location. We can also use them to calculate the net distance through which the particles diffuse in a given time.

Example 24.7 Calculating the net distance of diffusion

Calculate the net distance travelled on average by particles in a time t if they are diffusing in a medium with diffusion constant D .

Method We need to calculate the probability that a particle will be found at a certain distance from the origin, and then calculate the average by weighting each distance by that probability.

Answer The number of particles in a slab of thickness dx and area A at x , where the molar concentration is c , is $cAN_A dx$. The probability that any of the $N_0 = n_0N_A$ particles is in the slab is therefore $cAN_A dx/N_0$. If the particle is in the slab, it has travelled a distance x from the origin. Therefore, the mean distance travelled by all the particles is the sum of each x weighted by the probability of its occurrence:

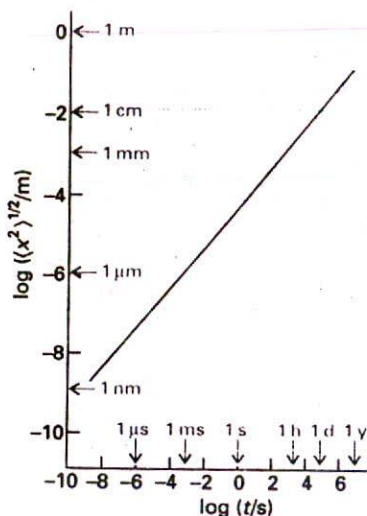
$$\begin{aligned}\langle x \rangle &= \int_0^{\infty} \frac{xcAN_A}{N_0} dx = \frac{1}{(\pi Dt)^{1/2}} \int_0^{\infty} x e^{-x^2/4Dt} dx \\ &= 2 \left(\frac{Dt}{\pi} \right)^{1/2}\end{aligned}$$

Comment The average distance of diffusion varies as the square root of the lapsed time. If we use the Stokes-Einstein relation for the diffusion coefficient, the mean distance travelled by particles of radius a in a solvent of viscosity η is

$$\langle x \rangle = \left(\frac{2kTt}{3\pi^2\eta a} \right)^{1/2}$$

Self-test 24.7 Derive an expression for the root mean square distance travelled by diffusing particles in a time t .

$$[\langle x^2 \rangle]^{1/2} = (2Dt)^{1/2}$$



24.25 The root mean square distance covered by particles with $D = 5 \times 10^{-10} \text{ m}^2 \text{ s}^{-1}$. Note the great slowness of diffusion.

As shown in Example 24.7, the average distance travelled by a diffusing particle in a time t (in an arrangement like that illustrated in Fig. 24.24) is

$$\langle x \rangle = 2 \left(\frac{Dt}{\pi} \right)^{1/2} \quad (81)$$

and the root mean square distance travelled in the same time is

$$\langle x^2 \rangle^{1/2} = (2Dt)^{1/2} \quad (82)$$

The latter is a valuable measure of the spread of particles when they can diffuse in both directions from the origin (for then $\langle x \rangle = 0$ at all times). The root mean square distance travelled by particles with a typical diffusion coefficient ($D = 5 \times 10^{-10} \text{ m}^2 \text{ s}^{-1}$) is illustrated in Fig. 24.25. The graph shows that diffusion is a very slow process (which is why solutions are stirred, to encourage mixing by convection).

24.13 The statistical view

An intuitive picture of diffusion is of the particles moving in a series of small steps and gradually migrating from their original positions. We shall explore this idea using a model in which the particles can jump through a distance λ in a time τ . The total distance travelled by a particle in a time t is therefore $t\lambda/\tau$. However, the particle will not necessarily be found at that distance from the origin. The direction of each step may be different, and the net distance travelled must take the changing directions into account.

If we simplify the discussion by allowing the particles to travel only along a straight line (the x -axis), and for each step (to the left or the right) to be through the same distance λ , then we obtain the **one-dimensional random walk**.¹⁰ We show in the *Justification* below that the probability of a particle being at a distance x from the origin after a time t is

$$P = \left(\frac{2\tau}{\pi t} \right)^{1/2} e^{-x^2/2t\lambda^2} \quad (83)$$

Justification 24.9

Consider a one-dimensional random walk in which each step is through a distance λ to the left or right. The net distance travelled after N steps is equal to the difference between the number of steps to the right (N_R) and to the left (N_L), and is $(N_R - N_L)\lambda$. We write $n = N_R - N_L$ and the total number of steps as $N = N_R + N_L$.

The number of ways of performing a walk with a given net distance of travel $n\lambda$ is the number of ways of making N_R steps to the right and N_L steps to the left, and is given by the binomial coefficient

$$W = \frac{N!}{N_L!N_R!} = \frac{N!}{\left\{ \frac{1}{2}(N+n) \right\}! \left\{ \frac{1}{2}(N-n) \right\}!}$$

The probability of the net distance walked being $n\lambda$ is

$$\begin{aligned} P &= \frac{\text{number of paths with } N_R \text{ steps to the right}}{\text{total number of steps}} \\ &= \frac{W}{2^N} = \frac{N!}{\left\{ \frac{1}{2}(N+n) \right\}! \left\{ \frac{1}{2}(N-n) \right\}! 2^N} \end{aligned}$$

The use of Stirling's approximation (Section 19.1a) in the form

$$\ln x! \approx \ln(2\pi)^{1/2} + \left(x + \frac{1}{2}\right) \ln x - x$$

¹⁰ The same model was used in the discussion of a one-dimensional random coil in Section 23.6.

gives (after quite a lot of algebra)

$$\ln P = \ln \left(\frac{2}{\pi N} \right)^{1/2} - \frac{1}{2}(N+n+1) \ln \left(1 + \frac{n}{N} \right) - \frac{1}{2}(N-n+1) \ln \left(1 - \frac{n}{N} \right)$$

For small net distances ($n \ll N$) we can use the approximation $\ln(1 \pm x) \approx \pm x - \frac{1}{2}x^2$, and so obtain

$$\ln P \approx \ln \left(\frac{2}{\pi N} \right)^{1/2} - n^2/2N$$

At this point, we note that the number of steps taken in a time t is $N = t/\tau$ and the net distance travelled from the origin is $x = n\lambda$. Substitution of these quantities into the equation just derived gives an expression that rearranges into eqn 83.

The differences of detail between eqns 79 and 83 arise from the fact that in the present calculation the particles can migrate in either direction from the origin. Moreover, they can be found only at discrete points separated by λ instead of being anywhere on a continuous line. The fact that the two expressions are so similar suggests that diffusion can indeed be interpreted as the outcome of a large number of steps in random directions.

We can now relate the coefficient D to the step length λ and the rate at which the jumps occur. Thus, by comparing the two exponents in eqns 79 and 83 we can immediately write down the Einstein–Smoluchowski equation:

$$D = \frac{\lambda^2}{2\tau} \quad (84)$$

Illustration

Suppose that an SO_4^{2-} ion jumps through its own diameter each time it makes a move in an aqueous solution; then, because $D = 1.1 \times 10^{-9} \text{ m}^2 \text{ s}^{-1}$ and $a = 210 \text{ pm}$ (as deduced from mobility measurements), it follows from $\lambda = 2a$ that $\tau = 80 \text{ ps}$. Because τ is the time for one jump, the ion makes 1×10^{10} jumps per second.

The Einstein–Smoluchowski relation is the central connection between the microscopic details of particle motion and the macroscopic parameters relating to diffusion (for example, the diffusion coefficient and, through the Stokes–Einstein relation, the viscosity). It also brings us back full circle to the properties of the perfect gas. For, if we interpret λ/τ as \bar{c} , the mean speed of the molecules, and interpret λ as a mean free path, then we can recognize in the Einstein–Smoluchowski equation exactly the same expression as we obtained from the kinetic theory of gases, eqn 11. That is, the diffusion of a perfect gas is a random walk with an average step size equal to the mean free path.

Checklist of key ideas

Molecular motion in gases

- transport properties
- diffusion
- thermal conduction
- electric conduction
- viscosity
- effusion

24.1 Collisions with walls and surfaces

- collision flux (3)
- collision frequency

24.2 The rate of effusion

- Graham's law of effusion
- Knudsen method

24.3 Migration down gradients

- flux
- Fick's first law of diffusion (6)
- diffusion coefficient
- coefficient of thermal conductivity

- Newtonian flow
- coefficient of viscosity

24.4 Transport properties of a perfect gas

- diffusion coefficient of a perfect gas (11)

- coefficient of thermal conductivity of a perfect gas (16)
- viscosity of a perfect gas (21)
- Poiseuille's formula (23)

Motion in liquids

24.5 The structures of liquids

- radial distribution function
- long-range order
- short-range order
- virial
- Monte Carlo method
- molecular dynamics
- mesophase
- liquid crystal
- smectic phase
- nematic phase
- cholesteric phase

24.6 Molecular motion in liquids

- inelastic neutron scattering

24.7 The conductivities of electrolyte solutions

- polarization
- conductance
- conductivity (29)
- molar conductivity (30)
- strong electrolyte
- weak electrolyte
- Kohlrausch's law (31)
- limiting molar conductivity
- law of the independent migration of ions (32)
- degree of ionization (36)
- Ostwald's dilution law (39)

24.8 The mobilities of ions

- drift speed (43)
- hydrodynamic (Stokes) radius
- Grotthuss mechanism
- mobility of ion (44)
- mobility and conductivity (46)
- transport number (50)
- limiting transport number

- transport number and conductivity (55)
- moving boundary method
- indicator solution
- leading solution
- Hittorf method
- cell with transference

24.9 Conductivities and ion-ion interactions

- relaxation effect
- electrophoretic effect
- Debye-Hückel-Onsager theory (59)
- Green-Kubo relation (60)
- correlation function

Diffusion

24.10 The thermodynamic view

- thermodynamic force (63)
- thermodynamic force due to a concentration gradient (65)
- Einstein relation (70)

- Nernst-Einstein equation (72)
- Stokes-Einstein equation (73)
- Walden's rule

24.11 The diffusion equation

- diffusion equation (75)
- convection
- convective flux
- generalized diffusion equation (78)
- capillary technique
- diaphragm technique

24.12 Diffusion probabilities

- root mean square migration distance (82)

24.13 The statistical view

- one-dimensional random walk
- probability of location (83)
- Einstein-Smoluchowski equation (84)

Further reading

Articles of general interest

- H.G. Herz, B.M. Braun, K.J. Müller, and R. Mauer, What is the physical significance of the pictures representing the Grotthuss H⁺ conductance mechanism? *J. Chem. Educ.* **64**, 777 (1987).
- N. Agmon, The Grotthuss mechanism. *Chem. Phys. Letts.* **244**, 456 (1995).
- B.L. Earl, Confusion in the expressions for transport coefficients. *J. Chem. Educ.* **66**, 147 (1989).
- T. Kenney, Graham's law: defining gas velocities. *J. Chem. Educ.* **67**, 871 (1990).
- B.J. Alder and A.J. Ladd, Simulation by molecular dynamics. In *Encyclopedia of applied physics* (ed. G.L. Trigg), **18**, 281. VCH, New York (1997).
- J.D. Lister and R. Shashidhar, Structure of liquid crystals. In *Encyclopedia of applied physics* (ed. G.L. Trigg), **8**, 515. VCH, New York (1994).
- N.E. Cusack, Structure of simple liquids. In *Encyclopedia of applied physics* (ed. G.L. Trigg), **8**, 533. VCH, New York (1994).
- D.G. Leaist, Diffusion and ionic conduction in liquids. In *Encyclopedia of applied physics* (ed. G.L. Trigg), **5**, 661. VCH, New York (1993).

Texts and sources of data and information

- P.J. Collings, *Liquid crystals: Nature's delicate phase of matter*. Wiley, New York (1991).
- G.A. Krestov, et al., *Ionic solvation*. Ellis Horwood/Prentice-Hall, Hemel Hempstead (1993).
- W. Kauzmann, *Kinetic theory of gases*. Addison-Wesley, Reading (1966).
- J.O. Hirschfelder, C.F. Curtiss, and R.B. Bird, *The molecular theory of gases and liquids*. Wiley, New York (1954).
- D. Tabor, *Gases, liquids, and solids*. Cambridge University Press (1979).
- A.J. Walton, *Three phases of matter*. Oxford University Press (1983).
- R.B. Bird, W.E. Stewart, and E.N. Lightfoot, *Transport phenomena*. Wiley, New York (1960).
- M. Spiro, Determination of transference numbers. In *Techniques of chemistry* (ed. A. Weissberger and B.W. Rossiter), **2A**, 205. Wiley-Interscience, New York (1971).
- A.J. Bard and L.R. Faulkner, *Electrochemical methods: fundamentals and applications*. Wiley, New York (1980).
- P.J. Dunlop, B.J. Steel, and J.E. Lane, Experimental methods for studying diffusion in liquids, gases, and solids. In *Techniques of*

chemistry (ed. A. Weissberger and B.W. Rossiter), 4, 205. Wiley-Interscience, New York (1972).

J. Crank, *The mathematics of diffusion*. Clarendon Press, Oxford (1975).

J.S. Rowlinson and F.L. Swinton, *Liquids and liquid mixtures*. Butterworth, London (1982).

J.N. Murrell and A.D. Jenkins, *Properties of liquids and solutions*. Wiley-Interscience, New York (1994).

A.R. Leach, *Molecular modelling: principles and applications*. Longman, Harlow (1996).

D. Frenkel and B. Smit, *Understanding molecular simulation*. Academic Press, San Diego (1996).

M.P. Allen and D. Tildesley, *Computer simulation of liquids*. Clarendon Press, Oxford (1986).

Exercises

24.1 (a) A solid surface with dimensions $2.5 \text{ mm} \times 3.0 \text{ mm}$ is exposed to argon gas at 90 Pa and 500 K. How many collisions do the Ar atoms make with this surface in 15 s?

24.1 (b) A solid surface with dimensions $3.5 \text{ mm} \times 4.0 \text{ cm}$ is exposed to helium gas at 111 Pa and 1500 K. How many collisions do the He atoms make with this surface in 10 s?

24.2 (a) An effusion cell has a circular hole of diameter 2.50 mm. If the molar mass of the solid in the cell is 260 g mol^{-1} and its vapour pressure is 0.835 Pa at 400 K, by how much will the mass of the solid decrease in a period of 2.00 h?

24.2 (b) An effusion cell has a circular hole of diameter 3.00 mm. If the molar mass of the solid in the cell is 300 g mol^{-1} and its vapour pressure is 0.224 Pa at 450 K, by how much will the mass of the solid decrease in a period of 24.00 h?

24.3 (a) Calculate the flux of energy arising from a temperature gradient of 2.5 K m^{-1} in a sample of argon in which the mean temperature is 273 K.

24.3 (b) Calculate the flux of energy arising from a temperature gradient of 3.5 K m^{-1} in a sample of hydrogen in which the mean temperature is 260 K.

24.4 (a) Use the experimental value of the thermal conductivity of neon (Table 24.1) to estimate the collision cross-section of Ne atoms at 273 K.

24.4 (b) Use the experimental value of the thermal conductivity of nitrogen (Table 24.1) to estimate the collision cross-section of N_2 molecules at 298 K.

24.5 (a) In a double-glazed window, the panes of glass are separated by 5.0 cm. What is the rate of transfer of heat by conduction from the warm room (25°C) to the cold exterior (-10°C) through a window of area 1.0 m^2 ? What power of heater is required to make good the loss of heat?

24.5 (b) Two sheets of copper of area 1.50 m^2 are separated by 10.0 cm. What is the rate of transfer of heat by conduction from the warm sheet (50°C) to the cold sheet (-10°C)? What is the rate of loss of heat?

24.6 (a) A manometer was connected to a bulb containing carbon dioxide under slight pressure. The gas was allowed to escape through a small pinhole, and the time for the manometer reading to drop from 75 cm to 50 cm was 52 s. When the experiment was repeated using

nitrogen (for which $M = 28.01 \text{ g mol}^{-1}$) the same fall took place in 42 s. Calculate the molar mass of carbon dioxide.

24.6 (b) A manometer was connected to a bulb containing nitrogen under slight pressure. The gas was allowed to escape through a small pinhole, and the time for the manometer reading to drop from 65.1 cm to 42.1 cm was 18.5 s. When the experiment was repeated using a fluorocarbon gas, the same fall took place in 82.3 s. Calculate the molar mass of the fluorocarbon.

24.7 (a) A space vehicle of internal volume 3.0 m^3 is struck by a meteor and a hole of radius 0.10 mm is formed. If the oxygen pressure within the vehicle is initially 80 kPa and its temperature 298 K, how long will the pressure take to fall to 70 kPa?

24.7 (b) A container of internal volume 22.0 m^3 was punctured, and a hole of radius 0.050 mm was formed. If the nitrogen pressure within the vehicle is initially 122 kPa and its temperature 293 K, how long will the pressure take to fall to 105 kPa?

24.8 (a) Use the experimental value of the coefficient of viscosity for neon (Table 24.1) to estimate the collision cross-section of Ne atoms at 273 K.

24.8 (b) Use the experimental value of the coefficient of viscosity for nitrogen (Table 24.1) to estimate the collision cross-section of the molecules at 273 K.

24.9 (a) Calculate the inlet pressure required to maintain a flow rate of $9.5 \times 10^5 \text{ L h}^{-1}$ of nitrogen at 293 K flowing through a pipe of length 8.50 m and diameter 1.00 cm. The pressure of gas as it leaves the tube is 1.00 bar. The volume of the gas is measured at that pressure.

24.9 (b) Calculate the inlet pressure required to maintain a flow rate of $8.70 \text{ cm}^3 \text{ s}^{-1}$ of nitrogen at 300 K flowing through a pipe of length 10.5 m and diameter 15 mm. The pressure of gas as it leaves the tube is 1.00 bar. The volume of the gas is measured at that pressure.

24.10 (a) Calculate the viscosity of air at (a) 273 K, (b) 298 K, (c) 1000 K. Take $\sigma \approx 0.40 \text{ nm}^2$. (The experimental values are $173 \mu\text{P}$ at 273 K, $182 \mu\text{P}$ at 20°C , and $394 \mu\text{P}$ at 600°C .)

24.10 (b) Calculate the viscosity of benzene vapour at (a) 273 K, (b) 298 K, (c) 1000 K. Take $\sigma \approx 0.88 \text{ nm}^2$.

24.11 (a) Calculate the thermal conductivities of (a) argon, (b) helium at 300 K and 1.0 mbar. Each gas is confined in a cubic vessel of side 10 cm, one wall being at 310 K and the one opposite at

295 K. What is the rate of flow of energy as heat from one wall to the other in each case?

24.11 (b) Calculate the thermal conductivities of (a) neon, (b) nitrogen at 300 K and 15 mbar. Each gas is confined in a cubic vessel of side 15 cm, one wall being at 305 K and the one opposite at 295 K. What is the rate of flow of energy as heat from one wall to the other in each case?

24.12 (a) The viscosity of carbon dioxide was measured by comparing its rate of flow through a long narrow tube (using Poiseuille's formula) with that of argon. For the same pressure differential, the same volume of carbon dioxide passed through the tube in 55 s as that of argon in 83 s. The viscosity of argon at 25°C is 208 μP ; what is the viscosity of carbon dioxide? Estimate the molecular diameter of carbon dioxide.

24.12 (b) The viscosity of a chlorofluorocarbon (CFC) was measured by comparing its rate of flow through a long narrow tube (using Poiseuille's formula) with that of argon. For the same pressure differential, the same volume of the CFC passed through the tube in 72.0 s as that of argon in 18.0 s. The viscosity of argon at 25°C is 208 μP ; what is the viscosity of the CFC? Estimate the molecular diameter of the CFC. Take $M = 200 \text{ g mol}^{-1}$.

24.13 (a) Calculate the thermal conductivity of argon ($C_{V,m} = 12.5 \text{ JK}^{-1} \text{ mol}^{-1}$, $\sigma = 0.36 \text{ nm}^2$) at room temperature (20°C).

24.13 (b) Calculate the thermal conductivity of nitrogen ($C_{V,m} = 20.8 \text{ JK}^{-1} \text{ mol}^{-1}$, $\sigma = 0.43 \text{ nm}^2$) at room temperature (20°C).

24.14 (a) Calculate the diffusion constant of argon at 25°C and (a) 1.00 Pa, (b) 100 kPa, (c) 10.0 MPa. If a pressure gradient of 0.10 atm cm^{-1} is established in a pipe, what is the flow of gas due to diffusion?

24.14 (b) Calculate the diffusion constant of nitrogen at 25°C and (a) 10.0 Pa, (b) 100 kPa, (c) 15.0 MPa. If a pressure gradient of 0.20 bar m^{-1} is established in a pipe, what is the flow of gas due to diffusion?

24.15 (a) The mobility of a chloride ion in aqueous solution at 25°C is $7.91 \times 10^{-8} \text{ m}^2 \text{ s}^{-1} \text{ V}^{-1}$. Calculate the molar ionic conductivity.

24.15 (b) The mobility of an acetate ion in aqueous solution at 25°C is $4.24 \times 10^{-8} \text{ m}^2 \text{ s}^{-1} \text{ V}^{-1}$. Calculate the molar ionic conductivity.

24.16 (a) The mobility of a Rb^+ ion in aqueous solution is $7.92 \times 10^{-8} \text{ m}^2 \text{ s}^{-1} \text{ V}^{-1}$ at 25°C. The potential difference between two electrodes placed in the solution is 35.0 V. If the electrodes are 8.00 mm apart, what is the drift speed of the Rb^+ ion?

24.16 (b) The mobility of a Li^+ ion in aqueous solution is $4.01 \times 10^{-8} \text{ m}^2 \text{ s}^{-1} \text{ V}^{-1}$ at 25°C. The potential difference between two electrodes placed in the solution is 12.0 V. If the electrodes are 1.00 cm apart, what is the drift speed of the ion?

24.17 (a) What fraction of the total current is carried by Li^+ when current flows through an aqueous solution of LiBr at 25°C?

24.17 (b) What fraction of the total current is carried by Cl^- when current flows through an aqueous solution of NaCl at 25°C?

24.18 (a) The limiting molar conductivities of KCl , KNO_3 , and AgNO_3 are 14.99 $\text{mS m}^2 \text{ mol}^{-1}$, 14.50 $\text{mS m}^2 \text{ mol}^{-1}$, and

13.34 $\text{mS m}^2 \text{ mol}^{-1}$, respectively (all at 25°C). What is the limiting molar conductivity of AgCl at this temperature?

24.18 (b) The limiting molar conductivities of NaI , NaCH_3CO_2 , and $\text{Mg}(\text{CH}_3\text{CO}_2)_2$ are 12.69 $\text{mS m}^2 \text{ mol}^{-1}$, 9.10 $\text{mS m}^2 \text{ mol}^{-1}$, and 18.78 $\text{mS m}^2 \text{ mol}^{-1}$, respectively (all at 25°C). What is the limiting molar conductivity of MgI_2 at this temperature?

24.19 (a) At 25°C the molar ionic conductivities of Li^+ , Na^+ , and K^+ are 3.87 $\text{mS m}^2 \text{ mol}^{-1}$, 5.01 $\text{mS m}^2 \text{ mol}^{-1}$, and 7.35 $\text{mS m}^2 \text{ mol}^{-1}$, respectively. What are their mobilities?

24.19 (b) At 25°C the molar ionic conductivities of F^- , Cl^- , and Br^- are 5.54 $\text{mS m}^2 \text{ mol}^{-1}$, 7.635 $\text{mS m}^2 \text{ mol}^{-1}$, and 7.81 $\text{mS m}^2 \text{ mol}^{-1}$, respectively. What are their mobilities?

24.20 (a) The mobility of a NO_3^- ion in aqueous solution at 25°C is $7.40 \times 10^{-8} \text{ m}^2 \text{ s}^{-1} \text{ V}^{-1}$. Calculate its diffusion coefficient in water at 25°C.

24.20 (b) The mobility of a CH_3CO_2^- ion in aqueous solution at 25°C is $4.24 \times 10^{-8} \text{ m}^2 \text{ s}^{-1} \text{ V}^{-1}$. Calculate its diffusion coefficient in water at 25°C.

24.21 (a) The diffusion coefficient of CCl_4 in heptane at 25°C is $3.17 \times 10^{-9} \text{ m}^2 \text{ s}^{-1}$. Estimate the time required for a CCl_4 molecule to have a root mean square displacement of 5.0 mm.

24.21 (b) The diffusion coefficient of I_2 in hexane at 25°C is $4.05 \times 10^{-9} \text{ m}^2 \text{ s}^{-1}$. Estimate the time required for an iodine molecule to have a root mean square displacement of 1.0 cm.

24.22 (a) Estimate the effective radius of a sucrose molecule in water at 25°C given that its diffusion coefficient is $5.2 \times 10^{-10} \text{ m}^2 \text{ s}^{-1}$ and that the viscosity of water is 1.00 cP.

24.22 (b) Estimate the effective radius of a glycine molecule in water at 25°C given that its diffusion coefficient is $1.055 \times 10^{-9} \text{ m}^2 \text{ s}^{-1}$ and that the viscosity of water is 1.00 cP.

24.23 (a) The diffusion coefficient for molecular iodine in benzene is $2.13 \times 10^{-9} \text{ m}^2 \text{ s}^{-1}$. How long does a molecule take to jump through about one molecular diameter (approximately the fundamental jump length for translational motion)?

24.23 (b) The diffusion coefficient for CCl_4 in heptane is $3.17 \times 10^{-9} \text{ m}^2 \text{ s}^{-1}$ and its viscosity is 0.387 $\text{kg m}^{-1} \text{ s}^{-1}$. How long does a molecule take to jump through about one molecular diameter (approximately the fundamental jump length for translational motion)?

24.24 (a) What is the root mean square distance travelled by an iodine molecule in benzene at 25°C in 1.0 s?

24.24 (b) What is the root mean square distance travelled by a sucrose molecule in water at 25°C in 1.0 s?

24.25 (a) About how long, on average, does it take for the molecules in Exercise 24.24a to drift to a point (a) 1.0 mm, (b) 1.0 cm from their starting points?

24.25 (b) The diffusion coefficient of a particular kind of t-RNA molecule is $D = 1.0 \times 10^{-11} \text{ m}^2 \text{ s}^{-1}$ in the medium of a cell interior. How long does it take molecules produced in the cell nucleus to reach the walls of the cell at a distance 1.0 μm , corresponding to the radius of the cell?

Problems

Numerical problems

24.1 Enrico Fermi, the great Italian scientist, was a master at making good approximate calculations based on little or no actual data. Hence, such calculations are often called 'Fermi calculations'. Do a Fermi calculation on how long it would take for a gaseous air-borne cold virus of molar mass 100 kg mol^{-1} to travel the distance between two conversing people 1.0 m apart by diffusion in still air.

24.2 Calculate the ratio of the thermal conductivities of gaseous hydrogen at 300 K to gaseous hydrogen at 10 K. Be circumspect, and think about the modes of motion that are thermally active at the two temperatures.

24.3 In the Knudsen method for the determination of vapour pressure, a weighed amount of a sample is heated inside a container, in the wall of which there is a small hole. The mass loss over a period of time can be related to the vapour pressure at the temperature of the experiment. If Δw is the mass lost in an interval Δt through a circular hole of radius R , find an expression relating the vapour pressure, p , to Δw and Δt . A Knudsen cell was used to determine the vapour pressure of germanium at 1000°C . During an interval of 7200 s the mass loss through a hole of radius 0.50 mm amounted to 43 μg . What is the vapour pressure of germanium at 1000°C ? Assume the gas to be monatomic.

24.4 In a study of the catalytic properties of a titanium surface it was necessary to maintain the surface free from contamination. Calculate the collision frequency per square centimetre of surface made by O_2 molecules at (a) 100 kPa, (b) 1.00 Pa and 300 K. Estimate the number of collisions made with a single surface atom in each second. The conclusions underline the importance of working at very low pressures (much lower than 1 Pa, in fact) in order to study the properties of uncontaminated surfaces. Take the nearest-neighbour distance as 291 pm.

24.5 The nuclide ^{244}Bk (berkelium) decays by producing α particles, which capture electrons and form He atoms. Its half-life is 4.4 h. A sample of mass 1.0 mg was placed in a container of volume 1.0 cm^3 that was impermeable to α radiation, but there was also a hole of radius $2.0 \mu\text{m}$ in the wall. What is the pressure of helium at 298 K, inside the container after (a) 1.0 h, (b) 10 h?

24.6 An atomic beam is designed to function with (a) cadmium, (b) mercury. The source is an oven maintained at 380 K, there being a small slit of dimensions $1.0 \text{ cm} \times 1.0 \times 10^{-3} \text{ cm}$. The vapour pressure of cadmium is 0.13 Pa and that of mercury is 152 kPa at this temperature. What is the atomic current (the number of atoms per unit time) in the beams?

24.7 Conductivities are often measured by comparing the resistance of a cell filled with the sample to its resistance when filled with some standard solution, such as aqueous potassium chloride. The conductivity of water is 76 mS m^{-1} at 25°C and the conductivity of $0.100 \text{ mol L}^{-1} \text{ KCl(aq)}$ is 1.1639 S m^{-1} . A cell had a resistance of 33.21Ω when filled with $0.100 \text{ mol L}^{-1} \text{ KCl(aq)}$ and 300.0Ω when

filled with $0.100 \text{ mol L}^{-1} \text{ CH}_3\text{COOH}$. What is the molar conductivity of acetic acid at that concentration and temperature?

24.8 The resistances of a series of aqueous NaCl solutions, formed by successive dilution of a sample, were measured in a cell with cell constant (the constant C in the relation $\kappa = C/R$) 0.2063 cm^{-1} . The following values were found:

$c/(\text{mol L}^{-1})$	0.00050	0.0010	0.0050	0.010	0.020	0.050
R/Ω	3314	1669	342.1	174.1	89.08	37.14

Verify that the molar conductivity follows Kohlrausch's law and find the limiting molar conductivity. Determine the coefficient \mathcal{K} . Use the value of \mathcal{K} (which should depend only on the nature, not the identity of the ions) and the information that $\lambda(\text{Na}^+) = 5.01 \text{ mS m}^2 \text{ mol}^{-1}$ and $\lambda(\text{I}^-) = 7.68 \text{ mS m}^2 \text{ mol}^{-1}$ to predict (a) the molar conductivity, (b) the conductivity, (c) the resistance it would show in the cell, of $0.010 \text{ mol L}^{-1} \text{ NaI(aq)}$ at 25°C .

24.9 After correction for the water conductivity, the conductivity of a saturated aqueous solution of AgCl at 25°C was found to be 0.1887 mS m^{-1} . What is the solubility of silver chloride at this temperature?

24.10 What are the drift speeds of Li^+ , Na^+ , and K^+ in water when a potential difference of 10 V is applied across a 1.00 cm conductivity cell? How long would it take an ion to move from one electrode to the other? In conductivity measurements it is normal to use alternating current: what are the displacements of the ions in (a) centimetres, (b) solvent diameters, about 300 pm, during a half cycle of 1.0 kHz applied potential?

24.11 The mobilities of H^+ and Cl^- at 25°C in water are $3.623 \times 10^{-7} \text{ m}^2 \text{ s}^{-1} \text{ V}^{-1}$ and $7.91 \times 10^{-8} \text{ m}^2 \text{ s}^{-1} \text{ V}^{-1}$, respectively. What proportion of the current is carried by the protons in 1.0 mM HCl(aq) ? What fraction do they carry when the NaCl is added to the acid so that the solution is 1.0 mol L^{-1} in the salt? Note how concentration as well as mobility governs the transport of current.

24.12 In a moving boundary experiment on KCl the apparatus consisted of a tube of internal diameter 4.146 mm, and it contained aqueous KCl at a concentration of 0.021 mol L^{-1} . A steady current of 18.2 mA was passed, and the boundary advanced as follows:

$\Delta t/\text{s}$	200	400	600	800	1000
x/mm	64	128	192	254	318

Find the transport number of K^+ , its mobility, and its ionic conductivity.

24.13 The proton possesses abnormal mobility in water, but does it behave normally in liquid ammonia? To investigate this question, a moving-boundary technique was used to determine the transport number of NH_4^+ in liquid ammonia (the analogue of H_3O^+ in liquid water) at -40°C (J. Baldwin, J. Evans, and J.B. Gill, *J. Chem. Soc. A*, 3389 (1971)). A steady current of 5.000 mA was passed for 2500 s, during which time the boundary formed between mercury(II) iodide

and ammonium iodide solutions in ammonia moved 286.9 mm in a 0.013 65 mol kg⁻¹ solution and 92.03 mm in a 0.042 55 mol kg⁻¹ solution. Calculate the transport number of NH₄⁺ at these concentrations, and comment on the mobility of the proton in liquid ammonia. The bore of the tube is 4.146 mm and the density of liquid ammonia is 0.682 g cm⁻³.

24.14 A dilute solution of potassium permanganate in water at 25°C was prepared. The solution was in a horizontal tube of length 10 cm, and at first there was a linear gradation of intensity of the purple solution from the left (where the concentration was 0.100 mol L⁻¹) to the right (where the concentration was 0.050 mol L⁻¹). What is the magnitude and sign of the thermodynamic force acting on the solute (a) close to the left face of the container, (b) in the middle, (c) close to the right face? Give the force per mole and force per molecule in each case.

24.15 Estimate the diffusion coefficients and the effective hydrodynamic radii of the alkali metal cations in water from their mobilities at 25°C. Estimate the approximate number of water molecules that are dragged along by the cations. Ionic radii are given in Table 21.3.

24.16 Nuclear magnetic resonance can be used to determine the mobility of molecules in liquids. A set of measurements on methane in carbon tetrachloride showed that its diffusion coefficient is 2.05 × 10⁻⁹ m² s⁻¹ at 0°C and 2.89 × 10⁻⁹ m² s⁻¹ at 25°C. Deduce what information you can about the mobility of methane in carbon tetrachloride.

24.17 A concentrated sucrose solution is poured into a cylinder of diameter 5.0 cm. The solution consisted of 10 g of sugar in 5.0 cm³ of water. A further 1.0 L of water is then poured very carefully on top of the layer, without disturbing the layer. Ignore gravitational effects, and pay attention only to diffusional processes. Find the concentration at 5.0 cm above the lower layer after a lapse of (a) 10 s, (b) 1.0 y.

Theoretical problems

24.18 Show how the ratio of two transport numbers t' and t'' for two cations in a mixture depends on their concentrations c' and c'' , and their mobilities u' and u'' .

24.19 Confirm that eqn 79 is a solution of the diffusion equation with the correct initial value.

24.20 The diffusion equation is valid when many elementary steps are taken in the time interval of interest; but the random walk calculation lets us discuss distributions for short times as well as for long. Use eqn 83 to calculate the probability of being six paces from the origin (that is, at $x = 6\lambda$) after (a) four, (b) six, (c) twelve steps.

24.21 Write a program or use mathematical software to calculate P in a one-dimensional random walk, and evaluate the probability of being at $x = n\lambda$ for $n = 6, 10, 14, \dots, 60$. Compare the numerical value with the analytical value in the limit of a large number of steps. At what value of n is the discrepancy no more than 0.1 per cent?

Additional problems supplied by Carmen Giunta and Charles Trapp

24.22 A.K. Srivastava, R.A. Smart, and S.D. Patankar (*J. Chem. Eng. Data* 41, 431 (1996)) measured the conductance of several salts in a binary solvent mixture of water and a dipolar aprotic solvent 1,3-dioxolan-2-one (ethylene carbonate). They report the following conductances at 25°C in a solvent 80 per cent 1,3-dioxolan-2-one by mass.

	Nal	KI
$c/(\text{mmol L}^{-1})$	32.02	20.28
$A_m/(\text{S cm}^2 \text{ mol}^{-1})$	50.26	51.99
$c/(\text{mmol L}^{-1})$	17.68	10.88
$A_m/(\text{S cm}^2 \text{ mol}^{-1})$	42.45	45.91

Calculate A_m° for Nal and KI in this solvent and $\lambda^\circ(\text{Na}) - \lambda^\circ(\text{K})$. Compare your results to the analogous quantities in aqueous solution using Table 24.4 in the Data section.

24.23 A. Fenghour, W.A. Wakeham, V. Vesovic, J.T.R. Watson, J. Millat, and E. Vogel (*J. Phys. Chem. Ref. Data* 24, 1649 (1995)) have compiled an extensive table of viscosity coefficients for ammonia in the liquid and vapour phases. Deduce the effective molecular diameter of NH₃ based on each of the following vapour-phase viscosity coefficients: (a) $\eta = 9.08 \times 10^{-6}$ kg m⁻¹ s⁻¹ at 270 K and 1.00 bar; (b) $\eta = 1.749 \times 10^{-5}$ kg m⁻¹ s⁻¹ at 490 K and 10.0 bar.

24.24 Interstellar space is quite a different medium from the gaseous environments we commonly encounter on Earth. For instance, a typical density of the medium is about 1 atom cm⁻³ and that atom is typically H; the effective temperature due to stellar background radiation is about 10 000 K. Estimate the diffusion coefficient and thermal conductivity of H under these conditions. (Comment. Energy is in fact transferred much more effectively by radiation.)

24.25 G. Bakale, K. Lacmann, and W.F. Schmidt (*J. Phys. Chem.* 100, 12477 (1996)) measured the mobility of singly charged C₆₀⁻ ions in a variety of nonpolar solvents. In cyclohexane at 22°C, the mobility is 1.1 cm² V⁻¹ s⁻¹. Estimate the effective radius of the C₆₀⁻ ion. The viscosity of the solvent is 0.93 × 10⁻³ kg m⁻¹ s⁻¹. Comment. The researchers interpreted the substantial difference between this



25

The rates of chemical reactions



Empirical chemical kinetics

- 25.1 Experimental techniques
- 25.2 The rates of reactions
- 25.3 Integrated rate laws
- 25.4 Reactions approaching equilibrium
- 25.5 The temperature dependence of reaction rates

Accounting for the rate laws

- 25.6 Elementary reactions
- 25.7 Consecutive elementary reactions
- 25.8 Unimolecular reactions

Checklist of key ideas

Further reading

Exercises

Problems

This chapter is the first of a sequence that explores the rates of chemical reactions. The chapter begins with a discussion of the definition of reaction rate and outlines the techniques for its measurement. The results of such measurements show that reaction rates depend on the concentration of reactants (and products) in characteristic ways that can be expressed in terms of differential equations known as rate laws. The solutions of these equations are used to predict the concentrations of species at any time after the start of the reaction. The form of the rate law also provides insight into the series of elementary steps by which a reaction takes place. The key task in this connection is the construction of a rate law from a proposed mechanism and its comparison with experiment. Simple elementary steps have simple rate laws, and these rate laws can be combined together by invoking one or more approximations. These approximations include the concept of the rate-determining stage of a reaction, the steady-state concentration of a reaction intermediate, and the existence of a pre-equilibrium.

This chapter introduces the principles of **chemical kinetics**, the study of reaction rates, by showing how the rates of reactions may be measured and interpreted. The remaining chapters of this part of the text then develop this material in more detail and apply it to more complicated or more specialized cases. The rate of a chemical reaction might depend on variables under our control, such as the pressure, the temperature, and the presence of a catalyst, and we may be able to optimize the rate by the appropriate choice of conditions. The study of reaction rates also leads to an understanding of the mechanisms of reactions, their analysis into a sequence of elementary steps. We saw in Chapter 9 that the Second Law accounts for the direction of spontaneous change. Here we explore why spontaneous chemical reactions occur at a finite rate and are not simply instantaneous.

Empirical chemical kinetics

The first step in the kinetic analysis of reactions is to establish the stoichiometry of the reaction and identify any side reactions. The basic data of chemical kinetics are then the

concentrations of the reactants and products at different times after a reaction has been initiated. The rates of most chemical reactions are sensitive to the temperature, so in conventional experiments the temperature of the reaction mixture must be held constant throughout the course of the reaction. This requirement puts severe demands on the design of an experiment. Gas-phase reactions, for instance, are often carried out in a vessel held in contact with a substantial block of metal. Liquid-phase reactions, including flow reactions, must be carried out in an efficient thermostat. Special efforts have to be made to study reactions at low temperatures, as in the study of the kinds of reactions that take place in interstellar clouds. Thus, supersonic expansion of the reaction gas can be used to attain temperatures as low as 10 K. Non-isothermal conditions are sometimes employed. For instance, the shelf-life of an expensive pharmaceutical may be explored by slowly raising the temperature of a single sample.

25.1 Experimental techniques

The method used to monitor concentrations depends on the species involved and the rapidity with which their concentrations change. Many reactions reach equilibrium over periods of minutes or hours, and several techniques may then be used to follow the changing concentrations.

(a) Monitoring the progress of a reaction

A reaction in which at least one component is a gas might result in an overall change in pressure in a system of constant volume, so its progress may be followed by recording the variation of pressure with time.

Example 25.1 Monitoring the variation in pressure

Predict how the total pressure varies during the gas-phase decomposition
 $2\text{N}_2\text{O}_5(\text{g}) \rightarrow 4\text{NO}_2(\text{g}) + \text{O}_2(\text{g})$.

Method The total pressure (at constant volume and temperature and assuming perfect gas behaviour) is proportional to the number of gas-phase molecules. Therefore, because each mole of N_2O_5 gives rise to $\frac{5}{2}$ mol of gas molecules, we can expect the pressure to rise to $\frac{5}{2}$ times its initial value. To confirm this conclusion, express the progress of the reaction in terms of the fraction, α , of N_2O_5 molecules that have reacted.

Answer Let the initial pressure be p_0 and the initial amount of N_2O_5 molecules present be n . When a fraction α of the N_2O_5 molecules has decomposed, the amounts of the components in the reaction mixture are:

	N_2O_5	NO_2	O_2	Total
Amount:	$n(1 - \alpha)$	$2\alpha n$	$\frac{1}{2}\alpha n$	$n(1 + \frac{3}{2}\alpha)$

When $\alpha = 0$ the pressure is p_0 , so at any stage the total pressure is

$$p = (1 + \frac{3}{2}\alpha)p_0$$

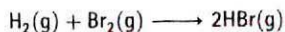
When the reaction is complete, the pressure will have risen to $\frac{5}{2}$ times its initial value.

Self-test 25.1 Repeat the calculation for $2\text{NOBr}(\text{g}) \rightarrow 2\text{NO}(\text{g}) + \text{Br}_2(\text{g})$.

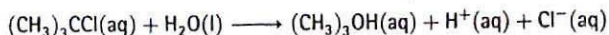
$$[p = (1 + \frac{1}{2}\alpha)p_0]$$

Spectrophotometry, the measurement of the intensity of absorption in a particular spectral region, is widely applicable, and is especially useful when one substance in the

reaction mixture has a strong characteristic absorption in a conveniently accessible region of the electromagnetic spectrum. For example, the progress of the reaction



can be followed by measuring the absorption of visible light by bromine. If the reaction changes the number or type of ions present in a solution, then it may be followed by monitoring the electrical conductivity of the solution. The replacement of neutral molecules by ionic products can result in dramatic changes in the conductivity, as in the reaction



If hydrogen ions are produced or consumed, the reaction may be followed by monitoring the pH of the solution.

Other methods of determining composition include mass spectrometry, gas chromatography, nuclear magnetic resonance, and electron spin resonance (for reactions involving radicals).

(b) Application of the techniques

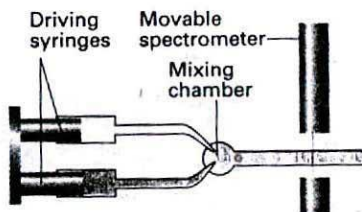
In a real-time analysis the composition of the system is analysed while the reaction is in progress. Either a small sample is withdrawn or the bulk solution is monitored. In the quenching method the reaction is stopped after it has been allowed to proceed for a certain time, and the composition is analysed at leisure. The quenching (of the entire mixture or of a sample drawn from it) can be achieved either by cooling suddenly, by adding the mixture to a large volume of solvent, or by rapid neutralization of an acid reagent. This method is suitable only for reactions that are slow enough for there to be little reaction during the time it takes to quench the mixture. Many current investigations study fast reactions, which we shall take to be reactions complete in less than about 1 s (and often very much less), and the present thrust of chemical kinetics is to ever shorter timescales. With special laser techniques it is now possible to observe processes occurring in a few tens of femtoseconds.

In the **flow method** the reactants are mixed as they flow together in a chamber (Fig. 25.1). The reaction continues as the thoroughly mixed solutions flow through the outlet tube, and observation of the composition at different positions along the tube is equivalent to the observation of the reaction mixture at different times after mixing. The disadvantage of conventional flow techniques is that a large volume of reactant solution is necessary. This disadvantage is particularly important for fast reactions, because to spread the reaction over a length of tube the flow must be rapid. The **stopped-flow technique** avoids this disadvantage (Fig. 25.2). The suitability of the stopped-flow technique to the study of small samples means that it is appropriate for biochemical reactions, and it has been widely used to study the kinetics of enzyme action.

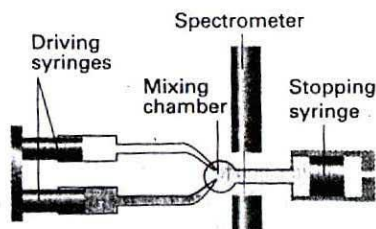
In **flash photolysis** the gaseous or liquid sample is exposed to a brief photolytic flash of light, and then the contents of the reaction chamber are monitored. Most work is now done with lasers with flashes of about 10 ns duration, but many studies are carried out at 1 ps, and some are done on a femtosecond timescale. Either emission or absorption spectroscopy may be used to monitor the reaction, and the spectra are recorded electronically at a series of times following the flash.

25.2 The rates of reactions

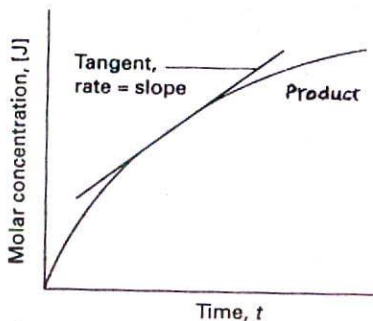
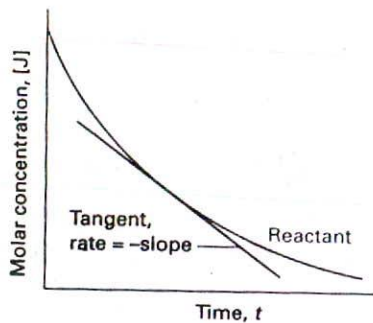
Reaction rates depend on the composition and the temperature of the reaction mixture. The next few sections look at these observations in more detail.



25.1 The arrangement used in the flow technique for studying reaction rates. The reactants are injected into the mixing chamber at a steady rate. The location of the spectrometer corresponds to different times after initiation.



25.2 In the stopped-flow technique the reagents are driven quickly into the mixing chamber by the driving syringes and then the time dependence of the concentrations is monitored.



25.3 The definition of (instantaneous) rate as the slope of the tangent drawn to the curve showing the variation of concentration with time. For negative slopes, the sign is changed when reporting the rate, so all reaction rates are positive.

(a) The definition of rate

Consider a reaction of the form $A + 2B \rightarrow 3C + D$, in which at some instant the molar concentration of a participant J is $[J]$. The instantaneous rate of consumption of one of the reactants at a given time is $-d[R]/dt$, where R is A or B . This rate is a positive quantity (Fig. 25.3). The rate of formation of one of the products (C or D , which we denote P) is $d[P]/dt$ (note the difference in sign). This rate is also positive.

It follows from the stoichiometry for the reaction $A + 2B \rightarrow 3C + D$ that

$$\frac{d[D]}{dt} = \frac{1}{3} \frac{d[C]}{dt} = -\frac{d[A]}{dt} = -\frac{1}{2} \frac{d[B]}{dt}$$

so there are several rates connected with the reaction. The problem of having several possibly different rates to describe the same reaction is avoided by defining the unique rate of reaction, v , as

$$v = \frac{1}{\nu_J} \frac{d[J]}{dt} \quad [1]$$

where ν_J is the stoichiometric number of substance J , with ν_J negative for reactants and positive for products (recall the notation introduced in Section 2.7b). Now there is a single rate for the entire reaction (for the chemical equation as written). With molar concentrations in moles per litre and time in seconds, reaction rates are reported in moles per litre per second ($\text{mol L}^{-1} \text{s}^{-1}$).

Illustration

If the rate of formation of NO in the reaction $2\text{NOBr}(\text{g}) \rightarrow 2\text{NO}(\text{g}) + \text{Br}_2(\text{g})$ is reported as $1.6 \times 10^{-4} \text{ mol L}^{-1} \text{ s}^{-1}$, we use $\nu_{\text{NO}} = +2$ to report that $v = 8.0 \times 10^{-5} \text{ mol L}^{-1} \text{ s}^{-1}$. Because $\nu_{\text{NOBr}} = -2$ it follows that $d[\text{NOBr}]/dt = -1.6 \times 10^{-4} \text{ mol L}^{-1} \text{ s}^{-1}$. The rate of consumption of NOBr is therefore $1.6 \times 10^{-4} \text{ mol L}^{-1} \text{ s}^{-1}$.

Self-test 25.2 The rate of change of molar concentration of CH_3 radicals in the reaction $2\text{CH}_3(\text{g}) \rightarrow \text{CH}_3\text{CH}_3(\text{g})$ was reported as $d[\text{CH}_3]/dt = -1.2 \text{ mol L}^{-1} \text{ s}^{-1}$ under particular conditions. What are (a) the rate of reaction and (b) the rate of formation of CH_3CH_3 ?

[(a) $0.60 \text{ mol L}^{-1} \text{ s}^{-1}$, (b) $0.60 \text{ mol L}^{-1} \text{ s}^{-1}$]

(b) Rate laws and rate constants

The rate of reaction is often found to be proportional to the concentrations of the reactants raised to a power. For example, the rate of a reaction may be found to be proportional to the molar concentrations of two reactants A and B , in which case we write

$$v = k[A][B] \quad (2)$$

where each concentration is raised to the first power. The coefficient k is called the **rate constant** for the reaction. The rate constant is independent of the concentrations but depends on the temperature. An experimentally determined equation of this kind is called the **rate law** of the reaction. More formally, a rate law is an equation that expresses the rate of reaction as a function of the concentrations of all the species present in the overall chemical equation for the reaction at some time:

$$v = f([A], [B], \dots) \quad [3]$$

The rate law of a reaction is determined experimentally, and cannot in general be inferred from the chemical equation for the reaction. The reaction of hydrogen and bromine, for

example, has a very simple stoichiometry, $\text{H}_2(\text{g}) + \text{Br}_2(\text{g}) \rightarrow 2\text{HBr}(\text{g})$, but its rate law is complicated:

$$v = \frac{k[\text{H}_2][\text{Br}_2]^{3/2}}{[\text{Br}_2] + k'[\text{HBr}]} \quad (4)$$

In certain cases the rate law does reflect the stoichiometry of the reaction, but that is either a coincidence or reflects a feature of the underlying reaction mechanism (see later).

A practical application of a rate law is that, once we know the law and the value of the rate constant, we can predict the rate of reaction from the composition of the mixture. Moreover, as we shall see later, by knowing the rate law, we can go on to predict the composition of the reaction mixture at a later stage of the reaction. Moreover, a rate law is a guide to the mechanism of the reaction, for any proposed mechanism must be consistent with the observed rate law.

(c) Reaction order

Many reactions are found to have rate laws of the form

$$v = k[\text{A}]^a[\text{B}]^b \dots \quad (5)$$

The power to which the concentration of a species (a product or a reactant) is raised in a rate law of this kind is the *order* of the reaction with respect to that species. A reaction with the rate law in eqn 2 is first-order in A and first-order in B. The overall order of a reaction with a rate law like that in eqn 5 is the sum of the individual orders, $a + b + \dots$. The rate law in eqn 2 is therefore second-order overall.

A reaction need not have an integral order, and many gas-phase reactions do not. For example, a reaction having the rate law

$$v = k[\text{A}]^{1/2}[\text{B}] \quad (6)$$

is half-order in A, first-order in B, and three-halves order overall. Some reactions obey a zero-order rate law, and therefore have a rate that is independent of the concentration of the reactant (so long as some is present). Thus, the catalytic decomposition of phosphine (PH_3) on hot tungsten at high pressures has the rate law

$$v = k \quad (7)$$

The PH_3 decomposes at a constant rate until it has almost entirely disappeared. Only heterogeneous reactions can have rate laws that are zero-order overall.

When a rate law is not of the form in eqn 5, the reaction does not have an overall order and may not even have definite orders with respect to each participant. Thus, although eqn 4 shows that the reaction of hydrogen and bromine is first-order in H_2 , the reaction has an indefinite order with respect to both Br_2 and HBr and has no overall order.

These remarks point to three problems. First, we must see how to identify the rate law and obtain the rate constant from the experimental data. We concentrate on this aspect in this chapter. Second, we must see how to construct reaction mechanisms that are consistent with the rate law. We shall introduce the techniques of doing so in this chapter and develop them further in Chapter 26. Third, we must account for the values of the rate constants and explain their temperature dependence. We shall see a little of what is involved in this chapter, but leave the details until Chapter 27.

(d) The determination of the rate law

The determination of a rate law is simplified by the isolation method in which the concentrations of all the reactants except one are in large excess. If B is in large excess, for example, then to a good approximation its concentration is constant throughout the

reaction. Although the true rate law might be $v = k[A][B]$, we can approximate $[B]$ by $[B]_0$ and write

$$v = k'[A] \quad k' = k[B]_0 \quad (8)$$

which has the form of a first-order rate law. Because the true rate law has been forced into first-order form by assuming that the concentration of B is constant, it is called a **pseudofirst-order rate law**. The dependence of the rate on the concentration of each of the reactants may be found by isolating them in turn (by having all the other substances present in large excess), and so constructing a picture of the overall rate law.

In the **method of initial rates**, which is often used in conjunction with the isolation method, the rate is measured at the beginning of the reaction for several different initial concentrations of reactants. We shall suppose that the rate law for a reaction with A isolated is $v = k[A]^a$; then its initial rate, v_0 , is given by the initial values of the concentration of A, and we write $v_0 = k[A]_0^a$. Taking logarithms gives:

$$\log v_0 = \log k + a \log [A]_0 \quad (9)$$

For a series of initial concentrations, a plot of the logarithms of the initial rates against the logarithms of the initial concentrations of A should be a straight line with slope a .

Example 25.2 Using the method of initial rates

The recombination of iodine atoms in the gas phase in the presence of argon was investigated and the order of the reaction was determined by the method of initial rates. The initial rates of reaction of $2I(g) + Ar(g) \rightarrow I_2(g) + Ar(g)$ were as follows:

$[I]_0 / (10^{-5} \text{ mol L}^{-1})$	1.0	2.0	4.0	6.0
$v_0 / (\text{mol L}^{-1} \text{ s}^{-1})$	(a) 8.70×10^{-4}	3.48×10^{-3}	1.39×10^{-2}	3.13×10^{-2}
	(b) 4.35×10^{-3}	1.74×10^{-2}	6.96×10^{-2}	1.57×10^{-1}
	(c) 8.69×10^{-3}	3.47×10^{-2}	1.38×10^{-1}	3.13×10^{-1}

The Ar concentrations are (a) $1.0 \times 10^{-3} \text{ mol L}^{-1}$, (b) $5.0 \times 10^{-3} \text{ mol L}^{-1}$, and (c) $1.0 \times 10^{-2} \text{ mol L}^{-1}$. Determine the orders of reaction with respect to the I and Ar atom concentrations and the rate constant.

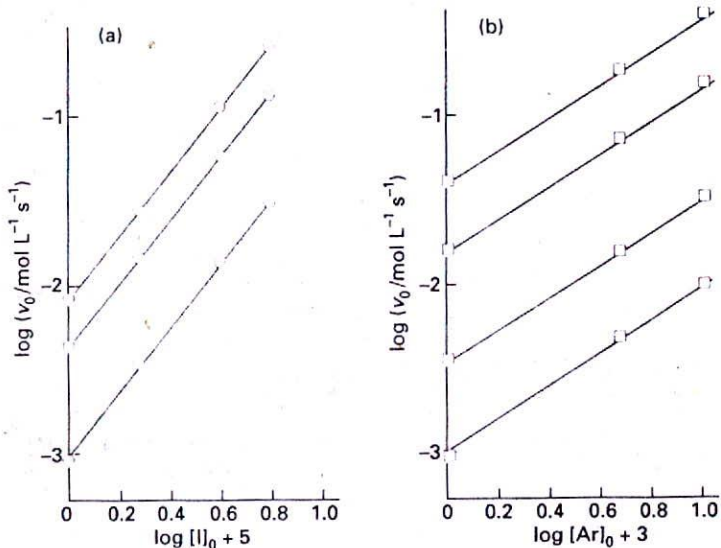
Method Plot the logarithm of the initial rate, $\log v_0$, against $\log [I]_0$ for a given concentration of Ar, and, separately, against $\log [Ar]_0$ for a given concentration of I. The slopes of the two lines are the orders of reaction with respect to I and Ar, respectively. The intercept with the vertical axis gives $\log k$.

Answer The plots are shown in Fig. 25.4. The slopes are 2 and 1 respectively, so the (initial) rate law is

$$v_0 = k[I]_0^2[Ar]_0$$

This rate law signifies that the reaction is second-order in [I], first-order in [Ar], and third-order overall. The intercept corresponds to $k = 9 \times 10^9 \text{ mol}^{-2} \text{ L}^2 \text{ s}^{-1}$.

Comment The units of k come automatically from the calculation, and are always such as to convert the product of concentrations to concentration per unit time (for example, $\text{mol L}^{-1} \text{ s}^{-1}$).



25.4 The plot of $\log v_0$ against (a) $\log[I]_0$ for a given $[Ar]_0$, and (b) $\log[Ar]_0$ for a given $[I]_0$.

Self-test 25.3 The initial rate of a reaction depended on concentration of a substance J as follows:

$[J]_0/(10^{-3} \text{ mol L}^{-1})$	5.0	8.2	17	30
$v_0/(10^{-7} \text{ mol L}^{-1} \text{ s}^{-1})$	3.6	9.6	41	130

Determine the order of the reaction with respect to J and calculate the rate constant.

$$[2, 1.4 \times 10^{-2} \text{ L mol}^{-1} \text{ s}^{-1}]$$

The method of initial rates might not reveal the full rate law, for the products may participate in the reaction and affect the rate. For example, products participate in the synthesis of HBr, because eqn 4 shows that the full rate law depends on the concentration of HBr. To avoid this difficulty, the rate law should be fitted to the data throughout the reaction. The fitting may be done, in simple cases at least, by using a proposed rate law to predict the concentration of any component at any time, and comparing it with the data. A law should also be tested by observing whether the addition of products or, for gas-phase reactions, a change in the surface-to-volume ratio in the reaction chamber affects the rate.

25.3 Integrated rate laws

Rate laws are differential equations. Therefore, we must integrate them if we want to find the concentrations as a function of time. Even the most complex rate laws may be integrated numerically. However, in a number of simple cases analytical solutions are easily obtained, and prove to be very useful. We shall examine a few of these simple cases here, and illustrate the computational approach in Chapter 26.

(a) First-order reactions

As shown in the *Justification* below, the first-order rate law for the consumption of a reactant A

$$\frac{d[A]}{dt} = -k[A] \quad (10a)$$

has the solution

$$\ln \left(\frac{[A]}{[A]_0} \right) = -kt \quad [A] = [A]_0 e^{-kt} \quad (10b)$$

These two equations are versions of an integrated rate law, the integrated form of the rate law.

Justification 25.1

Equation 10a rearranges to

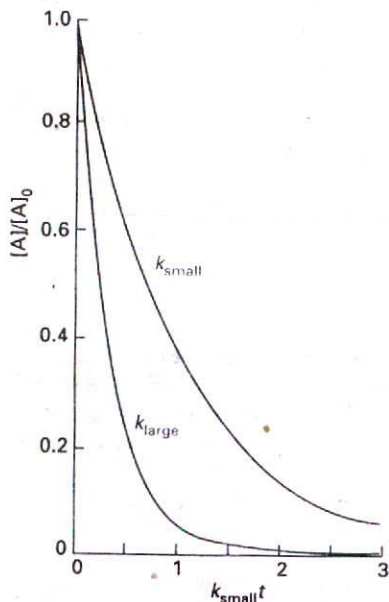
$$\frac{d[A]}{[A]} = -k dt$$

which can be integrated directly because k is a constant independent of t . Initially (at $t = 0$) the concentration of A is $[A]_0$, and at a later time t it is $[A]$, so we make these values the limits of the integrals and write

$$\int_{[A]_0}^{[A]} \frac{d[A]}{[A]} = -k \int_0^t dt$$

Because the integral of $1/x$ is $\ln x$, eqn 10b is obtained immediately.

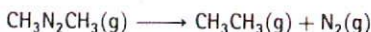
Equation 10b shows that, if $\ln ([A]/[A]_0)$ is plotted against t , then a first-order reaction will give a straight line of slope $-k$. Some rate constants determined in this way are given in Table 25.1. The second expression in eqn 10b shows that in a first-order reaction the reactant concentration decreases exponentially with time with a rate determined by k (Fig. 25.5).



25.5 The exponential decay of the reactant in a first-order reaction. The larger the rate constant, the more rapid the decay: here $k_{\text{large}} = 3k_{\text{small}}$.

Example 25.3 Analysing a first-order reaction

The variation in the partial pressure of azomethane with time was followed at 600 K, with the results given below. Confirm that the decomposition



is first-order in azomethane, and find the rate constant at 600 K.

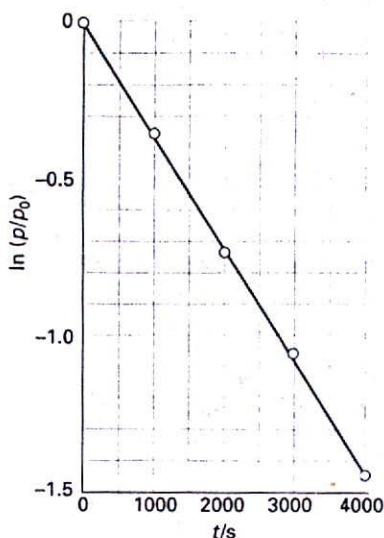
t/s	0	1000	2000	3000	4000
$p/(10^{-2} \text{ Torr})$	8.20	5.72	3.99	2.78	1.94

Method As indicated in the text, to confirm that a reaction is first-order, plot $\ln ([A]/[A]_0)$ against time and expect a straight line. Because the partial pressure of a gas is proportional to its concentration, it is equivalent to plot $\ln (p/p_0)$ against t . If a straight line is obtained, its slope can be identified with $-k$.

Table 25.1* Kinetic data for first-order reactions

Reaction	Phase	$\theta/^\circ\text{C}$	k/s^{-1}	$t_{1/2}$
$2\text{N}_2\text{O}_5 \rightarrow 4\text{NO}_2 + \text{O}_2$	g	25	3.38×10^{-5}	5.70 h
$2\text{N}_2\text{O}_5 \rightarrow 4\text{NO}_2 + \text{O}_2$	$\text{Br}_2(\text{l})$	25	4.27×10^{-5}	4.51 h
$\text{C}_2\text{H}_6 \rightarrow 2\text{CH}_3$	g	700	5.36×10^{-4}	21.6 min

*More values are given in the Data section at the end of this volume.



25.6 The determination of the rate constant of a first-order reaction: a straight line is obtained when $\ln[A]$ (or, as here, $\ln p$) is plotted against t ; the slope gives k .

Answer We draw up the following table:

t/s	0	1000	2000	3000	4000
$\ln(p/p_0)$	1	-0.360	-0.720	-1.082	-1.441

Figure 25.6 shows the plot of $\ln(p/p_0)$ against t . The plot is straight, confirming a first-order reaction, and its slope is -3.6×10^{-4} . Therefore, $k = 3.6 \times 10^{-4} \text{ s}^{-1}$.

Self-test 25.4 In a particular experiment, it was found that the concentration of N_2O_5 in liquid bromine varied with time as follows:

t/s	0	200	400	600	1000
$[\text{N}_2\text{O}_5]/\text{mol L}^{-1}$	0.110	0.073	0.048	0.032	0.014

Confirm that the reaction is first-order in N_2O_5 and determine the rate constant.

$$[k = 2.1 \times 10^{-3} \text{ s}^{-1}]$$

(b) Half-lives

A useful indication of the rate of a first-order chemical reaction is the **half-life**, $t_{1/2}$, of a substance, the time taken for the concentration of a reactant to fall to half its initial value. The time for $[A]$ to decrease from $[A]_0$ to $\frac{1}{2}[A]_0$ in a first-order reaction is given by eqn 10b as

$$kt_{1/2} = -\ln\left(\frac{\frac{1}{2}[A]_0}{[A]_0}\right) = -\ln\frac{1}{2} = \ln 2$$

Hence

$$t_{1/2} = \frac{\ln 2}{k} \quad (11)$$

($\ln 2 = 0.693$.) The main point to note about this result is that, for a first-order reaction, the half-life of a reactant is independent of its initial concentration. Hence, if the concentration of A at some arbitrary stage of the reaction is $[A]$, then it will have fallen to $\frac{1}{2}[A]$ after a further interval of $(\ln 2)/k$. Some half-lives are given in Table 25.1.

(c) Second-order reactions

We show in the *Justification* below that the integrated form of the second-order rate law

$$\frac{d[A]}{dt} = -k[A]^2 \quad (12a)$$

is

$$\frac{1}{[A]} - \frac{1}{[A]_0} = kt \quad [A] = \frac{[A]_0}{1 + kt[A]_0} \quad (12b)$$

Justification 25.2

Equation 12a is integrated by rearranging it to

$$-\frac{d[A]}{[A]^2} = kdt$$

Table 25.2* Kinetic data for second-order reactions

Reaction	Phase	$\theta/^\circ\text{C}$	$k/(\text{L mol}^{-1} \text{s}^{-1})$
$2\text{NOBr} \rightarrow 2\text{NO} + \text{Br}_2$	g	10	0.80
$2\text{I} \rightarrow \text{I}_2$	g	23	7×10^9
$\text{CH}_3\text{Cl} + \text{CH}_3\text{O}^-$	$\text{CH}_3\text{OH}(\text{l})$	20	2.29×10^{-6}

*More values are given in the *Data section*.

The concentration of A is $[A]_0$ at $t = 0$ and $[A]$ at a general time t later. Therefore, this expression integrates as follows:

$$-\int_{[A]_0}^{[A]} \frac{d[A]}{[A]^2} = k \int_0^t dt$$

Because the integral of $1/x^2$ is $-1/x$, we obtain eqn 12b by substitution of the limits.

The first expression in eqn 12b shows that to test for a second-order reaction we should plot $1/[A]$ against t and expect a straight line. The slope of the graph is k . Some rate constants determined in this way are given in Table 25.2. The second expression lets us predict the concentration of A at any time after the start of the reaction. It shows that the concentration of A approaches zero more slowly than in a first-order reaction with the same initial rate (Fig. 25.7).

It follows from eqn 12b by substituting $t = t_{1/2}$ and $[A] = \frac{1}{2}[A]_0$ that the half-life of a species A that is consumed in a second-order reaction is

$$t_{1/2} = \frac{1}{k[A]_0} \quad (13)$$

Therefore, unlike in a first-order reaction, the half-life of a substance in a second-order reaction varies with the initial concentration. A practical consequence is that species that decay by second-order reactions (which includes some environmentally harmful substances) may persist in low concentrations for long periods because their half-lives are long when their concentrations are low.

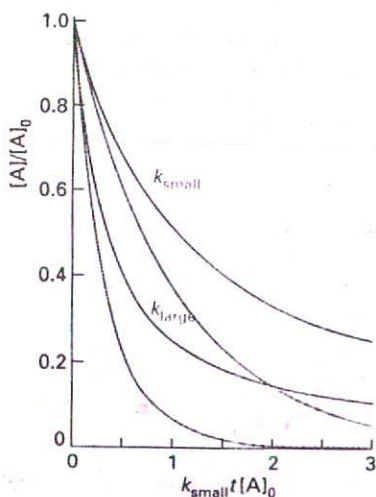
Another type of second-order reaction is one that is first-order in each of two reactants A and B:

$$\frac{d[A]}{dt} = -k[A][B] \quad (14)$$

Such a rate law cannot be integrated until we know how the concentration of B is related to that of A. For example, if the reaction is $\text{A} + \text{B} \rightarrow \text{P}$, where P denotes products, and the initial concentrations are $[A]_0$ and $[B]_0$, then it is shown in the *Justification* below that at a time t after the start of the reaction, the concentrations satisfy the relation

$$\ln \left(\frac{[B]/[B]_0}{[A]/[A]_0} \right) = ([B]_0 - [A]_0)kt \quad (15)$$

Therefore, a plot of the expression on the left against t should be a straight line from which k can be obtained. Note that, if $[A]_0 = [B]_0$, the solutions are those already given in eqn 12b (but this solution cannot be found simply by setting $[A]_0 = [B]_0$ in eqn 15).



25.7 The variation with time of the concentration of a reactant in a second-order reaction. The grey line is the corresponding decay in a first-order reaction with the same initial rate. For this illustration, $k_{\text{large}} = 3k_{\text{small}}$.

Justification 25.3

It follows from the reaction stoichiometry that, when the concentration of A has fallen to $[A]_0 - x$, the concentration of B will have fallen to $[B]_0 - x$ (because each A that disappears entails the disappearance of one B). It follows that

$$\frac{d[A]}{dt} = -k([A]_0 - x)([B]_0 - x)$$

Then, because $d[A]/dt = -dx/dt$, the rate law is

$$\frac{dx}{dt} = k([A]_0 - x)([B]_0 - x)$$

The initial condition is that $x = 0$ when $t = 0$, so the integration required is

$$\int_0^x \frac{dx}{([A]_0 - x)([B]_0 - x)} = k \int_0^t dt$$

The integral on the right is simply kt . It follows that

$$\begin{aligned} kt &= \int_0^x \frac{dx}{([A]_0 - x)([B]_0 - x)} \\ &= \frac{1}{[B]_0 - [A]_0} \int_0^x \left\{ \frac{1}{[A]_0 - x} - \frac{1}{[B]_0 - x} \right\} dx \\ &= \frac{1}{[B]_0 - [A]_0} \left\{ \ln \left(\frac{[A]_0}{[A]_0 - x} \right) - \ln \left(\frac{[B]_0}{[B]_0 - x} \right) \right\} \end{aligned}$$

This expression can be simplified and rearranged into eqn 15 by combining the two logarithms and noting that $[A] = [A]_0 - x$ and $[B] = [B]_0 - x$.

Similar calculations may be carried out to find the integrated rate laws for other orders, and some are listed in Table 25.3.

25.4 Reactions approaching equilibrium

Because all the laws considered so far disregard the possibility that the reverse reaction is important, none of them describes the overall rate when the reaction is close to equilibrium. At that stage the products may be so abundant that the reverse reaction must be taken into account. In practice, however, most kinetic studies are made on reactions that are far from equilibrium, and the reverse reactions are unimportant.

(a) First-order reactions close to equilibrium

We can explore the variation of the composition with time close to chemical equilibrium by considering the reaction in which A forms B and both forward and reverse reactions are first-order (as in some isomerizations). The scheme we consider is



The concentration of A is reduced by the forward reaction (at a rate $k[\text{A}]$) but it is increased by the reverse reaction (at a rate $k'[\text{B}]$). The net rate of change is therefore

$$\frac{d[A]}{dt} = -k[A] + k'[B] \quad (17)$$

Table 25.3 Integrated rate laws

Order	Reaction	Rate law*	$t_{1/2}$
0	$A \rightarrow P$	$v = k$ $kt = x$ for $0 \leq x \leq [A]_0$	$\frac{[A]_0}{2k}$
1	$A \rightarrow P$	$v = k[A]$ $kt = \ln \frac{[A]_0}{[A]_0 - x}$	$\frac{\ln 2}{k}$
2	$A \rightarrow P$	$v = k[A]^2$ $kt = \frac{x}{[A]_0([A]_0 - x)}$	$\frac{1}{k[A]_0}$
	$A + B \rightarrow P$	$v = k[A][B]$ $kt = \frac{1}{[B]_0 - [A]_0} \ln \frac{[A]_0([B]_0 - x)}{([A]_0 - x)[B]_0}$	
	$A + 2B \rightarrow P$	$v = k[A][B]$ $kt = \frac{1}{[B]_0 - 2[A]_0} \ln \frac{[A]_0([B]_0 - 2x)}{([A]_0 - x)[B]_0}$	
	A \rightarrow P with autocatalysis		
		$v = k[A][P]$ $kt = \frac{1}{[A]_0 + [P]_0} \ln \frac{[A]_0([P]_0 + x)}{([A]_0 - x)[P]_0}$	
3	$A + 2B \rightarrow P$	$v = k[A][B]^2$ $kt = \frac{2x}{(2[A]_0 - [B]_0)([B]_0 - 2x)[B]_0} + \frac{1}{(2[A]_0 - [B]_0)^2} \ln \frac{[A]_0([B]_0 - 2x)}{([A]_0 - x)[B]_0}$	
$n \geq 2$	$A \rightarrow P$	$v = k[A]^n$ $kt = \frac{1}{n-1} \left\{ \frac{1}{([A]_0 - x)^{n-1}} - \frac{1}{[A]_0^{n-1}} \right\}$	$\frac{2^{n-1} - 1}{(n-1)k[A]_0^{n-1}}$

* $x = [P]$, and $v = dx/dt$.

If the initial concentration of A is $[A]_0$, and no B is present initially, then at all times $[A] + [B] = [A]_0$. Therefore,

$$\frac{d[A]}{dt} = -k[A] + k'([A]_0 - [A]) = -(k+k')[A] + k'[A]_0 \quad (18)$$

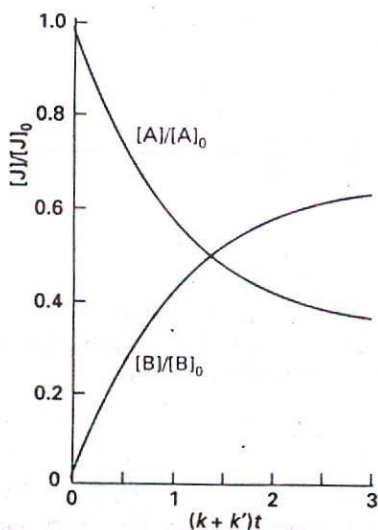
The solution of this first-order differential equation (as may be checked by differentiation) is

$$[A] = \frac{k' + ke^{-(k+k')t}}{k+k'} [A]_0 \quad (19)$$

The time dependence predicted by this equation is drawn in Fig. 25.8.

As $t \rightarrow \infty$, the concentrations reach their equilibrium values, which are given by eqn 19 as:

$$[A]_{\text{eq}} = \frac{k'[A]_{\text{eq}}}{k+k'} \quad [B]_{\text{eq}} = [A]_0 - [A]_{\text{eq}} = \frac{k[A]_0}{k+k'} \quad (20)$$



25.8 The approach of concentrations to their equilibrium values as predicted by eqn 19 for a reaction $A \rightleftharpoons B$ that is first-order in each direction, and for which $k = 2k'$.

It follows that the equilibrium constant of the reaction is

$$K = \frac{[B]_{\text{eq}}}{[A]_{\text{eq}}} = \frac{k}{k'} \quad (21)$$

Exactly the same conclusion can be reached—more simply, in fact—by noting that, at equilibrium, the forward and reverse rates must be the same, so

$$k[A]_{\text{eq}} = k'[B]_{\text{eq}} \quad (22)$$

This relation rearranges into eqn 21.

Equation 21 is very important, because it relates the thermodynamic quantity, the equilibrium constant, to quantities relating to rates. The practical importance of eqn 21 is that, if one of the rate constants can be measured, then the other may be obtained if the equilibrium constant is known.

For a more general reaction, the overall equilibrium constant can be expressed in terms of the rate constants for all the intermediate stages of the reaction mechanism:

$$K = \frac{k_a}{k'_a} \times \frac{k_b}{k'_b} \times \dots$$

where the k s are the rate constants for the individual steps and the k' s are for the corresponding reverse steps.

(b) Relaxation methods

The term relaxation denotes the return of a system to equilibrium. It is used in chemical kinetics to indicate that an externally applied influence has shifted the equilibrium position of a reaction, normally suddenly, and that the reaction is adjusting to the equilibrium composition characteristic of the new conditions (Fig. 25.9). We shall consider the response of reaction rates to a temperature jump, a sudden change in temperature. We know from Section 9.3a that the equilibrium composition of a reaction depends on the temperature (provided $\Delta_r H^\ominus$ is nonzero), so a shift in temperature acts as a perturbation on the system. One way of achieving a temperature jump is to discharge a capacitor through a sample made conducting by the addition of ions, but laser or microwave discharges can also be used. Temperature jumps of between 5 and 10 K can be achieved in about 1 μs . Some equilibria are also sensitive to pressure, and pressure-jump techniques may then also be used.

When a sudden temperature increase is applied to a simple $A \rightleftharpoons B$ equilibrium that is first-order in each direction, we show in the *Justification* below that the composition relaxes exponentially to the new equilibrium composition:

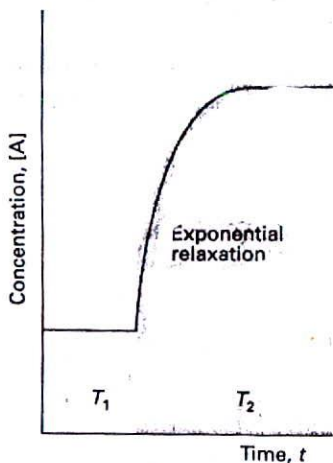
$$x = x_0 e^{-t/\tau} \quad \frac{1}{\tau} = k_a + k_b \quad (23)$$

where x is the departure from equilibrium at the new temperature and x_0 is the departure from equilibrium immediately after the temperature jump.

Justification 25.4

In the following analysis, we need to keep track of the fact that rate constants depend on temperature. At the initial temperature, when the rate constants are k'_a and k'_b , the net rate of change of $[A]$ is

$$\frac{d[A]}{dt} = -k'_a[A] + k'_b[B]$$



25.9 The relaxation to the new equilibrium composition when a reaction initially at equilibrium at a temperature T_1 is subjected to a sudden change of temperature, which takes it to T_2 .

At equilibrium under these conditions, $d[A]/dt = 0$, and the concentrations are $[A]_{\text{eq}}'$ and $[B]_{\text{eq}}'$. Therefore,

$$k_a'[A]_{\text{eq}}' = k_b'[B]_{\text{eq}}'$$

When the temperature is increased suddenly, the rate constants change to k_a and k_b , but the concentrations of A and B remain for an instant at their old equilibrium values. As the system is no longer at equilibrium, it readjusts to the new equilibrium concentrations, which are now given by

$$k_a[A]_{\text{eq}} = k_b[B]_{\text{eq}}$$

and it does so at a rate that depends on the new rate constants.

We write the deviation of [A] from its new equilibrium value as x , so $[A] = x + [A]_{\text{eq}}$ and $[B] = [B]_{\text{eq}} - x$. The concentration of A then changes as follows:

$$\frac{d[A]}{dt} = -k_a(x + [A]_{\text{eq}}) + k_b(-x + [B]_{\text{eq}}) = -(k_a + k_b)x$$

because the two terms involving the equilibrium concentrations cancel. Because $d[A]/dt = dx/dt$, this equation is a first-order differential equation with the solution given in eqn 23.

Equation 23 shows that the concentrations of A and B relax into the new equilibrium at a rate determined by the sum of the two new rate constants. Because the equilibrium constant under the new conditions is $K = k_a/k_b$, its value may be combined with the relaxation time measurement to find the individual k_a and k_b .

Example 25.4 Analysing a temperature-jump experiment

The $\text{H}_2\text{O}(\text{l}) \rightarrow \text{H}^+(\text{aq}) + \text{OH}^-(\text{aq})$ reaction relaxes to equilibrium with a time constant $37 \mu\text{s}$ at 298 K and $\text{pH} \approx 7$, and $\text{p}K_w = 14.01$. Given that the forward reaction is first-order and the reverse is second-order overall, calculate the rate constants for the forward and reverse reactions.

Method We need to derive an expression for the relaxation time, τ , in terms of k_1 (forward, first-order reaction) and k_2 (reverse, second-order reaction). We can proceed as above, but it will be necessary to make the assumption that the deviation from equilibrium (x) is so small that terms in x^2 can be neglected. Relate k_1 and k_2 through the equilibrium constant, but be careful with units because K_w is dimensionless.

Answer The forward rate at the final temperature is $k_1[\text{H}_2\text{O}]$ and the reverse rate is $k_2[\text{H}^+][\text{OH}^-]$. The net rate of formation of H_2O is

$$\frac{d[\text{H}_2\text{O}]}{dt} = -k_1[\text{H}_2\text{O}] + k_2[\text{H}^+][\text{OH}^-]$$

We write $[\text{H}_2\text{O}] = [\text{H}_2\text{O}]_{\text{eq}} + x$, $[\text{H}^+] = [\text{H}^+]_{\text{eq}} - x$, and $[\text{OH}^-] = [\text{OH}^-]_{\text{eq}} - x$, and obtain

$$\begin{aligned} \frac{dx}{dt} &= -(k_1 + k_2([\text{H}^+]_{\text{eq}} + [\text{OH}^-]_{\text{eq}}))x \\ &\quad - k_1[\text{H}_2\text{O}]_{\text{eq}} + k_2[\text{H}^+]_{\text{eq}}[\text{OH}^-]_{\text{eq}} + k_2x^2 \\ &\approx -(k_1 + k_2([\text{H}^+]_{\text{eq}} + [\text{OH}^-]_{\text{eq}}))x \end{aligned}$$

where we have neglected the term in x^2 and used the equilibrium condition to eliminate the terms that are independent of x . It follows that

$$\frac{1}{\tau} = k_1 + k_2([\text{H}^+]_{\text{eq}} + [\text{OH}^-]_{\text{eq}})$$

The equilibrium condition is

$$k_1[\text{H}_2\text{O}]_{\text{eq}} = k_2[\text{H}^+]_{\text{eq}}[\text{OH}^-]_{\text{eq}}$$

From this expression it follows that

$$\frac{k_1}{k_2} = \frac{[\text{H}^+]_{\text{eq}}[\text{OH}^-]_{\text{eq}}}{[\text{H}_2\text{O}]_{\text{eq}}} = \frac{K_w (\text{mol L}^{-1})^2}{[\text{H}_2\text{O}]_{\text{eq}}} = \frac{K_w}{55.6} \text{ mol L}^{-1}$$

because the molar concentration of pure water is 55.6 mol L^{-1} . If we write $K = K_w/55.6 = 1.8 \times 10^{-16}$, we obtain

$$\begin{aligned} \frac{1}{\tau} &= k_2\{(K \text{ mol L}^{-1}) + [\text{H}^+]_{\text{eq}} + [\text{OH}^-]_{\text{eq}}\} \\ &= k_2\{K + K_w^{1/2} + K_w^{1/2}\} \text{ mol L}^{-1} = (2.0 \times 10^{-7}) \times k_2 \text{ mol L}^{-1} \end{aligned}$$

Hence,

$$k_2 = \frac{1}{(3.7 \times 10^{-5} \text{ s}) \times (2.0 \times 10^{-7} \text{ mol L}^{-1})} = 1.4 \times 10^{11} \text{ L mol}^{-1} \text{ s}^{-1}$$

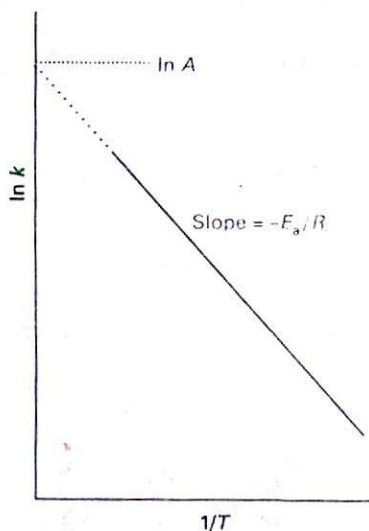
It follows that

$$k_1 = k_2 K \text{ mol L}^{-1} = 2.4 \times 10^{-5} \text{ s}^{-1}$$

Comment Notice how we keep track of units: K and K_w are dimensionless; k_2 is expressed in $\text{L mol}^{-1} \text{ s}^{-1}$; and k_1 is expressed in s^{-1} . The reaction is faster in ice, where $k_2 = 8.6 \times 10^{12} \text{ L mol}^{-1} \text{ s}^{-1}$.

Self-test 25.5 Derive an expression for the relaxation time of a concentration when the reaction $\text{A} + \text{B} \rightleftharpoons \text{C} + \text{D}$ is second-order in both directions.

$$[1/\tau = k([\text{A}] + [\text{B}]_{\text{eq}} + k'([\text{C}] + [\text{D}]_{\text{eq}})]$$



25.10 The Arrhenius plot of $\ln k$ against $1/T$ for the decomposition of CH_3CHO , and the best straight line. The slope gives $-E_a/R$ and the intercept at $1/T = 0$ gives $\ln A$.

25.5 The temperature dependence of reaction rates

The rate constants of most reactions increase as the temperature is raised. Many reactions in solution fall somewhere in the range spanned by the hydrolysis of methyl ethanoate (where the rate constant at 35°C is 1.82 times that at 25°C) and the hydrolysis of sucrose (where the factor is 4.13).

(a) The Arrhenius parameters

It is found experimentally for many reactions that a plot of $\ln k$ against $1/T$ gives a straight line. This behaviour is normally expressed mathematically by introducing two parameters, one representing the intercept and the other the slope of the straight line, and writing the Arrhenius equation

$$\ln k = \ln A - \frac{E_a}{RT} \quad (24)$$

The parameter A , which is given by the intercept of the line at $1/T = 0$ (Fig. 25.10), is called the pre-exponential factor or the frequency factor. The parameter E_a , which is obtained

Table 25.4* Arrhenius parameters

(1) First-order reactions	A/s^{-1}	$E_a/(kJ\ mol^{-1})$
$CH_3NC \rightarrow CH_3CN$	3.98×10^{13}	160
$2N_2O_5 \rightarrow 4NO_2 + O_2$	4.94×10^{13}	103.4
(2) Second-order reactions	$A/(L\ mol^{-1}\ s^{-1})$	$E_a/(kJ\ mol^{-1})$
$OH + H_2 \rightarrow H_2O + H$	8.0×10^{10}	42
$NaC_2H_5O + CH_3I$ in ethanol	2.42×10^{11}	81.6

*More values are given in the *Data* section.

from the slope of the line ($-E_a/R$), is called the activation energy. Collectively the two quantities are called the Arrhenius parameters (Table 25.4).

Example 25.5 Determining the Arrhenius parameters

The rate of the second-order decomposition of acetaldehyde (ethanal, CH_3CHO) was measured over the temperature range 700–1000 K, and the rate constants are reported below. Find E_a and A .

T/K	700	730	760	790	810	840	910	1000
$k/(L\ mol^{-1}\ s^{-1})$	0.011	0.035	0.105	0.343	0.789	2.17	20.0	145

Method According to eqn 24, the data can be analysed by plotting $\ln(k/L\ mol^{-1}\ s^{-1})$ against $1/(T/K)$ and getting a straight line. The slope of this line is $(-E_a/R)/K$ and the intercept at $1/T = 0$ is $\ln A$.

Answer We draw up the following table:

$10^3\ K/T$	1.43	1.37	1.32	1.27	1.23	1.19	1.10	1.00
$\ln(k/L\ mol^{-1}\ s^{-1})$	-4.51	-3.35	-2.25	-1.07	-0.24	0.77	3.00	4.98

Now plot $\ln k$ against $1/T$ (Fig. 25.11). The least-squares best fit of the line is with slope -2.27×10^4 and intercept 27.7. Therefore,

$$E_a = (2.21 \times 10^4\ K) \times (8.3145\ J\ K^{-1}\ mol^{-1}) = 188\ kJ\ mol^{-1}$$

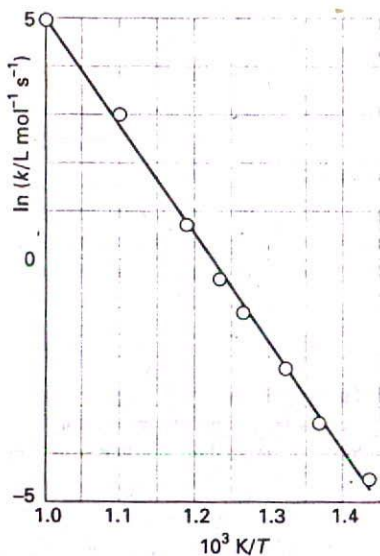
$$A = e^{27.0}\ L\ mol^{-1}\ s^{-1} = 1.1 \times 10^{12}\ L\ mol^{-1}\ s^{-1}$$

Comment Note that A has the same units as k . The slopes and intercepts of graphs are always dimensionless, and care must be taken to relate the numerical value to the physical quantity by noting how the data have been plotted. In practice, A is obtained from one of the midrange data values rather than by using a lengthy extrapolation.

Self-test 25.6 Determine A and E_a from the following data:

T/K	300	350	400	450	500
$k/(L\ mol^{-1}\ s^{-1})$	7.9×10^6	3.0×10^7	7.9×10^7	1.7×10^8	3.2×10^8

$$[8 \times 10^{10}\ L\ mol^{-1}\ s^{-1}, 23\ kJ\ mol^{-1}]$$



25.11 The Arrhenius plot using the data in Example 25.5.

The fact that E_a is given by the slope of the plot of $\ln k$ against $1/T$ means that the higher the activation energy, the stronger the temperature dependence of the rate constant (that is, the steeper the slope). A high activation energy signifies that the rate constant depends

strongly on temperature. If a reaction has zero activation energy, its rate is independent of temperature. In some cases the activation energy is negative, which indicates that the rate decreases as the temperature is raised. We shall see that such behaviour is a signal that the reaction has a complex mechanism.

The temperature dependence of some reactions is not Arrhenius-like, in the sense that a straight line is not obtained when $\ln k$ is plotted against $1/T$. However, it is still possible to define an activation energy as

$$E_a = RT^2 \frac{d \ln k}{dT} \quad [25]$$

This definition reduces to the earlier one (as the slope of a straight line) for a temperature-independent activation energy. However, the definition in eqn 25 is more general than eqn 24, because it allows E_a to be obtained from the slope (at the temperature of interest) of a plot of $\ln k$ against $1/T$ even if the Arrhenius plot is not a straight line. Non-Arrhenius behaviour is commonly a sign that quantum mechanical tunnelling is playing a significant role in the reaction.

(b) The interpretation of the parameters

For the present chapter we shall regard the Arrhenius parameters as purely empirical quantities that enable us to discuss the variation of rate constants with temperature. However, it is worth anticipating the interpretation of E_a in Section 27.1, which is motivated by writing eqn 24 as

$$k = A e^{-E_a/RT} \quad (26)$$

There we shall see that *the activation energy is the minimum kinetic energy that reactants must have in order to form products.* For example, in a gas-phase reaction there are numerous collisions each second, but only a tiny proportion are sufficiently energetic to lead to reaction. The fraction of collisions with a kinetic energy in excess of an energy E_a is given by the Boltzmann distribution as $e^{-E_a/RT}$. Hence, the exponential factor in eqn 26 can be interpreted as the fraction of collisions that have enough kinetic energy to lead to reaction.

The pre-exponential factor is a measure of the rate at which collisions occur irrespective of their energy. Hence, the product of A and the exponential factor, $e^{-E_a/RT}$, gives the rate of *successful* collisions. We shall develop these remarks in Chapter 27 and see that they have their analogues for reactions that take place in liquids.

Accounting for the rate laws

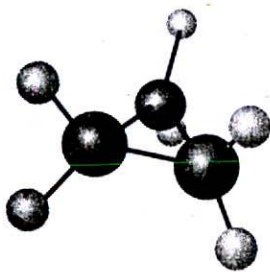
We now move on to the second stage of the analysis of kinetic data, their explanation in terms of a postulated reaction mechanism.

25.6 Elementary reactions

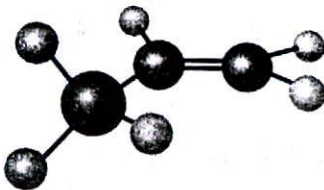
Most reactions occur in a sequence of steps called **elementary reactions**, each of which involves only a small number of molecules or ions. A typical elementary reaction is



(We do not specify the phase of the species in the chemical equation for an elementary reaction.) This equation signifies that an H atom attacks a Br_2 molecule to produce an HBr molecule and a Br atom. The **molecularity** of an elementary reaction is the number of molecules coming together to react in an elementary reaction. In a **unimolecular** reaction, a single molecule shakes itself apart or its atoms into a new arrangement, as in the isomerization of cyclopropane (1) to propene (2). In a **bimolecular** reaction, a pair of



1 Cyclopropane



2 Propene

molecules collide and exchange energy, atoms, or groups of atoms, or undergo some other kind of change. It is most important to distinguish molecularity from order:

Reaction order is an empirical quantity, and obtained from the experimental rate law.

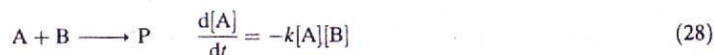
The **molecularity** refers to an elementary reaction proposed as an individual step in a mechanism.

The rate law of a unimolecular elementary reaction is first-order in the reactant:



where P denotes products (several different species may be formed). A unimolecular reaction is first-order because the number of A molecules that decay in a short interval is proportional to the number available to decay. (Ten times as many decay in the same interval when there are initially 1000 A molecules than when there are only 100 present.) Therefore, the rate of decomposition of A is proportional to its molar concentration.

An elementary bimolecular reaction has a second-order rate law:



A bimolecular reaction is second-order because its rate is proportional to the rate at which the reactant species meet, which in turn is proportional to their concentrations. Therefore, if we believe that a reaction is a single-step, bimolecular process, we can write down the rate law (and then go on to test it). Bimolecular elementary reactions are believed to account for many homogeneous reactions, such as the dimerizations of alkenes and dienes and reactions such as



(where 'alc' signifies alcohol solution). The mechanism of this reaction is believed to be the single elementary step



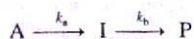
This mechanism is consistent with the observed rate law

$$v = k[\text{CH}_3\text{I}][\text{CH}_3\text{CH}_2\text{O}^-] \quad (29)$$

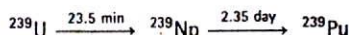
We shall see below how to string simple steps together into a mechanism and how to arrive at the corresponding rate law. For the present we emphasize that, *if the reaction is an elementary bimolecular process, then it has second-order kinetics but, if the kinetics are second-order, then the reaction might be complex.* The postulated mechanism can be explored only by detailed detective work on the system, and by investigating whether side products or intermediates appear during the course of the reaction. Detailed analysis of this kind was one of the ways, for example, in which the reaction $\text{H}_2(\text{g}) + \text{I}_2(\text{g}) \rightarrow 2\text{HI}(\text{g})$ was shown to proceed by a complex reaction. For many years the reaction had been accepted on good, but insufficiently meticulous evidence, as a fine example of a simple bimolecular reaction in which atoms exchanged partners during a collision.

25.7 Consecutive elementary reactions

Some reactions proceed through the formation of an intermediate (I), as in the consecutive unimolecular reactions



An example is the decay of a radioactive family, such as



(The times are half-lives.) We can discover the characteristics of this type of reaction by setting up the rate laws for the net rate of change of the concentration of each substance.

(a) The variation of concentrations with time

The rate of unimolecular decomposition of A is

$$\frac{d[A]}{dt} = -k_a[A] \quad (30)$$

and A is not replenished. The intermediate I is formed from A (at a rate $k_a[A]$) but decays to P (at a rate $k_b[I]$). The net rate of formation of I is therefore

$$\frac{d[I]}{dt} = k_a[A] - k_b[I] \quad (31)$$

The product P is formed by the unimolecular decay of I:

$$\frac{d[P]}{dt} = k_b[I] \quad (32)$$

We suppose that initially only A is present, and that its concentration is $[A]_0$.

The first of the rate laws, eqn 30, is an ordinary first-order decay, so we can write

$$[A] = [A]_0 e^{-k_a t} \quad (33)$$

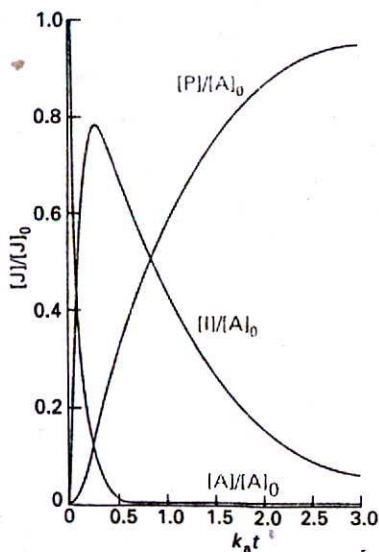
When this equation is substituted into eqn 31, and we set $[I]_0 = 0$, the solution is

$$[I] = \frac{k_a}{k_b - k_a} (e^{-k_a t} - e^{-k_b t}) [A]_0 \quad (34)$$

At all times $[A] + [I] + [P] = [A]_0$, so it follows that

$$[P] = \left\{ 1 + \frac{k_a e^{-k_b t} - k_b e^{-k_a t}}{k_b - k_a} \right\} [A]_0 \quad (35)$$

The concentration of the intermediate I rises to a maximum, and then falls to zero (Fig. 25.12). The concentration of the product P rises from zero towards $[A]_0$.



25.12 The concentrations of A, I, and P in the consecutive reaction scheme $A \rightarrow I \rightarrow P$. The curves are plots of eqns 33–35 with $k_a = 10k_b$. If the intermediate I is in fact the desired product, it is important to be able to predict when its concentration is greatest; see Example 25.6.

Example 25.6 Analysing consecutive reactions

Suppose that in an industrial batch process a substance A produces the desired compound I which goes on to decay to a worthless product C, each step of the reaction being first-order. At what time will I be present in greatest concentration?

Method The time dependence of the concentration of I is given by eqn 34. We can find the time at which [I] passes through a maximum, t_{\max} , by calculating $d[I]/dt$ and setting the resulting rate equal to zero.

Answer It follows from eqn 34 that

$$\frac{d[I]}{dt} = -\frac{k_a[A]_0(k_a e^{-k_a t} - k_b e^{-k_b t})}{k_b - k_a}$$

This rate is equal to zero when

$$k_a e^{-k_a t} = k_b e^{-k_b t}$$

Therefore,

$$t_{\max} = \frac{1}{k_a - k_b} \ln \frac{k_a}{k_b}$$

Comment For a given value of k_a , as k_b increases both the time at which [I] is a maximum and the yield of I increase.

Self-test 25.7 Calculate the maximum concentration of I and justify the last remark.

$$[I]_{\max}/[A]_0 = (k_a/k_b)^c, \quad c = k_b/(k_b - k_a)$$

(b) The rate-determining step

Suppose now that $k_b \gg k_a$; then, whenever an I molecule is formed, it decays rapidly into P. Because

$$e^{-k_b t} \ll e^{-k_a t} \quad k_b - k_a \approx k_b$$

eqn 35 reduces to

$$[P] \approx (1 - e^{-k_a t})[A]_0 \quad (36)$$

which shows that the formation of the final product P depends on only the smaller of the two rate constants. That is, the rate of formation of P depends on the rate at which I is formed, not on the rate at which I changes into P. For this reason, the step $A \rightarrow I$ is called the **rate-determining step** of the reaction. Its existence has been likened to building a six-lane highway up to a single-lane bridge: the traffic flow is governed by the rate of crossing the bridge. Similar remarks apply to more complicated reaction mechanisms, and in general the rate-determining step is the one with the smallest rate constant.

(c) The steady-state approximation

One feature of the calculation so far has probably not gone unnoticed: there is a considerable increase in mathematical complexity as soon as the reaction mechanism has more than a couple of steps. A reaction scheme involving many steps is nearly always unsolvable analytically, and alternative methods of solution are necessary. One approach is to integrate the rate laws numerically. An alternative approach, which continues to be widely used because it leads to convenient expressions and more readily digestible results, is to make an approximation.

The steady-state approximation assumes that, after an initial induction period, an interval during which the concentrations of intermediates, I, rise from zero, and during the major part of the reaction, the rates of change of concentrations of all reaction intermediates are negligibly small (Fig. 25.13):

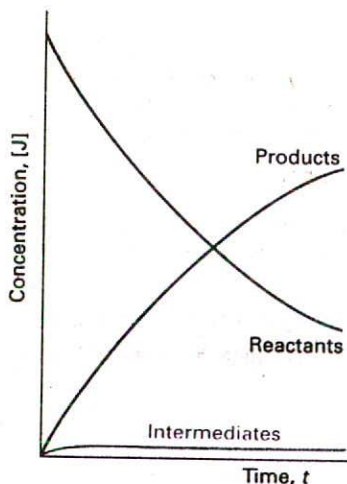
$$\frac{d[I]}{dt} \approx 0 \quad (37)$$

This approximation greatly simplifies the discussion of reaction schemes. For example, when we apply the approximation to the consecutive first-order mechanism, we set $d[I]/dt = 0$ in eqn 31, which then becomes

$$k_a[A] - k_b[I] \approx 0$$

Then

$$[I] \approx \frac{k_a}{k_b} [A] \quad (38)$$



25.13 The basis of the steady-state approximation. It is supposed that the concentrations of intermediates remain small and hardly change during most of the course of the reaction.

On substituting this value of $[I]$ into eqn 32, that equation becomes

$$\frac{d[P]}{dt} = k_b[I] \approx k_a[A] \quad (39)$$

and we see that P is formed by a first-order decay of A, with a rate constant k_a , the rate constant of the slower, rate-determining, step. We can write down the solution of this equation at once by substituting the solution for $[A]$, eqn 33, and integrating:

$$[P] = k_a[A]_0 \int_0^t e^{-k_a t'} dt' = (1 - e^{-k_a t})[A]_0 \quad (40)$$

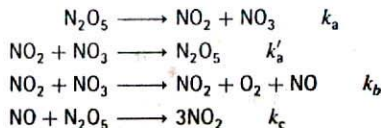
This is the same (approximate) result as before, eqn 36, but much more quickly obtained.

Example 25.7 Using the steady-state approximation

Devise the rate law for the decomposition of N_2O_5 ,



on the basis of the following mechanism:



Method First identify the intermediates (the species that occur in the reaction steps but do not appear in the overall reaction) and write expressions for their net rates of formation. Then, all net rates of change of the concentrations of intermediates are set equal to zero and the resulting equations are solved algebraically.

Answer The intermediates are NO and NO_3 ; the net rates of change of their concentrations are

$$\begin{aligned} \frac{d[NO]}{dt} &= k_b[NO_2][NO_3] - k_c[NO][N_2O_5] \approx 0 \\ \frac{d[NO_3]}{dt} &= k_a[N_2O_5] - k'_a[NO_2][NO_3] - k_b[NO_2][NO_3] \approx 0 \end{aligned}$$

The net rate of change of concentration of N_2O_5 is

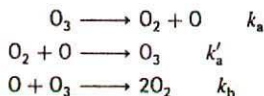
$$\frac{d[N_2O_5]}{dt} = -k_a[N_2O_5] + k'_a[NO_2][NO_3] - k_c[NO][N_2O_5]$$

and replacing the concentrations of the intermediates by using the equations above gives

$$\frac{d[N_2O_5]}{dt} = -\frac{2k_a k_b [N_2O_5]}{k'_a + k_b}$$

Comment The decomposition of N_2O_5 is problematic because its rate decreases more quickly than expected at low pressures. It is believed that this decrease is due to changes in the rate constants themselves (particularly k'_a).

Self-test 25.8 Derive the rate law for the decomposition of ozone in the reaction $2\text{O}_3(\text{g}) \rightarrow 3\text{O}_2(\text{g})$ on the basis of the (incomplete) mechanism



$$[d[\text{O}_3]/dt = -k_a k_b [\text{O}_3]^2 / (k'_a [\text{O}_2] + k_b [\text{O}_3])]$$

(d) Pre-equilibria

From a simple sequence of consecutive reactions we now turn to a slightly more complicated mechanism in which an intermediate I reaches an equilibrium with the reactants A and B:



The rate constants are k_a and k'_a for the forward and reverse reactions of the equilibrium and k_b for the final step. This scheme involves a pre-equilibrium, in which an intermediate is in equilibrium with the reactants. A pre-equilibrium arises when the rates of formation of the intermediate and its decay back into reactants are much faster than its rate of formation of products; thus, the condition is possible when $k'_a \gg k_b$ but not when $k_b \gg k'_a$. Because we assume that A, B, and I are in equilibrium, we can write

$$K = \frac{[\text{I}]}{[\text{A}][\text{B}]} \quad K = \frac{k_a}{k'_a} \quad (42)$$

In writing these equations, we are presuming that the rate of reaction of I to form P is too slow to affect the maintenance of the pre-equilibrium (see the example below). The rate of formation of P may now be written:

$$\frac{d[\text{P}]}{dt} = k_b [\text{I}] = k_b K [\text{A}][\text{B}] \quad (43)$$

This rate law has the form of a second-order rate law with a composite rate constant:

$$\frac{d[\text{P}]}{dt} = k [\text{A}][\text{B}] \quad k = k_b K = \frac{k_a k_b}{k'_a} \quad (44)$$

Example 25.8 Analysing a pre-equilibrium

Repeat the pre-equilibrium calculation but without ignoring the fact that I is slowly leaking away as it forms P.

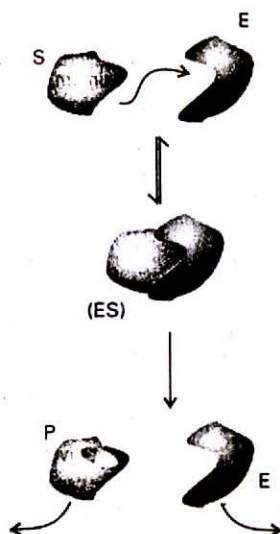
Method Begin by writing the net rates of change of the concentrations of the substances and then invoke the steady-state approximation for the intermediate I. Use the resulting expression to obtain the rate of change of the concentration of P.

Answer The net rates of change of P and I are

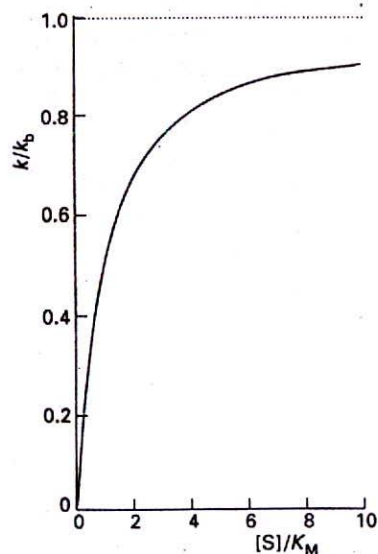
$$\begin{aligned} \frac{d[\text{P}]}{dt} &= k_b [\text{I}] \\ \frac{d[\text{I}]}{dt} &= k_a [\text{A}][\text{B}] - k'_a [\text{I}] - k_b [\text{I}] \approx 0 \end{aligned}$$

The second equation solves to

$$[\text{I}] \approx \frac{k_a [\text{A}][\text{B}]}{k'_a + k_b}$$



25.14 The basis of the Michaelis-Menten mechanism of enzyme action. Only a fragment of the large enzyme molecule E is shown.



25.15 The variation of the effective rate constant k with substrate concentration according to the Michaelis-Menten mechanism.

When we substitute this into the expression for the rate of formation of P, we obtain

$$\frac{d[P]}{dt} \approx k[A][B] \quad k = \frac{k_a k_b}{k'_a + k_b}$$

Comment This expression reduces to that in eqn 44 when the rate constant for the decay of I into products is much smaller than that for its decay into reactants, $k_b \ll k'_a$.

Self-test 25.9 Show that the pre-equilibrium mechanism in which $2A \rightleftharpoons I$ (K) followed by $I + B \rightarrow P$ (k_b) results in an overall third-order reaction.

$$[d[P]/dt = k_b K[A]^2[B]]$$

(e) The Michaelis-Menten mechanism

An example of a reaction in which an intermediate is formed is the Michaelis-Menten mechanism of enzyme action. The rate of an enzyme-catalysed reaction in which a substrate S is converted into products P is found to depend on the concentration of the enzyme E even though the enzyme undergoes no net change. The proposed mechanism, which is illustrated in Fig. 25.14, is



In this mechanism, ES denotes a bound state of the enzyme and its substrate. This mechanism has the same form as that treated in Example 25.8, so we can conclude at once that

$$[ES] = \frac{k_a [E][S]}{k'_a + k_b} \quad (46)$$

[E] and [S] are the concentrations of the free enzyme and free substrate. If $[E]_0$ is the total concentration of enzyme, then

$$[E] + [ES] = [E]_0 \quad (47)$$

Because only a little enzyme is added, the free substrate concentration is almost the same as the total substrate concentration, and we can ignore the fact that [S] differs slightly from $[S]_{\text{total}}$. Therefore,

$$[ES] = \frac{k_a ([E]_0 - [ES])[S]}{k'_a + k_b} \quad (48)$$

which rearranges to

$$[ES] = \frac{k_a [E]_0 [S]}{k'_a + k_b + k_a [S]} \quad (49)$$

It follows that the rate of formation of product is

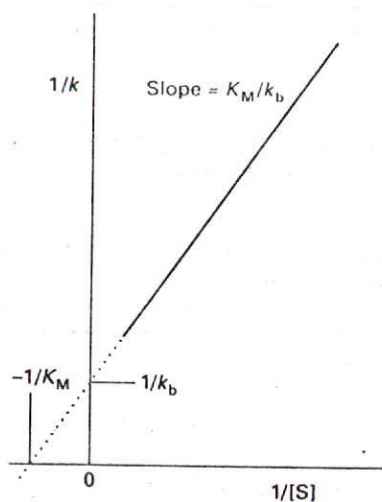
$$\frac{d[P]}{dt} = k[E]_0 \quad k = \frac{k_b [S]}{K_M + [S]} \quad (50)$$

where the Michaelis constant, K_M , is

$$K_M = \frac{k'_a + k_b}{k_a} \quad (51)$$

According to eqn 50, the rate of enzymolysis varies linearly with the enzyme concentration, but in a more complicated manner with the concentration of substrate (Fig. 25.15). Thus, when $[S] \gg K_M$, the rate law in eqn 50 reduces to

$$\frac{d[P]}{dt} = k_b [E]_0 \quad (52)$$



25.16 A Lineweaver-Burk plot for the analysis of an enzymolysis that proceeds by a Michaelis-Menten mechanism, and the significance of the intercepts and the slope.

and is zero-order in S. This result means that under these conditions the rate is constant: there is so much S present that it remains at effectively the same concentration even though products are being formed. Moreover, the rate of formation of products is a maximum, and $k_b[E]_0$ is called the **maximum velocity** of the enzymolysis; k_b itself is called the **maximum turnover number**. When so little S is present that $[S] \ll K_M$, the rate of formation of products is

$$\frac{d[P]}{dt} = \frac{k_b}{K_M} [E]_0 [S] \quad (53)$$

Now the rate is proportional to $[S]$ as well as to $[E]_0$.

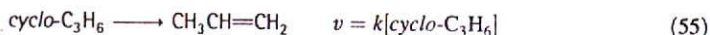
It follows from eqn 50 that

$$\frac{1}{k} = \frac{1}{k_b} + \frac{K_M}{k_b[S]} \quad (54)$$

Hence, a **Lineweaver-Burk plot** of $1/k$ against $1/[S]$ will give k_b (from the intercept at $1/[S] = 0$) and K_M (from the slope, K_M/k_b , Fig. 25.16). However, the plot cannot give the individual rate constants k_a and k'_a that appear in K_M . The stopped-flow technique can give the additional data needed, because the rate of formation of the enzyme-substrate complex can be found by monitoring its concentration after mixing enzyme and substrate. This procedure gives k_a , and k'_a can then be found by combining this result with the value of K_M .

25.8 Unimolecular reactions

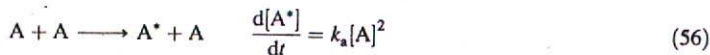
A number of gas-phase reactions follow first-order kinetics, as in the isomerization of cyclopropane mentioned earlier:



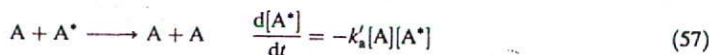
The problem with the interpretation of first-order rate laws is that presumably a molecule acquires enough energy to react as a result of its collisions with other molecules. However, collisions are simple bimolecular events, so how can they result in a first-order rate law? First-order gas-phase reactions are widely called 'unimolecular reactions' because they also involve an elementary unimolecular step in which the reactant molecule changes into the product. This term must be used with caution, though, because the overall mechanism has bimolecular as well as unimolecular steps.

(a) The Lindemann-Hinshelwood mechanism

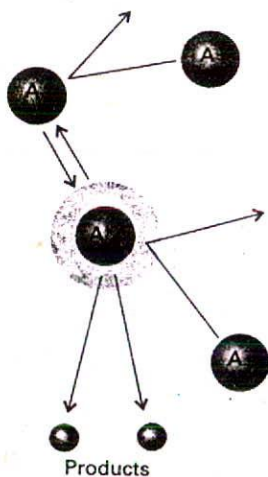
The first successful explanation of unimolecular reactions was provided by Frederick Lindemann in 1921 and then elaborated by Cyril Hinshelwood. In the **Lindemann-Hinshelwood mechanism** it is supposed that a reactant molecule A becomes energetically excited by collision with another A molecule (Fig. 25.17):



The energized molecule might lose its excess energy by collision with another molecule:



Alternatively, the excited molecule might shake itself apart and form products P. That is, it might undergo the unimolecular decay



25.17 A representation of the Lindemann-Hinshelwood mechanism of unimolecular reactions. The species A is excited by collision with A, and the excited A molecule (A^*) may either be deactivated by a collision with A or go on to decay by a unimolecular process to form products.

If the unimolecular step is slow enough to be the rate-determining step, the overall reaction will have first-order kinetics, as observed. This conclusion can be demonstrated explicitly by applying the steady-state approximation to the net rate of formation of A^* :

$$\frac{d[A^*]}{dt} = k_a[A]^2 - k'_a[A][A^*] - k_b[A^*] \approx 0 \quad (59)$$

This equation solves to

$$[A^*] = \frac{k_a[A]^2}{k_b + k'_a[A]} \quad (60)$$

so the rate law for the formation of P is

$$\frac{d[P]}{dt} = k_b[A^*] = \frac{k_a k_b [A]^2}{k_b + k'_a[A]} \quad (61)$$

At this stage the rate law is not first-order. However, if the rate of deactivation by (A^* , A) collisions is much greater than the rate of unimolecular decay, in the sense that

$$k'_a[A^*][A] \gg k_b[A^*] \quad \text{or} \quad k'_a[A] \gg k_b$$

then we can neglect k_b in the denominator and obtain

$$\frac{d[P]}{dt} \approx k[A] \quad k = \frac{k_a k_b}{k'_a} \quad (62)$$

Equation 62 is a first-order rate law, as we set out to show.

The Lindemann-Hinshelwood mechanism can be tested because it predicts that, as the concentration (and therefore the partial pressure) of A is reduced, the reaction should switch to overall second-order kinetics. Thus, when $k'_a[A] \ll k_b$, the rate law in eqn 61 is

$$\frac{d[P]}{dt} \approx k_a[A]^2 \quad (63)$$

The physical reason for the change of order is that at low pressures the rate-determining step is the bimolecular formation of A^* . If we write the full rate law in eqn 61 as

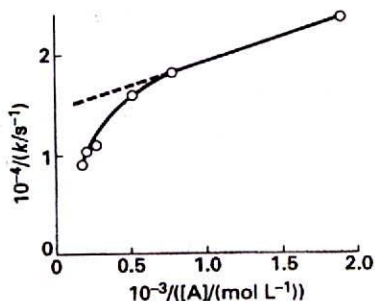
$$\frac{d[P]}{dt} = k[A] \quad k = \frac{k_a k_b [A]}{k_b + k'_a[A]} \quad (64)$$

then the expression for the effective rate-constant, k , can be rearranged to

$$\frac{1}{k} = \frac{k'_a}{k_a k_b} + \frac{1}{k_a[A]} \quad (65)$$

Hence, a test of the theory is to plot $1/k$ against $1/[A]$, and to expect a straight line.

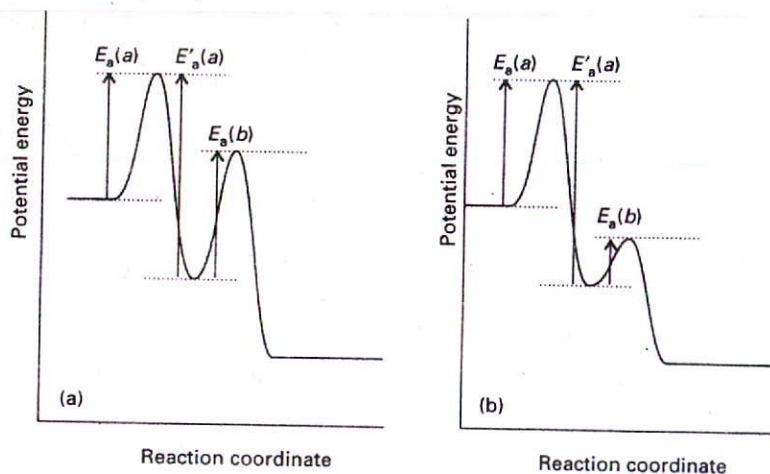
Whereas the Lindemann-Hinshelwood mechanism agrees in general with the switch in order of unimolecular reactions, it does not agree in detail. A typical graph of $1/k$ against $1/[A]$ is shown in Fig. 25.18. The graph has a pronounced curvature, corresponding to a larger value of k (a smaller value of $1/k$) at high pressures (low $1/[A]$) than would be expected by extrapolation of the reasonably linear low pressure (high $1/[A]$) data.



25.18 The pressure dependence of the unimolecular isomerization of *trans*-CHD=CHD showing a pronounced departure from the straight line predicted by eqn 65 based on the Lindemann-Hinshelwood mechanism.

(b) The activation energy of a composite reaction

Although the rate of each step of a complex mechanism might increase with temperature and show Arrhenius behaviour, is that true of a composite reaction? To answer this question, we consider the high-pressure limit of the Lindemann-Hinshelwood mechanism as



25.19 For a reaction with a pre-equilibrium, there are three activation energies to take into account, two referring to the reversible steps of the pre-equilibrium and one for the final step. The relative magnitudes of the activation energies determine whether the overall activation energy is (a) positive or (b) negative.

expressed in eqn 62. If each of the rate constants has an Arrhenius-like temperature dependence, we can use eqn 26 for each of them, and write

$$\begin{aligned}
 k &= \frac{k_a k_b}{k'_a} = \frac{(A(a)e^{-E_a(a)/RT})(A(b)e^{-E_a(b)/RT})}{(A'(a)e^{-E'_a(a)/RT})} \\
 &= \frac{A(a)A(b)}{A'(a)} e^{-\{E_a(a)+E_a(b)-E'_a(a)\}/RT}
 \end{aligned} \quad (66)$$

That is, the composite rate constant k has an Arrhenius-like form with activation energy

$$E_a = E_a(a) + E_a(b) - E'_a(a) \quad (67)$$

Moreover, provided $E_a(a) + E_a(b) > E'_a(a)$, the activation energy is positive and the rate increases with temperature. However, it is conceivable that $E_a(a) + E_a(b) < E'_a(a)$ (Fig. 25.19), in which case the activation energy is negative and the rate will decrease as the temperature is raised. There is nothing remarkable about this behaviour: all it means is that the reverse reaction (corresponding to the deactivation of A^*) is so sensitive to temperature that its rate increases sharply as the temperature is raised, and depletes the steady-state concentration of A^* . The Lindemann-Hinshelwood mechanism is an unlikely candidate for this type of behaviour because the deactivation of A^* has only a small activation energy, but there are reactions with analogous mechanisms in which a negative activation energy is observed.

When we examine the general rate law given in eqn 61, it is clear that the temperature dependence may be difficult to predict because each rate constant in the expression for k increases with temperature, and the outcome depends on whether the terms in the numerator dominate those in the denominator, or vice versa. The fact that so many reactions do show Arrhenius-like behaviour with positive activation energies suggests that their rate laws are in a 'simple' regime, like eqn 63 rather than eqn 61, and that the temperature dependence is dominated by the activation energy of the rate-determining stage. An enzyme reaction can show an even more complicated temperature dependence, because the enzyme may become denatured as the temperature is raised, and hence cease to function.

Checklist of key ideas

- chemical kinetics

Empirical chemical kinetics

25.1 Experimental techniques

- real-time analysis
 quenching method
 flow method
 stopped-flow technique
 flash photolysis

25.2 The rates of reactions

- rate of consumption
 rate of formation
 rate of reaction (1)
 rate constant
 rate law (3)
 reaction order (5)
 first-order reaction
 overall order
 zero-order rate law (7)
 isolation method

- pseudofirst-order rate law
 method of initial rates

25.3 Integrated rate laws

- integrated rate law
 first-order integrated rate law (10)
 half-life (11)
 second-order integrated rate law (12)
 half-life of second-order process (13)

25.4 Reactions approaching equilibrium

- integrated reversible rate laws
 equilibrium constants and rate constants (21)
 relaxation
 temperature jump
 pressure jump

25.5 The temperature dependence of reaction rates

- Arrhenius equation (24)
 pre-exponential factor
 frequency factor
 activation energy
 Arrhenius parameters
 formal definition of activation energy (25)

Accounting for the rate laws

25.6 Elementary reactions

- elementary reaction
 molecularity
 unimolecular reaction
 bimolecular reaction
 rate laws for elementary reactions (27, 28)

25.7 Consecutive elementary reactions

- integrated rate law for consecutive reactions
 rate-determining step
 steady-state approximation (37)
 induction period
 pre-equilibrium (41)
 Michaelis-Menten mechanism
 Michaelis constant
 maximum velocity (of enzymolysis) (52)
 maximum turnover number
 Lineweaver-Burk plot (54)

25.8 Unimolecular reactions

- Lindemann-Hinshelwood mechanism
 effective rate constant (65)
 composite activation energy (67)

Further reading

Articles of general interest

E. Levin and J.G. Eberhart, Simplified rate-law integration for reactions that are first-order in each of the two reactants.

J. Chem. Educ. **66**, 705 (1989).

M.N. Berberan-Santos and J.M.G. Martinho, Integration of kinetic rate equations by matrix methods. *J. Chem. Educ.* **67**, 375 (1990).

J.C. Reeve, Some provocative opinions on the terminology of chemical kinetics. *J. Chem. Educ.* **68**, 728 (1991).

H. Maskill, The extent of reaction and chemical kinetics. *Educ. in Chem.* **21**, 122 (1984).

S.R. Logan, The meaning and significance of "the activation energy" of a chemical reaction. *Educ. in Chem.* **23**, 148 (1986).

J.G. Eberhardt and E. Levin, A simplified integration technique for reaction rate laws of integral order in several substances. *J. Chem. Educ.* **72**, 193 (1995).

G.I. Gellene, Application of kinetic approximations to the $A + B \rightleftharpoons C$ reaction system. *J. Chem. Educ.* **72**, 196 (1995).

S. Bluestone and K.Y. Yan, A method to find the rate constants

in chemical kinetics of a complex reaction. *J. Chem. Educ.* **72**, 884 (1995).

H. Bisswanger, Proteins and enzymes. In *Encyclopedia of applied physics* (ed. G.L. Trigg), **15**, 185. VCH, New York (1996).

R.W. Carr, Chemical kinetics. In *Encyclopedia of applied physics* (ed. G.L. Trigg), **3**, 345. VCH, New York (1992).

Texts and sources of data and information

M.J. Pilling and P.W. Seakins, *Reaction kinetics*. Oxford University Press (1995).

S.R. Logan, *Fundamentals of chemical kinetics*. Longman, Harlow (1996).

J.I. Steinfeld, J.S. Francisco, and W.L. Hase, *Chemical kinetics and dynamics*. Prentice-Hall, Englewood Cliffs (1989).

K.A. Connors, *Chemical kinetics*. VCH, Weinheim (1990).

K.J. Laidler, *Chemical kinetics*. Harper & Row, New York (1987).

I.H. Siegel, *Enzyme kinetics*. Wiley-Interscience, New York (1993).

C.H. Bamford and C.F. Tipper (ed.), *Comprehensive chemical kinetics*, Vols 1–26. Elsevier, Amsterdam (1969–86).

R.G. Compton (ed.), *Comprehensive chemical kinetics*, Vols 27–33. Elsevier, Amsterdam (1987–92).

B.B. Chance, Rapid flow methods. In *Techniques of chemistry* (ed. G.G. Hammes), 6B, 5. Wiley-Interscience, New York (1974).

G.G. Hammes, Temperature-jump methods. In *Techniques of chemistry* (ed. G.G. Hammes), 6B, 147. Wiley-Interscience, New York (1974).

W. Knoch, Pressure-jump methods. In *Techniques of chemistry* (ed. G.G. Hammes), 6B, 187. Wiley-Interscience, New York (1974).

Exercises

25.1 (a) The rate of the reaction $A + 2B \rightarrow 3C + D$ was reported as $1.0 \text{ mol L}^{-1} \text{ s}^{-1}$. State the rates of formation and consumption of the participants.

25.1 (b) The rate of the reaction $A + 3B \rightarrow C + 2D$ was reported as $1.0 \text{ mol L}^{-1} \text{ s}^{-1}$. State the rates of formation and consumption of the participants.

25.2 (a) The rate of formation of C in the reaction $2A + B \rightarrow 2C + 3D$ is $1.0 \text{ mol L}^{-1} \text{ s}^{-1}$. State the reaction rate, and the rates of formation or consumption of A, B, and D.

25.2 (b) The rate of consumption of B in the reaction $A + 3B \rightarrow C + 2D$ is $1.0 \text{ mol L}^{-1} \text{ s}^{-1}$. State the reaction rate, and the rates of formation or consumption of A, C, and D.

25.3 (a) The rate law for the reaction in Exercise 25.1a was found to be $v = k[A][B]$. What are the units of k ? Express the rate law in terms of the rates of formation and consumption of (a) A, (b) C.

25.3 (b) The rate law for the reaction in Exercise 25.1b was found to be $v = k[A][B]^2$. What are the units of k ? Express the rate law in terms of the rates of formation and consumption of (a) A, (b) C.

25.4 (a) The rate law for the reaction in Exercise 25.2a was reported as $d[C]/dt = k[A][B][C]$. Express the rate law in terms of the reaction rate; what are the units for k in each case?

25.4 (b) The rate law for the reaction in Exercise 25.2b was reported as $d[C]/dt = k[A][B][C]^{-1}$. Express the rate law in terms of the reaction rate; what are the units for k in each case?

25.5 (a) At 518°C , the rate of decomposition of a sample of gaseous acetaldehyde, initially at a pressure of 363 Torr, was 1.07 Torr s^{-1} when 5.0 per cent had reacted and 0.76 Torr s^{-1} when 20.0 per cent had reacted. Determine the order of the reaction.

25.5 (b) At 400 K, the rate of decomposition of a gaseous compound initially at a pressure of 12.6 kPa, was 9.71 Pa s^{-1} when 10.0 per cent had reacted and 7.67 Pa s^{-1} when 20.0 per cent had reacted. Determine the order of the reaction.

25.6 (a) At 518°C , the half-life for the decomposition of a sample of gaseous acetaldehyde (ethanal) initially at 363 Torr was 410 s. When the pressure was 169 Torr, the half-life was 880 s. Determine the order of the reaction.

25.6 (b) At 400 K, the half-life for the decomposition of a sample of a gaseous compound initially at 55.5 kPa was 340 s. When the pressure was 28.9 kPa, the half-life was 178 s. Determine the order of the reaction.

25.7 (a) The rate constant for the first-order decomposition of N_2O_5 in the reaction $2\text{N}_2\text{O}_5(\text{g}) \rightarrow 4\text{NO}_2(\text{g}) + \text{O}_2(\text{g})$ is $k = 3.38 \times 10^{-5} \text{ s}^{-1}$ at 25°C . What is the half-life of N_2O_5 ? What will be the pressure, initially 500 Torr, (a) 10 s, (b) 10 min after initiation of the reaction?

25.7 (b) The rate constant for the first-order decomposition of a compound A in the reaction $2A \rightarrow P$ is $k = 2.78 \times 10^{-7} \text{ s}^{-1}$ at 25°C . What is the half-life of A? What will be the pressure, initially 32.1 kPa, (a) 10 h, (b) 50 h after initiation of the reaction?

25.8 (a) A second-order reaction of the type $A + B \rightarrow P$ was carried out in a solution that was initially 0.050 mol L^{-1} in A and 0.080 mol L^{-1} in B. After 1.0 h the concentration of A had fallen to 0.020 mol L^{-1} . (a) Calculate the rate constant. (b) What is the half-life of the reactants?

25.8 (b) A second-order reaction of the type $A + 2B \rightarrow P$ was carried out in a solution that was initially 0.075 mol L^{-1} in A and 0.080 mol L^{-1} in B. After 1.0 h the concentration of A had fallen to 0.045 mol L^{-1} . (a) Calculate the rate constant. (b) What is the half-life of the reactants?

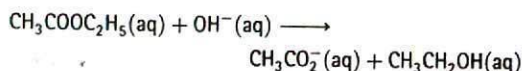
25.9 (a) If the rate laws are expressed with (a) concentrations in moles per litre, (b) pressures in kilopascals, what are the units of the second-order and third-order rate constants?

25.9 (b) If the rate laws are expressed with (a) concentrations in molecules per metre cubed, (b) pressures in newtons per metre squared, what are the units of the second-order and third-order rate constants?

25.10 (a) The half-life for the (first-order) radioactive decay of ^{14}C is 5730 y (it emits β rays with an energy of 0.16 MeV). An archaeological sample contained wood that had only 72 per cent of the ^{14}C found in living trees. What is its age?

25.10 (b) One of the hazards of nuclear explosions is the generation of ^{90}Sr and its subsequent incorporation in place of calcium in bones. This nuclide emits β rays of energy 0.55 MeV, and has a half-life of 28.1 y. Suppose $1.00 \mu\text{g}$ was absorbed by a newly born child. How much will remain after (a) 18 y, (b) 70 y if none is lost metabolically?

25.11 (a) The second-order rate constant for the reaction



is $0.11 \text{ L mol}^{-1} \text{ s}^{-1}$. What is the concentration of ester after (a) 10 s, (b) 10 min when ethyl acetate is added to sodium hydroxide so that the initial concentrations are $[\text{NaOH}] = 0.050 \text{ mol L}^{-1}$ and $[\text{CH}_3\text{COOC}_2\text{H}_5] = 0.100 \text{ mol L}^{-1}$?

25.11 (b) The second-order rate constant for the reaction $\text{A} + 2\text{B} \rightarrow \text{C} + \text{D}$ is $0.21 \text{ L mol}^{-1} \text{ s}^{-1}$. What is the concentration of C after (a) 10 s, (b) 10 min when the reactants are mixed with initial concentrations of $[\text{A}] = 0.025 \text{ mol L}^{-1}$ and $[\text{B}] = 0.150 \text{ mol L}^{-1}$?

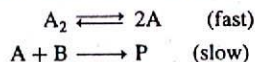
25.12 (a) A reaction $2\text{A} \rightarrow \text{P}$ has a second-order rate law with $k = 3.50 \times 10^{-4} \text{ L mol}^{-1} \text{ s}^{-1}$. Calculate the time required for the concentration of A to change from 0.260 mol L^{-1} to 0.011 mol L^{-1} .

25.12 (b) A reaction $2\text{A} \rightarrow \text{P}$ has a third-order rate law with $k = 3.50 \times 10^{-4} \text{ L}^2 \text{ mol}^{-2} \text{ s}^{-1}$. Calculate the time required for the concentration of A to change from 0.077 mol L^{-1} to 0.021 mol L^{-1} .

25.13 (a) The rate constant for the decomposition of a certain substance is $2.80 \times 10^{-3} \text{ L mol}^{-1} \text{ s}^{-1}$ at 30°C and $1.38 \times 10^{-2} \text{ L mol}^{-1} \text{ s}^{-1}$ at 50°C . Evaluate the Arrhenius parameters of the reaction.

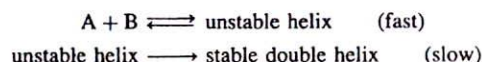
25.13 (b) The rate constant for the decomposition of a certain substance is $1.70 \times 10^{-2} \text{ L mol}^{-1} \text{ s}^{-1}$ at 24°C and $2.01 \times 10^{-2} \text{ L mol}^{-1} \text{ s}^{-1}$ at 37°C . Evaluate the Arrhenius parameters of the reaction.

25.14 (a) The reaction mechanism



involves an intermediate A. Deduce the rate law for the reaction.

25.14 (b) Consider the following mechanism for renaturation of a double helix from its strands A and B:



Derive the rate equation for the formation of the double helix and express the rate constant of the renaturation reaction in terms of the rate constants of the individual steps.

25.15 (a) Show that $t_{1/2} \propto 1/[\text{A}]^{n-1}$ for a reaction that is n th-order in A.

25.15 (b) Deduce an expression for the time it takes for the concentration of a substance to fall to one-third its initial value in an n th-order reaction.

25.16 (a) The enzyme-catalysed conversion of a substrate at 25°C has a Michaelis constant of 0.035 mol L^{-1} . The rate of the reaction is $1.15 \times 10^{-3} \text{ mol L}^{-1} \text{ s}^{-1}$ when the substrate concentration is 0.110 mol L^{-1} . What is the maximum velocity of this enzymolysis?

25.16 (b) The enzyme-catalysed conversion of a substrate at 25°C has a Michaelis constant of 0.042 mol L^{-1} . The rate of the reaction is $2.45 \times 10^{-4} \text{ mol L}^{-1} \text{ s}^{-1}$ when the substrate concentration is 0.890 mol L^{-1} . What is the maximum velocity of this enzymolysis?

25.17 (a) The effective rate constant for a gaseous reaction which has a Lindemann-Hinshelwood mechanism is $2.50 \times 10^{-4} \text{ s}^{-1}$ at 1.30 kPa and $2.10 \times 10^{-5} \text{ s}^{-1}$ at 12 Pa . Calculate the rate constant for the activation step in the mechanism.

25.17 (b) The effective rate constant for a gaseous reaction which has a Lindemann-Hinshelwood mechanism is $1.7 \times 10^{-3} \text{ s}^{-1}$ at 1.09 kPa and $2.2 \times 10^{-4} \text{ s}^{-1}$ at 25 Pa . Calculate the rate constant for the activation step in the mechanism.

25.18 (a) The $\text{p}K_a$ of NH_4^+ is 9.25 at 25°C . The rate constant at 25°C for the reaction of NH_4^+ and OH^- to form aqueous NH_3 is $4.0 \times 10^{10} \text{ L mol}^{-1} \text{ s}^{-1}$. Calculate the rate constant for proton transfer to NH_3 . What relaxation time would be observed if a temperature jump were applied to a solution of $0.15 \text{ mol L}^{-1} \text{ NH}_3(\text{aq})$ at 25°C ?

25.18 (b) The equilibrium $\text{A} \rightleftharpoons \text{B} + \text{C}$ at 25°C is subjected to a temperature jump. The measured relaxation time is $3.0 \mu\text{s}$. The equilibrium constant for the system is 2.0×10^{-16} at 25°C , and the equilibrium concentrations of B and C at 25°C are both $2.0 \times 10^{-4} \text{ mol L}^{-1}$. Calculate the rate constants for the first-order forward and second-order reverse reactions.

Problems

Numerical problems

25.1 The data below apply to the formation of urea from ammonium cyanate, $\text{NH}_4\text{CNO} \rightarrow \text{NH}_2\text{CONH}_2$. Initially 22.9 g of ammonium cyanate was dissolved in enough water to prepare 1.00 L of solution. Determine the order of the reaction, the rate constant, and the mass of ammonium cyanate left after 300 min .

t/min	0	20.0	50.0	65.0	150
$m(\text{urea})/\text{g}$	0	7.0	12.1	13.8	17.7

25.2 The data below apply to the reaction, $(\text{CH}_3)_3\text{CBr} + \text{H}_2\text{O} \rightarrow (\text{CH}_3)_3\text{COH} + \text{HBr}$. Determine the order of the

reaction, the rate constant, and the molar concentration of $(\text{CH}_3)_3\text{CBr}$ after 43.8 h .

t/h	0	3.15	6.20	10.00	18.30	30.80
$[(\text{CH}_3)_3\text{CBr}]/(10^{-2} \text{ mol L}^{-1})$	10.39	8.96	7.76	6.39	3.53	2.07

25.3 The thermal decomposition of an organic nitrile produced the following data:

$t/(10^3 \text{ s})$	0	2.00	4.00	6.00	8.00	10.00	12.00	∞
$[\text{nitrile}]/(\text{mol L}^{-1})$	1.10	0.86	0.67	0.52	0.41	0.32	0.25	0

Determine the order of the reaction and the rate constant.

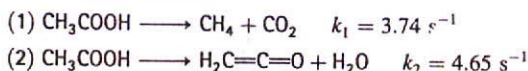
25.4 The following data have been obtained for the decomposition of $\text{N}_2\text{O}_5(\text{g})$ at 67°C according to the reaction $2\text{N}_2\text{O}_5(\text{g}) \rightarrow 4\text{NO}_2(\text{g}) + \text{O}_2(\text{g})$. Determine the order of the reaction, the rate constant, and the half-life. It is not necessary to obtain the result graphically; you may do a calculation using estimates of the rates of change of concentration.

t/min	0	1	2	3	4	5
$[\text{N}_2\text{O}_5]/(\text{mol L}^{-1})$	1.000	0.705	0.497	0.349	0.246	0.173

25.5 A first-order decomposition reaction is observed to have the following rate constants at the indicated temperatures. Estimate the activation energy.

$k/(10^{-3} \text{ s}^{-1})$	2.46	45.1	576
$\theta/^\circ\text{C}$	0	20.0	40.0

25.6 The gas-phase decomposition of acetic acid at 1189 K proceeds by way of two parallel reactions:



What is the maximum percentage yield of the ketene CH_2CO obtainable at this temperature?

25.7 The composition of a liquid-phase reaction $2\text{A} \rightarrow \text{B}$ was followed by a spectrophotometric method with the following results:

t/min	0	10	20	30	40	∞
$[\text{B}]/(\text{mol L}^{-1})$	0	0.089	0.153	0.200	0.230	0.312

Determine the order of the reaction and its rate constant.

25.8 Sucrose is readily hydrolysed to glucose and fructose in acidic solution. The hydrolysis is often monitored by measuring the angle of rotation of plane-polarized light passing through the solution. From the angle of rotation the concentration of sucrose can be determined. An experiment on the hydrolysis of sucrose in 0.50 M HCl(aq) produced the following data:

t/min	0	14	39	60	80	110	140	170	210
$[\text{sucrose}]/(\text{mol L}^{-1})$	0.316	0.300	0.274	0.256	0.238	0.211	0.190	0.170	0.146

Determine the rate constant of the reaction and the average lifetime of a sucrose molecule.

25.9 The ClO radical decays rapidly by way of the reaction, $2\text{ClO} \rightarrow \text{Cl}_2 + \text{O}_2$. The following data have been obtained:

$t/(10^{-3} \text{ s})$	0.12	0.62	0.96	1.60	3.20	4.00	5.75
$[\text{ClO}]/(10^{-6} \text{ mol L}^{-1})$	8.49	8.09	7.10	5.79	5.20	4.77	3.95

Determine the rate constant of the reaction.

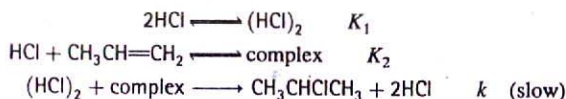
25.10 Cyclopropane isomerizes into propene when heated to 500°C in the gas phase. The extent of conversion for various initial pressures has been followed by gas chromatography by allowing the reaction to proceed for a time with various initial pressures:

p_0/Torr	200	200	400	400	600	600
t/s	100	200	100	200	100	200
p/Torr	186	173	373	347	559	520

where p_0 is the initial pressure and p is the final pressure of cyclopropane. What are the order and rate constant for the reaction under these conditions?

25.11 The addition of hydrogen halides to alkenes has played a fundamental role in the investigation of organic reaction mechanisms. In one study (M.J. Haugh and D.R. Dalton, *J. Amer. Chem. Soc.* 97, 5674 (1975)), high pressures of hydrogen chloride (up to 25 atm) and propene (up to 5 atm) were examined over a range of temperatures and the amount of 2-chloropropane formed was determined by NMR. Show that if the reaction $\text{A} + \text{B} \rightarrow \text{P}$ proceeds for a short time δt , the concentration of product follows $[\text{P}]/[\text{A}] = k[\text{A}]^{m-1}[\text{B}]^n \delta t$ if the reaction is m th-order in A and n th-order in B. In a series of runs the ratio of [chloropropane] to [propene] was independent of [propene] but the ratio of [chloropropane] to [HCl] for constant amounts of propene depended on [HCl]. For $\delta t \approx 100 \text{ h}$ (which is short on the timescale of the reaction) the latter ratio rose from zero to 0.05, 0.03, 0.01 for $p(\text{HCl}) = 10 \text{ atm}$, 7.5 atm, 5.0 atm, respectively. What are the orders of the reaction with respect to each reactant?

25.12 Show that the following mechanism can account for the rate law of the reaction in Problem 25.11:



What further tests could you apply to verify this mechanism?

25.13 In the experiments described in Problems 25.11 and 25.12 an inverse temperature dependence of the reaction rate was observed, the overall rate of reaction at 70°C being roughly one-third that at 19°C . Estimate the apparent activation energy and the activation energy of the rate-determining step given that the enthalpies of the two equilibria are both of the order of -14 kJ mol^{-1} .

25.14 The second-order rate constants for the reaction of oxygen atoms with aromatic hydrocarbons have been measured (R. Atkinson and J.N. Pitts, *J. Phys. Chem.* 79, 295 (1975)). In the reaction with benzene the rate constants are $1.44 \times 10^7 \text{ L mol}^{-1} \text{ s}^{-1}$ at 300.3 K , $3.03 \times 10^7 \text{ L mol}^{-1} \text{ s}^{-1}$ at 341.2 K , and $6.9 \times 10^7 \text{ L mol}^{-1} \text{ s}^{-1}$ at 392.2 K . Find the pre-exponential factor and activation energy of the reaction.

25.15 In Problem 25.10 the isomerization of cyclopropane over a limited pressure range was examined. If the Lindemann mechanism of first-order reactions is to be tested we also need data at low pressures. These have been obtained (H.O. Pritchard, R.G. Sowden, and A.F. Trotman-Dickenson, *Proc. R. Soc. A* 217, 563 (1953)):

p/Torr	84.1	11.0	2.89	0.569	0.120	0.067
$10^4 k_{\text{eff}}/\text{s}^{-1}$	2.98	2.23	1.54	0.857	0.392	0.303

Test the Lindemann theory with these data.

25.16 The initial rate of O_2 production by the action of an enzyme on a substrate was measured for a range of substrate concen-

trations; the data are below. Evaluate the Michaelis constant for the reaction.

$[S]/(\text{mol L}^{-1})$	0.050	0.017	0.010	0.0050	0.0020
$v/(\text{mm}^3 \text{min}^{-1})$	16.6	12.4	10.1	6.6	3.3

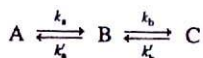
Theoretical problems

25.17 The equilibrium $A \rightleftharpoons B$ is first-order in both directions. Derive an expression for the concentration of A as a function of time when the initial molar concentrations of A and B are $[A]_0$ and $[B]_0$. What is the final composition of the system?

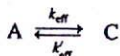
25.18 Derive an integrated expression for a second-order rate law $v = k[A][B]$ for a reaction of stoichiometry $2A + 3B \rightarrow P$.

25.19 Derive the integrated form of a third-order rate law $v = k[A]^2[B]$ in which the stoichiometry is $2A + B \rightarrow P$ and the reactants are initially present in (a) their stoichiometric proportions, (b) with B present initially in twice the amount.

25.20 Set up the rate equations for the reaction mechanism:



Show that the mechanism is equivalent to



under specified circumstances.

25.21 Show that the ratio $t_{1/2}/t_{3/4}$, where $t_{1/2}$ is the half-life and $t_{3/4}$ is the time for the concentration of A to decrease to $\frac{3}{4}$ of its initial value (implying that $t_{3/4} < t_{1/2}$) can be written as a function of n alone, and can therefore be used as a rapid assessment of the order of a reaction.

25.22 Many enzyme-catalysed reactions are consistent with a modified version of the Michaelis-Menten mechanism in which the second step is also reversible. For this mechanism obtain an expression for the rate of formation of product and find its limiting behaviour for large and small concentrations of substrate.

25.23 Derive an equation for the steady-state rate of the sequence of reactions $A \rightleftharpoons B \rightleftharpoons C \rightleftharpoons D$, with $[A]$ maintained at a fixed value and the product D removed as soon as it is formed.

Additional problems supplied by Carmen Giunta and Charles Trapp

25.24 *Prebiotic reactions* are reactions that might have occurred under the conditions prevalent on the Earth before the first living creatures emerged and that can lead to analogues of molecules necessary for life as we now know it. To qualify, a reaction must proceed with favourable rates and equilibria. M.P. Robertson and S.I. Miller (*Science* 268, 702 (1995)) have studied the prebiotic synthesis of 5-substituted uracils, among them 5-hydroxymethyluracil (HMU). Amino acid analogues can be formed from HMU under prebiotic conditions by reaction with various nucleophiles, such as H_2S , HCN, indole, imidazole, etc. For the synthesis of HMU (the uracil

analogue of serine) from uracil and formaldehyde (HCHO), the rate of addition is given by $\log k/(\text{L mol}^{-1} \text{s}^{-1}) = 11.75 - 5488/(T/\text{K})$ (at pH = 7), and $\log K = -1.36 + 1794/(T/\text{K})$. For this reaction, calculate the rates and equilibrium constants over a range of temperatures corresponding to possible prebiotic conditions, such as 0–50°C, and plot them against temperature. Also, calculate the activation energy and the standard reaction Gibbs energy and enthalpy at 25°C. Prebiotic conditions are not likely to be standard conditions. Speculate about how the actual values of the reaction Gibbs energy and enthalpy might differ from the standard values. Do you expect that the reaction would still be favourable?

25.25 For the second-order reaction $A + B \rightarrow \text{Products}$, the rate of reaction, v , may be written

$$v = \frac{dx}{dt} = k([A]_0 - x)([B]_0 + x)$$

where x is the decrease in concentration of A or B as a result of reaction. What are the conditions for the rate to be a maximum and a minimum? Draw a graph of v against x and, noting that v and x cannot be negative, identify the portion of the curve that corresponds to reality.

25.26 For the consecutive reaction $A \rightarrow I \rightarrow P$, Fig. 25.12 shows $[I]$ plotted against time for $k_a = 10k_b$. For $[A]_0 = 1.0 \text{ mol L}^{-1}$ and $k_a = 1.0 \text{ min}^{-1}$, plot $[I]$ against t for $k_a/k_b = 5, 1, \text{ and } 0.5$. For each case determine the time at which $[I]$ reaches a maximum.

25.27 For the only $A + B \rightarrow P$ reaction in Table 25.3, find an expression for x as a function of time.

25.28 T. Gierczak, R.K. Talukdar, S.C. Herndon, G.L. Vaghjiani, and A.R. Ravishankara (*J. Phys. Chem. A* 101, 3125 (1997)) measured the rate constants for the elementary bimolecular gas-phase reaction of methane with the hydroxyl radical over a range of temperatures of importance to atmospheric chemistry. Deduce the Arrhenius parameters A and E_a from the following measurements.

T/K	295	295	223	218
$k/(10^6 \text{ L mol}^{-1} \text{ s}^{-1})$	3.70	3.55	0.494	0.452
T/K	213	206	200	195
$k/(10^6 \text{ L mol}^{-1} \text{ s}^{-1})$	0.379	0.295	0.241	0.217

25.29 The oxidation of HSO_3^- by O_2 in aqueous solution is a reaction of importance to the processes of acid rain formation and flue gas desulfurization. R.E. Connick, Y.-X. Zhang, S. Lee, R. Adamic, and P. Chieng (*Inorg. Chem.* 34, 4543 (1995)) report that the reaction $2\text{HSO}_3^- + \text{O}_2 \rightarrow 2\text{SO}_4^{2-} + 2\text{H}^+$ follows the rate law $v = k[\text{HSO}_3^-]^2[\text{H}^+]^2$. Given a pH of 5.6 and an oxygen molar concentration of $2.4 \times 10^{-4} \text{ mol L}^{-1}$ (both presumed constant), an initial HSO_3^- molar concentration of $5 \times 10^{-5} \text{ mol L}^{-1}$, and a rate constant of $3.6 \times 10^6 \text{ L}^3 \text{ mol}^{-3} \text{ s}^{-1}$, what is the initial rate of reaction? How long would it take for HSO_3^- to reach half its initial concentration?

25.30 Chlorine atoms react rapidly with ozone in the gas-phase bimolecular reaction $\text{Cl} + \text{O}_3 \rightarrow \text{ClO} + \text{O}_2$ with $k_2 = (1.7 \times 10^{10} \text{ L mol}^{-1} \text{ s}^{-1})e^{-260/(T/\text{K})}$ (W.B. DeMore, S.P. Sander, D.M. Golden, R.F. Hampson, M.J. Kurylo, C.J. Howard, A.R. Ravishankara, C.E. Kolb, and M.J. Molina, *Chemical kinetics and*

photochemical data for use in stratospheric modeling: Evaluation Number 11, JPL Publication 94-26 (1994)). Estimate the rate of this reaction at (a) 20 km, where $[\text{Cl}] = 5 \times 10^{-17} \text{ mol L}^{-1}$, $[\text{O}_3] = 8 \times 10^{-9} \text{ mol L}^{-1}$, and $T = 220 \text{ K}$; (b) 45 km, where $[\text{Cl}] = 3 \times 10^{-15} \text{ mol L}^{-1}$, $[\text{O}_3] = 8 \times 10^{-11} \text{ mol L}^{-1}$, and $T = 270 \text{ K}$.

25.31 T. Gierczak, R.K. Talukdar, S.C. Herndon, G.L. Vaghjiani, and A.R. Ravishankara (*J. Phys. Chem. A* 101, 3125 (1997)) measured the rate constants for the bimolecular gas-phase reaction of methane with the hydroxyl radical $\text{CH}_4(\text{g}) + \text{OH}(\text{g}) \rightarrow \text{CH}_3(\text{g}) + \text{H}_2\text{O}(\text{g})$ and found $A = 1.13 \times 10^9 \text{ L mol}^{-1} \text{ s}^{-1}$ and $E_a = 14.1 \text{ kJ mol}^{-1}$ for the Arrhenius parameters. Reaction with OH is the main path by which CH_4 is removed from the lower atmosphere. (a) Estimate the rate of consumption of CH_4 . Take the average OH concentration to be $1.5 \times 10^{-21} \text{ mol L}^{-1}$, that of CH_4 to be $4.0 \times 10^{-8} \text{ mol L}^{-1}$, and the

temperature to be -10°C . (b) Estimate the global annual mass of CH_4 consumed by this reaction (which is slightly less than the amount introduced to the atmosphere) given an effective volume for the Earth's lower atmosphere of $4 \times 10^{21} \text{ L}$.

25.32 P.W. Seakins, M.J. Pilling, L.T. Niiranen, D. Gutman, and L.N. Krasnoperov (*J. Phys. Chem.* 96, 9847 (1992)) measured the forward and reverse rate constants for the gas-phase reaction $\text{C}_2\text{H}_5(\text{g}) + \text{HBr}(\text{g}) \rightarrow \text{C}_2\text{H}_6(\text{g}) + \text{Br}(\text{g})$ and used their findings to compute thermodynamic parameters for C_2H_5 . The reaction is bimolecular in both directions with Arrhenius parameters $A = 1.0 \times 10^9 \text{ L mol}^{-1} \text{ s}^{-1}$, $E_a = -4.2 \text{ kJ mol}^{-1}$ for the forward reaction and $k' = 1.4 \times 10^{11} \text{ L mol}^{-1} \text{ s}^{-1}$, $E_a = 53.3 \text{ kJ mol}^{-1}$ for the reverse reaction. Compute $\Delta_r H^\ominus$, S_m^\ominus , and $\Delta_r G^\ominus$ of C_2H_5 at 298 K.